Claudius Gros

Complex and Adaptive Dynamical Systems

A Primer

Springer Complexity

Springer Complexity is an interdisciplinary program publishing the best research and academic-level teaching on both fundamental and applied aspects of complex systems – cutting across all traditional disciplines of the natural and life sciences, engineering, economics, medicine, neuroscience, social and computer science.

Complex Systems are systems that comprise many interacting parts with the ability to generate a new quality of macroscopic collective behavior the manifestations of which are the spontaneous formation of distinctive temporal, spatial or functional structures. Models of such systems can be successfully mapped onto quite diverse "real-life" situations like the climate, the coherent emission of light from lasers, chemical reaction-diffusion systems, biological cellular networks, the dynamics of stock markets and of the internet, earthquake statistics and prediction, freeway traffic, the human brain, or the formation of opinions in social systems, to name just some of the popular applications.

Although their scope and methodologies overlap somewhat, one can distinguish the following main concepts and tools: self-organization, nonlinear dynamics, synergetics, turbulence, dynamical systems, catastrophes, instabilities, stochastic processes, chaos, graphs and networks, cellular automata, adaptive systems, genetic algorithms and computational intelligence.

The two major book publication platforms of the Springer Complexity program are the monograph series "Understanding Complex Systems" focusing on the various applications of complexity, and the "Springer Series in Synergetics", which is devoted to the quantitative theoretical and methodological foundations. In addition to the books in these two core series, the program also incorporates individual titles ranging from textbooks to major reference works.

Claudius Gros

Complex and Adaptive Dynamical Systems

A Primer

With 98 Figures and 10 Tables

Springer

Claudius Gros

Universität Frankfurt
Institut für Theoretische Physik
Max-von-Laue-Str. 1
60438 Frankfurt, Germany

Für meine Eltern,
meinem verstorbenen Vater
und meiner grossartigen Mutter

Contents

About this Book

From Evolving Networks to Cognitive Systems Theory This textbook covers a wide range of concepts, notions and phenomena of a truly interdisciplinary subject of rapidly growing importance. Complex system theory deals with dynamical systems containing a very large number of variables, showing a plethora of emergent features, arising in a broad range of contexts. A central focus of these notes is the notion of complexity arising within evolving and dynamical network structures, such as the gene expression networks at the basis of all living, adaptive ecological networks or neural networks for cognitive information processing.

Complex systems theory ultimately forms the basis of our long-standing quest for exploring and understanding cognitive systems in general and our brain in particular – the mammalian brain is probably the most complex of all adaptive networks known to humanity.

Readership and Preconditions This primer is intended for graduate students or scientists from natural sciences, engineering or neuroscience. Technically, the reader should have a basic knowledge of ordinary and partial differential equations and of probability distributions. This textbook is suitable both for studies in conjunction with teaching courses as well as for the individual reader.

Course Material and the Modular Approach When used for teaching, this primer is suitable for a course running over 40–60 lecture hours, depending on the pace and on the number of chapters covered. Essentially all mathematical transformations are performed on a step-by-step basis and in general the reader should have no problem following the respective derivations.

Individual chapters, apart from the first two, having an introductory character, may be skipped whenever time considerations demand it. I have followed a basic modular approach and the individual chapters are, as far as possible, independent of each other. Notwithstanding, cross references between the different chapters are included throughout the text, since interrelations between distinct topics are helpful for a thorough understanding.

Style This interdisciplinary primer sets a high value on conveying concepts and notions within their respective mathematical settings. Believing that a concise style helps the reader to go through the material I mostly abstained from long text passages with general background explanations or philosophical considerations. Widespread use has been made of paragraph headings, with the intention to facilitate scientific reading in this way.

A Primer to Scientific Common-Sense Knowledge To a certain extent one can regard this textbook as a primer to a wide range of scientific common-sense knowledge regarding complex systems. Basic knowledge about life's organizational principles, to give an example, such as the notion of "life at the edge of chaos", is important in today's world to an educated scientist. Other areas of scientific common-sense knowledge discussed in this primer include network theory, which has applications ranging from social networks to gene expression networks, the fundamentals of evolution, cognitive systems theory and the basic principles of dynamical systems theory.

Content All of the chapters making up this book deal with a subject worth devoting an entire course to. This book addresses readers interested in multidisciplinary aspects; I have consequently tried to present succinct expositions of the fundamental notions and concepts on the basis of the subjects treated in the individual chapters.

1. *Graph Theory and Small-World Networks*
    Networks, ranging from neural networks, social networks, ecological networks to gene expression networks, are at the basis of many complex systems. Networks tend to be adaptive and evolving. Network theory is therefore a prerequisite for a thorough understanding of adaptive and/or complex systems.

2. *Chaos, Bifurcations and Diffusion*
    This chapter introduces basic notions of dynamical systems theory, such as attractors, bifurcations, deterministic chaos, diffusion and stochastic resonances, many of which are used throughout these notes. Complexity emergent from dynamical systems containing many variables, the central theme of this textbook, is ultimately based on the concepts of classical dynamical systems theory, treated in this chapter, which deals with differential equations involving a handful of variables.

3. *Random Boolean Networks*
    A prime model for complex systems with an infinite number of variables are random graphs with boolean variables. It allows for the characterization of typical dynamical behaviors, e.g. "frozen" vs. "chaotic", which are of relevance in many contexts. Of especial importance are random boolean networks for the fundamentals in the realm of life, leading to the notion of "life at the edge of chaos".

4. *Cellular Automata and Self-Organized Criticality*
    Regular dynamical systems on lattices, the cellular automata, allow detailed studies of the dynamics of complex systems, a key issue being the organizational principle necessary for a dynamical system to show the emergent phenomenon of "self-organized criticality".

5. *Statistical Modeling of Darwinian Evolution*
   Evolution of living organisms is, without a doubt, the paradigm for an adaptive and complex dynamical system, that of interacting species. Key concepts such as the "error catastrophe" and "hypercycles" for the prebiotic evolution are discussed within the standard statistical approach.
6. *Synchronization Phenomena*
   When many distinct computational units interact, which is a typical situation in complex systems, they might evolve synchronously, in phase, or rather independently. Synchronization is an issue of wide ranging importance, from the outbreak of epidemics to the definition of objects in cortical circuits.
7. *Elements of Cognitive Systems Theory*
   The most complex of any known dynamical systems, and probably also the least understood of all, is the brain. It constitutes the biological support for the human cognitive system, supposedly the most evolved cognitive system known to date. Basic principles and important concepts of cognitive systems theory are developed in this chapter.

The basic material and mathematical notions for the course are developed in the first two chapters. The scientific investigations of complex systems are just beginning and the subjects chosen in Chaps. 3–7 are of exemplary importance for this rapidly developing field.

Exercises and Suggestions for Individual Studies Towards the end of each individual chapter a selection of exercises is presented. Some of them deal with simple extensions of the material, such as a proof of a specific formula or the application of a method discussed in the main text to a different or related problem. Other exercises are of the form of small work studies, such as the numerical implementation via a C++ or Maple code of a basic model, with the objective to obtain a hands-on experience with an interesting phenomenon from the investigation of the results obtained from the simulation runs.

This interdisciplinary field is very suitable for making an inroad with a basic research project. The suggestions for work studies presented in the respective exercise sections therefore also serve as guides and motivations for a first step towards scientific research in this field, which in the end may possibly lead to research goals developed by the individual reader. It is a highly satisfying experience and is truly recommended.

References and Literature The section "Further Reading" at the end of each individual chapter contains references to standard introductory textbooks and review articles, and to some articles for further in-depth studies dealing with selected issues treated within the respective chapter. Certain original research literature containing some of the first investigations of phenomena discussed in the respective chapter is also selectively listed whenever of scientific or historical interest.

Complexity and Our Future Human society constitutes an adaptive network with "intelligent vertices", us as individuals. On a larger scale, intricate interrelations between industrial companies, political parties and pressure groups, non-governmental

organizations (NGOs) of the civil society and many other constituent components defy any encompassing analysis. The complex dynamical system denoted human society will remain beyond our predictive capacities for many years to come.[1]

Nevertheless complexity theory represents a fundamental tool for long-term modeling and scenario building. A good understanding of possible emergent behaviors, of chaotic vs. regular evolution processes and of stability analysis is clearly very helpful when trying to study and model the long-term consequences of human actions today. The theory of complex and adaptive dynamical systems is a basic tool for genuine futurology.

The Future of Life and of Our Civilization On a personal note the author believes, in this context, that the long-term perspective is of central importance as a guideline for global human actions today, in view of our capability to change the very face of the earth. We are living at a point in history where we, the constituents of human society, are not capable of directly controlling the global and dynamical developments of this very society, an example of what one denotes an emergent behavior – the sum is more than its parts.

We are nevertheless the central actors within human society and the long-term developments and trends are determined by the underlying principles, by the long-term guidelines to our actions and planning. A stronger focus on long-term perspectives and developments, for all the positive outlook it may provide, for the perils to our civilization and to life on earth it might reveal, is of central importance, in the view of the author, at this point in history. The reader thinking along similar lines is invited to visit the organization Future 25 [2], which is dedicated to the "future of life and humanity on earth, the planets and in the universe".

---

[1] It is unlikely that we will ever develop a deep enough understanding of our society, to say on the level of the "psychohistory" of Isaac Asimov's Foundation trilogy, that we may truly predict long-term global developments.

[2] http://www.future25.org.

Chapter 1
Graph Theory and Small-World Networks

Dynamical networks constitute a very wide class of complex and adaptive systems. Examples range from ecological prey–predator networks to the gene expression and protein networks constituting the basis of all living creatures as we know it. The brain is probably the most complex of all adaptive dynamical systems and is at the basis of our own identity, in the form of a sophisticated neural network. On a social level we interact through social networks, to give a further example – networks are ubiquitous through the domain of all living creatures.

A good understanding of network theory is therefore of basic importance for complex system theory. In this chapter we will discuss the most important concepts of graph[1] theory and basic realizations of possible network organizations.

1.1 Random Graphs

1.1.1 The Small-World Effect

Six or more billion humans live on earth today and it might seem that the world is a big place. But, as an Italian proverb says,

"Tutto il mondo é paese"   –   "The world is a village".

The network of who knows whom – the network of acquaintances – is indeed quite densely webbed. Modern scientific investigations mirror this century-old proverb.

Social Networks Stanley Milgram performed a by now famous experiment in the 1960s. He distributed a number of letters addressed to a stockbroker in Boston to a random selection of people in Nebraska. The task was to send these letters to the addressee (the stockbroker) via mail to an acquaintance of the respective sender. In other words, the letters were to be sent via a social network.

---

[1] Mathematicians generally prefer the term "graph" instead of "network".
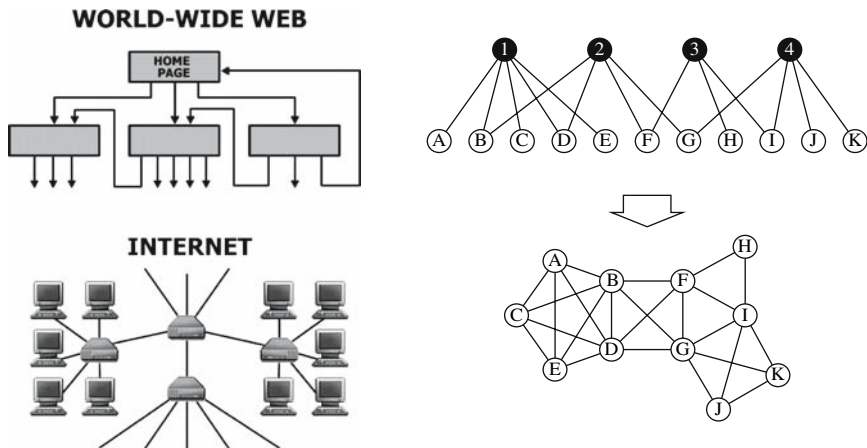
Fig. 1.1 *Left*: Illustration of the network structure of the world-wide web and of the Internet (from Albert and Barabási, 2002). *Right*: Construction of a graph (*bottom*) from an underlying bipartite graph (*top*). The filled circles correspond to movies and the open circles to actors cast in the respective movies (from Newman, Strogatz and Watts, 2001)

The initial recipients of the letters clearly did not know the Boston stockbroker on a first-name basis. Their best strategy was to send their letter to someone whom they felt was closer to the stockbroker, socially or geographically: perhaps someone they knew in the financial industry, or a friend in Massachusetts.

Six Degrees of Separation About 20% of Milgram's letters did eventually reach their destination. Milgram found that it had only taken an average of six steps for a letter to get from Nebraska to Boston. This result is by now dubbed "six degrees of separation" and it is possible to connect any two persons living on earth via the social network in a similar number of steps.

> *The Small-World Effect. The "small-world effect" denotes the result that the average distance linking two nodes belonging to the same network can be orders of magnitude smaller than the number of nodes making up the network.*

The small world effect occurs in all kinds of networks. Milgram originally examined the networks of friends. Other examples for social nets are the network of film actors or that of baseball players, see Fig. 1.1. Two actors are linked by an edge in this network whenever they co-starred at least once in the same movie. In the case of baseball players the linkage is given by the condition to have played at least once on the same team.

Networks are Everywhere Social networks are but just one important example of a communication network. Most human communication takes place directly among individuals. The spreading of news, rumors, jokes and of diseases takes place by contact between individuals. And we are all aware that rumors and epidemic infections can spread very fast in densely webbed social networks.
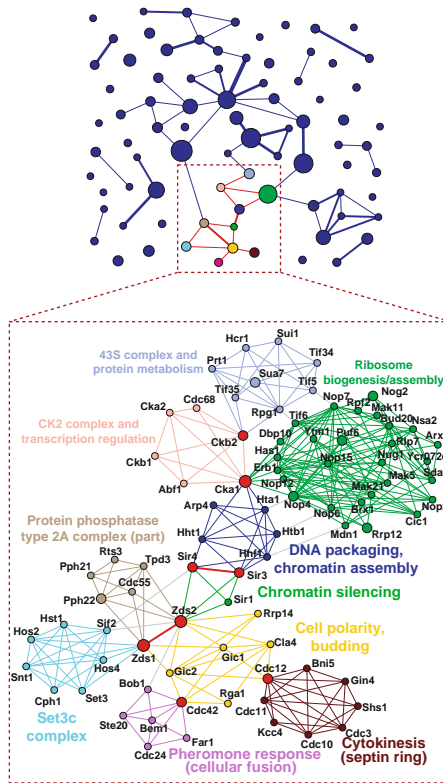
Fig. 1.2 A protein interaction network, showing a complex interplay between highly connected hubs and communities of subgraphs with increased densities of edges (from Palla et al., 2005)

Communication networks are ubiquitous. Well known examples are the Internet and the world-wide web, see Fig. 1.1. Inside a cell the many constituent proteins form an interacting network, as illustrated in Fig. 1.2. The same is of course true for artificial neural networks as well as for the networks of neurons that build up the brain. It is therefore important to understand the statistical properties of the most important network classes.

1.1.2 Basic Graph-Theoretical Concepts

The simplest type of network is the random graph. It is characterized by only two numbers: By the number of vertices N and by the average degree z, also called the coordination number.

Coordination Number. The coordination number z is the average number of links per vertex, i.e. there are a total of $Nz/2$ connections in the network.

Alternatively we can define the probability p to find a given link.
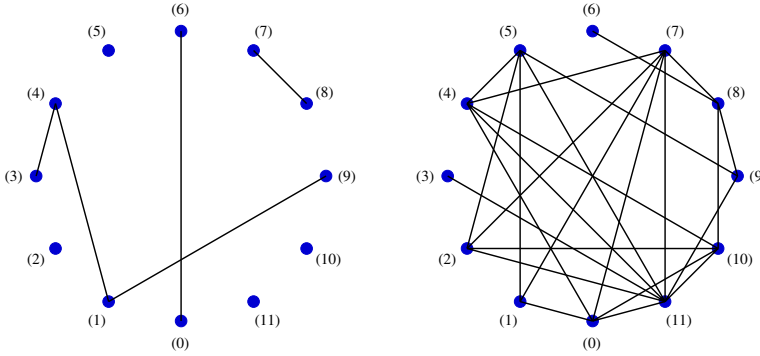
Fig. 1.3 Random graphs with $N = 12$ vertices and different connection probabilities $p = 0.0758$ (*left*) and $p = 0.3788$ (*right*). The three mutually connected vertices (0,1,7) contribute to the clustering coefficient and the fully interconnected set of sites (0,4,10,11) is a clique in the network on the right

> *Connection Probability.* *The probability that a given edge occurs is called the connection probability p.*

Erdös–Rényi Random Graphs We can construct a specific type of random graph simply by taking N nodes, also called vertices and by drawing $Nz/2$ lines, the edges, between randomly chosen pairs of nodes, compare Fig. 1.3. This type of random graph is called an Erdös–Rényi random graph after two mathematicians who studied this type of graph extensively. In Sect. 1.2 we will introduce and study other types of random graphs.

Most of the following discussion will be valid for all types of random graphs, we will explicitly state whenever we specialize to Erdös–Rényi graphs.

The Thermodynamic Limit In random graphs the relation between z and p is given simply by

$$p = \frac{Nz}{2} \frac{2}{N(N-1)} = \frac{z}{N-1} \ . \tag{1.1}$$

> *The Thermodynamic Limit.* *The limit where the number of elements making up a system diverges to infinity is called the "thermodynamic limit" in physics. A quantity is* extensive *if it is proportional to the number of constituting elements, and* intensive *if it scales to a constant in the thermodynamic limit.*

We note that $p = p(N) \to 0$ in the thermodynamic limit $N \to \infty$ for intensive $z \sim O(N^0)$, compare Eq. (1.1).

Network Diameter and the Small-World Effect As a first parameter characterizing a network we discuss the diameter of a network.

> *Network Diameter.* *The network diameter is the maximum degree of separation between all pairs of vertices.*

For a random network with N vertices and coordination number z we have

$$z^D \approx N, \qquad D \propto \log N / \log z , \qquad (1.2)$$

since any node has z neighbors, z^2 next-nearest neighbors and so on. The logarithmic increase in the number of degrees of separation with the size of the network is characteristic of small-world networks. $\log N$ increases very slowly with N and the network diameter therefore remains small even for networks containing a large number of nodes N.

> *Average Distance. The average distance ℓ is the average of the minimal path length between all pairs of nodes of a network.*

The average distance ℓ is generally closely related to the diameter D; it has the same scaling as the number of nodes N.

The Hyperlink Network Every web page contains links to other web pages, thus forming a network of hyperlinks. In 1999 there were about $N \simeq 0.8 \times 10^9$ documents on the web, but the average distance between documents was only about 19. The WWW is growing rapidly; in 2007 estimates for the total number of web pages resulted in $N \simeq (20 - 30) \times 10^9$, with the size of the Internet backbone, viz the number of Internet servers, being about $\simeq 0.1 \times 10^9$.

Clustering in Networks Real networks have strong local recurrent connections, compare, e.g. the protein network illustrated in Fig. 1.2, leading to distinct topological elements, such as loops and clusters.

> *The Clustering Coefficient. The clustering coefficient C is the average fraction of pairs of neighbors of a node that are also neighbors of each other.*

The clustering coefficient is a normalized measure of loops of length 3. In a fully connected network, in which everyone knows everyone else, $C = 1$.

In a random graph a typical site has $z(z-1)/2$ pairs of neighbors. The probability of an edge to be present between a given pair of neighbors is $p = z/(N-1)$, see Eq. (1.1). The clustering coefficient, which is just the probability of a pair of neighbors to be interconnected is therefore

Table 1.1 The number of nodes N, average degree of separation ℓ, and clustering coefficient C, for three real-world networks. The last column is the value which C would take in a random graph with the same size and coordination number, $C_{\text{rand}} = z/N$ (from Watts and Strogatz, 1998)

Network	N	ℓ	C	C_{rand}
Movie actors	225 226	3.65	0.79	0.00027
Neural network	282	2.65	0.28	0.05
Power grid	4941	18.7	0.08	0.0005
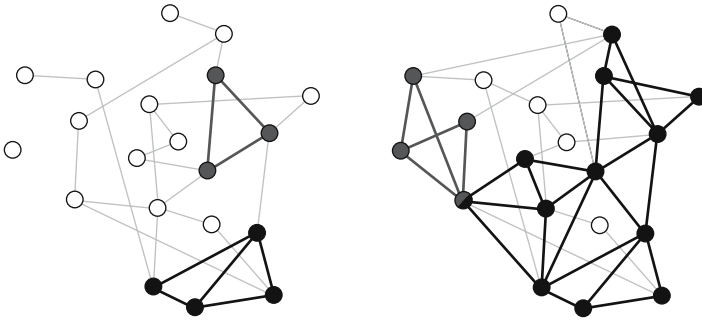
Fig. 1.4 *Left*: Highlighted are three three-site cliques. *Right*: A percolating network of three-site cliques (from Derenyi, Palla and Vicsek, 2005)

$$C_{\text{rand}} \;=\; \frac{z}{N-1} \;\approx\; \frac{z}{N} \;. \tag{1.3}$$

It is very small for large random networks and scales to zero in the thermodynamic limit. In Table 1.1 the respective clustering coefficients for some real-world networks and for the corresponding random networks are listed for comparison.

Cliques and Communities The clustering coefficient measures the normalized number of triples of fully interconnected vertices. In general, any fully connected subgraph is denoted a clique.

> *Cliques. A clique is a set of vertices for which (a) every node is connected by an edge to every other member of the clique and (b) no node outside the clique is connected to all members of the clique.*

The term "clique" comes from social networks. A clique is a group of friends where everybody knows everybody else. The number of cliques of size K in an Erdös–Rényi graph with N vertices and linking probability p is

$$\binom{N}{K} p^{K(K-1)/2} \left(1 - p^K\right)^{N-K} \;.$$

The only cliques occurring in random graphs in the thermodynamic limit have the size 2, since $p = z/N$. For an illustration see Fig. 1.4.

Another term used is *community*. It is mathematically not as strictly defined as "clique", it roughly denotes a collection of strongly overlapping cliques, viz of subgraphs with above-the-average densities of edges.

Clustering for Real-World Networks Most real-world networks have a substantial clustering coefficient, which is much greater than $O(N^{-1})$. It is immediately evident from an inspection, for example of the protein network presented in Fig. 1.2, that the underlying "community structure" gives rise to a high clustering coefficient.

In Table 1.1, we give some values of C, together with the average distance ℓ, for three different networks:

– the network of collaborations between movie actors
– the neural network of the worm *C. Elegans*, and
– the Western Power Grid of the United States.

Also given in Table 1.1 are the values C_{rand} that the clustering coefficient would have for random graphs of the same size and coordination number. Note that the real-world value is systematically higher than that of random graphs. Clustering is important for real-world graphs. These are small-world graphs, as indicated by the small values for the average distances ℓ given in Table 1.1.

Erdös–Rényi random graphs obviously do not match the properties of real-world networks well. In Sect. 1.4 we will discuss generalizations of random graphs that approximate the properties of real-world graphs much better. Before that, we will discuss some general properties of random graphs in more detail.

Bipartite Networks Many real-world graphs have an underlying bipartite structure, see Fig. 1.1.

> *Bipartite Graphs.   A bipartite graph has two kinds of vertices with links only between vertices of unlike kinds.*

Examples are networks of managers, where one kind of vertex is a company and the other kind of vertex the managers belonging to the board of directors. When eliminating one kind of vertex, in this case it is customary to eliminate the companies, one retains a social network; the network of directors, as illustrated in Fig. 1.1. This network has a high clustering coefficient, as all boards of directors are mapped onto cliques of the respective social network.

1.1.3 Properties of Random Graphs

So far we have considered averaged quantities of random graphs, like the average coordination number or degree z.

> *Degree of a Vertex.   The degree k of the vertex is the number of edges linking it to this node.*

The distribution of the degree characterizes general random and non-random graphs.

> *Degree Distribution.   If X_k is the number of vertices having the degree k, then $p_k = X_k/N$ is called the degree distribution, where N is the total number of nodes.*

Degree Distribution for Erdös–Rényi Graphs The probability of any node to have k edges is

$$p_k = \binom{N-1}{k} p^k (1-p)^{N-1-k} , \qquad (1.4)$$

for an Erdös–Rényi network, where p is the link connection probability. For large $N \gg k$ we can approximate the degree distribution p_k by

$$p_k \simeq e^{-pN} \frac{(pN)^k}{k!} = e^{-z} \frac{z^k}{k!}, \tag{1.5}$$

where z is the average coordination number, compare Eq. (1.1). We have used

$$\lim_{N \to \infty} \left(1 - \frac{x}{N}\right)^N = e^{-x}, \qquad \binom{N-1}{k} = \frac{(N-1)!}{k!(N-1-k)!} \simeq \frac{(N-1)^k}{k!},$$

and $(N-1)^k p^k = z^k$, see Eq. (1.1). Equation (1.5) is a Poisson distribution with the mean

$$\langle k \rangle = \sum_{k=0}^{\infty} k e^{-z} \frac{z^k}{k!} = z e^{-z} \sum_{k=1}^{\infty} \frac{z^{k-1}}{(k-1)!} = z,$$

as expected.

Ensemble Fluctuations In general, two specific realizations of random graphs differ. Their properties coincide on the average, but not on the level of individual links. With "ensemble" one denotes the set of possible realizations.

In an ensemble of random graphs with fixed p and N the degree distribution X_k/N will be slightly different from one realization to the next. On the average it will be given by

$$\frac{1}{N} \langle X_k \rangle = p_k. \tag{1.6}$$

Here $\langle \ldots \rangle$ denotes the ensemble average. One can go one step further and calculate the probability $P(X_k = R)$ that in a realization of a random graph the number of vertices with degree k equals R. It is given in the large-N limit by

$$P(X_k = R) = e^{-\lambda_k} \frac{(\lambda_k)^R}{R!}, \qquad \lambda_k = \langle X_k \rangle. \tag{1.7}$$

Note the similarity to Eq. (1.5) and that the mean $\lambda_k = \langle X_k \rangle$ is in general extensive while the mean z of the degree distribution (1.5) is intensive.

Scale-Free Graphs Scale-free graphs are defined by a power-law degree distribution

$$p_k \sim \frac{1}{k^{\alpha}}, \qquad \alpha > 1. \tag{1.8}$$

Typically, for real-world graphs, this scaling $\sim k^{-\alpha}$ holds only for large degrees k. For theoretical studies we will mostly assume, for simplicity, that the functional dependence Eq. (1.8) holds for all k. The power-law distribution can be normalized if

$$\lim_{K \to \infty} \sum_{k=0}^{K} p_k \approx \lim_{K \to \infty} \int_{k=0}^{K} p_k \propto \lim_{K \to \infty} K^{1-\alpha} < \infty,$$

i.e. when $\alpha > 1$. The average degree is finite if

$$\lim_{K\to\infty} \sum_{k=0}^{K} k\, p_k \;\propto\; \lim_{K\to\infty} K^{-\alpha+2} \;<\; \infty\,, \qquad \alpha > 2\,.$$

A power-law functional relation is called scale-free, since any rescaling $k \to ak$ can be reabsorbed into the normalization constant.

Scale-free functional dependencies are also called *critical*, since they occur generally at the critical point of a phase transition. We will come back to this issue recurrently in the following chapters.

Graph Spectra   Any graph G with N nodes can be represented by a matrix encoding the topology of the network, the adjacency matrix.

The Adjacency Matrix.   The $N \times N$ adjacency matrix $\hat{A}$ has elements $A_{ij} = 1$ if nodes i and j are connected and $A_{ij} = 0$ if they are not connected.

The adjacency matrix is symmetric and consequently has N real eigenvalues.

The Spectrum of a Graph.   The spectrum of a graph G is given by the set of eigenvalues λ_i of the adjacency matrix $\hat{A}$.

A graph with N nodes has N eigenvalues λ_i and it is useful to define the corresponding "spectral density"

$$\rho(\lambda) \;=\; \frac{1}{N} \sum_j \delta(\lambda - \lambda_j), \qquad \int d\lambda\, \rho(\lambda) = 1\,, \tag{1.9}$$

where $\delta(\lambda)$ is the Dirac delta function.

Green's Function[2]   The spectral density $\rho(\lambda)$ can be evaluated once the Green's function $G(\lambda)$,

$$G(\lambda) \;=\; \frac{1}{N} Tr\left[\frac{1}{\lambda - \hat{A}}\right] \;=\; \frac{1}{N} \sum_j \frac{1}{\lambda - \lambda_j}\,, \tag{1.10}$$

is known. Here $Tr[\ldots]$ denotes the trace over the matrix $(\lambda - \hat{A})^{-1} \equiv (\lambda\,\hat{I} - \hat{A})^{-1}$, where $\hat{I}$ is the identity matrix. Using the formula

$$\lim_{\varepsilon\to 0} \frac{1}{\lambda - \lambda_j + i\epsilon} \;=\; P\frac{1}{\lambda - \lambda_j} - i\pi\delta(\lambda - \lambda_j)\,,$$

where P denotes the principal part[3], we find the relation

---

[2] The reader without prior experience with Green's functions may skip the following derivation and pass directly to the result, namely to Eq. (1.13).

[3] Taking the principal part signifies that one has to consider the positive and the negative contributions to the $1/\lambda$ divergences carefully.

$$\rho(\lambda) = -\frac{1}{\pi} \lim_{\varepsilon \to 0} Im G(\lambda + i\varepsilon) \,. \tag{1.11}$$

The Semi-Circle Law The graph spectra can be evaluated for random matrices for the case of small link densities $p = z/N$, where z is the average connectivity. Starting from a random site we can connect on the average to z neighboring sites and from there on to $z - 1$ next-nearest neighboring sites, and so on:

$$G(\lambda) = \cfrac{1}{\lambda - \cfrac{z}{\lambda - \cfrac{z-1}{\lambda - \cfrac{z-1}{\lambda - \dots}}}} \approx \frac{1}{\lambda - z G(\lambda)} \,, \tag{1.12}$$

where we have approximated $z - 1 \approx z$ in the last step. Equation (1.12) is also called the "self-retracting path approximation" and can be derived by evoking a mapping to Green's function of a particle moving along the vertices of the graph. It constitutes a self-consistency equation for $G = G(\lambda)$, with the solution

$$G^2 - \frac{\lambda}{z} G + \frac{1}{z} = 0, \qquad G = \frac{\lambda}{2z} - \sqrt{\frac{\lambda^2}{4z^2} - \frac{1}{z}} \,,$$

since $\lim_{\lambda \to \infty} G(\lambda) = 0$. The spectral density Eq. (1.11) then takes the form

$$\rho(\lambda) = \begin{cases} \sqrt{4z - \lambda^2}/(2\pi z) & \text{if } \lambda^2 < 4z \\ 0 & \text{if } \lambda^2 > 4z \end{cases} \tag{1.13}$$

of a half-ellipse also known as "Wigner's law", or the "semi-circle law".

Loops and the Clustering Coefficient The total number of triangles, viz the overall number of loops of length 3 in a network is $C(N/3)(z - 1)z/2$, where C is the clustering coefficient. This number is related to the adjacency matrix via

$$C\frac{N}{3}\frac{z(z-1)}{2} = \text{number of triangles} = \frac{1}{6} \sum_{i_1, i_2, i_3} A_{i_1 i_2} A_{i_2 i_3} A_{i_3 i_1} \,,$$

since three sites i_1, i_2 and i_3 are interconnected only when the respective entries of the adjacency matrix are unity. The sum of the right-hand side of above relation is also denoted a "moment" of the graph spectrum. The factors $1/3$ and $1/6$ on the left-hand side and on the right-hand side account for overcountings.

Moments of the Spectral Density The graph spectrum is directly related to certain topological features of a graph via its moments. The lth moment of $\rho(\lambda)$ is given by

$$\int d\lambda \, \lambda^l \rho(\lambda) = \frac{1}{N} \sum_{j=1}^{N} (\lambda_j)^l$$

$$= \frac{1}{N} \text{Tr}\left[A^l\right] = \frac{1}{N} \sum_{i_1, i_2, \dots, i_l} A_{i_1 i_2} A_{i_2 i_3} \cdots A_{i_l i_1} \,, \tag{1.14}$$

Step A   Step B
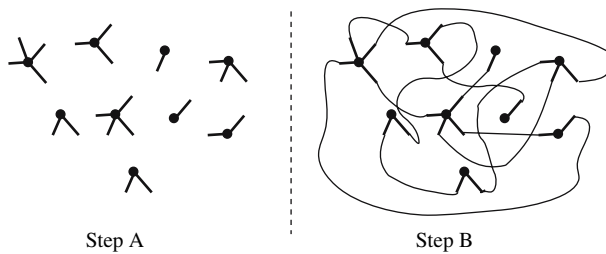
Fig. 1.5 Construction procedure of a random network with nine vertices and degrees $X_1 = 2$, $X_2 = 3$, $X_3 = 2$, $X_4 = 2$. In step A the vertices with the desired number of stubs (degrees) are constructed. In step B the stubs are connected randomly

as one can see from Eq. (1.9). The lth moment of $\rho(\lambda)$ is therefore equivalent to the number of closed paths of length l, the number of all paths of length l returning to the starting point.

1.2 Generalized Random Graphs

1.2.1 Graphs with Arbitrary Degree Distributions

In order to generate random graphs that have non-Poisson degree distributions we may choose a specific set of degrees.

The Degree Sequence. A degree sequence is a specified set $\{k_i\}$ of the degrees for the vertices $i = 1 \ldots N$.

Construction of Networks with Arbitrary Degree Distribution The degree sequence can be chosen in such a way that the fraction of vertices having degree k will tend to the desired degree distribution

$$p_k, \qquad N \to \infty$$

in the thermodynamic limit. The network can then be constructed in the following way:

1. Assign k_i "stubs" (ends of edges emerging from a vertex) to every vertex $i = 1, \ldots, N$.
2. Iteratively choose pairs of stubs at random and join them together to make complete edges.

When all stubs have been used up, the resulting graph is a random member of the ensemble of graphs with the desired degree sequence. Figure 1.5 illustrates the construction procedure.

The Average Degree and Clustering The mean number of neighbors is the coordination number

$$z = \langle k \rangle = \sum_k k\, p_k \ .$$

The probability that one of the second neighbors of a given vertex is also a first neighbor, scales as N^{-1} for random graphs, regardless of the degree distribution, and hence can be ignored in the limit $N \to \infty$.

Degree Distribution of Neighbors Consider a given vertex A and a vertex B that is a neighbor of A, i.e. A and B are linked by an edge.

We are now interested in the degree distribution for vertex B, viz in the degree distribution of a neighbor vertex of A, where A is an arbitrary vertex of the random network with degree distribution p_k. As a first step we consider the average degree of a neighbor node.

A high-degree vertex has more edges connected to it. There is then a higher chance that any given edge on the graph will be connected to it, with this chance being directly proportional to the degree of the vertex. Thus the probability distribution of the degree of the vertex to which an edge leads is proportional to $k p_k$ and not just to p_k.

Distribution of the Outgoing Edges of a Neighbor Vertex When we are interested in determining the size of loops or the size of connected components in a random graph, we are normally interested not in the complete degree of the vertex reached by following an edge from A, but in the number of edges emerging from such a vertex that do not lead back to A, because the latter contains all information about the number of second neighbors of A.

The number of new edges emerging from B is just the degree of B minus one and its correctly normalized distribution is therefore

$$q_{k-1} = \frac{k\, p_k}{\sum_j j p_j}, \qquad q_k = \frac{(k+1)p_{k+1}}{\sum_j j p_j} \ , \tag{1.15}$$

since $k p_k$ is the degree distribution of a neighbor. The average number of outgoing edges of a neighbor vertex is then

$$\sum_{k=0}^{\infty} k q_k = \frac{\sum_{k=0}^{\infty} k(k+1)p_{k+1}}{\sum_j j p_j} = \frac{\sum_{k=1}^{\infty} (k-1)k p_k}{\sum_j j p_j}$$

$$= \frac{\langle k^2 \rangle - \langle k \rangle}{\langle k \rangle} \ . \tag{1.16}$$

Number of Next-Nearest Neighbors We denote with

$$z_m, \qquad z_1 = \langle k \rangle \equiv z$$

the average number of m-nearest neighbors. Equation (1.16) gives the average number of vertices two steps away from the starting vertex A via a particular neighbor

vertex. Multiplying this by the mean degree of A, namely $z_1 \equiv z$, we find that the mean number of second neighbors z_2 of a vertex is

$$z_2 = \langle k^2 \rangle - \langle k \rangle . \tag{1.17}$$

z_2 for the Erdös–Rényi graph The degree distribution of an Erdös–Rényi graph is the Poisson distribution, $p_k = e^{-z} z^k / k!$, see Eq. (1.5). We obtain for the average degree of a neighbor vertex, Eq. (1.17),

$$z_2 = \sum_{k=0}^{\infty} k^2 e^{-z} \frac{z^k}{k!} - z = z e^{-z} \sum_{k=1}^{\infty} (k-1+1) \frac{z^{k-1}}{(k-1)!} - z$$
$$= z^2 = \langle k \rangle^2 .$$

The mean number of second neighbors of a vertex in an Erdös–Rényi random graph is just the square of the mean number of first neighbors. This is a special case however. For most degree distributions, Eq. (1.17) will be dominated by the term $\langle k^2 \rangle$, so the number of second neighbors is roughly the mean square degree, rather than the square of the mean. For broad distributions these two quantities can be very different.

Number of Far Away Neighbors The average number of edges emerging from a second neighbor, and not leading back to where we came from, is also given by Eq. 1.16, and indeed this is true at any distance m away from vertex A. The average number of neighbors at a distance m is then

$$z_m = \frac{\langle k^2 \rangle - \langle k \rangle}{\langle k \rangle} z_{m-1} = \frac{z_2}{z_1} z_{m-1} , \tag{1.18}$$

where $z_1 \equiv z = \langle k \rangle$ and z_2 are given by Eq. (1.17). Iterating this relation we find

$$z_m = \left[\frac{z_2}{z_1} \right]^{m-1} z_1 . \tag{1.19}$$

The Giant Connected Cluster Depending on whether z_2 is greater than z_1 or not, Eq. (1.19) will either diverge or converge exponentially as m becomes large:

$$\lim_{m \to \infty} z_m = \begin{cases} \infty & \text{if } z_2 > z_1 \\ 0 & \text{if } z_2 < z_1 \end{cases} , \tag{1.20}$$

$z_1 = z_2$ is the percolation point. In the second case the total number of neighbors

$$\sum_m z_m = z_1 \sum_{m=1}^{\infty} \left[\frac{z_2}{z_1} \right]^{m-1} = \frac{z_1}{1 - z_2/z_1} = \frac{z_1^2}{z_1 - z_2}$$

is finite even in the thermodynamic limit, in the first case it is infinite. The network decays, for $N \to \infty$, into non-connected components when the total number of neighbors is finite.

The Giant Connected Component.   When the largest cluster of a graph encompasses a finite fraction of all vertices, in the thermodynamic limit, it is said to form a giant connected component (GCC).

If the total number of neighbors is infinite, then there must be a giant connected component. When the total number of neighbors is finite, there can be no GCC.

The Percolation Threshold   When a system has two or more possibly macroscopically different states, one speaks of a phase transition.

Percolation Transition.   When the structure of an evolving graph goes from a state in which two (far away) sites are on the average connected/not connected one speaks of a percolation transition.

This phase transition occurs precisely at the point where $z_2 = z_1$. Making use of Eq. (1.17), $z_2 = \langle k^2 \rangle - \langle k \rangle$, we find that this condition is equivalent to

$$\langle k^2 \rangle - 2\langle k \rangle \; = \; 0, \qquad \sum_{k=0}^{\infty} k(k-2)p_k \; = \; 0 \,. \qquad (1.21)$$

We note that, because of the factor $k(k-2)$, vertices of degree zero and degree two do not contribute to the sum. The number of vertices with degree zero or two therefore affects neither the phase transition nor the existence of the giant component.

– Vertices of degree zero are not connected to any other node, they do not contribute to the network topology.
– Vertices of degree two act as intermediators between two other nodes. Removing vertices of degree two does not change the topological structure of a graph.

One can therefore remove (or add) vertices of degree two or zero without affecting the existence of the giant component.

Clique Percolation   Edges correspond to cliques with $Z = 2$ sites (see page 6). The percolation transition can then also be interpreted as a percolation of 2-site cliques. It is then clear that the concept of percolation can be generalized to that of percolation of cliques with Z sites, see Fig. 1.4 for an illustration.

The Average Vertex–Vertex Distance   Below the percolation threshold the average vertex–vertex distance ℓ is finite and the graph decomposes into an infinite number of disconnected subclusters.

Disconnected Subclusters.   A disconnected subcluster or subgraph constitutes a subset of vertices for which (a) there is at least one path in between all pairs of nodes making up the subcluster and (b) there is no path between a member of the subcluster and any out-of-subcluster vertex.

Well above the percolation transition, ℓ is given approximately by the condition $z_\ell \simeq N$:

$$\log(N/z_1) \;=\; (\ell-1)\log(z_2/z_1), \qquad \ell \;=\; \frac{\log(N/z_1)}{\log(z_2/z_1)} + 1 \,, \qquad (1.22)$$

using Eq. (1.19). For the special case of the Erdös–Rényi random graph, for which $z_1 = z$ and $z_2 = z^2$, this expression reduces to the standard formula (1.2),

$$\ell \;=\; \frac{\log N - \log z}{\log z} + 1 \;=\; \frac{\log N}{\log z}\,.$$

The Clustering Coefficient of Generalized Random Graphs The clustering coefficient C denotes the probability that two neighbors i and j of a particular vertex A have stubs that do interconnect. The probability that two given stubs are connected is $1/(zN-1) \approx 1/zN$, since zN is the total number of stubs. We then have, compare Eq. (1.16),

$$C = \frac{\langle k_i k_j\rangle}{Nz} = \frac{\langle k_i\rangle\langle k_j\rangle}{Nz} = \frac{1}{Nz}\left[\sum_k k q_k\right]^2$$

$$= \frac{1}{Nz}\left[\frac{\langle k^2\rangle - \langle k\rangle}{\langle k\rangle}\right]^2 = \frac{z}{N}\left[\frac{\langle k^2\rangle - \langle k\rangle}{\langle k\rangle^2}\right]^2 \,, \qquad (1.23)$$

since the distributions of two neighbors i and j are statistically independent.

The clustering coefficient vanishes in the thermodynamic limit $N \to \infty$, as expected. However, it may have a very big leading coefficient, especially for degree distributions with fat tails. The differences listed in Table 1.1, between the measured clustering coefficient C and the value $C_{\mathrm{rand}} = z/N$ for Erdös–Rényi graphs, are partly due to the fat tails in the degree distributions p_k of the corresponding networks.

1.2.2 Probability Generating Function Formalism

Network theory is about the statistical properties of graphs. A very powerful method from probability theory is the generating function formalism, which we will discuss now and apply later on.

Probability Generating Functions We define by

$$G_0(x) \;=\; \sum_{k=0}^{\infty} p_k x^k \qquad (1.24)$$

the *generating function* $G_0(x)$ for the probability distribution p_k. The generating function $G_0(x)$ contains all information present in p_k. We can recover p_k from $G_0(x)$ simply by differentiation:

$$p_k \;=\; \frac{1}{k!}\left.\frac{\mathrm{d}^k G_0}{\mathrm{d}x^k}\right|_{x=0}. \qquad (1.25)$$

One says that the function G_0 "generates" the probability distribution p_k.

The Generating Function for Degree Distribution of Neighbors We can also define a generating function for the distribution q_k, Eq. (1.15), of the other edges leaving a vertex that we reach by following an edge in the graph:

$$G_1(x) = \sum_{k=0}^{\infty} q_k x^k = \frac{\sum_{k=0}^{\infty}(k+1)p_{k+1}x^k}{\sum_j j p_j} = \frac{\sum_{k=0}^{\infty} k p_k x^{k-1}}{\sum_j j p_j}$$

$$= \frac{G_0'(x)}{z} \,, \tag{1.26}$$

where $G_0'(x)$ denotes the first derivative of $G_0(x)$ with respect to its argument.

Properties of Generating Functions Probability generating functions have a couple of important properties:

1. Normalization: The distribution p_k is normalized and hence

$$G_0(1) = \sum_k p_k = 1 \,. \tag{1.27}$$

2. Mean: A simple differentiation

$$G_0'(1) = \sum_k k p_k = \langle k \rangle \tag{1.28}$$

   yields the average degree $\langle k \rangle$.
3. Moments: The nth moment $\langle k^n \rangle$ of the distribution p_k is given by

$$\langle k^n \rangle = \sum_k k^n p_k = \left[\left(x\frac{\mathrm{d}}{\mathrm{d}x}\right)^n G_0(x)\right]_{x=1} \,. \tag{1.29}$$

The Generating Function for Independent Random Variables Let us assume that we have two random variables. As an example we consider two dice. Throwing the two dice are two independent random events. The joint probability to obtain $k = 1,\ldots,6$ with the first die and $l = 1,\ldots,6$ with the second dice is $p_k p_l$. This probability function is generated by

$$\sum_{k,l} p_k p_l x^{k+l} = \left(\sum_k p_k x^k\right)\left(\sum_l p_l x^l\right) \,,$$

i.e. by the product of the individual generating functions. This is the reason why generating functions are so useful in describing combinations of independent random events.

As an application consider n randomly chosen vertices. The sum $\sum_i k_i$ of the respective degrees has a cumulative degree distribution, which is generated by

$$\left[G_0(x)\right]^n \,.$$

The Generating Function of the Poisson Distribution As an example we consider the Poisson distribution, Eq. (1.5). Using Eq. (1.24) we obtain

$$G_0(x) = e^{-z} \sum_{k=0}^{\infty} \frac{z^k}{k!} x^k = e^{z(x-1)} . \tag{1.30}$$

This is the generating function for the Poisson distribution. The generating function $G_1(x)$ for the outgoing edges of a neighbor is, see Eq. (1.26),

$$G_1(x) = \frac{G_0'(x)}{z} = e^{z(x-1)} . \tag{1.31}$$

Thus, for the case of the Poisson distribution we have, as expected, $G_1(x) = G_0(x)$.

Further Examples of Generating Functions As a second example, consider a graph with an exponential degree distribution:

$$p_k = (1 - e^{-1/\kappa}) e^{-k/\kappa}, \qquad \sum_{k=0}^{\infty} p_k = \frac{1 - e^{-1/\kappa}}{1 - e^{-1/\kappa}} = 1 , \tag{1.32}$$

where κ is a constant. The generating function for this distribution is

$$G_0(x) = (1 - e^{-1/\kappa}) \sum_{k=0}^{\infty} e^{-k/\kappa} x^k = \frac{1 - e^{-1/\kappa}}{1 - x e^{-1/\kappa}} , \tag{1.33}$$

and

$$z = G_0'(1) = \frac{e^{-1/\kappa}}{1 - e^{-1/\kappa}}, \qquad G_1(x) = \frac{G_0'(x)}{z} = \left[\frac{1 - e^{-1/\kappa}}{1 - x e^{-1/\kappa}} \right]^2 . \tag{1.34}$$

As a third example, consider a graph in which all vertices have degree 0, 1, 2, or 3 with probabilities $p_0 \ldots p_3$. Then the generating functions take the form of simple polynomials

$$G_0(x) = p_3 x^3 + p_2 x^2 + p_1 x + p_0, \tag{1.35}$$

$$G_1(x) = q_2 x^2 + q_1 x + q_0 = \frac{3 p_3 x^2 + 2 p_2 x + p_1}{3 p_3 + 2 p_2 + p_1} . \tag{1.36}$$

1.2.3 Distribution of Component Sizes

The Absence of Closed Loops We consider here a network below the percolation transition and are interested in the distribution of the sizes of the individual subclusters. The calculations will crucially depend on the fact that the generalized random graphs considered here do not have any significant clustering nor any closed loops.
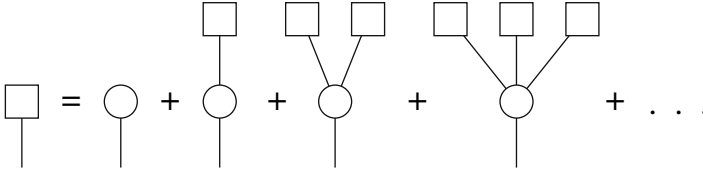
Fig. 1.6 Graphical representation of the self-consistency Eq. (1.37) for the generating function $H_1(x)$, represented by the *box*. A single vertex is represented by a *circle*. The subcluster connected to an incoming vertex can be either a single vertex or an arbitrary number of subclusters of the same type connected to the first vertex (from Newman et al., 2001)

Closed Loops.   A set of edges linking vertices

$$i_1 \rightarrow i_2 \ \ldots \ i_n \rightarrow i_1$$

is called a closed loop of length n.

In physics jargon, all finite components are *tree-like*. The number of closed loops of length 3 corresponds to the clustering coefficient C, viz to the probability that two of your friends are also friends of each other. For random networks $C = [\langle k^2 \rangle - \langle k \rangle]^2/(z^3 N)$, see Eq. (1.23), tends to zero as $N \rightarrow \infty$.

Generating Function for the Size Distribution of Components   We define by

$$H_1(x) \ = \ \sum_m h_m^{(1)} x^m$$

the generating function that generates the distribution of cluster sizes containing a given vertex j, which is linked to a specific incoming edge, see Fig. 1.6. That is, $h_m^{(1)}$ is the probability that the such-defined cluster contains m nodes.

Self-Consistency Condition for $H_1(x)$ We note the following:

1. The first vertex j belongs to the subcluster with probability 1, its generating function is x.
2. The probability that the vertex j has k outgoing stubs is q_k.
3. At every stub outgoing from vertex j there is a subcluster.
4. The total number of vertices consists of those generated by $H_1(x)$ plus the starting vertex.

The number of outgoing edges k from vertex j is described by the distribution function q_k, see Eq. (1.15). The total size of the k clusters is generated by $[H_1(x)]^k$, as a consequence of the multiplication property of generating functions discussed in Sect. 1.2.2. The self-consistency equation for the total number of vertices reachable is then

$$H_1(x) \ = \ x \sum_{k=0}^{\infty} q_k [H_1(x)]^k \ = \ x G_1(H_1(x)) \,, \tag{1.37}$$

where we have made use of Eq. (1.26).

The Embedding Cluster Distribution Function The quantity that we actually want to know is the distribution of the sizes of the clusters to which the entry vertex belongs. We note that

1. The number of edges emanating from a randomly chosen vertex is distributed according to the degree distribution p_k.
2. Every edge leads to a cluster whose size is generated by $H_1(x)$.

The size of a complete component is thus generated by

$$H_0(x) = x \sum_{k=0}^{\infty} p_k [H_1(x)]^k = x G_0(H_1(x)), \tag{1.38}$$

where the prefactor x corresponds to the generating function of the starting vertex. The complete distribution of component sizes is given by solving Eq. (1.37) self-consistently for $H_1(x)$ and then substituting the result into Eq. (1.38).

The Mean Component Size The calculation of $H_1(x)$ and $H_0(x)$ in closed form is not possible. We are, however, interested only in the first moment, viz the mean component size, see Eq. (1.28).

The component size distribution is generated by $H_0(x)$, Eq. (1.38), and hence the mean component size below the percolation transition is

$$\langle s \rangle = H_0'(1) = \left[G_0(H_1(x)) + x G_0'(H_1(x)) H_1'(x) \right]_{x=1}$$
$$= 1 + G_0'(1) H_1'(1), \tag{1.39}$$

where we have made use of the normalization

$$G_0(1) = H_1(1) = H_0(1) = 1.$$

of generating functions, see Eq. (1.27). The value of $H_1'(1)$ can be calculated from Eq. (1.37) by differentiating:

$$H_1'(x) = G_1(H_1(x)) + x G_1'(H_1(x)) H_1'(x), \tag{1.40}$$

$$H_1'(1) = \frac{1}{1 - G_1'(1)}.$$

Substituting this into (1.39) we find

$$\langle s \rangle = 1 + \frac{G_0'(1)}{1 - G_1'(1)}. \tag{1.41}$$

We note that

$$G'_0(1) = \sum_k k\, p_k \; = \; \langle k \rangle \; = \; z_1, \tag{1.42}$$

$$G'_1(1) = \frac{\sum_k k(k-1)p_k}{\sum_k k p_k} \; = \; \frac{\langle k^2 \rangle - \langle k \rangle}{\langle k \rangle} \; = \; \frac{z_2}{z_1} \; ,$$

where we have made use of Eq. (1.17). Substitution into (1.41) then gives the average component size below the transition as

$$\langle s \rangle \; = \; 1 + \frac{z_1^2}{z_1 - z_2} \; . \tag{1.43}$$

This expression has a divergence at $z_1 = z_2$. The mean component size diverges at the percolation threshold, compare Sect. 1.2, and the giant connected component forms.

1.3 Robustness of Random Networks

Fat tails in the degree distributions p_k of real-world networks (only slowly decaying with large k) increase the robustness of the network. That is, the network retains functionality even when a certain number of vertices or edges is removed. The Internet remains functional, to give an example, even when a substantial number of Internet routers have failed.

Removal of Vertices We consider a graph model in which each vertex is either "active" or "inactive". Inactive vertices are nodes that have either been removed, or are present but non-functional. We denote by

$$b(k) \; = \; b_k$$

the probability that a vertex is active. The probability can be, in general, a function of the degree k. The generating function

$$F_0(x) \; = \; \sum_{k=0}^{\infty} p_k\, b_k\, x^k, \qquad F_0(1) \; = \; \sum_k p_k\, b_k \; \leq \; 1 \; , \tag{1.44}$$

generates the probabilities that a vertex has degree k and is present. The normalization $F_0(1)$ is equal to the fraction of all vertices that are present.

Distribution of Connected Clusters By analogy with Eq. (1.26) we define by

$$F_1(x) \; = \; \frac{\sum_k k\, p_k\, b_k\, x^{k-1}}{\sum_k k\, p_k} \; = \; \frac{F'_0(x)}{z} \tag{1.45}$$

the (non-normalized) generating function for the degree distribution of neighbor sites. The distribution of the sizes of connected clusters reachable from a given vertex, $H_0(x)$, or from a given edge, $H_1(x)$, is generated respectively by the normalized functions

$$H_0(x) = 1 - F_0(1) + xF_0(H_1(x)), \qquad H_0(1) = 1,$$
$$H_1(x) = 1 - F_1(1) + xF_1(H_1(x)), \qquad H_1(1) = 1 , \qquad (1.46)$$

which are logical equivalents of Eqs. (1.37) and (1.38).

Random Failure of Vertices First we consider the case of random failure of vertices. In this case, the probability

$$b_k \equiv b \leq 1, \qquad F_0(x) = b\,G_0(x), \qquad F_1(x) = b\,G_1(x)$$

of a vertex being present is independent of the degree k and just equal to a constant b, which means that

$$H_0(x) = 1 - b + bxG_0(H_1(x)), \qquad H_1(x) = 1 - b + bxG_1(H_1(x)), \qquad (1.47)$$

where $G_0(x)$ and $G_1(x)$ are the standard generating functions for the degree of a vertex and of a neighboring vertex, Eqs. (1.24) and (1.26). This implies that the mean size of a cluster of connected and present vertices is

$$\langle s \rangle = H_0'(1) = b + bG_0'(1)H_1'(1) = b + \frac{b^2 G_0'(1)}{1 - bG_1'(1)} = b\left[1 + \frac{bG_0'(1)}{1 - bG_1'(1)}\right],$$

where we have followed the derivation presented in Eq. (1.40) in order to obtain $H_1'(1) = b/(1 - bG_1'(1))$. With Eq. (1.42) for $G_0'(1) = z_1 = z$ and $G_1'(1) = z_2/z_1$ we obtain the generalization

$$\langle s \rangle = b + \frac{b^2 z_1^2}{z_1 - bz_2} \qquad (1.48)$$

of Eq. (1.43). The model has a phase transition at the critical value of b

$$b_c = \frac{z_1}{z_2} = \frac{1}{G_1'(1)} . \qquad (1.49)$$

If the fraction b of the vertices present in the network is smaller than the critical fraction b_c, then there will be no giant component. This is the point at which the network ceases to be functional in terms of connectivity. When there is no giant component, connecting paths exist only within small isolated groups of vertices, but no long-range connectivity exists. For a communication network such as the Internet, this would be fatal.

For networks with fat tails, however, we expect that the number of next-nearest neighbors z_2 is large compared to the number of nearest neighbors z_1 and that b_c is consequently small. The network is robust as one would need to take out a substantial fraction of the nodes before it would fail.

Random Failure of Vertices in Scale-Free Graphs We consider a pure power-law degree distribution

$$p_k \sim \frac{1}{k^\alpha}, \qquad \int \frac{dk}{k^\alpha} < \infty, \qquad \alpha > 1 \,,$$

see Eq. (1.8) and also Sect. 1.5. The first two moments are

$$z_1 = \langle k \rangle \sim \int dk \,(k/k^\alpha), \qquad \langle k^2 \rangle \sim \int dk \,(k^2/k^\alpha) \,.$$

Noting that the number of next-nearest neighbors $z_2 = \langle k^2 \rangle - \langle k \rangle$, Eq. (1.17), we can identify three regimes:

- $\underline{1 < \alpha \leq 2}$: $z_1 \to \infty$, $z_2 \to \infty$
  $b_c = z_1/z_2$ is arbitrary in the thermodynamic limit $N \to \infty$.
- $\underline{2 < \alpha \leq 3}$: $z_1 < \infty$, $z_2 \to \infty$
  $b_c = z_1/z_2 \to 0$ in the thermodynamic limit. Any number of vertices can be randomly removed with the network remaining above the percolation limit. The network is extremely robust.
- $\underline{3 < \alpha}$: $z_1 < \infty$, $z_2 < \infty$
  $b_c = z_1/z_2$ can acquire any value and the network has normal robustness.

Biased Failure of Vertices What happens when one sabotages the most important sites of a network? This is equivalent to removing vertices in decreasing order of their degrees, starting with the highest degree vertices. The probability that a given node is active then takes the form

$$b_k = \theta(k_{\max} - k) \,, \tag{1.50}$$

where $\theta(x)$ is the Heaviside step function

$$\theta(x) = \begin{cases} 0 & \text{for } x < 0 \\ 1 & \text{for } x \geq 0 \end{cases} \,. \tag{1.51}$$

This corresponds to setting the upper limit of the sum in Eq. (1.44) to $k_{\max}$.

Differentiating Eq. (1.46) with respect to x yields

$$H_1'(1) = F_1(H_1(1)) + F_1'(H_1(1))\,H_1'(1), \qquad H_1'(1) = \frac{F_1(1)}{1 - F_1'(1)} \,,$$

as $H_1(1) = 1$. The phase transition occurs when $F_1'(1) = 1$,

$$\frac{\sum_{k=1}^{\infty} k(k-1)p_k b_k}{\sum_{k=1}^{\infty} kp_k} \;=\; \frac{\sum_{k=1}^{k_{\max}} k(k-1)p_k}{\sum_{k=1}^{\infty} kp_k} \;=\; 1 \;, \tag{1.52}$$

where we used the definition Eq. (1.45) for $F_1(x)$.

Biased Failure of Vertices for Scale-Free Networks Scale-free networks have a power-law degree distribution, $p_k \propto k^{-\alpha}$. We can then rewrite Eq. (1.52) as

$$H_{k_c}^{(\alpha-2)} - H_{k_c}^{(\alpha-1)} \;=\; H_{\infty}^{(\alpha-1)} \;, \tag{1.53}$$

where $H_n^{(r)}$ is the nth harmonic number of order r:

$$H_n^{(r)} \;=\; \sum_{k=1}^{n} \frac{1}{k^r} \;. \tag{1.54}$$

The number of vertices present is $F_0(1)$, see Eq. (1.44), or $F_0(1)/\sum_k p_k$, since the degree distribution p_k is normalized. If we remove a certain fraction f_c of the vertices we reach the transition determined by Eq. (1.53):

$$f_c \;=\; 1 - \frac{F_0(1)}{\sum_k p_k} \;=\; 1 - \frac{H_{k_c}^{(\alpha)}}{H_{\infty}^{(\alpha)}} \;. \tag{1.55}$$

It is impossible to determine k_c from (1.53) and (1.55) to get f_c in closed form. One can, however, solve Eq. (1.53) numerically for k_c and substitute it into Eq. (1.55). The results are shown in Fig. 1.7, as a function of the exponent α. The network is very susceptible with respect to a biased removal of highest-degree vertices.

- A removal of more than about 3% of the highest degree vertices always leads to a destruction of the giant connected component. Maximal robustness is achieved for $\alpha \approx 2.2$, which is actually close to the exponents measured in some real-world networks.
- Networks with $\alpha < 2$ have no finite mean, $\sum_k k/k^2 \to \infty$, and therefore make little sense physically.
- Networks with $\alpha > \alpha_c = 3.4788\ldots$ have no giant connected component. The critical exponent α_c is given by the percolation condition $H_{\infty}^{(\alpha-2)} = 2H_{\infty}^{(\alpha-1)}$, see Eq. (1.21).

1.4 Small-World Models

Random graphs and random graphs with arbitrary degree distribution show no clustering in the thermodynamic limit, in contrast to real-world networks. It is therefore important to find methods to generate graphs that have a finite clustering coefficient and, at the same time, the small-world property.
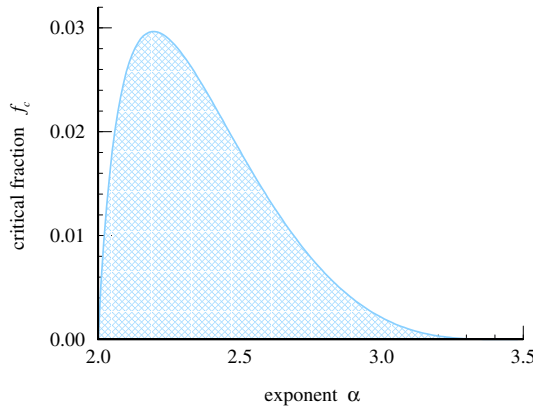
Fig. 1.7 The critical fraction f_c of vertices, Eq. (1.55). Removing a fraction greater than f_c of highest degree vertices from a scale-free network, with a power-law degree distribution $p_k \sim k^{-\alpha}$ drives the network below the percolation limit. For a smaller loss of highest degree vertices (*shaded area*) the giant connected component remains intact (from Newman, 2002)

Clustering in Lattice Models Lattice models and random graphs are two extreme cases of network models. In Fig. 1.8 we illustrate a simple one-dimensional lattice with connectivity $z = 2, 4$. We consider periodic boundary conditions, viz the chain wraps around itself in a ring. We then can calculate the clustering coefficient C exactly.

– The One-Dimensional Lattice: The number of clusters can be easily counted. One finds

$$C = \frac{3(z-2)}{4(z-1)} , \tag{1.56}$$

which tends to $3/4$ in the limit of large z.

– Lattices with Dimension d: Square or cubic lattices have dimension $d = 2, 3$, respectively. The clustering coefficient for general dimension d is

$$C = \frac{3(z-2d)}{4(z-d)} , \tag{1.57}$$

which generalizes Eq. (1.56). We note that the clustering coefficient tends to $3/4$ for $z \gg 2d$ for regular hypercubic lattices in all dimensions.

Distances in Lattice Models Regular lattices do not show the small-world effect. A regular hypercubic lattice in d dimensions with linear size L has $N = L^d$ vertices. The average vertex–vertex distance increases as L, or equivalently as

$$\ell \approx N^{1/d} .$$

The Watts and Strogatz Model Watts and Strogatz have proposed a small-world model that interpolates smoothly between a regular lattice and an Erdös–Rényi random graph. The construction starts with a one-dimensional lattice, see Fig. 1.9(a).
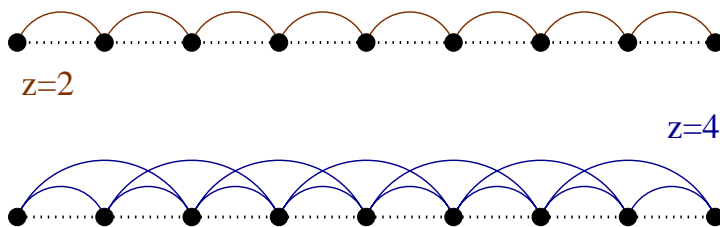
Fig. 1.8 Regular linear graphs with connectivities $z = 2$ (*top*) and $z = 4$ (*bottom*)

One goes through all the links of the lattice and rewires the link with some probability p.

Rewiring Probability. We move one end of every link with the probability p to a new position chosen at random from the rest of the lattice.

For small p this process produces a graph that is still mostly regular but has a few connections that stretch long distances across the lattice as illustrated in Fig. 1.9(a). The average coordination number of the lattice is by construction still the initial degree z. The number of neighbors of any particular vertex can, however, be greater or smaller than z.

The Newman and Watts Model A variation of the Watts–Strogatz model has been suggested by Newman and Watts. Instead of rewiring links between sites as in Fig. 1.9(a), extra links, also called "shortcuts", are added between pairs of sites chosen at random, but no links are removed from the underlying lattice, see Fig. 1.9(b). This model is somewhat easier to analyze than the original Watts and Strogatz model, because it is not possible for any region of the graph to become disconnected from the rest, whereas this can happen in the original model.

The small-world models illustrated in Fig. 1.9, have an intuitive justification for social networks. Most people are friends with their immediate neighbors. Neighbors on the same street, people that they work with or their relatives. However, some people are also friends with a few far away persons. Far away in a social sense, like people in other countries, people from other walks of life, acquaintances from previous eras of their lives, and so forth. These long-distance acquaintances are represented by the long-range links in the small-world models illustrated in Fig. 1.9.

Properties of the Watts and Strogatz Model In Fig. 1.10 the clustering coefficient and the average path length are shown as a function of the rewiring probability p. The key result is that there is a parameter range, say $p \approx 0.01 - 0.1$, where the network still has a very high clustering coefficient and already a small average path length, as observed in real-world networks. Similar results hold for the Newman–Watts model.
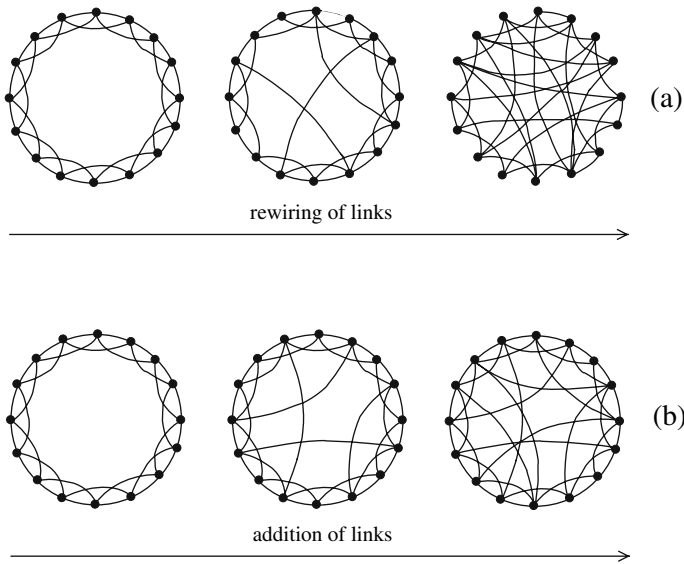
Fig. 1.9 Small-world networks in which the crossover from a regular lattice to a random network is realized. (**a**) The original Watts–Strogatz model with the rewiring of links. (**b**) The network with the addition of shortcuts (from Dorogovtsev and Mendes, 2002)

1.5 Scale-Free Graphs

Evolving Networks Most real-world networks are *open*, i.e. they are formed by the continuous addition of new vertices to the system. The number of vertices, N, increases throughout the lifetime of the network, as it is the case for the WWW, which grows exponentially by the continuous addition of new web pages. The small world networks discussed in Sect. 1.4 are, however, constructed for a fixed number of nodes N, growth is not considered.

Preferential Connectivity Random network models assume that the probability that two vertices are connected is random and uniform. In contrast, most real networks exhibit the "rich-get-richer" phenomenon.

> *Preferential Connectivity.   When the probability for a new vertex to connect to any of the existing nodes is not uniform for an open network we speak of preferential connectivity.*

A newly created web page, to give an example, will include links to well-known sites with a quite high probability. Popular web pages will therefore have both a high number of incoming links and a high growth rate for incoming links. The growth of vertices in terms of edges is therefore in general not uniform.

Barabási–Albert Model We start with m_0 unconnected vertices. The preferential attachment growth process can then be carried out in two steps:

Fig. 1.10 The clustering coefficient $C(p)$ and the average path length $L(p)$, as a function of the rewiring probability for the Watts and Strogatz model, compare Fig. 1.9 (from Watts and Strogatz, 1998)
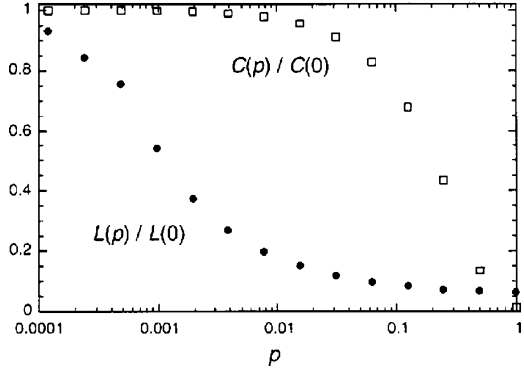
– Growth: At every time step we add a new vertex and $m \le m_0$ stubs.
– Preferential Attachment: We connect the m stubs to vertices already present with the probability

$$\Pi(k_i) = k_i / \sum_j k_j \,, \tag{1.58}$$

viz we have chosen the attachment probability $\Pi(k_i)$ to be linearly proportional to the number of links already present. Other functional dependencies for $\Pi(k_i)$ are of course possible, but they are not considered here.

After t time steps this model leads to a network with $N = t + m_0$ vertices and mt edges, see Fig. 1.11. We will now show that the preferential rule leads to a scale-free degree distribution

$$p_k \sim k^{-\gamma} \qquad \gamma > 1 \,, \tag{1.59}$$

with $\gamma = 3$.

Time-Dependent Connectivities The time dependence of the degree of a given vertex can be calculated analytically using a mean-field approach. We are interested in vertices with large degrees k; the scaling relation Eq. (1.59) is defined asymptotically for the limit $k \to \infty$. We may therefore assume k to be continuous:

$$\Delta k_i(t) \equiv k_i(t+1) - k_i(t) \approx \frac{\partial k_i}{\partial t}$$
$$= A\,\Pi(k_i) = A\,\frac{k_i}{\sum_{j=1}^{m_0+t-1} k_j} \,, \tag{1.60}$$

where $\Pi(k_i) = k_i / \sum_j k_j$ is the attachment probability. The overall number of new links is proportional to a normalization constant A, which is hence determined by the sum rule

$$\sum_i \Delta k_i(t) \equiv m = A\,\frac{\sum_i k_i}{\sum_j k_j} = A \,,$$

where the sum runs over the already existing nodes. At every time step m new edges are attached to the existing links. The total number of connectivities is then $\sum_j k_j = 2m(t-1)$. We thus obtain
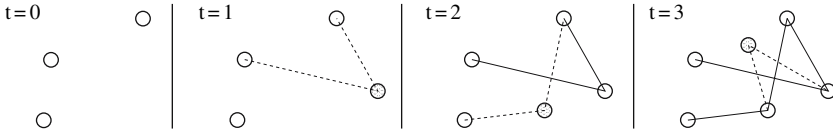
Fig. 1.11 Illustration of the preferential attachment model for an evolving network. At $t = 0$ the system consists of $m_0 = 3$ isolated vertices. At every time step a new vertex (*shaded circle*) is added, which is connected to $m = 2$ vertices, preferentially to the vertices with high connectivity, determined by the rule Eq. (1.58)

$$\frac{\partial k_i}{\partial t} = \frac{mk_i}{2m(t-1)} = \frac{k_i}{2(t-1)} \approx \frac{k_i}{2t} . \tag{1.61}$$

Note that Eq. (1.60) is not well defined for $t = 1$, since there are no existing edges present in the system. In principle preferential attachment needs some starting connectivities to work. We have therefore set $t - 1 \approx t$ in Eq. (1.61), since we are only interested in the long-time behaviour.

Adding Times Equation (1.61) can be easily solved taking into account that every vertex i is characterized by the time $t_i = N_i - m_0$ that it was added to the system with $m = k_i(t_i)$ initial links:

$$k_i(t) = m \left(\frac{t}{t_i}\right)^{0.5}, \qquad t_i = t m^2 / k_i^2 . \tag{1.62}$$

Older nodes, i.e. those with smaller t_i, increase their connectivity faster than the younger vertices, viz those with bigger t_i, see Fig. 1.12. For social networks this mechanism is dubbed the rich-gets-richer phenomenon.

The number of nodes $N(t) = m_0 + t$ is identical to the number of adding times,

$$t_1, \dots, t_{m_0} = 0, \qquad t_{m_0+j} = j, \qquad j = 1, 2, \dots ,$$

where we have defined the initial m_0 nodes to have adding times zero.

Integrated Probabilities Using (1.62), the probability that a vertex has a connectivity $k_i(t)$ smaller than a certain k, $P(k_i(t) < k)$ can be written as

$$P(k_i(t) < k) = P(t_i > \frac{m^2 t}{k^2}) . \tag{1.63}$$

The adding times are uniformly distributed, compare Fig. 1.12, and the probability $P(t_i)$ to find an adding time t_i is then

$$P(t_i) = \frac{1}{m_0 + t}, \tag{1.64}$$

just the inverse of the total number of adding times, which coincides with the total number of nodes. $P(t_i > m^2 t / k^2)$ is therefore the cumulative number of adding times
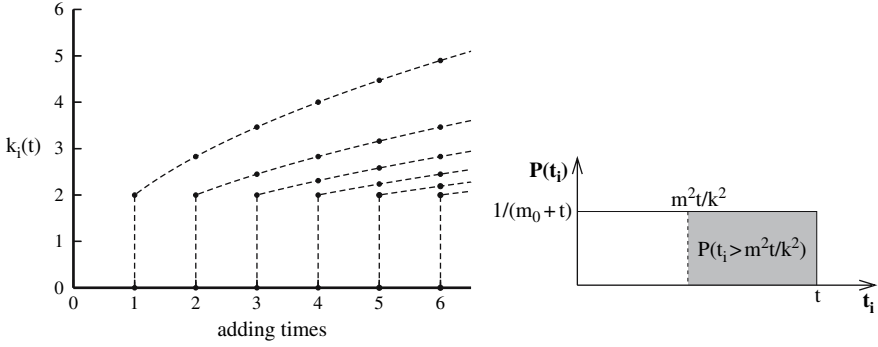
Fig. 1.12 *Left*: Time evolution of the connectivities for vertices with adding times $t = 1, 2, 3, \ldots$ and $m = 2$, following Eq. (1.62). *Right*: The integrated probability, $P(k_i(t) < k) = P(t_i > tm^2/k^2)$, see Eq. (1.63)

t_i larger than $m^2 t / k^2$, multiplied with the probability $P(t_i)$ (Eq. (1.64)) to add a new node:

$$P(t_i > \frac{m^2 t}{k^2}) = \left(t - \frac{m^2 t}{k^2}\right) \frac{1}{m_0 + t} . \tag{1.65}$$

Scale-Free Degree Distribution The degree distribution p_k then follows from Eq. (1.65) via a simple differentiation,

$$p_k = \frac{\partial P(k_i(t) < k)}{\partial k} = \frac{\partial P(t_i > m^2 t / k^2)}{\partial k} = \frac{2m^2 t}{m_0 + t} \frac{1}{k^3} , \tag{1.66}$$

in accordance with Eq. (1.59). The degree distribution Eq. (1.66) has a well defined limit $t \to \infty$, approaching a stationary distribution. We note that $\gamma = 3$, which is independent of the number m of added links per new site. This result indicates that growth and preferential attachment play an important role for the occurrence of a power-law scaling in the degree distribution. To verify that both ingredients are really necessary, we now investigate a variant of above model.

Growth with Random Attachment We examine then whether growth alone can result in a scale-free degree distribution. We assume random instead of preferential attachment. The growth equation for the connectivity k_i of a given node i, compare Eqs. (1.60) and (1.64), then takes the form

$$\frac{\partial k_i}{\partial t} = \frac{m}{m_0 + (t - 1)} . \tag{1.67}$$

The m new edges are linked randomly at time t to the $(m_0 + t - 1)$ nodes present at the previous time step. Solving Eq. (1.67) for k_i, with the initial condition $k_i(t_i) = m$, we obtain

$$k_i = m\left[\ln(m_0 + t - 1) - \ln(m_0 + t_i - 1) + 1 \right], \tag{1.68}$$

which is a logarithmic increase with time. The probability that vertex i has connectivity $k_i(t)$ smaller than k is then

$$
P(k_i(t) < k) = P\left(t_i > (m_0 + t - 1)\exp(1 - \frac{k}{m}) - m_0 + 1\right)
$$
$$
= \left[t - (m_0 + t - 1)\exp(1 - \frac{k}{m}) - m_0 + 1\right]\frac{1}{m_0 + t}\,, \quad (1.69)
$$

where we assumed that we add the vertices uniformly in time to the system. Using

$$
p_k = \frac{\partial P(k_i(t) < k)}{\partial k}
$$

and assuming long times, we find

$$
p_k = \frac{1}{m}e^{1-k/m} = \frac{e}{m}\exp(-\frac{k}{m})\,. \quad (1.70)
$$

Thus for a growing network with random attachment we find a characteristic degree

$$
k^* = m\,, \quad (1.71)
$$

which is identical to half of the average connectivities of the vertices in the system, since $\langle k \rangle = 2m$. Random attachment does not lead to a scale-free degree distribution. Note that p_k in Eq. (1.70) is not properly normalized, nor in Eq. (1.66), since we used a large-k approximation during the respective derivations.

Internal Growth with Preferential Attachment The original preferential attachment model yields a degree distribution $p_k \sim k^{-\gamma}$ with $\gamma = 3$. Most social networks such as the WWW and the Wikipedia network, however, have exponents $2 < \gamma < 3$, with the exponent γ being relatively close to 2. It is also observed that new edges are mostly added in between existing nodes, albeit with (internal) preferential attachment.

We can then generalize the preferential attachment model discussed above in the following way:

– Vertex Growth: At every time step a new vertex is added.
– Link Growth: At every time step m new edges are added.
– External Preferential Attachment: With probability $r \in [0, 1]$ any one of the m new edges is added between the new vertex and an existing vertex i, which is selected with a probability $\propto \Pi(k_i)$, see Eq. (1.58).
– Internal Preferential Attachment: With probability $1 - r$ any one of the m new edges is added in between two existing vertices i and j, which are selected with a probability $\propto \Pi(k_i)\Pi(k_j)$.

The model reduces to the original preferential attachment model in the limit $r \to 1$. The scaling exponent γ can be evaluated along the lines used above for the case $r = 1$. One finds

$$p_k \sim \frac{1}{k^\gamma}, \qquad \gamma = 1 + \frac{1}{1 - r/2} . \qquad (1.72)$$

The exponent $\gamma = \gamma(r)$ interpolates smoothly between 2 and 3, with $\gamma(1) = 3$ and $\gamma(0) = 2$. For most real-world graphs r is quite small; most links are added internally. Note, however, that the average connectivity $\langle k \rangle = 2m$ remains constant, since one new vertex is added for $2m$ new stubs.

Exercises

DEGREE DISTRIBUTION

Online network databases can be found on the Internet. Write a program and evaluate for a network of your choice the degree distribution p_k, the clustering coefficient C and compare it with the expression (1.23) for a generalized random net with the same p_k.

ENSEMBLE FLUCTUATIONS

Derive Eq. (1.7) for the distribution of ensemble fluctuations. In the case of difficulties Albert and Barabási (2002) can be consulted. Alternatively, check Eq. (1.7) numerically.

SELF-RETRACING PATH APPROXIMATION

Look at Brinkman and Rice (1970) and prove Eq. (1.12). This derivation is only suitable for readers with a solid training in physics.

CLUSTERING COEFFICIENT

Prove Eq. (1.56) for the clustering coefficient of one-dimensional lattice graphs. Facultatively, generalize this formula to a d-dimensional lattice with links along the main axis.

SCALE-FREE GRAPHS

Write a program that implements preferential attachments and calculate the resulting degree distribution p_k. If you are adventurous, try alternative functional dependencies for the attachment probability $\Pi(k_i)$ instead of the linear assumption (1.58).

SIR MODEL

Consult `http://xxx.arxiv.org/abs/cond-mat/0201433`, M.E.J. Newman, *Exact solutions of epidemic models on networks* and solve the susceptible (S), infective (I), removed (R) model for spreading of diseases in social networks by a generalization of the techniques discussed in Sect. 1.3.

Further Reading

For further studies several books (Watts, 1999; Dorogovtsev and Mendes, 2003) and review articles (Albert and Barabási, 2002; Dorogovtsev and Mendes, 2002) are recommended.

The interested reader might delve into some of the original literature on, e.g. the original Watts and Strogatz (1998) small-world model, the Newman and Watts (1999) model, the mean-field solution of the preferential attachment model (Barabási, Albert and Jeong, 1999), the formulation of the concept of clique percolation (Derenyi, Palla and Vicsek, 2005), an early study of the WWW (Albert, Jeong and Barabási, 1999), a recent study of the time evolution of the Wikipedia network (Capocci et al., 2006), a study regarding the community structure of real-world networks (Palla et al., 2005) or the mathematical basis of graph theory (Erdös and Rényi, 1959). A good starting point is Milgram's (1967) account of his by now famous experiment, which led to the law of 'six degrees of separation' (Guare, 1990).

ALBERT, R., JEONG, H.; BARABÁSI, A.-L 1999 Diameter of the world-wide web. *Nature* **401**, 130–131.

ALBERT, R., BARABÁSI, A.-L. 2002 Statistical mechanics of complex networks. *Review of Modern Physics* **74**, 47–97.

BARABASI, A.L., ALBERT, R., JEONG, H. (1999) Mean-field theory for scale-free random networks. *Physica A* **272**, 173–187.(1999)

BRINKMAN, W.F., RICE, T.M. Single-particle excitations in magnetic insulators. Physical Review B *2* **1324-1338**, (1970).

CAPOCCI, A. ET AL. 2006 Preferential attachment in the growth of social networks: The internet encyclopedia Wikipedia *Physical Review E* **74**, 036116.

DERENYI, I., PALLA, G., VICSEK, T. 2005 Clique percolation in random networks. *Physical Review Letters* **94**, 160202.

DOROGOVTSEV, S.N., MENDES, J.F.F. 2002 Evolution of networks. *Advances in Physics* **51**, 1079–1187.

DOROGOVTSEV, S.N., MENDES, J.F.F. 2003 *Evolution of networks. From biological nets to the Internet and WWW.* Oxford University Press.

ERDÖS, P., RÉNYI, A. 1959 On random graphs. *Publications Mathematicae* **6**, 290–297.

GUARE, J. 1990 *Six degrees of separation: A play.* Vintage.

MILGRAM, S. 1967 The small world problem. *Psychology Today* **2**, 60–67.

MOUKARZEL, C.F. 1999 Spreading and shortest paths in systems with sparse long-range connections. *Physics Review E* **60**, 6263–6266.

NEWMAN, M.E.J. 2002 *Random graphs as models of networks.* `http://arxiv.org/abs/cond-mat/0202208`.

NEWMAN, M.E.J., WATTS, D.J. 1999 Renormalization group analysis of the small world network model. *Physics Letters A* **263**, 341–346.

NEWMAN, M.E.J., STROGATZ, S.H., WATTS, D.J. 2001 Random graphs with arbitrary degree distributions and their applications. *Physical Review E* **64**, 026118.

PALLA, G., DERENYI, I., FARKAS, I., VICSEK, T. 2005 Uncovering the overlapping community structure of complex networks in nature and society. *Nature* **435**, 814–818.

WATTS, D.J. 1999 *Small Worlds: The dynamics of networks between order and randomness.* Princeton University Press (Princeton).

WATTS, D.J., STROGATZ, S.H. 1998 Collective dynamics of small world networks. *Nature* **393**, 440–442.

Chapter 2
Chaos, Bifurcations and Diffusion

Complex system theory deals with dynamical systems containing very large numbers of variables. It extends dynamical system theory, which deals with dynamical systems containing a few variables. A good understanding of dynamical systems theory is therefore a prerequisite when studying complex systems.

In this chapter we introduce important concepts, like regular and irregular behavior, attractors and Lyapunov exponents, bifurcation, and deterministic chaos from the realm of dynamical system theory. A short introduction to dissipative and stochastic, viz noisy systems is given further on, together with two important examples out of noise-controlled dynamics, namely stochastic escape and stochastic resonance.

2.1 Basic Concepts of Dynamical Systems Theory

Dynamical systems theory deals with the properties of coupled differential equations, determining the time evolution of a few, typically a handful of variables. Many interesting concepts have been developed and we will present a short overview covering the most important phenomena.

Fixpoints and Limiting Cycles We start by discussing an elementary non-linear rotator, just to illustrate some procedures that are typical for dynamical systems theory. We consider a two-dimensional system $\mathbf{x} = (x,y)$. Using the polar coordinates

$$x(t) \;=\; r(t)\cos(\varphi(t)), \qquad y(t) \;=\; r(t)\sin(\varphi(t)) , \qquad (2.1)$$

we assume that the following non-linear differential equations:

$$\dot{r} \;=\; (\Gamma - r^2)\,r, \qquad \dot{\varphi} \;=\; \omega \qquad (2.2)$$

govern the dynamical behavior. The typical orbits $(x(t),y(t))$ are illustrated in Fig. 2.1. The limiting behavior of Eq. (2.2) is
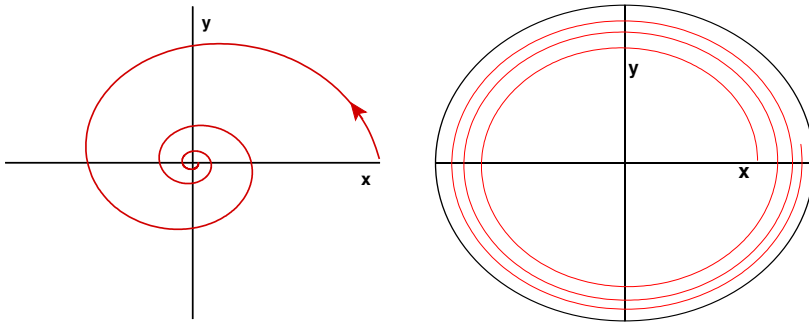
Fig. 2.1 The solution of the non-linear rotator equations (2.1) and (2.2) for $\Gamma < 0$ (*left*) and $\Gamma > 0$ (*right*)

$$\lim_{t \to \infty} \begin{bmatrix} x(t) \\ y(t) \end{bmatrix} = \begin{cases} \begin{bmatrix} 0 \\ 0 \end{bmatrix} & \Gamma < 0 \\ \begin{bmatrix} r_c \cos(\omega t) \\ r_c \sin(\omega t) \end{bmatrix} & \Gamma = r_c^2 > 0 \end{cases} . \tag{2.3}$$

In the first case, $\Gamma < 0$, we have a stable fixpoint; in the second case, $\Gamma > 0$, the dynamics approaches a limiting cycle.

> *Bifurcation.   When a dynamical system, described by a set of parameterized differential equations, changes qualitatively, as a function of an external parameter, the nature of its long-time limiting behavior in terms of fixpoints or limiting cycles, one speaks of a bifurcation.*

The dynamical system (2.1) and (2.2) shows a bifurcation at $\Gamma = 0$. A fixpoint turns into a limiting cycle at $\Gamma = 0$, and one denotes this specific type of bifurcation as a "Hopf bifurcation".

First-Order Differential Equations Let us consider the third-order differential equation

$$\frac{d^3}{dt^3} x(t) = f(x, \dot{x}, \ddot{x}) . \tag{2.4}$$

Using

$$x_1(t) = x(t), \qquad x_2(t) = \dot{x}(t), \qquad x_3(t) = \ddot{x}(t) , \tag{2.5}$$

we can rewrite (2.4) as a first-order differential equation:

$$\frac{d}{dt} \begin{bmatrix} x_1 \\ x_2 \\ x_3 \end{bmatrix} = \begin{bmatrix} x_2 \\ x_3 \\ f(x_1, x_2, x_3) \end{bmatrix} .$$

Autonomous Systems It is then generally true that one can reduce any set of coupled differential equations to a set of first-order differential equations by introducing an appropriate number of additional variables. We therefore consider in the following only first-order, ordinary differential equations such as

Fig. 2.2 The Poincaré map
$\mathbf{x} \to \mathbf{P(x)}$
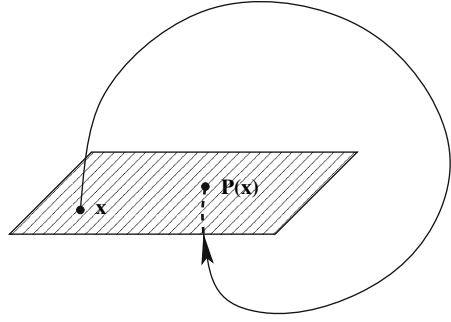
$$\frac{d\mathbf{x}(t)}{dt} = \mathbf{f}(\mathbf{x}(t)), \qquad \mathbf{x}, \mathbf{f} \in \mathbb{R}^d, \qquad t \in [-\infty, +\infty], \qquad (2.6)$$

when time is continuous, or, equivalently, maps such as

$$\mathbf{x}(t+1) = \mathbf{g}(\mathbf{x}(t)), \qquad \mathbf{x}, \mathbf{g} \in \mathbb{R}^d, \qquad t = 0, 1, 2, \dots \qquad (2.7)$$

when time is discrete. An evolution equation of type Eq. (2.6) is denoted "autonomous", since it does not contain an explicit time dependence. A system of type $\dot{\mathbf{x}} = \mathbf{f}(t, \mathbf{x})$ is dubbed "non-autonomous".

The Phase Space. One denotes by "phase space" the space spanned by all allowed values of the variables entering the set of first-order differential equations defining the dynamical system.

The phase space depends on the representation. For a two-dimensional system (x, y) the phase space is just $\mathbb{R}^2$, but in the polar coordinates Eq. (2.1) it is

$$\left\{ (r, \varphi) \, \middle| \, r \in [0, \infty], \, \varphi \in [0, 2\pi[\right\}.$$

Orbits and Trajectories A particular solution $\mathbf{x}(t)$ of the dynamical system Eq. (2.6) can be visualized as a "trajectory", also denoted "orbit", in phase space. Any orbit is uniquely determined by the set of "initial conditions", $\mathbf{x}(0) \equiv \mathbf{x}_0$, since we are dealing with first-order differential equations.

The Poincaré Map It is difficult to illustrate graphically the motion of $\mathbf{x}(t)$ in d dimensions. Our retina as well as our print media are two-dimensional and it is therefore convenient to consider a plane Σ in $\mathbb{R}^d$ and the points $\mathbf{x}^{(i)}$ of the intersection of an orbit γ with Σ, see Fig. 2.2.

For the purpose of illustration let us consider the plane

$$\Sigma = \{ (x_1, x_2, 0, \dots, 0) \, | \, x_1, x_2 \in \mathbb{R} \}$$

and the sequence of intersections (see Fig. 2.2)

$$\mathbf{x}^{(i)} \;=\; (x_1^{(i)}, x_2^{(i)}, 0, \ldots, 0), \qquad (i = 1, 2, \ldots)$$

which define the *Poincaré map*

$$\mathbf{P}: \; \mathbf{x}^{(i)} \; \mapsto \; \mathbf{x}^{(i+1)} \,.$$

The Poincaré map is therefore a discrete map of the type of Eq. (2.7), which can be constructed for continuous-time dynamical systems like Eq. (2.6). The Poincaré map is very useful, since we can print and analyze it directly. A periodic orbit, to give an example, would show up in the Poincaré map as the identity mapping.

Constants of Motion and Ergodicity We mention here a few general concepts from the theory of dynamical systems.

- The Constant of Motion: A function $F(\mathbf{x})$ on phase space $\mathbf{x} = (x_1, \ldots, x_d)$ is called a "constant of motion" or a "conserved quantity" if it is conserved under the time evolution of the dynamical system, i.e. when

$$\frac{\mathrm{d}}{\mathrm{d}t} F(\mathbf{x}(t)) \;=\; \sum_{i=1}^{d} \left(\frac{\partial}{\partial x_i} F(\mathbf{x}) \right) \dot{x}_i(t) \;\equiv\; 0$$

  holds for all times t. In many mechanical systems the energy is a conserved quantity.
- Ergodicity: A dynamical system in which orbits come arbitrarily close to any allowed point in the phase space, irrespective of the initial condition, is called ergodic.

  All conserving systems of classical mechanics, obeying Hamiltonian dynamics, are ergodic. The ergodicity of a mechanical system is closely related to "Liouville's theorem", which will be discussed in Sect. 2.3.1.

  Ergodicity holds only modulo conserved quantities, as is the case for the energy in many mechanical systems. Then, only points in the phase space having the same energy as the trajectory considered are approached arbitrarily close.
- Attractors: A bounded region in phase space to which orbits with certain initial conditions come arbitrarily close is called an attractor.

  Attractors can be isolated points (fixpoints), limiting cycles or more complex objects.
- The Basin of Attraction: The set of initial conditions that leads to orbits approaching a certain attractor arbitrarily closely is called the basin of attraction.

It is clear that ergodicity and attractors are mutually exclusive: An ergodic system cannot have attractors and a dynamical system with one or more attractors cannot be ergodic.

Mechanical Systems and Integrability A dynamical system of type

$$\ddot{x}_i = f_i(\boldsymbol{x}, \dot{\boldsymbol{x}}), \qquad i = 1, \ldots, f$$

is denoted a "mechanical system" since all equations of motion in classical mechanics are of this form, e.g. Newton's law. f is called the degree of freedom and
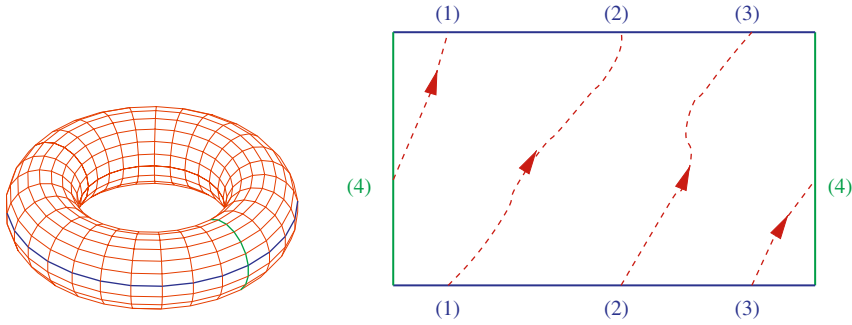
Fig. 2.3 A KAM-torus. *Left*: The torus can be cut along two lines (*vertical/horizontal*) and un-folded. *Right*: A closed orbit on the unfolded torus with $\omega_1/\omega_2 = 3/1$. The numbers indicate points that coincide after refolding (periodic boundary conditions)

a mechanical system can be written as a set of coupled first-order differential equations with $2f$ variables

$$(x_1 \ldots x_f, v_1 \ldots v_f), \qquad v_i = \dot{x}_i, \qquad i = 1, \ldots, N$$

constituting the phase space, with $\mathbf{v} = (v_1, \ldots, v_f)$ being denoted the generalized velocity. A mechanical system is *integrable* if there are $\alpha = 1, \ldots, f$ independent constants of motion $F_\alpha(\mathbf{x}, \dot{\mathbf{x}})$ with

$$\frac{d}{dt} F_\alpha(\mathbf{x}, \dot{\mathbf{x}}) = 0, \qquad \alpha = 1, \ldots, f .$$

The motion in the $2f$-dimensional phase space $(x_1 \ldots x_f, v_1 \ldots v_f)$ is then restricted to an f-dimensional subspace, which is an f-dimensional torus, see Fig. 2.3.

An example of an integrable mechanical system is the Kepler problem, viz the motion of the earth around the sun. Integrable systems, however, are very rare, but they constitute important reference points for the understanding of more general dynamical systems. A classical example of a non-integrable mechanical system is the three-body problem, viz the combined motion of earth, moon and sun around each other.

The KAM Theorem Kolmogorov, Arnold and Moser (KAM) have examined the question of what happens to an integrable system when it is perturbed. Let us consider a two-dimensional torus, as illustrated in Fig. 2.3. The orbit wraps around the torus with frequencies ω_1 and ω_2, respectively. A key quantity is the ratio of revolution frequencies ω_1/ω_2; it might be rational or irrational.

We remember that any irrational number r may be approximated with arbitrary accuracy by a sequence of quotients

$$\frac{m_1}{s_1}, \frac{m_2}{s_2}, \frac{m_3}{s_3}, \ldots \qquad s_1 < s_2 < s_3 < \ldots$$

with ever larger denominators s_i. A number r is "very irrational" when it is difficult to approximate r by such a series of rational numbers, viz when very large denominators s_i are needed to achieve a certain given accuracy $|r - m/s|$.

The KAM theorem states that orbits with rational ratios of revolution frequencies ω_1/ω_2 are the most unstable under a perturbation of an integrable system and that tori are most stable when this ratio is very irrational.

Gaps in the Saturn Rings A spectacular example of the instability of rational KAM-tori are the gaps in the rings of the planet Saturn.

The time a particle orbiting in Cassini's gap (between the A-ring and the B-ring, $r = 118\,000$ km) would need around Saturn is exactly half the time the "shepherdmoon" Mimas needs to orbit Saturn. The quotient of the revolving frequencies is $2:1$. Any particle orbiting in Cassini's gap is therefore unstable against the perturbation caused by Mimas and it is consequently thrown out of its orbit.

2.2 The Logistic Map and Deterministic Chaos

Chaos The notion of "chaos" plays an important role in dynamical systems theory. A chaotic system is defined as a system that cannot be predicted within a given numerical accuracy. At first sight this seems to be a surprising concept, since differential equations of type Eq. (2.6), which do not contain any noise or randomness, are perfectly deterministic. Once the starting point is known, the resulting trajectory can be calculated for all times. Chaotic behavior can arise nevertheless, due to an exponential sensitivity to the initial conditions.

> *Deterministic Chaos. A deterministic dynamical system that shows exponential sensibility of the time development on the initial conditions is called chaotic.*

This means that a very small change in the initial condition can blow up even after a short time. When considering real-world applications, when models need to be determined from measurements containing inherent errors and limited accuracies, an exponential sensitivity can result in unpredictability. A well known example is the problem of long-term weather prediction.

The Logistic Map One of the most cherished models in the field of deterministic chaos is the logistic map of the interval $[0,1]$ onto itself:

$$x_{n+1} = f(x_n) \equiv r x_n (1 - x_n), \qquad x_n \in [0,1], \qquad r \in [0,4], \qquad (2.8)$$

where we have used the notation $x(t+n) = x_n$. The logistic map is illustrated in Fig. 2.4. The logistic map shows, despite its apparent simplicity, an infinite series of bifurcations and a transition to chaos.

Biological Interpretation We may consider $x_n \in [0,1]$ as standing for the population density of a reproducing species in the year n. In this case the factor
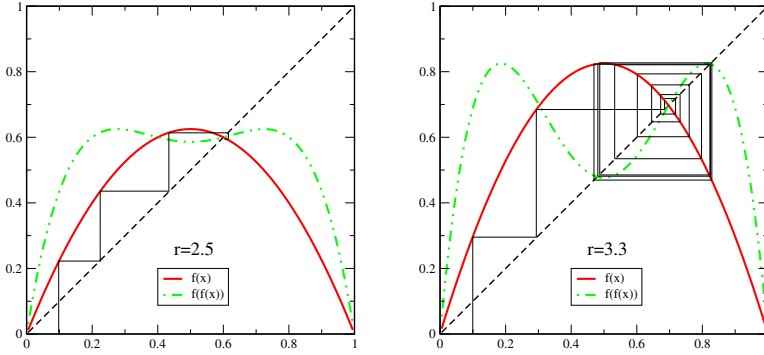
Fig. 2.4 Illustration of the logistic map $f(x)$ (*thick solid line*) and of the iterated logistic map $f(f(x))$ (*thick dot-dashed line*) for $r = 2.5$ (*left*) and $r = 3.3$ (*right*). Also shown is an iteration of $f(x)$, starting from $x = 0.1$ (*thin solid line*) Note, that the fixpoint $f(x) = x$ is stable/unstable for $r = 2.5$ and $r = 3.3$, respectively. The orbit is attracted to a fixpoint of $f(f(x))$ for $r = 3.3$, corresponding to a cycle of period 2 for $f(x)$

$r(1 - x_n) \in [0, 4]$ is the number of offspring per year, which is limited in the case of high population densities $x \to 1$, when resources become scarce. The classical example is that of a herd of reindeer on an island.

Knowing the population density x_n in a given year n we may predict via Eq. (2.8) the population density for all subsequent years exactly; the system is deterministic. Nevertheless the population shows irregular behavior for certain values of r, which one calls "chaotic".

Fixpoints of the Logistic Map We start considering the fixpoints of $f(x)$:

$$x = rx(1 - x) \qquad \Longleftrightarrow \qquad x = 0 \quad \text{or} \quad 1 = r(1 - x) .$$

The non-trivial fixpoint is then

$$1/r = 1 - x, \qquad x^{(1)} = 1 - 1/r, \qquad r_1 < r, \qquad r_1 = 1 . \qquad (2.9)$$

It occurs only for $r_1 < r$, with $r_1 = 1$, due to the restriction $x^{(1)} \in [0, 1]$.

Stability of the Fixpoint We examine the stability of $x^{(1)}$ against perturbations by linearization of Eq. (2.8), using

$$y_n = x_n - x^{(1)}, \qquad x_n = x^{(1)} + y_n, \qquad y_n \ll 1 .$$

We obtain

$$\begin{aligned} x^{(1)} + y_{n+1} &= r(x^{(1)} + y_n)(1 - x^{(1)} - y_n) \\ &= rx^{(1)}(1 - x^{(1)} - y_n) + ry_n(1 - x^{(1)} - y_n) . \end{aligned}$$

Using the fixpoint condition $x^{(1)} = f(x^{(1)})$ and neglecting terms $\sim y_n^2$, we obtain

$$y_{n+1} = -rx^{(1)}y_n + ry_n(1 - x^{(1)}) = r(1 - 2x^{(1)})y_n,$$

and, using Eq. (2.9), we find

$$y_{n+1} = r(1 - 2(1 - 1/r))y_n = (2 - r)y_n = (2 - r)^{n+1}y_0 . \tag{2.10}$$

The perturbation y_n increases/decreases in magnitude for $|2 - r| > 1$ and $|2 - r| < 1$, respectively. Noting that $r \in [1, 4]$, we find

$$|2 - r| < 1 \qquad \Longleftrightarrow \qquad \boxed{r_1 < r < r_2} \qquad \begin{array}{l} r_1 = 1 \\ r_2 = 3 \end{array} \tag{2.11}$$

for the region of stability of $x^{(1)}$.

Fixpoints of Period 2 For $r > 3$ a fixpoint of period 2 appears, which is a fixpoint of the iterated function

$$f(f(x)) = rf(x)(1 - f(x)) = r^2 x(1 - x)(1 - rx(1 - x)).$$

The fixpoint equation $x = f(f(x))$ leads to the cubic equation

$$1 = r^2(1 - rx + rx^2) - r^2 x(1 - rx + rx^2),$$
$$0 = r^3 x^3 - 2r^3 x^2 + (r^3 + r^2)x + 1 - r^2 . \tag{2.12}$$

In order to find the roots of Eq. (2.12) we use the fact that $x = x^{(1)} = 1 - 1/r$ is a stationary point of both $f(x)$ and $f(f(x))$, see Fig. 2.4. We divide (2.12) by the root $(x - x^{(1)}) = (x - 1 + 1/r)$:

$$(r^3 x^3 - 2r^3 x^2 + (r^3 + r^2)x + 1 - r^2) : (x - 1 + 1/r) =$$

$$r^3 x^2 - (r^3 + r^2)x + (r^2 + r) .$$

The two new fixpoints of $f(f(x))$ are therefore the roots of

$$x^2 - \left(1 + \frac{1}{r}\right)x + \left(\frac{1}{r} + \frac{1}{r^2}\right) = 0 .$$

We obtain

$$x_{\pm}^{(2)} = \frac{1}{2}\left(1 + \frac{1}{r}\right) \pm \sqrt{\frac{1}{4}\left(1 + \frac{1}{r}\right)^2 - \left(\frac{1}{r} + \frac{1}{r^2}\right)} . \tag{2.13}$$

Bifurcation We have two fixpoints for $r > 3$ and only one fixpoint for $r < 3$. What happens for $r = 3$?
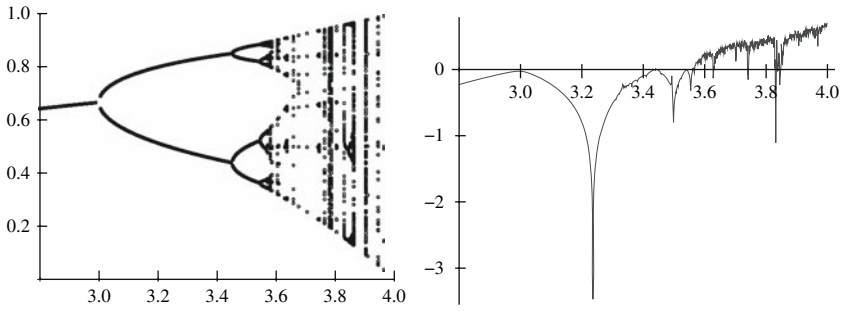
Fig. 2.5 The fixpoints of the (iterated) logistic map (*left*) and the corresponding Lyapunov exponents (*right*), as a function of the parameter r. Positive Lyapunov exponents λ indicate chaotic behavior

$$x_{\pm}^{(2)}(r=3) = \frac{1}{2}\frac{3+1}{3} \pm \sqrt{\frac{1}{4}\left(\frac{3+1}{3}\right)^2 - \left(\frac{3+1}{9}\right)}$$

$$= \frac{2}{3} = 1 - \frac{1}{3} = x^{(1)}(r=3) .$$

At $r = 3$ the fixpoint splits into two, see Fig. 2.5, a typical *bifurcation*.

More Bifurcations We may now carry out a stability analysis for $x_{\pm}^{(2)}$, just as we did for $x^{(1)}$. We find a critical value $r_3 > r_2$ such that

$$x_{\pm}^{(2)}(r) \text{ stable} \qquad \Longleftrightarrow \qquad \boxed{r_2 < r < r_3.} \qquad (2.14)$$

Going further on one finds an r_4 such that there are four fixpoints of period 4, that is of $f(f(f(f(x))))$, for $r_3 < r < r_4$. In general there are critical values r_n and r_{n+1} such that there are

$$2^{n-1} \text{ fixpoints } x^{(n)} \text{ of period } 2^{n-1} \qquad \Longleftrightarrow \qquad \boxed{r_n < r < r_{n+1}.}$$

The logistic map therefore shows iterated bifurcations. This, however, is not yet chaotic behavior.

Chaos in the Logistic Map The critical r_n for doubling of the period converge:

$$\lim_{n\to\infty} r_n \to r_\infty, \qquad r_\infty = 3.5699456\ldots$$

There are consequently no stable fixpoints of $f(x)$ or of the iterated logistic map in the region

$$r_\infty < r < 4 .$$

In order to characterize the sensitivity of Eq. (2.8) with respect to the initial condition, we consider two slightly different starting populations x_1 and x_1':

$$x_1 - x_1' = y_1, \qquad y_1 \ll 1 .$$

The key question is then whether the difference in populations

$$y_m = x_m - x_m'$$

is still small after m iterations. Using $x_1' = x_1 - y_1$ we find for $m = 2$

$$
\begin{aligned}
y_2 = x_2 - x_2' &= rx_1(1-x_1) - rx_1'(1-x_1') \\
&= rx_1(1-x_1) - r(x_1-y_1)(1-(x_1-y_1)) \\
&= rx_1(1-x_1) - rx_1(1-x_1+y_1) + ry_1(1-x_1+y_1) \\
&= -rx_1y_1 + ry_1(1-x_1+y_1) .
\end{aligned}
$$

Neglecting the term $\sim y_1^2$ we obtain

$$y_2 = -rx_1y_1 + ry_1(1-x_1) = r(1-2x_1)y_1 \equiv \epsilon y_1 .$$

For $|\epsilon| < 1$ the map is stable, as two initially different populations close in with time passing. For $|\epsilon| > 1$ they diverge; the map is "chaotic".

Lyapunov Exponents We define via

$$|\epsilon| = e^\lambda$$

the *Lyapunov exponent* $\lambda = \lambda(r)$:

$$\lambda < 0 \Leftrightarrow \text{stability}, \qquad \lambda > 0 \Leftrightarrow \text{instability} .$$

For positive Lyapunov exponents the time development is exponentially sensitive to the initial conditions and shows chaotic features. This is indeed observed in nature, e.g. for populations of reindeer on isolated islands, as well as for the logistic map for $r_\infty < r < 4$, compare Fig. 2.5.

Routes to Chaos The chaotic regime $r_\infty < r < 4$ of the logistic map connects to the regular regime $0 < r < r_\infty$ with increasing period doubling. One speaks of a "route to chaos via period-doubling". The study of chaotic systems is a wide field of research and a series of routes leading from regular to chaotic behavior have been found. Two important alternative routes to chaos are:

– The Intermittency route to chaos.
  The trajectories are almost periodic; they are interdispersed with regimes of irregular behaviour. The occurrence of these irregular bursts increases until the system becomes irregular.
– Ruelle–Takens–Newhouse route to chaos.
  A strange attractor appears in a dissipative system after two (Hopf) bifurcations.

As a function of an external parameter a fixpoint evolves into a limiting cycle (Hopf bifurcation), which then turns into a limiting torus, which subsequently turns into a strange attractor.

2.3 Dissipation and Adaption

In the preceding sections, we discussed deterministic dynamical systems, viz systems for which the time evolution can be computed exactly, at least in principle, once the initial conditions are known. We now turn to "stochastic systems", i.e. dynamical systems that are influenced by noise and fluctuations.

2.3.1 Dissipative Systems and Strange Attractors

Friction and Dissipation Friction plays an important role in real-world systems. One speaks also of "dissipation" since energy is dissipated away by friction in physical systems.

The total energy, however, is conserved in nature and friction then just stands for a transfer process of energy; when energy is transferred from a system we observe, like a car on a motorway with the engine turned off, to a system not under observation, such as the surrounding air. In this case the combined kinetic energy of the car and the thermal energy of the air body is constant; the air heats up a little bit while the car slows down.

The Mathematical Pendulum As an example we consider the damped "mathematical pendulum"

$$\ddot{\phi} + \gamma\dot{\phi} + \omega_0^2 \sin\phi = 0 , \tag{2.15}$$

which describes a pendulum with a rigid bar, capable of turning over completely, with ϕ corresponding to the angle between the bar and the vertical. The mathematical pendulum reduces to the damped harmonic oscillator for small $\phi \approx \sin\phi$, which is damped/critical/overdamped for $\gamma < 2\omega_0$, $\gamma = 2\omega_0$ and $\gamma > 2\omega_0$.

Normal Coordinates Transforming the damped mathematical pendulum Eq. (2.15) to a set of coupled first-order differential equations via $x = \phi$ and $\dot{\phi} = y$ one gets

$$\begin{aligned} \dot{x} &= y \\ \dot{y} &= -\gamma y - \omega_0^2 \sin x . \end{aligned} \tag{2.16}$$

The phase space is $x \in \mathbb{R}^2$, with $x = (x, y)$. For all $\gamma > 0$ the motion approaches one of the equivalent global fixpoints $(2\pi n, 0)$ for $t \to \infty$ and $n \in \mathbb{Z}$.

Phase Space Contraction Near an attractor the phase space contracts. We consider a three-dimensional phase space (x, y, x) for illustrational purposes. The quantity
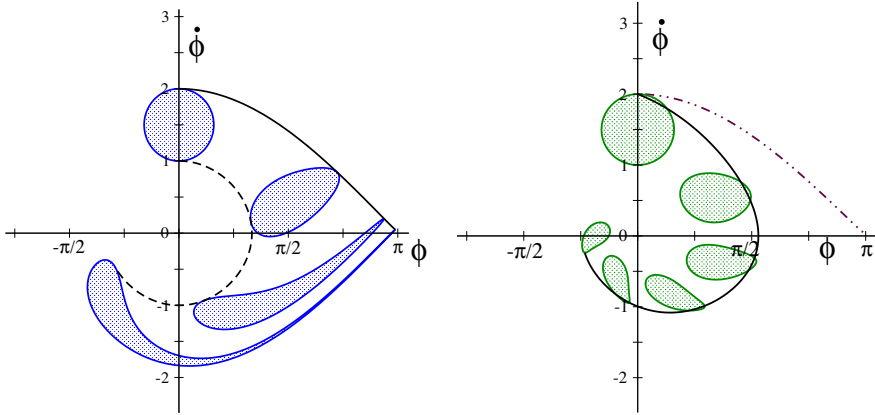
Fig. 2.6 Simulation of the mathematical pendulum $\ddot{\phi} = -\sin(\phi) - \gamma\dot{\phi}$. The *shaded regions* illustrate the evolution of the phase space volume for consecutive times, starting with $t = 0$ (top). *Left*: Dissipationless case $\gamma = 0$. The energy $E = \dot{\phi}^2/2 - \cos(\phi)$ is conserved as well as the phase space volume (Liouville's theorem). The *solid/dashed lines* are the trajectories for $E = 1$ and $E = -0.5$, respectively. *Right*: Case $\gamma = 0.4$. Note the contraction of the phase space volume

$$\Delta V(t) = \Delta x(t)\Delta y(t)\Delta y(t) = (x(t) - x'(t))(y(t) - y'(t))(y(t) - y'(t))$$

corresponds to a small volume of phase space. Its time evolution is given by

$$\frac{\mathrm{d}}{\mathrm{d}t}\Delta V = \Delta\dot{x}\Delta y\Delta y + \Delta x\Delta\dot{y}\Delta y + \Delta x\Delta y\Delta\dot{y},$$

or

$$\frac{\Delta\dot{V}}{\Delta x\Delta y\Delta z} = \frac{\Delta\dot{x}}{\Delta x} + \frac{\Delta\dot{y}}{\Delta y} + \frac{\Delta\dot{y}}{\Delta y} = \nabla\cdot\dot{\boldsymbol{x}}. \tag{2.17}$$

The time evolution of the phase space is illustrated in Fig. 2.6 for the case of the mathematical pendulum. An initially simply connected volume of the phase space thus remains under the effect of time evolution, but it might undergo substantial deformations.

> *Dissipative and Conserving Systems.*   *A dynamical system is dissipative, if its phase space volume contracts continuously, $\nabla\cdot\dot{\boldsymbol{x}} < 0$, for all $\boldsymbol{x}(t)$. The system is said to be conserving if the phase space volume is a constant of motion, viz if $\nabla\cdot\dot{\boldsymbol{x}} \equiv 0$.*

Mechanical systems, i.e. systems described by Hamiltonian mechanics, are all conserving in the above sense. One denotes this result from classical mechanics as "Liouville's theorem".

Mechanical systems in general have bounded and non-bounded orbits, depending on the energy. The planets run through bounded orbits around the sun, to give an

example, but some comets leave the solar system for ever on unbounded trajectories. One can easily deduce from Liouville's theorem, i.e. from phase space conservation, that bounded orbits are ergodic. This comes arbitrarily close to every point in phase space having the identical conserved energy.

Examples Dissipative systems are a special class of dynamical systems. Let us consider a few examples:

– For the damped mathematical pendulum Eq. (2.16) we find

$$\frac{\partial \dot{x}}{\partial x} = 0, \qquad \frac{\partial \dot{y}}{\partial y} = \frac{\partial[-\gamma y - \omega_0^2 \sin x]}{\partial y} = -\gamma \qquad \nabla \cdot \dot{x} = -\gamma < 0 .$$

The damped harmonic oscillator is consequently dissipative. It has a single fix-point $(0,0)$ and the basis of attraction is the full phase space (modulo 2π). Some examples of trajectories and phase space evolution are illustrated in Fig. 2.6.

– For the non-linear rotator defined by Eq. (2.2) we have

$$\frac{\partial \dot{r}}{\partial r} + \frac{\partial \dot{\varphi}}{\partial \varphi} = \Gamma - 3r^2 = \begin{cases} < 0 \text{ for } \Gamma < 0 \\ < 0 \text{ for } \Gamma > 0 \text{ and } r > r_c/\sqrt{3} \\ > 0 \text{ for } \Gamma > 0 \text{ and } 0 < r < r_c/\sqrt{3} \end{cases} , \qquad (2.18)$$

where $r_c = \sqrt{\Gamma}$ is the radius of the limiting cycle when $\Gamma > 0$. The system might either dissipate or take up energy, which is typical behavior of "adaptive systems" as we will discuss further in Sect. 2.3.2. Note that the phase space contracts both close to the fixpoint, for $\Gamma < 0$, and close to the limiting cycle, for $\Gamma > 0$.

Phase Space Contraction and Coordinate Systems The time development of a small phase space volume, Eq. 2.17, depends on the coordinate system chosen to represent the variables. As an example we reconsider the non-linear rotator defined by Eq. (2.2) in terms of the Cartesian coordinates $x = r\cos\varphi$ and $y = r\sin\varphi$.

The respective infinitesimal phase space volumes are related via the Jacobian,

$$\mathrm{d}x\,\mathrm{d}y = r\,\mathrm{d}r\,\mathrm{d}\varphi ,$$

and we find

$$\frac{\Delta \dot{V}}{\Delta V} = \frac{\dot{r}\Delta r\Delta\varphi + r\dot{\Delta r}\Delta\varphi + r\Delta r\dot{\Delta\varphi}}{r\Delta r\Delta\varphi} = \frac{\dot{r}}{r} + \frac{\partial \dot{r}}{\partial r} + \frac{\partial \dot{\varphi}}{\partial \varphi} = 2\Gamma - 4r^2 ,$$

compare Eqs. (2.2) and (2.18). The amount and even the sign of the phase space contraction can depend on the choice of the coordinate system.

The Lorenz Model A rather natural question is the possible existence of attractors with less regular behaviors, i.e. which are different from stable fixpoints, periodic or quasi-periodic motion. For this question we examine the Lorenz model

$$\frac{\mathrm{d}x}{\mathrm{d}t} = -\sigma(x - y),$$

$$\frac{dy}{dt} = -xz + rx - y, \tag{2.19}$$

$$\frac{dz}{dt} = xy - bz .$$

The classical values are $\sigma = 10$ and $b = 8/3$, with r being the control variable.

Fixpoints of the Lorenz Model A trivial fixpoint is $(0,0,0)$. The non-trivial fixpoints are

$$\begin{aligned} 0 &= -\sigma(x-y), & x &= y, \\ 0 &= -xz + rx - y, & z &= r-1, \\ 0 &= xy - bz, & x^2 &= y^2 = b(r-1) . \end{aligned}$$

It is easy to see by linear analysis that the fixpoint $(0,0,0)$ is stable for $r < 1$. For $r > 1$ it becomes unstable and two new fixpoints appear:

$$C_{+,-} = \left(\pm\sqrt{b(r-1)}, \pm\sqrt{b(r-1)}, r-1 \right) . \tag{2.20}$$

These are stable for $r < r_c = 24.74$ ($\sigma = 10$ and $b = 8/3$). For $r > r_c$ the behavior becomes more complicated and generally non-periodic.

Strange Attractors One can show, that the Lorenz model has positive Lyapunov exponents for $r > r_c$. It is chaotic with sensitive dependence on the initial conditions. The Lorenz model is at the same time dissipative, since

$$\frac{\partial \dot{x}}{\partial x} + \frac{\partial \dot{y}}{\partial y} + \frac{\partial \dot{z}}{\partial z} = -(\sigma + 1 + b) < 0, \qquad \sigma > 0, \ b > 0 . \tag{2.21}$$

The attractor of the Lorenz system therefore cannot be a smooth surface. Close to the attractor the phase space contracts. At the same time two nearby orbits are repelled due to the positive Lyapunov exponents. One finds a self-similar structure for the Lorenz attractor with a fractal dimension 2.06 ± 0.01. Such a structure is called a *strange attractor*.

   The Lorenz model has an important historical relevance in the development of chaos theory and is now considered a paradigmatic example of a chaotic system.

Fractals Self-similar structures are called fractals. Fractals can be defined by recurrent geometric rules; examples are the Sierpinski triangle and carpet (see Fig. 2.7) and the Cantor set. Strange attractors are normally *multifractals*, i.e. fractals with non-uniform self-similarity.

The Hausdorff Dimension An important notion in the theory of fractals is the "Hausdorff dimension". We consider a geometric structure defined by a set of points in d dimensions and the number $N(l)$ of d-dimensional spheres of diameter l needed to cover this set. If $N(l)$ scales like

$$N(l) \ \propto \ l^{-D_H}, \qquad \text{for} \qquad l \rightarrow 0 , \tag{2.22}$$
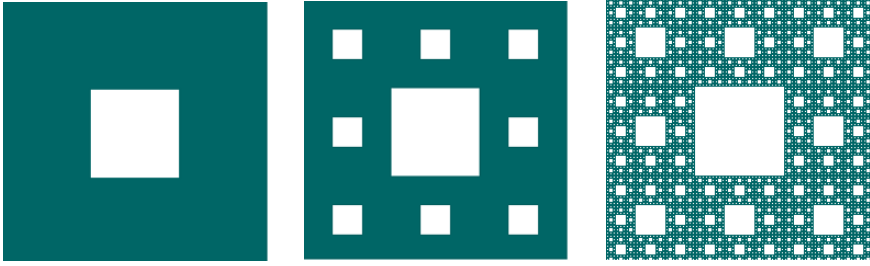
Fig. 2.7 The Sierpinski carpet and its iterative construction

then D_H is called the Hausdorff dimension of the set. Alternatively we can rewrite Eq. (2.22) as

$$\frac{N(l)}{N(l')} = \left(\frac{l}{l'}\right)^{-D_H}, \qquad D_H = -\frac{\log[N(l)/N(l')]}{\log[l/l']}, \qquad (2.23)$$

which is useful for self-similar structures (fractals).

The d-dimensional spheres necessary to cover a given geometrical structure will generally overlap. The overlap does not affect the value of the fractal dimension as long as the degree of overlap does not change qualitatively with decreasing diameter l.

The Hausdorff Dimension of the Sierpinski Carpet For the Sierpinski carpet we increase the number of points $N(l)$ by a factor of 8, compare Fig. 2.8, when we decrease the length scale l by a factor of 3 (see Fig. 2.7):

$$D_H \rightarrow -\frac{\log[8/1]}{\log[1/3]} = \frac{\log 8}{\log 3} \approx 1.8928.$$

2.3.2 Adaptive Systems

Adaptive Systems A general complex system is neither fully conserving nor fully dissipative. Adaptive systems will have periods where they take up energy and periods where they give energy back to the environment. An example is the non-linear rotator of Eq. (2.2), see also Eq. (2.18).

In general one affiliates with the term "adaptive system" the notion of complexity and adaption. Strictly speaking any dynamical system is adaptive if $\nabla \cdot \dot{x}$ may take both positive and negative values. In practice, however, it is usual to reserve the term adaptive system to dynamical systems showing a certain complexity, such as emerging behavior.

The Van der Pol Oscillator Circuits or mechanisms built for the purpose of controlling an engine or machine are intrinsically adaptive. An example is the van der Pol oscillator,
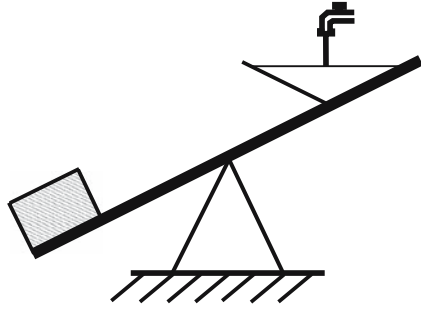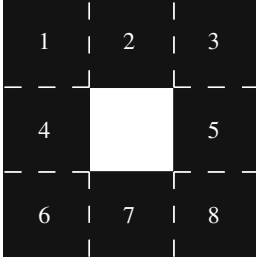
Fig. 2.8 *Left*: The fundamental unit of the Sierpinski carpet, compare Fig. 2.7, contains eight squares that can be covered by discs of an appropriate diameter. *Right*: The seesaw with a water container at one end; an example of an oscillator that takes up/disperses takes up/disperses energy periodically

$$\ddot{x} - \epsilon(1-x^2)\dot{x} + x = 0, \qquad \begin{aligned} \dot{x} &= y \\ \dot{y} &= \epsilon(1-x^2)y - x \end{aligned} \qquad (2.24)$$

where $\epsilon > 0$ and where we have used the phase space variables $\boldsymbol{x} = (x,y)$. We evaluate the time evolution $\nabla \cdot \dot{\boldsymbol{x}}$ of the phasespace volume,

$$\nabla \cdot \dot{\boldsymbol{x}} = +\epsilon(1-x^2) .$$

The oscillator takes up/dissipates energy for $x^2 < 1$ and $x^2 > 1$, respectively. A simple mechanical example for a system with similar properties is illustrated in Fig. 2.8

Secular Perturbation Theory We consider a perturbation expansion in ϵ. The solution of Eq. (2.24) is

$$x_0(t) = a e^{i(\omega_0 t + \phi)} + c.c., \qquad \omega_0 = 1 , \qquad (2.25)$$

for $\epsilon = 0$. We note that the amplitude a and phase ϕ are arbitrary in Eq. (2.25). The perturbation $\epsilon(1-x^2)\dot{x}$ might change, in principle, also the given frequency $\omega_0 = 1$ by an amount $\propto \epsilon$. In order to account for this "secular perturbation" we make the ansatz

$$x(t) = \left[A(T)e^{it} + A^*(T)e^{-it}\right] + \epsilon x_1 + \cdots, \qquad A(T) = A(\epsilon t) , \qquad (2.26)$$

which differs from the usual expansion $x(t) \rightarrow x_0(t) + \epsilon x'(t) + \cdots$ of the full solution $x(t)$ of a dynamical system with respect to a small parameter ϵ.

Expansion From Eq. (2.26) we find to the order $O(\epsilon^1)$

$$x^2 \approx A^2 e^{2it} + 2|A|^2 + (A^*)^2 e^{-2it} + 2\epsilon x_1 \left[A e^{it} + A e^{-it}\right]$$

$$\epsilon(1-x^2) \approx \epsilon(1-2|A|^2) - \epsilon \left[A^2 e^{2it} + (A^*)^2 e^{-2it}\right] \,,$$

$$\dot{x} \approx \left[(\epsilon A_T + iA)\, e^{it} + c.c.\right] + \epsilon \dot{x}_1, \qquad A_T = \frac{\partial A(T)}{\partial T}$$

$$\epsilon(1-x^2)\dot{x} = \epsilon(1-2|A|^2) \left[iAe^{it} - iA^* e^{-it}\right]$$
$$- \epsilon \left[A^2 e^{2it} + (A^*)^2 e^{-2it}\right] \left[iAe^{it} - iA^* e^{-it}\right]$$

and

$$\ddot{x} = \left[\left(\epsilon^2 A_{TT} + 2i\epsilon A_T - A\right) e^{it} + c.c.\right] + \epsilon \ddot{x}_1$$
$$\approx \left[(2i\epsilon A_T - A)\, e^{it} + c.c.\right] + \epsilon \ddot{x}_1 \,.$$

Substituting these expressions into Eq. (2.24) we obtain in the order $O(\epsilon^1)$

$$\ddot{x}_1 + x_1 = \left(-2iA_T + iA - i|A|^2 A\right) e^{it} - iA^3 e^{3it} + c.c. \qquad (2.27)$$

The Solvability Condition Equation (2.27) is identical to a driven harmonic oscillator, which will be discussed in the chapter "Synchronization Phenomena" in more detail. The time dependencies

$$\sim e^{it} \qquad \text{and} \qquad \sim e^{3it}$$

of the two terms on the right-hand side of Eq. (2.27) are proportional to the unperturbed frequency $\omega_0 = 1$ and to $3\omega_0$, respectively.

The term $\sim e^{it}$ is therefore exactly at resonance and would induce a diverging response $x_1 \to \infty$, in contradiction to the perturbative assumption made by ansatz (2.26). Its prefactor must therefore vanish:

$$A_T = \frac{\partial A}{\partial T} = \frac{1}{2}\left(1-|A|^2\right) A, \qquad \frac{\partial A}{\partial t} = \frac{\epsilon}{2}\left(1-|A|^2\right) A \,, \qquad (2.28)$$

where we have used $T = \epsilon t$. The solubility condition Eq. (2.28) can be written as

$$\dot{a}e^{i\phi} + i\dot{\phi}\, a e^{i\phi} = \frac{\epsilon}{2}\left(1-a^2\right) a e^{i\phi}$$

in phase-magnitude representation $A(t) = a(t)e^{i\phi(t)}$, or

$$\dot{a} = \epsilon \left(1-a^2\right) a/2,$$
$$\dot{\phi} \sim O(\epsilon^2) \,. \qquad (2.29)$$

The system takes up energy for $a < 1$ and the amplitude a increases until the saturation limit $a \to 1$, the conserving point. For $a > 1$ the system dissipates energy to the environment and the amplitude a decreases, approaching unity for $t \to \infty$, just as we discussed in connection with Eq. (2.2).
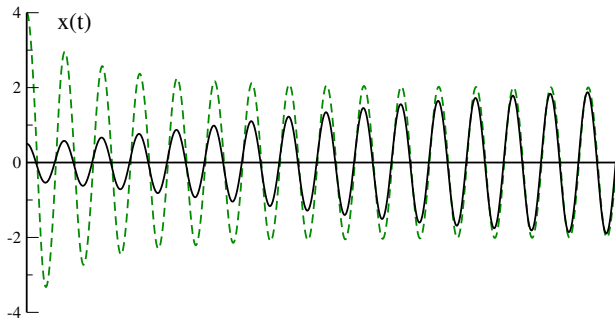
Fig. 2.9 The solution of the van der Pol oscillator, Eq. (2.24), for small ϵ and two different initial conditions. Note the self-generated amplitude stabilization

The solution $x(t) \approx 2a\cos(t)$, compare Eqs. (2.26) and (2.29), of the van der Pol equations therefore constitutes an amplitude-regulated oscillation, as illustrated in Fig. 2.9. This behavior was the technical reason for historical development of the control systems that are described by the van der Pol equation (2.24).

Liénard Variables For large ϵ it is convenient to define, compare Eq. (2.24), with

$$\epsilon \frac{\mathrm{d}}{\mathrm{d}t} Y(t) = \ddot{x}(t) - \epsilon \left(1 - x^2(t)\right) \dot{x}(t) = -x(t) \tag{2.30}$$

or

$$\epsilon \dot{Y} = \ddot{X} - \epsilon \left(1 - X^2\right) \dot{X}, \qquad X(t) = x(t),$$

the Liénard variables $X(t)$ and $Y(t)$. Integration of $\dot{Y}$ with respect to t yields

$$\epsilon Y = \dot{X} - \epsilon \left(X - \frac{X^3}{3}\right) ,$$

where we have set the integration constant to zero. We obtain, together with Eq. (2.30),

$$\begin{aligned} \dot{X} &= c\left(Y - f(X)\right) \\ \dot{Y} &= -X/c \end{aligned} \qquad f(X) = X^3/3 - X , \tag{2.31}$$

where we have set $c \equiv \epsilon$, as we are now interested in the case $c \gg 1$.

Relaxation Oscillations We discuss the solution of the van der Pol oscillator Eq. (2.31) for a large driving c graphically, compare Fig. 2.10, by considering the flow $(\dot{X}, \dot{Y})$ in phase space (X, Y). For $c \gg 1$ there is a separation of time scales,

$$(\dot{X}, \dot{Y}) \sim (c, 1/c), \qquad \dot{X} \gg \dot{Y} ,$$

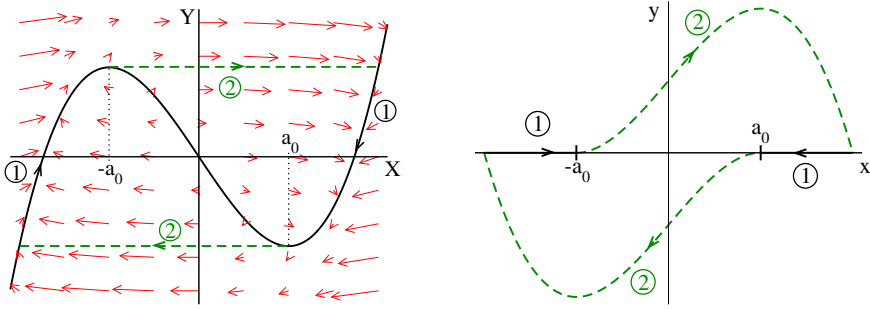which leads to the following dynamical behavior:

Fig. 2.10 Van der Pol oscillator for a large driving $c \equiv \epsilon$. *Left*: The relaxation oscillations with respect to the Liénard variables Eq. (2.31). The arrows indicate the flow $(\dot{X}, \dot{Y})$, for $c = 3$, see Eq. (2.31). Also shown is the $\dot{X} = 0$ isocline $Y = -X + X^3/3$ (*solid line*) and the limiting cycle, which includes the *dashed line with an arrow* and part of the isocline. *Right*: The limiting cycle in terms of the original variables $(x, y) = (x, \dot{x}) = (x, v)$. Note that $X(t) = x(t)$

– Starting at a general $(X(t_0), Y(t_0))$ the orbit develops very fast $\sim c$ and nearly horizontally until it hits the "isocline"[1]

$$\dot{X} = 0, \qquad Y = f(X) = -X + X^3/3 . \qquad (2.32)$$

– Once the orbit is close to the $\dot{X} = 0$ isocline $Y = -X + X^3/3$ the motion slows down and it develops slowly, with a velocity $\sim 1/c$ close-to (but not exactly on) the isocline (Eq. (2.32)).
– Once the slow motion reaches one of the two local extrema of the isocline it cannot follow the isocline any more and makes a rapid transition with $Y \approx$ const. until it hits the other branch of the $\dot{X} = 0$ isocline.

The orbit therefore relaxes rapidly towards a limiting oscillatory trajectory, illustrated in Fig. 2.10, with the time needed to perform a whole oscillation depending on the relaxation constant c; therefore the term "relaxation oscillation". We will discuss relaxation oscillators further in the chapter "Synchronization Phenomena".

2.4 Diffusion and Transport

Deterministic vs. Stochastic Time Evolution So far we have discussed some concepts and examples of deterministic dynamical systems, governed by sets of coupled differential equations without noise or randomness. At the other extreme are diffusion processes for which the random process dominates the dynamics.

Dissemination of information through social networks is one of many examples where diffusion processes plays a paramount role. The simplest model of diffusion

---

[1] The term isocline stands for "equal slope" in ancient Greek.

is the Brownian motion, which is the erratic movement of grains suspended in liquid observed by the botanist Robert Brown as early as 1827. Brownian motion became the prototypical example of a stochastic process after the seminal works of Einstein and Langevin at the beginning of the 20th century.

2.4.1 Random Walks, Diffusion and Lévy Flights

One-Dimensional Diffusion We consider the random walk of a particle along a line, with the equal probability $1/2$ to move left/right at every time step. The probability

$$p_t(x), \qquad x = 0, \pm 1, \pm 2, \ldots, \qquad t = 0, 1, 2, \ldots$$

to find the particle at time t at position x obeys the master equation

$$p_{t+1}(x) \;=\; \frac{1}{2}\,p_t(x-1) + \frac{1}{2}\,p_t(x+1) \,. \tag{2.33}$$

In order to obtain the limit of continuous time and space, we introduce explicitly the steps Δx and Δt in space and time, and write

$$\frac{p_{t+\Delta t}(x) - p_t(x)}{\Delta t} \;=\; \frac{(\Delta x)^2}{2\Delta t}\,\frac{p_t(x+\Delta x) + p_t(x-\Delta x) - 2p_t(x)}{(\Delta x)^2}\,. \tag{2.34}$$

Now, taking the limit $\Delta x, \Delta t \to 0$ in such a way that $(\Delta x)^2/(2\Delta t)$ remains finite, we obtain the diffusion equation

$$\frac{\partial p(x,t)}{\partial t} \;=\; D\,\frac{\partial^2 p(x,t)}{\partial x^2} \qquad D = \frac{(\Delta x)^2}{2\Delta t}\,. \tag{2.35}$$

Solution of the Diffusion Equation The solution to Eq. (2.35) is readily obtained as[2]

$$p(x,t) \;=\; \frac{1}{\sqrt{4\pi Dt}}\,\exp\!\left(-\frac{x^2}{4Dt}\right), \qquad \int_{-\infty}^{\infty} dx\,\rho(x,t) \;=\; 1\,. \tag{2.36}$$

From Eq. (2.36) one concludes that the variance of the displacement follows diffusive behavior, i.e.

$$\langle x^2(t)\rangle \;=\; 2Dt\,, \qquad \bar{x} \;=\; \sqrt{\langle x^2(t)\rangle} \;=\; \sqrt{2Dt}\,. \tag{2.37}$$

Diffusive transport is characterized by transport sublinear in time in contrast to ballistic transport with $x = vt$, as illustrated in Fig. 2.11.

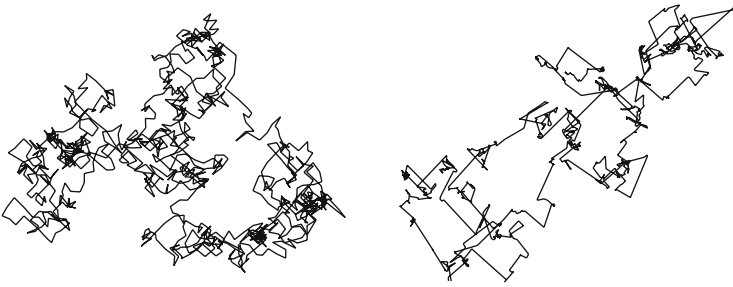[2] Note: $\int e^{-x^2/a}\,dx = \sqrt{a\pi}$.

Fig. 2.11 Examples of random walkers with scale-free distributions $\sim |\Delta x|^{1+\beta}$ for the real-space jumps, see Eq. (2.38). *Left*: $\beta = 3$, which falls into the universality class of standard Brownian motion. *Right*: $\beta = 0.5$, a typical Levy flight. Note the occurrence of longer-ranged jumps in conjunction with local walking

Lévy Flights We can generalize the concept of a random walker, which is at the basis of ordinary diffusion, and consider a random walk with distributions $p(\Delta t)$ and $p(\Delta x)$ for waiting times Δt_i and jumps Δx_i, at every step $i = 1, 2, \ldots$ of the walk, as illustrated in Fig. 2.12. One may assume scale-free distributions

$$p(\Delta t) \sim \frac{1}{(\Delta t)^{1+\alpha}}, \qquad p(\Delta x) \sim \frac{1}{(\Delta x)^{1+\beta}}, \qquad \alpha, \beta > 0 . \qquad (2.38)$$

If $\alpha > 1$ (finite mean waiting time) and $\beta > 2$ (finite variance), nothing special happens. In this case the central limiting theorem for well behaved distribution functions is valid for the spatial component and one obtains standard Brownian diffusion. Relaxing the above conditions one finds four regimes: normal Brownian diffusion, "Lévy flights", fractional Brownian motion, also denoted "subdiffusion" and generalized Lévy flights termed "ambivalent processes". Their respective scaling laws are listed in Table 2.1 and two examples are shown in Fig. 2.11.

Lévy flights occur in a wide range of processes, such as in the flight patterns of wandering albatrosses or in human travel habits, which seem to be characterized by a generalized Lévy flight with $\alpha, \beta \approx 0.6$.

Diffusion of Information Within Networks Diffusion occurs in many circumstances. Let us consider here the diffusion of information through a social network. This is an interesting issue as the control of information is an important aspect of social influence and prestige.

Table 2.1 The four regimes of a generalized walker with distribution functions, Eq. (2.38), characterized by scalings $\propto (\Delta t)^{-1-\alpha}$ and $\propto (\Delta x)^{-1-\beta}$ for the waiting times Δt and jumps Δx, as depicted in Fig. 2.12

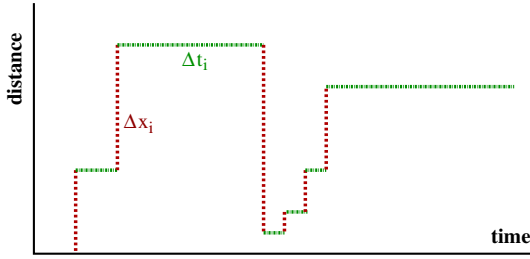|			
$\alpha > 1$	$\beta > 2$	$\bar{x} \sim \sqrt{t}$	Ordinary diffusion
$\alpha > 1$	$0 < \beta < 2$	$\bar{x} \sim t^{1/\beta}$	Lévy flights
$0 < \alpha < 1$	$\beta > 2$	$\bar{x} \sim t^{\alpha/2}$	Subdiffusion
$0 < \alpha < 1$	$0 < \beta < 2$	$\bar{x} \sim t^{\alpha/\beta}$	Ambivalent processes

Fig. 2.12 A random walker with distributed waiting times Δt_i and jumps Δx_i may become a generalized Lévy flight

Consider a network of $i = 1, \ldots, N$ vertices connected by edges with weight W_{ij}, corresponding to the elements of the weighted adjacency matrix. We denote by

$$\rho_i(t), \qquad \sum_{i=1}^{N} \rho_i(t) = 1$$

the density of information present at time t and vertex i.

Flow of Information The information flow can then be described by the master equation

$$\rho_i(t+1) = \rho_i(t) + J_i^{(+)}(t)\Delta t - J_i^{(-)}(t)\Delta t , \qquad (2.39)$$

where $J_i^{(\pm)}(t)$ denotes the density of information entering $(+)$ and leaving $(-)$ vertex i per time interval Δt, given by

$$J_i^{(+)}(t) = \sum_j \frac{W_{ij}}{\sum_k W_{kj}} \rho_j(t), \qquad J_i^{(-)}(t) = \sum_j \frac{W_{ji}}{\sum_k W_{ki}} \rho_i(t) = \rho_i(t) .$$

Introducing the time step $\Delta t = 1$ and the expressions for $J_i^{(\pm)}(t)$ into Eq. (2.39) we find

$$\frac{\rho_i(t+\Delta t) - \rho_i(t)}{\Delta t} = \frac{\partial}{\partial t} \rho_i(t) = \sum_j T_{ij} \rho_j(t) - \rho_i(t) , \qquad (2.40)$$

where we have performed the limit $\Delta t \to 0$ and defined

$$T_{ij} = \frac{W_{ij}}{\sum_k W_{kj}} .$$

This equation can easily be cast into the following matrix form:

$$\frac{\partial}{\partial t} \rho(t) = \mathbf{D} \rho(t), \qquad D_{ij} = T_{ij} - \delta_{ij} , \qquad (2.41)$$

where $\rho = (\rho_1, \ldots, \rho_N)$. It resembles the diffusion equation (2.34), so we may denote $\mathbf{D} = (D_{ij})$ as the diffusion matrix (or operator). Physically, Eq. (2.40) means

that $\mathbf{T} = (T_{ij})$ transfers (propagates) the energy density $\rho(t)$ one step forward in time. Due to this property, $\mathbf{T}$ has been termed the "transfer matrix".

The Stationary State When no new information is created we may expect the distribution of information to settle into a stationary state

$$\frac{\partial \rho_i(t)}{\partial t} \to 0, \qquad \rho_i(t) \to \rho_i(\infty) .$$

Formally, the stationary state corresponds to the unitary eigenvalue of $\mathbf{T}$, see Eq. (2.40). Here we assume

$$\rho_i(\infty) \propto \sum_j W_{ji} , \tag{2.42}$$

in Eq. (2.40):

$$\sum_j \frac{W_{ij}}{\sum_k W_{kj}} \sum_k W_{kj} = \sum_l W_{li}, \qquad \sum_j W_{ij} = \sum_l W_{li} . \tag{2.43}$$

Consequently, a global steady state has the form of the ansatz (2.42) when the weight of incoming links $\sum_j W_{ij}$ equals the weight of outgoing links $\sum_l W_{li}$ for every vertex i. That is if there are no sinks or sources for information. The condition Eq. (2.43) is fulfilled for symmetric weight matrices with $W_{ij} = W_{ji}$.

2.4.2 The Langevin Equation and Diffusion

Diffusion as a Stochastic Process Langevin proposed to describe the diffusion of a particle by the stochastic differential equation

$$m\dot{v} = -m\gamma v + \xi(t), \qquad < \xi(t) >= 0, \qquad < \xi(t)\xi(t') >= Q\delta(t - t'), \tag{2.44}$$

where $v(t)$ is the velocity of the particle and $m > 0$ its mass.

(i)   The term $-m\gamma v$ on the right-hand-side of Eq. (2.44) corresponds to a damping term, the friction being proportional to $\gamma > 0$.

(ii) $\xi(t)$ is a stochastic variable, viz noise. The brackets $< \ldots >$ denote ensemble averages, i.e. averages over different noise realizations.

(iii) As *white noise* (in contrast to *colored noise*) one denotes noise with a flat power spectrum (as white light), viz $< \xi(t)\xi(t') > \propto \delta(t - t')$.

(iv) The constant Q is a measure for the strength of the noise.

Solution of the Langevin Equation Considering a specific noise realization $\xi(t)$, one finds

$$v(t) = v_0 e^{-\gamma t} + \frac{e^{-\gamma t}}{m} \int_0^t dt'\, e^{\gamma t'} \xi(t') \tag{2.45}$$

for the solution of the Langevin Eq. (2.44), where $v_0 \equiv v(0)$.

Mean Velocity For the ensemble average $< v(t) >$ of the velocity one finds

$$< v(t) > = v_0\, e^{-\gamma t} + \frac{e^{-\gamma t}}{m} \int_0^t dt'\, e^{\gamma t'} \underbrace{< \xi(t') >}_{0} = v_0\, e^{-\gamma t} \,. \tag{2.46}$$

The average velocity decays exponentially to zero.

Mean Square Velocity For the ensemble average $< v^2(t) >$ of the velocity squared one finds

$$\begin{aligned}
< v^2(t) > &= v_0^2 e^{-2\gamma t} + \frac{2 v_0\, e^{-2\gamma t}}{m} \int_0^t dt'\, e^{\gamma t'} \underbrace{< \xi(t') >}_{0} \\[2mm]
&+ \frac{e^{-2\gamma t}}{m^2} \int_0^t dt' \int_0^t dt''\, e^{\gamma t'}\, e^{\gamma t''} \underbrace{< \xi(t')\xi(t'') >}_{Q\,\delta(t'-t'')} \\[2mm]
&= v_0^2 e^{-2\gamma t} + \frac{Q\, e^{-2\gamma t}}{m^2} \underbrace{\int_0^t dt'\, e^{2\gamma t'}}_{(e^{2\gamma t}-1)/(2\gamma)}
\end{aligned}$$

and finally

$$< v^2(t) > = v_0^2 e^{-2\gamma t} + \frac{Q}{2\gamma m^2}\left(1 - e^{-2\gamma t}\right) \,. \tag{2.47}$$

For long times the average squared velocity

$$\lim_{t\to\infty} < v^2(t) > = \frac{Q}{2\gamma m^2} \tag{2.48}$$

becomes, as expected, independent of the initial velocity v_0. Equation (2.48) shows explicitly that the dynamics is driven exclusively by the stochastic process $\propto Q$ for long time scales.

The Langevin Equation and Diffusion The Langevin equation is formulated in terms of the particle velocity. In order to make connection with the time evolution of a real-space random walker, Eq. (2.37), we multiply the Langevin equation (2.44) by x and take the ensemble average:

$$< x\dot{v} > = -\gamma < xv > + \frac{1}{m} < x\xi > \,. \tag{2.49}$$

We note that

$$xv = x\dot{x} = \frac{d}{dt}\frac{x^2}{2}, \qquad x\dot{v} = x\ddot{x} = \frac{d^2}{dt^2}\frac{x^2}{2} - \dot{x}^2, \qquad < x\xi > = x < \xi > = 0 \,.$$

We then find for Eq. (2.49)

$$\frac{d^2}{dt^2}\frac{<x^2>}{2} - <v^2> = -\gamma\frac{d}{dt}\frac{<x^2>}{2}$$

or

$$\frac{d^2}{dt^2}<x^2> + \gamma\frac{d}{dt}<x^2> = 2<v^2> = \frac{Q}{\gamma m^2}, \tag{2.50}$$

where we have used the long-time result Eq. (2.48) for $<v^2>$. The solution of Eq. (2.50) is

$$<x^2> = \left[\gamma t - 1 + e^{-\gamma t}\right]\frac{Q}{\gamma^3 m^2}. \tag{2.51}$$

For long times we find

$$\lim_{t\to\infty} <x^2> = \frac{Q}{\gamma^2 m^2}t \equiv 2Dt, \qquad D = \frac{Q}{2\gamma^2 m^2} \tag{2.52}$$

diffusive behavior, compare Eq. (2.37). This shows that diffusion is microscopically due to a stochastic process, since $D \propto Q$.

2.5 Noise-Controlled Dynamics

Stochastic Systems A set of first-order differential equations with a stochastic term is generally denoted a "stochastic system". The Langevin equation (2.44) discussed in Sect. 2.4.2 is a prominent example. The stochastic term corresponds quite generally to noise. Depending on the circumstances, noise might be very important for the long-term dynamical behavior. Some examples of this are as follows:

– Neural Networks: Networks of interacting neurons are responsible for the cognitive information processing in the brain. They must remain functional also in the presence of noise and need to be stable as stochastic systems. In this case the introduction of a noise term to the evolution equation should not change the dynamics qualitatively. This postulate should be valid for the vast majorities of biological networks.
– Diffusion: The Langevin equation reduces, in the absence of noise, to a damped motion without an external driving force, with $v = 0$ acting as a global attractor. The stochastic term is therefore essential in the long-time limit, leading to diffusive behavior.
– Stochastic Escape and Stochastic Resonance: A particle trapped in a local minimum may escape this minimum by a noise-induced diffusion process; a phenomenon called "stochastic escape". Stochastic escape in a driven bistable system leads to an even more subtle consequence of noise-induced dynamics, the "stochastic resonance".

2.5.1 Stochastic Escape

Drift Velocity We generalize the Langevin equation (2.44) and consider an external potential $V(x)$,

$$m\dot{v} = -m\gamma v + F(x) + \xi(t), \qquad F(x) = -V'(x) = -\frac{d}{dx}V(x), \qquad (2.53)$$

where v, m are the velocity and the mass of the particle, $< \xi(t) >= 0$ and $< \xi(t)\xi(t') >= Q\delta(t-t')$. In the absence of damping ($\gamma = 0$) and noise ($Q = 0$), Eq. (2.53) reduces to Newton's law.

We consider for a moment a constant force $F(x) = F$ and the absence of noise, $\xi(t) \equiv 0$. The system then reaches an equilibrium for $t \to \infty$ when relaxation and force cancel each other:

$$m\dot{v}_D = -m\gamma v_D + F \equiv 0, \qquad v_D = \frac{F}{\gamma m}. \qquad (2.54)$$

v_D is called the "drift velocity". A typical example is the motion of electrons in a metallic wire. An applied voltage, which leads an electric field along the wire, induces an electrical current (Ohm's law). This results in the drifting electrons being continuously accelerated by the electrical field, while bumping into lattice imperfections or colliding with the lattice vibrations, i.e. the phonons.

The Fokker-Planck Equation We consider now an ensemble of particles diffusing in an external potential, and denote with $P(x,t)$ the density of particles at location x and time t. Particle number conservation defines the particle current density $J(x,t)$ via the continuity equation

$$\frac{\partial P(x,t)}{\partial t} + \frac{\partial J(x,t)}{\partial x} = 0. \qquad (2.55)$$

There are two contributions, J_{v_D} and J_ξ, to the total particle current density. The particle current density is

$$J_{v_D} = v_D P(x,t)$$

when the particles move uniformly with drift velocity v_D. For the contribution J_ξ of the noise term $\sim \xi(t)$ to the particle current density $J(x,t)$ we remind ourselves of the diffusion equation (2.35)

$$\frac{\partial P(x,t)}{\partial t} = D\frac{\partial^2 P(x,t)}{\partial x^2} \equiv -\frac{\partial J_\xi(x,t)}{\partial x} \qquad J_\xi = -D\frac{\partial P(x,t)}{\partial x}. \qquad (2.56)$$

Rewriting the diffusion equation in the above fashion turns it into a continuity equation and allows us to determine the functional form for J_ξ. Using the relation $D = Q/(2\gamma^2 m^2)$, see Eq. (2.52), and including the drift term we find
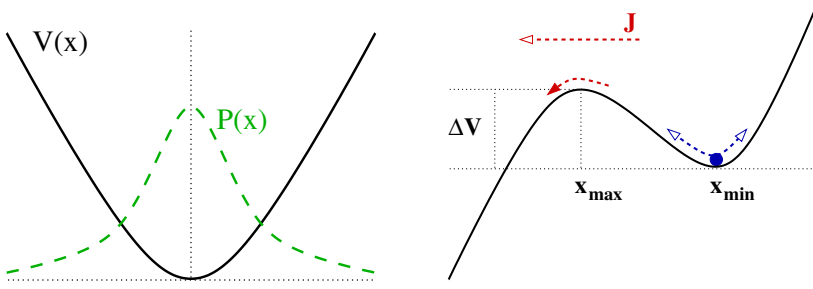
Fig. 2.13 *Left*: Stationary distribution $P(x)$ of diffusing particles in a harmonic potential $V(x)$. *Right*: Stochastic escape from a local minimum, with $\Delta V = V(x_{\max}) - V(x_{\min})$ being the potential barrier height and J the escape current

$$J(x,t) \;=\; v_D P(x,t) - D\frac{\partial P(x,t)}{\partial x} \;=\; \frac{F}{\gamma m} P(x,t) - \frac{Q}{2\gamma^2 m^2}\frac{\partial P(x,t)}{\partial x} \qquad (2.57)$$

for the total current density $J = J_{v_D} + J_\xi$ of diffusing particles. The continuity equation (2.55) together with expression (2.57) for the total particle current density is denoted as the Fokker–Planck or Smoluchowski equation for the density distribution $P(x,t)$.

The Harmonic Potential We consider the harmonic confining potential

$$V(x) \;=\; \frac{f}{2}x^2, \qquad F(x) \;=\; -fx\,,$$

and a stationary density distribution,

$$\frac{\mathrm{d}P(x,t)}{\mathrm{d}t} \;=\; 0 \qquad \Longrightarrow \qquad \frac{\mathrm{d}J(x,t)}{\mathrm{d}x} \;=\; 0\,.$$

Expression (2.57) yields then the differential equation

$$\frac{\mathrm{d}}{\mathrm{d}x}\left[\frac{fx}{\gamma m} + \frac{Q}{2\gamma^2 m^2}\frac{\mathrm{d}}{\mathrm{d}x}\right]P(x) \;=\; 0 \;=\; \frac{\mathrm{d}}{\mathrm{d}x}\left[\beta fx + \frac{\mathrm{d}}{\mathrm{d}x}\right]P(x),$$

with $\beta = 2\gamma m/Q$ and where for the stationary distribution function $P(x) = \lim_{t\to\infty} P(x,t)$. We find

$$\boxed{P(x) \;=\; A e^{-\beta \frac{f}{2}x^2} \;=\; A e^{-\beta V(x)}} \qquad A = \sqrt{\frac{f\gamma m}{\pi Q}}, \qquad (2.58)$$

where the prefactor is determined by the normalization condition $\int \mathrm{d}x P(x) = 1$. The density of diffusing particles in a harmonic trap is Gaussian-distributed, see Fig. 2.13.

The Escape Current We now consider particles in a local minimum, as depicted in Fig. 2.13. Without noise, the particle will oscillate around the local minimum eventually coming to a standstill $x \to x_{\min}$ under the influence of friction.

With noise, the particle will have a small but finite probability

$$\propto e^{-\beta \Delta V}, \qquad \Delta V = V(x_{\max}) - V(x_{\min})$$

to reach the next saddlepoint , where ΔV is the potential difference between the saddlepoint and the local minimum, see Fig. 2.13.

The solution Eq. (2.58) for the stationary particle distribution in an external potential $V(x)$ has a constant total current J, see Eq. (2.57), which depends on the form of the potential. For the case of the harmonic potential the steady state current vanishes.

For the type of potentials relevant for the phenomena of stochastic escape, as illustrated in Fig. 2.13, the steady state current is proportional to the probability a particle has to reach the saddlepoint. The escape current is then

$$J(x,t)\Big|_{x=x_{\max}} \propto e^{-\beta \, [V(x_{\max}) - V(x_{\min})]} \, ,$$

when approximating the functional dependence of $P(x)$ with that valid for the harmonic potential, Eq. (2.58).

Kramer's Escape When the escape current is finite, there is a finite probability per unit of time for the particle to escape the local minima, the *Kramer's escape rate* r_K,

$$r_K = \frac{\omega_{\max} \omega_{\min}}{2\pi \gamma} \exp\left[-\beta \left(V(x_{\max}) - V(x_{\min})\right)\right] , \qquad (2.59)$$

where the prefactors $\omega_{\min} = \sqrt{|V''(x_{\min})|/m}$ and $\omega_{\max} = \sqrt{|V''(x_{\max})|/m}$ can be derived from a more detailed calculation, and where $\beta = 2\gamma m/Q$.

Stochastic Escape in Evolution Stochastic escape occurs in many real-world systems. Noise allows the system to escape from a local minimum where it would otherwise remain stuck for eternity.

As an example, we mention stochastic escape from a local fitness maximum (in evolution fitness is to be maximized) by random mutations that play the role of noise. These issues will be discussed in more detail in Chap. 5.

2.5.2 Stochastic Resonance

The Driven Double-Well Potential We consider diffusive dynamics in a driven double-well potential, see Fig. 2.14,

$$\dot{x} = -V'(x) + A_0 \cos(\Omega t) + \xi(t), \qquad V(x) = -\frac{1}{2}x^2 + \frac{1}{4}x^4 . \qquad (2.60)$$
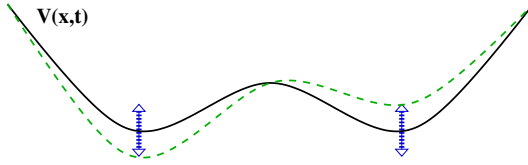
Fig. 2.14 The driven double-well potential, $V(x) - A_0 \cos(\Omega t)x$, compare Eq. (2.60). The driving force is small enough to retain the two local minima

The following is to be remarked:

- Equation (2.60) corresponds to the Langevin equation (2.53) in the limit of very large damping, $\gamma \gg m$, keeping $\gamma m \equiv 1$ constant (in dimensionless units).
- The potential in Eq. (2.60) is in normal form, which one can always achieve by rescaling the variables appropriately.
- The potential $V(x)$ has two minima x_0 at

$$-V'(x) = 0 = x - x^3 = x(1 - x^2), \qquad x_0 = \pm 1 .$$

  The local maximum $x_0 = 0$ is unstable.
- We assume that the periodic driving $\propto A_0$ is small enough, such that the effective potential $V(x) - A_0 \cos(\Omega t)x$ retains two minima at all times, compare Fig. 2.14.

Transient State Dynamics The system will stay close to one of the two minima, $x \approx \pm 1$, for most of the time when both A_0 and the noise strength are weak, see Fig. 2.15. This is an instance of "transient state dynamics", which will be discussed in more detail in Chap. 7. The system switches between a set of preferred states.

Switching Times An important question is then: How often does the system switch between the two preferred states $x \approx 1$ and $x \approx -1$? There are two time scales present:

- In the absence of external driving, $A_0 \equiv 0$, the transitions are noise driven and irregular, with the average switching time given by Kramer's lifetime $T_K = 1/r_K$, see Fig. 2.15. The system is translational invariant with respect to time and the ensemble averaged expectation value

$$< x(t) > = 0$$

  therefore vanishes in the absence of an external force.
- When $A_0 \neq 0$ the external force induces a reference time and a non-zero response $\bar{x}$,

$$< x(t) > = \bar{x} \cos(\Omega t - \bar{\phi}) , \tag{2.61}$$

  which follows the time evolution of the driving potential with a certain phase shift $\bar{\phi}$, see Fig. 2.16.
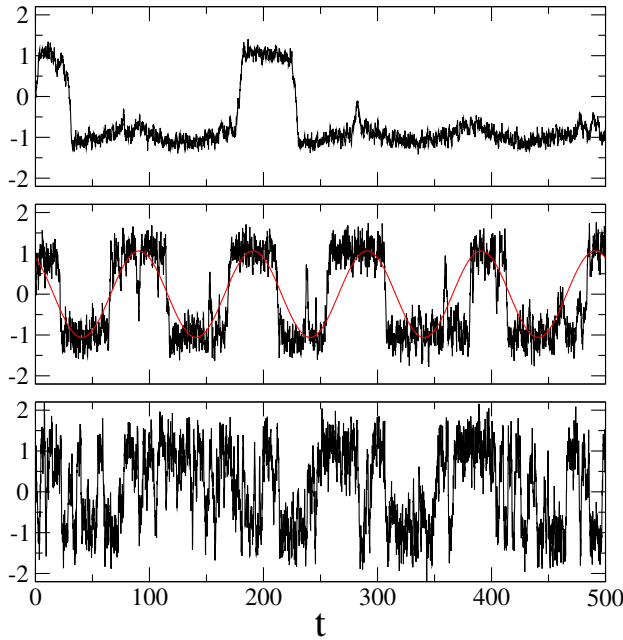
Fig. 2.15 Example trajectories $x(t)$ for the driven double-well potential. The strength and the period of the driving potential are $A_0 = 0.3$ and $2\pi/\Omega = 100$, respectively. The noise level Q is 0.05, 0.3 and 0.8 (*top/middle/bottom*), see Eq. (2.60)

The Resonance Condition When the time scale $2T_K = 2/r_K$ to switch back and forth due to the stochastic process equals the period $2\pi/\Omega$, we expect a large response $\bar{x}$, see Fig. 2.16. The time-scale matching condition

$$\frac{2\pi}{\Omega} \approx \frac{2}{r_K}$$

depends on the noise-level Q, via Eq. (2.59), for the Kramer's escape rate r_K. The response $\bar{x}$ first increases with rising Q and then becomes smaller again, for otherwise constant parameters, see Fig. 2.16. Therefore the name "stochastic resonance".

Stochastic Resonance and the Ice Ages The average temperature T_e of the earth differs by about $\Delta T_e \approx 10°C$ in between a typical ice age and the interglacial periods. Both states of the climate are locally stable.

– The Ice Age: The large ice covering increases the albedo of the earth and a larger part of sunlight is reflected back to space. The earth remains cool.
– The Interglacial Period: The ice covering is small and a larger portion of the sunlight is absorbed by the oceans and land. The earth remains warm.

A parameter of the orbit of the planet earth, the eccentricity, varies slightly with a period $T = 2\pi/\Omega \approx 10^5$ years. The intensity of the incoming radiation from the sun therefore varies with the same period. Long-term climate changes can therefore be modeled by a driven two-state system, i.e. by Eq. (2.60). The driving force, viz the
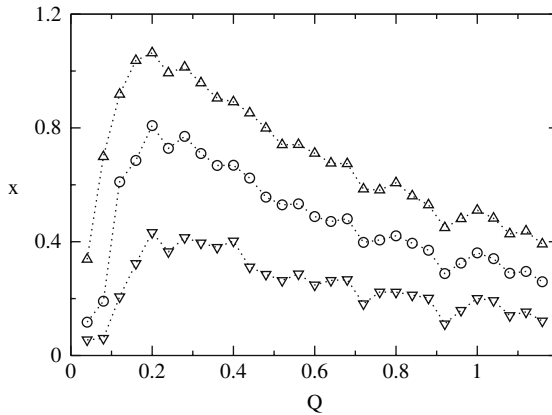
Fig. 2.16 The gain $\bar{x}$, see Eq. (2.61), as a function of noise level Q. The strength of the driving amplitude A_0 is 0.1, 0.2 and 0.3 (*bottom/middle/top* curves), see Eq. (2.60) and the period $2\pi/\Omega = 100$. The response $\bar{x}$ is very small for vanishing noise $Q = 0$, when the system performs only small-amplitude oscillations in one of the local minima

variation of the energy flux the earth receives from the sun, is however very small. The increase in the amount of incident sunlight is too weak to pull the earth out of an ice age into an interglacial period or vice versa. Random climatic fluctuation, like variations in the strength of the gulf stream, are needed to finish the job. The alternation of ice ages with interglacial periods may therefore be modeled as a stochastic resonance phenomenon.

Neural Networks and Stochastic Resonance Neurons are driven bistable devices operating in a noisy environment. It is therefore not surprising that stochastic resonance may play a role for certain neural network setups with undercritical driving.

Exercises

THE LORENZ MODEL

Perform the stability analysis of the fixpoint $(0,0,0)$ and of $C_{+,-} = (\pm\sqrt{b(r-1)}, \pm\sqrt{b(r-1)}, r-1)$ for the Lorenz model Eq. (2.19) with $r, b > 0$. Discuss the difference between the dissipative case and the ergodic case $\sigma = -1 - b$, see Eq. (2.21).

THE POINCARÉ MAP

For the Lorenz model Eq. (2.19) with $\sigma = 10$ and $\beta = 8/3$, evaluate numerically the Poincaré map for (a) $r = 22$ (regular regime) and the plane $z = 21$ and (b) $r = 28$ (chaotic regime) and the plane $z = 27$.

THE HAUSDORFF DIMENSION

Calculate the Hausdorff dimension of a straight line and of the Cantor set, which is generated by removing consecutively the middle-1/3 segment of a line having a given initial length.

THE DRIVEN HARMONIC OSCILLATOR

Solve the driven, damped harmonic oscillator

$$\ddot{x} + \gamma \dot{x} + \omega_0^2 x = \epsilon \cos(\omega t)$$

in the long-time limit. Discuss the behavior close to the resonance $\omega \to \omega_0$.

INFORMATION FLOW IN NETWORKS

Choose a not-too-big social network and examine numerically the flow of information, Eq. (2.39), through the network. Set the weight matrix W_{ij} identical to the adjacency matrix A_{ij}, with entries being either unity or zero. Evaluate the steady-state distribution of information and plot the result as a function of vertex degrees.

STOCHASTIC RESONANCE

Solve the driven double-well problem Eq. (2.60) numerically and try to reproduce Figs. 2.15 and 2.16.

Further Reading

For further studies we refer to introductory texts for dynamical system theory (Katok and Hasselblatt, 1995), classical dynamical systems (Goldstein, 2002), chaos (Schuster and Just, 2005; Devaney, 1989; Gutzwiller, 1990, Strogatz, 1994) and stochastic systems (Ross, 1982; Lasota and Mackey, 1994). Other textbooks on complex and/or adaptive systems are those by Schuster (2001) and Boccara (2003). For an alternative approach to complex system theory via Brownian agents consult Schweitzer (2003).

The interested reader may want to study some selected subjects in more depth, such as the KAM theorem (Ott, 2002), relaxation oscillators (Wang, 1999), stochastic resonance (Benzit, Sutera, Vulpiani, 1981; Gammaitoni et al., 1998), Lévy flights (Metzler and Klafter, 2000), the connection of Lévy flights to the patterns of wandering albatrosses (Viswanathan et al., 1996), human traveling (Brockmann, Hufnagel and Geisel, 2006) and diffusion of information in networks (Eriksen et al., 2003).

The original literature provides more insight, such as the seminal works of Einstein (1905) and Langevin (1908) on Brownian motion or the first formulation and study of the Lorenz (1963) model.

BENZIT, R., SUTERA, A., VULPIANI, A. 1981 The mechanism of stochastic resonance. *Journal of Physics A* **14**, L453-L457.

BROCKMANN, D., HUFNAGEL, L., GEISEL, T. 2006 The scaling laws of human travel. *Nature* **439**, 462.

BOCCARA, N. 2003 *Modeling Complex Systems.* Springer, Berlin.

DEVANEY, R.L. 1989 *An Introduction to Chaotic Dynamical Systems.* Addison-Wesley, Reading, MA.

EINSTEIN, A. 1905 Über die von der molekularkinetischen Theorie der Wärme geforderte Bewegung von in ruhenden Flüssigkeiten suspendierten Teilchen. *Annalen der Physik* **17**, 549.

ERIKSEN, K.A., SIMONSEN, I., MASLOV, S., SNEPPEN, K. 2003 Modularity and extreme edges of the Internet. *Physical Review Letters* **90**, 148701.

GAMMAITONI, L., HÄNGGI, P., JUNG, P., MARCHESONI, F. 1998 Stochastic resonance. *Review of Modern Physics* **70**, 223–287.

GOLDSTEIN, H. 2002 *Classical Mechanics.* 3rd Edition, Addison-Wesley, Reading, MA.

GUTZWILLER, M.C. 1990 *Chaos in classical and quantum mechanics.* Springer, New York.

KATOK, A., HASSELBLATT, B. 1995 *Introduction to the Modern Theory of Dynamical Systems.* Cambridge University Press.

LASOTA, A., MACKEY, M.C. 1994 *Chaos, fractals, and noise – Stochastic aspects of dynamics.* Springer, New York.

LANGEVIN, P. 1908 Sur la théorie du mouvement brownien. *Comptes Rendus* **146**, 530–532.

LORENZ, E.N. 1963 Deterministic nonperiodic flow. *Journal of the Atmospheric Sciences* **20**, 130–141.

METZLER, R., KLAFTER J. 2000 The random walk's guide to anomalous diffusion: a fractional dynamics approach *Physics Reports* **339**, 1.

OTT, E. 2002 *Chaos in Dynamical Systems.* Cambridge University Press.

ROSS, S.M. 1982 *Stochastic processes.* Wiley, New York.

SCHUSTER, H.G., JUST, W. 2005 *Deterministic Chaos.* 4. Edition, Wiley-VCH, New York.

SCHUSTER, H.G. 2001 *Complex Adaptive Systems.* Scator, Saarbrücken.

SCHWEITZER, F. 2003 *Brownian Agents and Active Particles: Collective Dynamics in the Natural and Social Sciences.* Springer, New York.

STROGATZ, S.H 1994 *Nonlinear Systems and Chaos.* Perseus Publishing .

VISWANATHAN, G.M., AFANASYEV, V., BULDYREV, S.V., MURPHY, E.J., PRINCE, P.A., STANLEY, H.E. 1996 Lévy flight search patterns of wandering albatrosses. *Nature* **381**, 413.

WANG, D.L. 1999 *Relaxation oscillators and networks.* In J.G. Webster (ed.), *Encyclopedia of Electrical and Electronic Engineers*, pp. 396–405, Wiley, New York.

Chapter 3
Random Boolean Networks

Complex system theory deals with dynamical systems containing a very large number of variables. The resulting dynamical behavior can be arbitrary complex and sophisticated. It is therefore important to have well controlled benchmarks, dynamical systems which can be investigated and understood in a controlled way for large numbers of variables.

Networks of interacting binary variables, i.e. boolean networks, constitute such canonical complex dynamical systems. They allow the formulation and investigation of important concepts like phase transition in the resulting dynamical state. They are also recognized to be the starting points for the modeling of gene expression and protein regulation networks; the fundamental networks at the basis of all life.

3.1 Introduction

Boolean Networks In this chapter, we describe the dynamics of a set of N binary variables.

Boolean Variables. A boolean or binary variable has two possible values, typically 0 and 1.

The actual values chosen for the binary variable are irrelevant; ± 1 is an alternative popular choice. These elements interact with each other according to some given interaction rules denoted as coupling functions.

Boolean Coupling Functions. A boolean function $\{0,1\}^K \to \{0,1\}$ maps K boolean variables onto a single one.

The dynamics of the system is considered to be discrete, $t = 0, 1, 2, \ldots$. The value of the variables at the next time step are determined by the choice of boolean coupling functions.
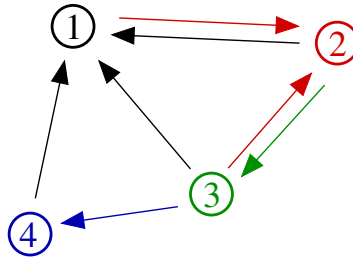
Fig. 3.1 Illustration of a boolean network with $N = 4$ sites. $\sigma_1(t+1)$ is determined by $\sigma_2(t)$, $\sigma_3(t)$ and $\sigma_4(t)$ ($K = 3$). The controlling elements of σ_2 are σ_1 and σ_3 ($K = 2$). The connectivity of σ_3 and σ_4 is $K = 1$

> *The Boolean Network.   The set of boolean coupling functions interconnecting the N boolean variables can be represented graphically by a directed network, the boolean network.*

In Fig. 3.1 a small boolean network is illustrated. Boolean networks at first sight seem to be quite esoteric, devoid of the practical significance for real-world phenomena. Why are they then studied so intensively?

Cell Differentiation in Terms of Stable Attractors The field of boolean networks was given the first big boost by the seminal study of Kauffman in the late 1960s. Kauffman casted the problem of gene expression in terms of a gene regulation network and introduced the so-called *N-K* model in this context. All cells of an animal contain the same genes and cell differentiation, i.e. the fact that a skin cell differs from a muscle cell, is due to differences in the gene activities in the respective cells. Kauffman proposed that different stable attractors, viz cycles, in his random boolean gene expression network correspond to different cells in the bodies of animals.

The notion is then that cell types correspond to different dynamical states of a complex system, i.e. the gene expression network, viz that gene regulation networks are the underpinnings of life. This proposal by Kauffman has received strong support from experimental studies in the last years. In Sect. 3.5.2 we will discuss the case of the yeast cell division cycle.

Boolean Networks are Everywhere Kauffman's original work on gene expression networks was soon generalized to a wide spectrum of applications, such as, to give a few examples, the modeling of neural networks by random boolean networks and of the "punctuated equilibrium" in long-term evolution; a concept that we will discuss in Chap. 5.

Dynamical systems theory (see Chap. 2) deals with dynamical systems containing a relatively small number of variables. General dynamical systems with large numbers of variables are very difficult to analyze and control. Random boolean networks can hence be considered, in a certain sense, as being of prototypical importance in this field, as they provide well defined classes of dynamical systems for which the thermodynamical limit $N \to \infty$ can be taken. They show chaotic as well as regular behavior, despite their apparent simplicity, and many other typical phenomena of dynamical systems. In the thermodynamic limit there can be phase transitions between chaotic and regular regimes. These are the issues studied in this chapter.

N–K Networks There are several types of random boolean networks. The most simple realization is the *N–K* model. It is made up of *N* boolean variables, each variable interacting exactly with *K* other randomly chosen variables. The respective coupling functions are also chosen randomly from the set of all possible boolean functions mapping *K* boolean inputs onto one boolean output.

There is no known realization of *N–K* models in nature. All real physical or biological problems have very specific couplings determined by the structure and the physical and biological interactions of the system considered. The topology of the couplings is, however, often very complex and, in many instances, completely unknown. It is then often a good starting point to model the real-world system by a generic model, like the *N–K* model.

Binary Variables Modeling real-world systems by a collection of interacting binary variables is often a simplification, as real-world variables are often continuous. For the case of the gene expression network, one just keeps two possible states for every single gene: active or inactive.

Thresholds, viz parameter regimes at which the dynamical behavior changes qualitatively, are wide-spread in biological systems. Examples are neurons, which fire or do not fire depending on the total strength of presynaptic activity. Similar thresholds occur in metabolic networks in the form of activation potentials for the chemical reactions involved. Modeling real-world systems based on threshold dynamics with binary variables is, then, a viable first step towards an understanding.

3.2 Random Variables and Networks

3.2.1 Boolean Variables and Graph Topologies

Variables We denote by

$$\{\sigma_1, \sigma_2, \ldots, \sigma_N\}, \qquad \sigma_i \in \{0,1\}, \qquad i = 1, 2, \ldots, N$$

the *N* binary variables.

Time Dependence Time is assumed to be discrete,

$$\sigma_i = \sigma_i(t), \qquad t = 1, 2, \ldots$$

The value of a given boolean element σ_i at the next time step is determined by the values of *K* controlling variables.

Controlling Elements. The controlling elements $\sigma_{j_1(i)}$, $\sigma_{j_2(i)}$, ..., $\sigma_{j_{K_i}(i)}$ *of a boolean variable* σ_i *determine its time evolution by*

$$\sigma_i(t+1) = f_i(\sigma_{j_1(i)}(t), \sigma_{j_2(i)}(t), \ldots, \sigma_{j_{K_i}(i)}(t)) . \tag{3.1}$$

Here f_i is a boolean function associated with σ_i. The set of controlling elements might include σ_i itself. Some exemplary boolean functions are given in Table 3.1.

State Space We denote by Σ_t the state of the system at time t,

$$\Sigma_t = \{\sigma_1(t), \sigma_2(t), \ldots, \sigma_N(t)\} . \tag{3.2}$$

Σ_t can be thought of as a vector pointing to one of the $\Omega = 2^N$ edges of an N-dimensional hypercube, where Ω is the number of possible configurations. For numerical implementations and simulations it is useful to consider Σ_t as the binary representation of an integer number $0 \le \Sigma_t < 2^N$.

Model Definition For a complete definition of the model we then need to specify several parameters:

- The Connectivity: The first step is to select the connectivity K_i of each element, i.e. the number of its controlling elements. With

$$\langle K \rangle = \frac{1}{N} \sum_{i=1}^{N} K_i$$

  the average connectivity is defined. Here we will consider mostly the case in which the connectivity is the same for all nodes: $K_i = K$, $i = 1, 2, \ldots, N$.
- The Linkages: The second step is to select the specific set of controlling elements $\{\sigma_{j_1(i)}, \sigma_{j_2(i)}, \ldots, \sigma_{j_{K_i}(i)}\}$ on which the element σ_i depends. See Fig. 3.1 for an illustration.
- The Evolution Rule: The third step is to choose the boolean function f_i determining the value of $\sigma_i(t+1)$ from the values of the linkages $\{\sigma_{j_1(i)}(t), \sigma_{j_2(i)}(t), \ldots, \sigma_{j_{K_i}(i)}(t)\}$.

Table 3.1 Examples of boolean functions of three arguments. (**a**) A particular random function. (**b**) A canalizing function of the first argument. When $\sigma_1 = 0$, the function value is 1. If $\sigma_1 = 1$, then the output can be either 0 or 1. (**c**) An additive function. The output is 1 (active) if at least two inputs are active. (**d**) The generalized XOR, which is true when the number of 1-bits is odd

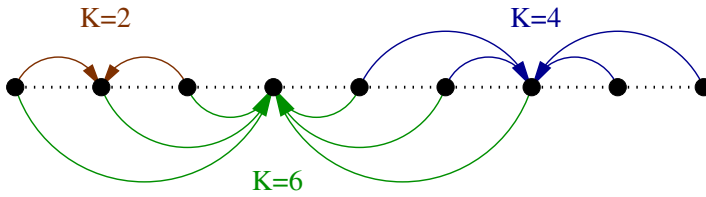| σ_1	σ_2	σ_3	$f(\sigma_1, \sigma_2, \sigma_3)$			
			Random	Canalizing	Additive	Gen. XOR
0	0	0	0	1	0	0
0	0	1	1	1	0	1
0	1	0	1	1	0	1
0	1	1	0	1	1	0
1	0	0	1	0	0	1
1	0	1	0	1	1	0
1	1	0	1	0	1	0
1	1	1	1	0	1	1

Fig. 3.2 Translational invariant linkages for a completely ordered one-dimensional lattice with connectivities $K = 2, 4, 6$

The Geometry of the Network The way the linkages are assigned determines the topology of the network and networks can have highly diverse topologies, see Chap. 1. It is custom to consider two special cases:

> *Lattice Assignment. The boolean variables σ_i are assigned to the nodes of a regular lattice. The K controlling elements $\{\sigma_{j_1(i)}, \sigma_{j_2(i)}, \ldots, \sigma_{j_K(i)}\}$ are then chosen in a regular, translational invariant manner, see Fig. 3.2 for an illustration.*

> *Uniform Assignment. In a uniform assignment the set of controlling elements are randomly drawn from all N sites of the network. This is the case for the N–K model, also called the* Kauffman net. *In terms of graph theory one also speaks of an Erdös–Rényi random graph.*

All intermediate cases are possible. Small-world networks, to give an example, with regular short-distance links and random long-distance links are popular models in network theory, as discussed extensively in Chap. 1.

3.2.2 Coupling Functions

Number of Coupling Functions The coupling function

$$ f_i : \quad \{\sigma_{j_1(i)}, \ldots, \sigma_{j_K(i)}\} \rightarrow \sigma_i $$

has 2^K different arguments. To each argument value one can assign either 0 or 1. Thus there are a total of

$$ N_f = 2^{\left(2^K\right)} = 2^{2^K} = \begin{cases} 4 & K = 1 \\ 16 & K = 2 \\ 256 & K = 3 \end{cases} \tag{3.3} $$

possible coupling functions. In Table 3.1 we present several examples for the case $K = 3$, out of the $2^{2^3} = 256$ distinct $K = 3$ boolean functions.

Types of Coupling Ensembles There are a range of different possible choices for the probability distribution of coupling functions. The following are some examples:

– Uniform Distribution: As introduced originally by Kauffman, the uniform distribution specifies all possible coupling functions to occur with the same probability $1/N_f$.
– Magnetization Bias[1]: The probability of a coupling function to occur is proportional to p if the outcome is 0 and proportional to $1-p$ if the outcome is 1.
– Forcing Functions: Forcing functions are also called "canalizing function". The function value is determined when one of its arguments, say $m \in \{1,\ldots,K\}$, is given a specific value, say $\sigma_m = 0$ (compare Table 3.1). The function value is not specified if the forcing argument has another value, here when $\sigma_m = 1$.
– Additive Functions: In order to simulate the additive properties of inter-neural synaptic activities one can choose

$$\sigma_i(t+1) \;=\; \Theta(f_i(t)), \qquad f_i(t) \;=\; h + \sum_{j=1}^{N} c_{ij}\,\sigma_j(t), \qquad c_{ij} \in \{0,1\}\,,$$

where $\Theta(x)$ is the Heaviside step function and h a bias. The value of $\sigma_i(t+1)$ depends only on a weighted sum of its controlling elements at time t.

Classification of Coupling Functions For small numbers of connectivity K one can completely classify all possible coupling functions:

– $K = 0$
There are only two constant functions, $f = 1$ and $f = 0$.
– $K = 1$

Apart from the two constant functions, which one may denote together by $\mathscr{A}$, there are the identity 1 and the negation $\neg\sigma$, which one can lump together into a class $\mathscr{B}$.

σ	Class $\mathscr{A}$	Class $\mathscr{B}$
0	0 1	0 1
1	0 1	1 0

– $K = 2$
There are four classes of functions $f(\sigma_1,\sigma_2)$, with each class being invariant under the interchange $0 \leftrightarrow 1$ in either the arguments or the value of f: $\mathscr{A}$ (constant functions), $\mathscr{B}_1$ (fully canalizing functions for which one of the arguments determines the output deterministically), $\mathscr{B}_2$ (normal canalizing functions), $\mathscr{C}$ (non-canalizing functions, sometimes also denoted "reversible functions"). Compare Table 3.2.

3.2.3 Dynamics

Model Realizations A given set of linkages and boolean functions $\{f_i\}$ defines what one calls a *realization* of the model. The dynamics then follows from Eq. (3.1). For the updating of all elements during one time step one has several choices:

---

[1] Magnetic moments often have only two possible directions (up or down in the language of spin-1/2 particles). A compound is hence magnetic when more moments point into one of the two possible directions, viz if the two directions are populated unequally.

- Synchronous Update: All variables $\sigma_i(t)$ are updated simultaneously.
- Serial Update (or asynchronous update): Only one variable is updated at every step. This variable may be picked at random or by some predefined ordering scheme.

The choice of updating does not affect thermodynamic properties, like the phase diagram discussed in Sect. 3.3.2. The occurrence and the properties of cycles and attractors, as discussed in Sect. 3.4, however, crucially depends on the form of update.

Selection of the Model Realization There are several alternatives for choosing the model realization during numerical simulations.

- The Quenched Model[2]: One specific realization of coupling functions is selected at the beginning and kept throughout all time.
- The Annealed Model[3]: A new realization is randomly selected after each time step. Then either the linkages or the coupling functions or both change with every update, depending on the choice of the algorithm.
- The Genetic Algorithm: If the network is thought to approach a predefined goal, one may employ a genetic algorithm in which the system slowly modifies its realization with passing time.

Real-world systems are normally modeled by quenched systems with synchronous updating. All interactions are then fixed for all times.

Cycles and Attractors Boolean dynamics correspond to a trajectory within a finite state space of size $\Omega = 2^N$. Any trajectory generated by a dynamical system with unmutable dynamical update rules, as for the quenched model, will eventually lead to a cyclical behavior. No trajectory can generate more than Ω distinct states in a row. Once a state is revisited,

$$\Sigma_t = \Sigma_{t-T}, \qquad T < \Omega ,$$

part of the original trajectory is retraced and cyclic behavior follows. The resulting cycle acts as an attractor for a set of initial conditions.

Table 3.2 The 16 boolean functions for $K = 2$. For the definition of the various classes see page 72 and Aldana, Coppersmith and Kadanoff (2003)

σ_1	σ_2	Class $\mathscr{A}$		Class $\mathscr{B}_1$				Class $\mathscr{B}_2$								Class $\mathscr{C}$	
0	0	1	0	0	1	0	1	1	0	0	0	0	1	1	1	1	0
0	1	1	0	0	1	1	0	0	1	0	0	1	0	1	1	0	1
1	0	1	0	1	0	0	1	0	0	1	0	1	1	0	1	0	1
1	1	1	0	1	0	1	0	0	0	0	1	1	1	1	0	1	0

---

[2] An alloy made up of two or more substances is said to be "quenched" when it is cooled so quickly that it remains stuck in a specific atomic configuration, which does not change anymore with time.

[3] A compound is said to be "annealed" when it has been kept long enough at elevated temperatures such that the thermodynamic stable configuration has been achieved.
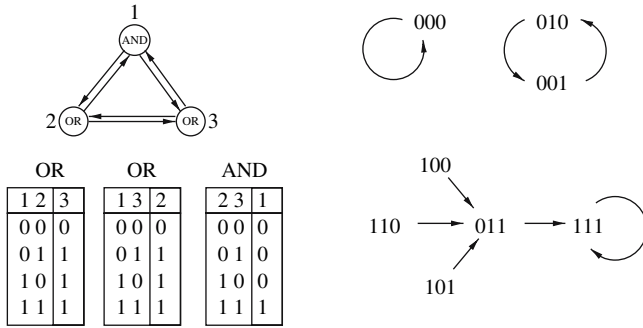
Fig. 3.3 A boolean network with $N = 3$ sites and connectivities $K_i \equiv 2$. *Left*: Definition of the network linkage and coupling functions. *Right*: The complete network dynamics (from Luque and Sole, 2000)

Cycles of length 1 are fixpoint attractors. The fixpoint condition $\sigma_i(t+1) = \sigma_i(t)$ ($i = 1, \ldots, N$) is independent of the updating rules, viz synchronous vs. asynchronous. The order of updating the individual σ_i is irrelevant when none of them changes.

An Example In Fig. 3.3 a network with $N = 3$ and $K = 2$ is fully defined. The time evolution of the $2^3 = 8$ states Σ_t is given for synchronous updating. One can observe one cycle of length 2 and two cycles of length 1 (fixpoints).

3.3 The Dynamics of Boolean Networks

3.3.1 The Flow of Information Through the Network

The Response to Changes For random models the value of any given variable σ_i, or its change with time, is, per se, meaningless. Of fundamental importance, however, for quenched models is its response to changes. We may either change the initial conditions, or some specific coupling function, and examine its effect on the time evolution of the variable considered.

Robustness Biological systems need to be robust. A gene regulation network, to give an example, for which even small damage routinely results in the death of the cell, will be at an evolutionary disadvantage with respect to a more robust gene expression set-up. Here we will examine the sensitivity of the dynamics with regard to the initial conditions. A system is robust if two similar initial conditions lead to similar long-time behavior.

The Hamming Distance and the Divergence of Orbits We consider two different initial states,

$$\Sigma_0 = \{\sigma_1(0), \sigma_2(0), \ldots, \sigma_N(0)\}, \qquad \tilde{\Sigma}_0 = \{\tilde{\sigma}_1(0), \tilde{\sigma}_2(0), \ldots, \tilde{\sigma}_N(0)\} .$$

Typically we are interested in the case when Σ_0 and $\tilde{\Sigma}_0$ are close, viz when they differ in the values of only a few elements. A suitable measure for the distance is the "Hamming distance" $D(t) \in [0, N]$,

$$D(t) = \sum_{i=1}^{N} \left(\sigma_i(t) - \tilde{\sigma}_i(t) \right)^2 , \qquad (3.4)$$

which is just the sum of elements that differ in Σ_0 and $\tilde{\Sigma}_0$. As an example we consider

$$\Sigma_1 = \{1, 0, 0, 1\}, \qquad \Sigma_2 = \{0, 1, 1, 0\}, \qquad \Sigma_3 = \{1, 0, 1, 1\} .$$

We have 4 for the Hamming distance Σ_1-Σ_2 and 1 for the Hamming distance Σ_1-Σ_3. If the system is robust, two close-by initial conditions will never move far apart with time passingwith passing time, in terms of the Hamming distance.

The Normalized Overlap The normalized overlap $a(t) \in [0, 1]$ between two configurations is defined as

$$a(t) = 1 - \frac{D(t)}{N} = 1 - \frac{1}{N} \sum_{i=1}^{N} \left(\sigma_i^2(t) - 2\sigma_i(t)\tilde{\sigma}_i(t) + \tilde{\sigma}_i^2(t) \right)$$

$$\approx \frac{2}{N} \sum_{i=1}^{N} \sigma_i(t)\tilde{\sigma}_i(t) , \qquad (3.5)$$

where we have assumed the absence of any magnetization bias, namely

$$\frac{1}{N} \sum_i \sigma_i^2 \approx \frac{1}{2} \approx \frac{1}{N} \sum_i \tilde{\sigma}_i^2 ,$$

in the last step. The normalized overlap Eq. (3.5) is then like a normalized scalar product between Σ and $\tilde{\Sigma}$. Two arbitrary states have, on the average, a Hamming distance of $N/2$ and a normalized overlap $a = 1 - D/N$ of $1/2$.

Information Loss/Retention for Long Time Scales The difference between two initial states Σ and $\tilde{\Sigma}$ can also be interpreted as an information for the system. One then has than two possible behaviors:

– Loss of Information: $\lim_{t \to \infty} a(t) \to 1$
  $a(t) \to 1$ implies that two states are identical, or that they differ only by a finite number of elements, in the thermodynamic limit. This can happen when two states are attracted by the same cycle. All information about the starting states is lost.
– Information Retention: $\lim_{t \to \infty} a(t) = a^* < 1$
  The system "remembers" that the two configurations were initially different, with the difference measured by the respective Hamming distance.

The system is very robust when information is routinely lost. Robustness depends on the value of a^* when information is kept. If $a^* > 0$ then two trajectories retain a certain similarity for all time scales.

Percolation of Information for Short Time Scales Above we considered how information present in initial states evolves for very long times. Alternatively one may ask, and this a typical question in dynamical system theory, how information is processed for short times. We write

$$D(t) \approx D(0) e^{\lambda t} , \qquad (3.6)$$

where $0 < D(0) \ll N$ is the initial Hamming distance and where λ is called the "Lyapunov exponent", which we discussed in somewhat more detail in Chap. 2.

The question is then whether two initially close trajectories, also called "orbits" within dynamical systems theory, converge or diverge initially. One may generally distinguish between three different types of behaviors or phases:

– The Chaotic Phase: $\lambda > 0$
  The Hamming distance grows exponentially, i.e. information is transferred to an exponential large number of elements. Two initially close orbits soon become very different. This behavior is found for large connectivities K and is not suitable for real-world biological systems.
– The Frozen Phase: $\lambda < 0$
  Two close trajectories typically converge, as they are attracted by the same attractor. This behavior arises for small connectivities K. The system is locally robust.
– The Critical Phase: $\lambda = 0$
  The Hamming distance then depends algebraically on time, $D(t) \propto t^\gamma$.

All three phases can be found in the N–K model when $N \to \infty$. We will now study the N–K model and determine its phase diagram.

3.3.2 The Mean-Field Phase Diagram

Mean-Field Theory We consider two initial states

$$\Sigma_0, \qquad \tilde{\Sigma}_0, \qquad D(0) = \sum_{i=1}^{N} \left(\sigma_i - \tilde{\sigma}_i \right)^2 .$$

We remember that the Hamming distance $D(t)$ measures the number of elements differing in Σ_t and $\tilde{\Sigma}_t$.

For the N–K model, every boolean coupling function f_i is as likely to occur and every variable is, on the average, a controlling element for K other variables. Therefore, the variables differing in Σ_t and $\tilde{\Sigma}_t$ affect on the average $KD(t)$ coupling functions, see Fig. 3.4 for an illustration. Every coupling function changes with
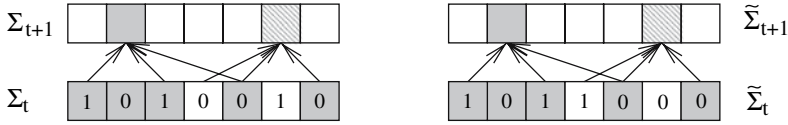
Fig. 3.4 The time evolution of the overlap between two states Σ_t and $\tilde{\Sigma}_t$. The vertices (given by the squares) can have values 0 or 1. Vertices with the same value in both states Σ_t and $\tilde{\Sigma}_t$ are highlighted by a gray background. The values of vertices at the next time step, $t+1$, can only differ if the corresponding arguments are different. Therefore, the vertex with gray background at time $t+1$ must be identical in both states. The vertex with the striped background can have different values in both states at time, $t+1$, with a probability $2p(1-p)$, where $p/(1-p)$ are the probabilities of having vertices with 0/1, respectively

probability half of its value, in the absence of a magnetization bias. The number of elements different in Σ_{t+1} and $\tilde{\Sigma}_{t+1}$, viz the Hamming distance $D(t+1)$ will then be

$$D(t+1) \;=\; \frac{K}{2}D(t), \qquad D(t) \;=\; \left(\frac{K}{2}\right)^t D(0) \;=\; D(0)\,e^{t\ln(K/2)}\,. \qquad (3.7)$$

The connectivity K then determines the phase of the N–K network:

- Chaotic $K > 2$
  Two initially close orbits diverge, the number of different elements, i.e. the relative Hamming distance grows exponentially with time t.
- Frozen $(K < 2)$
  The two orbits approach each other exponentially. All initial information contained $D(0)$ is lost.
- Critical $(K_c = 2)$
  The evolution of Σ_t relative to $\tilde{\Sigma}_t$ is driven by fluctuations. The power laws typical for critical regimes cannot be deduced within mean-field theory, which discards fluctuations.

The mean-field theory takes only average quantities into account. The evolution law $D(t+1) = (K/2)D(t)$ holds only on the average. Fluctuations, viz the deviation of the evolution from the mean-field prediction, are however of importance only close to a phase transition, i.e. close to the critical point $K = 2$.

The mean-field approximation generally works well for lattice physical systems in high spatial dimensions and fails in low dimensions, compare Chap. 2. The Kauffman network has no dimension per se, but the connectivity K plays an analogous role.

Phase Transitions in Dynamical Systems and the Brain The notion of a "phase transition" originally comes from physics, where it denotes the transition between two or more different physical phases, like ice, water and gas, see Chap. 2, which are well characterized by their respective order parameters.

The term phase transition therefore classically denotes a transition between two stationary states. The phase transition discussed here involves the characterization of

the overall behavior of a dynamical system. They are well defined phase transitions in the sense that $1 - a^*$ plays the role of an order parameter; its value uniquely characterizes the frozen phase and the chaotic phase in the thermodynamic limit.

An interesting, completely open and unresolved question is then, whether dynamical phase transitions play a role in the most complex dynamical system known, the mammalian brain. It is tempting to speculate that the phenomena of consciousness may result from a dynamical state characterized by a yet unknown order parameter. Were this true, then this phenomena would be "emergent" in the strict physical sense, as order parameters are rigorously defined only in the thermodynamic limit.

Let us stress, however, that these considerations are very speculative at this point. In Chap. 7, we will discuss a somewhat more down-to-earth approach to cognitive systems theory in general and to aspects of the brain dynamics in particular.

3.3.3 The Bifurcation Phase Diagram

In deriving Eq. (3.7) we assumed that the coupling functions f_i of the system acquire the values 0 and 1 with the same probability $p = 1/2$. We generalize this approach and consider the case of a magnetic bias in which the coupling functions are

$$f_i = \begin{cases} 0, & \text{with probability } p \\ 1, & \text{with probability } 1 - p \end{cases}.$$

For a given value of the bias p and connectivity K, there are critical values

$$K_c(p), \qquad p_c(K),$$

such that for $K < K_c$ ($K > K_c$) the system is in the frozen phase (chaotic phase). When we consider a fixed connectivity and vary p, then $p_c(K)$ separates the system into a chaotic phase and a frozen phase.

The Time Evolution of the Overlap We note that the overlap $a(t) = 1 - D(t)/N$ between two states Σ_t and $\tilde{\Sigma}_t$ at time t is the probability that two vertices have the same value both in Σ_t and in $\tilde{\Sigma}_t$. The probability that all arguments of the function f_i will be the same for both configurations is then

$$\rho_K = \left[a(t) \right]^K. \tag{3.8}$$

As illustrated by Fig. 3.4, the values at the next time step differ with a probability $2p(1-p)$, but only if the arguments of the coupling functions are non-different. Together with the probability that at least one controlling element has different values in Σ_t and $\tilde{\Sigma}_t$, $1 - \rho_K$, this gives the probability, $(1 - \rho_K)2p(1-p)$, of values being different in the next time step. We then have
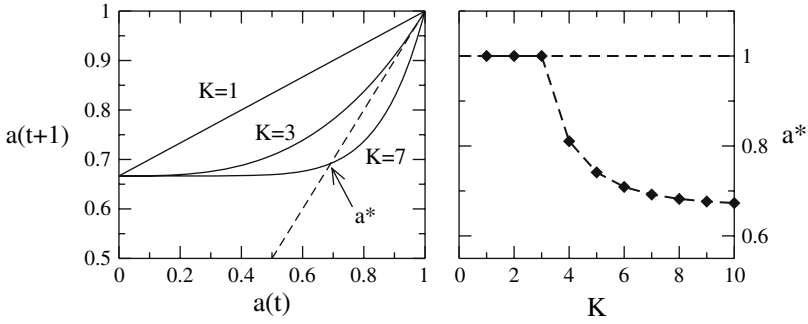
Fig. 3.5 Solution of the self-consistency condition $a^* = 1 - \left[1 - (a^*)^K\right]/K_c$, see Eq. (3.11). *Left:* Graphical solution equating both sides. *Right:* Numerical result for a^* for $K_c = 3$. The fixpoint $a^* = 1$ becomes unstable for $K > K_c = 3$

$$a(t+1) = 1 - (1 - \rho_K)\, 2p(1-p) = 1 - \frac{1 - [a(t)]^K}{K_c}, \tag{3.9}$$

where K_c is given in terms of p as

$$K_c = \frac{1}{2p(1-p)}, \qquad p_c^{1,2} = \frac{1}{2} \pm \sqrt{\frac{1}{4} - \frac{1}{2K}}. \tag{3.10}$$

The fixpoint a^* of Eq. (3.9) obeys

$$a^* = 1 - \frac{1 - [a^*]^K}{K_c}. \tag{3.11}$$

This self-consistency condition for the normalized overlap can be solved graphically or numerically by simple iterations, see Fig. 3.5.

Stability Analysis The trivial fixpoint

$$a^* = 1$$

always constitutes a solution of Eq. (3.11). We examine its stability under the time evolution Eq. (3.9) by considering a small deviation $\delta a_t > 0$ from the fixpoint solution, $a = a^* - \delta a_t$:

$$1 - \delta a_{t+1} = 1 - \frac{1 - [1 - \delta a_t]^K}{K_c}, \qquad \delta a_{t+1} \approx \frac{K\, \delta a_t}{K_c}. \tag{3.12}$$

The trivial fixpoint $a^* = 1$ therefore becomes unstable for $K/K_c > 1$, viz when $K > K_c = (2p(1-p))^{-1}$.

Bifurcation Equation (3.11) has two solutions for $K > K_c$, a stable fixpoint $a^* < 1$ and the unstable solution $a^* = 1$. One speaks of a bifurcation, which is shown in
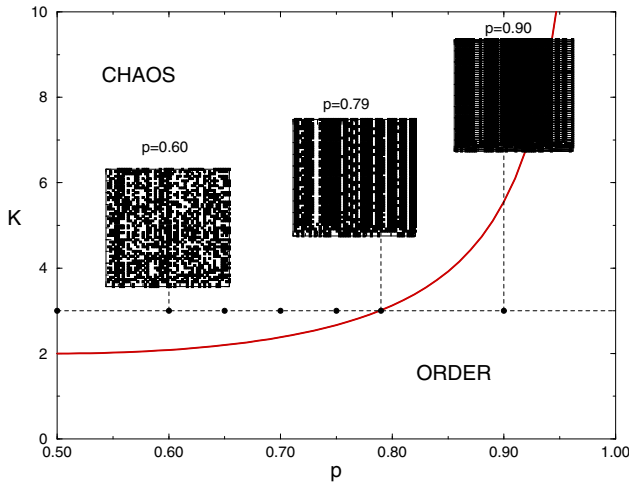
Fig. 3.6 Phase diagram for the N–K model. The curve separating the chaotic phase from the ordered (frozen) phase is $K_c = [2p(1-p)]^{-1}$. The insets are simulations for $N = 50$ networks with $K = 3$ and $p = 0.60$ (chaotic phase), $p = 0.79$ (on the critical line) and $p = 0.90$ (frozen phase). The site index runs horizontally, the time vertically. Notice the fluctuations for $p = 0.79$ (from Luque and Sole, 2000)

Fig. 3.5. We note that

$$K_c\Big|_{p=1/2} = 2 \,,$$

in agreement with our previous mean-field result, Eq. (3.7), and that

$$\lim_{K\to\infty} a^* = \lim_{K\to\infty}\left(1 - \frac{1-[a^*]^K}{K_c}\right) = 1 - \frac{1}{K_c} = 1 - 2p(1-p)\,,$$

since $a^* < 1$ for $K > K_c$, compare Fig. 3.5. Notice that $a^* = 1/2$ for $p = 1/2$ corresponds to the average normalized overlap for two completely unrelated states in the absence of the magnetization bias, $p = 1/2$. Two initial similar states then become completely uncorrelated for $t \to \infty$ in the limit of infinite connectivity K.

Rigidity of the Kauffman Net We can connect the results for the phase diagram of the N–K network illustrated in Fig. 3.6 with our discussion on robustness, see Sect. 3.3.1.

– The Chaotic Phase: $K > K_c$
  The infinite time normalized overlap a^* is less than 1 even when two trajectories Σ_t and $\tilde{\Sigma}_t$ start out very close to each other. a^*, however, always remains above the value expected for two completely unrelated states. This is so as the two orbits enter two different attractors consecutively, after which the Hamming distance remains constant, modulo small-scale fluctuations that do not contribute in the thermodynamic limit $N \to \infty$.
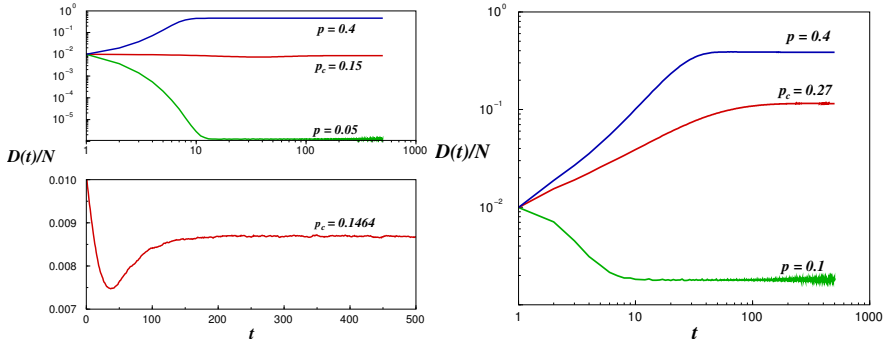
Fig. 3.7 Normalized Hamming distance $D(t)/N$ for a Kauffman net (*left*) and a square lattice (*right*) with $N = 10\,000$ variables, connectivity $K = 4$ and $D(0) = 100$, viz $D(0)/N = 0.01$. *Left*: (*top*) Frozen phase ($p = 0.05$), critical ($p_c \simeq 0.1464$) and chaotic ($p = 0.4$) phases, plotted with a logarithmic scale; (*bottom*) Hamming distance for the critical phase ($p = p_c$) but in a non-logarithmic graph. *Right*: Frozen phase ($p = 0.1$), critical ($p_c \simeq 0.27$) and chaotic ($p = 0.4$) phases, plotted with a logarithmic scale. Note that $a^* = \lim_{t\to\infty}(1 - D(t)/N) < 1$ in the frozen state of the lattice system, compare Fig. 3.5 (from Aldana, Coppersmith and Kadanoff, 2003)

- The Frozen Phase: $K < K_c$
  The infinite time overlap a^* is exactly one. All trajectories approach essentially the same configuration independently of the starting point, apart from fluctuations that vanish in the thermodynamic limit. The system is said to "order".

Lattice Versus Random Networks The complete loss of information in the ordered phase observed for the Kauffman net does not occur for lattice networks, for which $a^* < 1$ for any $K > 0$. This behavior of lattice systems is born out by the results of numerical simulations presented in Fig. 3.7. The finite range of the linkages in lattice systems allows them to store information about the initial data in spatially finite proportions of the system, specific to the initial state. For the Kauffman graph every region of the network is equally close to any other and local storage of information is impossible.

Percolation Transition in Lattice Networks For lattice boolean networks the frozen and chaotic phases cannot be distinguished by examining the value of the long-term normalized overlap a^*, as it is always smaller than unity. The lattice topology, however, allows for a connection with percolation theory. One considers a finite system, e.g. a 100×100 square lattice, and two states Σ_0 and $\tilde{\Sigma}_0$ that differ only along one edge. If the damage, viz the difference in between Σ_t and $\tilde{\Sigma}_t$ spreads for long times to the opposite edge, then the system is said to be percolating and in the chaotic phase. If the damage never reaches the opposite edge, then the system is in the frozen phase. Numerical simulations indicate, e.g. a critical $p_c \simeq 0.298$ for the two-dimensional square lattice with connectivity $K = 4$, compare Fig. 3.7.

Numerical Simulations The results of the mean-field solution for the Kauffman net are confirmed by numerical solutions of finite-size networks. In Fig. 3.7 the normalized Hamming distance, $D(t)/N$, is plotted for both Kauffman graphs and a two-dimensional squared lattice, both containing $N = 10\,000$ elements and connectivity $K = 4$.

For both cases results are shown for parameters corresponding to the frozen phase and to the chaotic phase, in addition to a parameter close to the critical line. Note that $1 - a^* = D(t)/N \to 0$ in the frozen phase for the random Kauffman network, but not for the lattice system.

3.3.4 Scale-Free Boolean Networks

Scale-Free Connectivity Distributions Scale-free connectivity distributions

$$P(K) = \frac{1}{\zeta(\gamma)} K^{-\gamma}, \qquad \zeta(\gamma) = \sum_{K=1}^{\infty} K^{-\gamma}, \qquad \gamma > 1 \qquad (3.13)$$

abound in real-world networks, as discussed in Chap. 1. Here $P(K)$ denotes the probability to draw a coupling function $f_i(\cdot)$ having Z arguments. The distribution Eq. (3.13) is normalizable for $\gamma > 1$.

The average connectivity $\langle K \rangle$ is

$$\langle K \rangle = \sum_{K=1}^{\infty} K P(K) = \begin{cases} \infty & \text{if } 1 < \gamma \leq 2 \\ \frac{\zeta(\gamma-1)}{\zeta(\gamma)} < \infty & \text{if } \gamma > 2 \end{cases}, \qquad (3.14)$$

where $\zeta(\gamma)$ is the Riemann zeta function.

Annealed Approximation We consider again two states Σ_t and $\tilde{\Sigma}_t$ and the normalized overlap

$$a(t) = 1 - D(t)/N,$$

which is identical to the probability that two vertices in Σ and $\tilde{\Sigma}$ have the same value. In Sect. 3.3.3 we derived, for a magnetization bias p,

$$a(t+1) = 1 - (1 - \rho_K) 2p(1-p) \qquad (3.15)$$

for the time-evolution of $a(t)$, where

$$\rho_K = [a(t)]^K \quad \to \quad \sum_{K=1}^{\infty} [a(t)]^K P(K) \qquad (3.16)$$

is the average probability that the $K = 1, 2, \ldots$ controlling elements of the coupling function $f_i()$ are all identical. In Eq. (3.16) we have generalized Eq. (3.8) to a non-constant connectivity distribution $P(K)$. We then find

$$a(t+1) \;=\; 1 - 2p(1-p)\left\{1 - \sum_{K=1}^{\infty} a^K(t)P(K)\right\} \;\equiv\; F(a)\,, \qquad (3.17)$$

compare Eq. (3.9). Effectively we have used here an annealed model, due to the statistical averaging in Eq. (3.16).

Fixpoints Within the Annealed Approximation In the limit $t \to \infty$, Eq. (3.17) becomes the self-consistency equation

$$a^* \;=\; F(a^*)\,,$$

for the fixpoint a^*, where $F(a)$ is defined as the right-hand-side of Eq. (3.17). Again, $a^* = 1$ is always a fixpoint of Eq. (3.17), since $\sum_K P(K) = 1$ per definition.

Stability of the Trivial Fixpoint We repeat the stability analysis of the trivial fixpoint $a^* = 1$ of Sect. 3.3.3 and assume a small deviation $\delta a > 0$ from a^*:

$$a^* - \delta a \;=\; F(a^* - \delta a) \;=\; F(a^*) - F'(a^*)\delta a, \qquad \delta a \;=\; F'(a^*)\delta a\,.$$

The fixpoint a^* becomes unstable if $F'(a^*) > 1$. We find for $a^* = 1$

$$1 \;=\; \lim_{a \to 1^-} \frac{\mathrm{d}F(a)}{\mathrm{d}a} = 2p(1-p)\sum_{k=1}^{\infty} KP(K)$$
$$= 2p(1-p)\langle K\rangle\,. \qquad (3.18)$$

For $\lim_{a\to 1^-} \mathrm{d}F(a)/\mathrm{d}a < 1$ the fixpoint $a^* = 1$ is stable, otherwise it is unstable. The phase transition is then given by

$$2p(1-p)\langle K\rangle \;=\; 1\,. \qquad (3.19)$$

For the classical $N\!-\!K$ model all elements have the same connectivity, $K_i = \langle K\rangle = K$, and Eq. (3.19) reduces to Eq. (3.12).

The Frozen and Chaotic Phases for the Scale-Free Model For $1 < \gamma \le 2$ the average connectivity is infinite, see Eq. (3.14). $F'(1) = 2p(1-p)\,\langle K\rangle$ is then always larger than unity and $a^* = 1$ unstable, as illustrated in Fig. 3.8. Equation (3.17) then has a stable fixpoint $a^* \ne 1$; the system is in the chaotic phase for all $p \in]0,1[$.

For $\gamma > 2$ the first moment of the connectivity distribution $P(K)$ is finite and the phase diagram is identical to that of the $N\!-\!K$ model shown in Fig. 3.6, with K replaced by $\zeta(\gamma_c - 1)/\zeta(\gamma_c)$. The phase diagram in γ–p space is presented in Fig. 3.8. One finds that $\gamma_c \in [2, 2.5]$ for any value of p. There is no chaotic scale-free network for $\gamma > 2.5$. It is interesting to note that $\gamma \in [2,3]$ for many real-world scale-free networks.
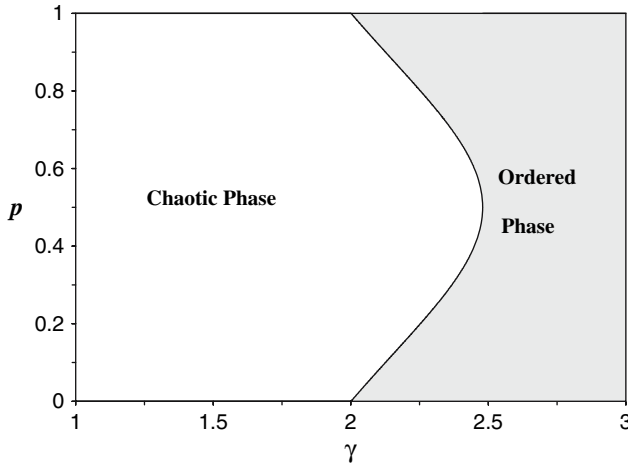
Fig. 3.8 Phase diagram for a scale-free boolean network with connectivity distribution $\propto K^{-\gamma}$. The average connectivity diverges for $\gamma < 2$ and the network is chaotic for all p (from Aldana and Cluzel, 2003)

3.4 Cycles and Attractors

3.4.1 Quenched Boolean Dynamics

Self-Retracting Orbits From now on we consider quenched systems for which the coupling functions $f_i(\sigma_{i_1}, \dots, \sigma_{i_K})$ are fixed for all times. Any orbit eventually partly retraces itself, since the state space $\Omega = 2^N$ is finite. The long-term trajectory is therefore cyclic.

> *Attractors. An attractor A_0 of a discrete dynamical system is a region $\{\Sigma_t\} \subset \Omega$ in phase space that maps completely onto itself under the time evolution $A_{t+1} = A_t \equiv A_0$.*

Attractors are typically cycles

$$\Sigma^{(1)} \quad \rightarrow \quad \Sigma^{(2)} \quad \rightarrow \quad \dots \quad \rightarrow \quad \Sigma^{(1)} \,,$$

see Figs. 3.3 and 3.9 for some examples. Fixed points are cycles of length 1.

> *The Attraction Basin.   The attraction basin B of an attractor A_0 is the set $\{\Sigma_t\} \subset \Omega$ for which there is a $T < \infty$ such that $\Sigma_T \in A_0$.*

The probability to end up in a given cycle is directly proportional, for randomly drawn initial conditions, to the size of its basin of attraction. The three-site network illustrated in Fig. 3.3 is dominated by the fixpoint $\{1,1,1\}$, which is reached with probability 5/8 for random initial starting states.
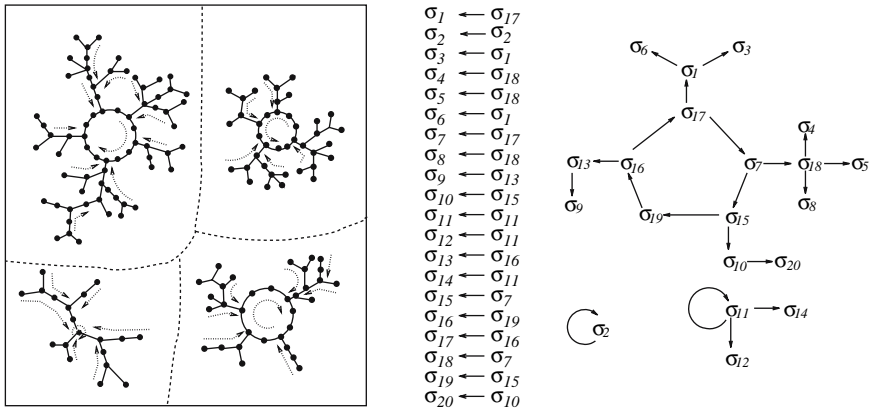
Fig. 3.9 Cycles and linkages. *Left*: Sketch of the state space where every bold point stands for a state $\Sigma_t = \{\sigma_1, \ldots, \sigma_N\}$. The state space decomposes into distinct attractor basins for each cycle attractor or fixpoint attractor. *Right*: Linkage loops for an $N = 20$ model with $K = 1$. The controlling elements are listed in the center column. Each arrow points from the controlling element toward the direct descendant. There are three modules of uncoupled variables (from Aldana, Coppersmith and Kadanoff, 2003)

Attractors are Everywhere Attractors and fixpoints are generic features of dynamical systems and are very important for their characterization, as they dominate the time evolution in state space within their respective basins of attraction. Random boolean networks allow for very detailed studies of the structure of attractors and of the connection to network topology. Of special interest in this context is how various properties of the attractors, like the cycle length and the size of the attractor basins, relate to the thermodynamic differences between the frozen phase and the chaotic phase. These are the issues that we shall now discuss.

Linkage Loops, Ancestors and Descendants Every variable σ_i can appear as an argument in the coupling functions for other elements; it is said to act as a controlling element. The collections of all such linkages can be represented graphically by a directed graph, as illustrated in Figs. 3.1, 3.3 and 3.9, with the vertices representing the individual binary variables. Any given element σ_i can then influence a large number of different states during the continued time evolution.

> *Ancestors and Descendants.*   *The elements a vertex affects consecutively via the coupling functions are called its descendants. Going backwards in time one find ancestors for each element.*

In the 20-site network illustrated in Fig. 3.9 the descendants of σ_{11} are σ_{11}, σ_{12} and σ_{14}.

When an element is its own descendant (and ancestor) it is said to be part of a "linkage loop". Different linkage loops can overlap, as is the case for the linkage loops

$$\sigma_1 \to \sigma_2 \to \sigma_3 \to \sigma_4 \to \sigma_1, \qquad \sigma_1 \to \sigma_2 \to \sigma_3 \to \sigma_1$$

shown in Fig. 3.1. Linkage loops are disjoint for $K = 1$, compare Fig. 3.9.

Modules and Time Evolution The set of ancestors and descendants determines the overall dynamical dependencies.

> *Module. The collection of all ancestors and descendants of a given element σ_i is called the module to which σ_i belongs.*

If we go through all variables σ_i, $i = 1,\ldots,N$ we find all modules, with every element belonging to one and only one specific module. Otherwise stated, disjoint modules correspond to disjoint subgraphs, the set of all modules constitute the full linkage graph. The time evolution is block-diagonal in terms of modules;: $\sigma_i(t)$ is independent of all variables not belonging to its own module, for all times t.

In lattice networks the clustering coefficient (see Chap. 1) is large and closed linkage loops occur frequently. For big lattice systems with a small mean linkage K we expect far away spatial regions to evolve independently, due the lack of long-range connections.

Lattice Nets versus Kauffman Nets For lattice systems the linkages are short-ranged and whenever a given element σ_j acts as a controlling element for another element σ_i there is a high probability that the reverse is also true, viz that σ_i is an argument of f_j.

The linkages are generally non-reciprocal for the Kauffman net; the probability for reciprocality is just K/N and vanishes in the thermodynamic limit for finite K. The number of disjoint modules in a random network therefore grows more slowly than the system size. For lattice systems, on the other hand, the number of modules is proportional to the size of the system. The differences between lattice and Kauffman networks translate to different cycle structures, as every periodic orbit for the full system is constructed out of the individual attractors of all modules present in the network considered.

3.4.2 The K = 1 Kauffman Network

We start our discussion of the cycle structure of Kauffman nets with the case $K = 1$, which can be solved exactly. The maximal length for a linkage loop $l_{\max}$ is on the average of the order of

$$l_{\max} \sim N^{1/2} . \tag{3.20}$$

The linkage loops determine the cycle structure together with the choice of the coupling ensemble. As an example we discuss the case of an $N = 3$ linkage loop.

The Three-site Linkage Loop with Identities For $K = 1$ there are only two non-constant coupling functions, i.e. the identity I and the negation $\neg$, see page 72. We start by considering the case of all the coupling functions being the identity:

$$ABC \;\rightarrow\; CAB \;\rightarrow\; BCA \;\rightarrow\; ABC \;\rightarrow\; \ldots ,$$

where we have denoted by A, B, C the values of the binary variables σ_i, $i = 1, 2, 3$. There are two cycles of length 1, in which all elements are identical. When the three elements are not identical, the cycle length is 3. The complete dynamics is then:

$$000 \rightarrow 000 \qquad\qquad 100 \rightarrow 010 \rightarrow 001 \rightarrow 100$$
$$111 \rightarrow 111 \qquad\qquad 011 \rightarrow 101 \rightarrow 110 \rightarrow 011$$

Three-Site Linkage Loops with Negations Let us consider now the case that all three coupling functions are negations:

$$ABC \;\rightarrow\; \bar{C}\bar{A}\bar{B} \;\rightarrow\; BCA \;\rightarrow\; \bar{A}\bar{B}\bar{C} \;\rightarrow\; \ldots$$

The cycle length is 2 if all elements are identical

$$000 \rightarrow 111 \rightarrow 000$$

and of length 6 if they are not.

$$100 \rightarrow 101 \rightarrow 001 \rightarrow 011 \rightarrow 010 \rightarrow 110 \rightarrow 100 \;.$$

The complete state space $\Omega = 2^3 = 8$ decomposes into two cycles, one of length 6 and one of length 2.

Three-Site Linkage Loops with a Constant Function Let us see what happens if any of the coupling functions are a constant function. For illustration purposes we consider the case of two constant functions 0 and 1 and the identity:

$$ABC \;\rightarrow\; 0A1 \;\rightarrow\; 001 \;\rightarrow\; 001 \;. \tag{3.21}$$

Generally it holds that the cycle length is 1 if any of the coupling functions is an identity and that there is then only a single fixpoint attractor. Equation (3.21) holds for all $A, B, C \in \{0, 1\}$; the basin of attraction for 001 is therefore the whole state space, and 001 is a global attractor.

   The Kauffman net can contain very large linkage loops for $K = 1$, see Eq. (3.20), but then the probability that a given linkage loop contains at least one constant function is also very high. The average cycle length therefore remains short for the $K = 1$ Kauffman net.

3.4.3 The K = 2 Kauffman Network

The $K = 2$ Kauffman net is critical, as discussed in Sects. 3.3.1 and 3.3.2. When physical systems undergo a (second-order) phase transition, power laws are expected right at the point of transition for many response functions; see the discussion in Chap. 2. It is therefore natural to expect the same for critical dynamical systems, such as a random boolean network.

This expectation was indeed initially born out of a series of mostly numerical investigations, which indicated that both the typical cycle lengths, as well as the mean number of different attractors, would grow algebraically with N, namely like $\sqrt{N}$. It was therefore tempting to relate many of the power laws seen in natural organisms to the behavior of critical random boolean networks.

Undersampling of the State Space The problem to determine the number and the length of cycles is, however, numerically very difficult. In order to extract power laws one has to simulate systems with large N. The state space $\Omega = 2^N$, however, grows exponentially, so that an exhaustive enumeration of all cycles is impossible. One has therefore to resort to a weighted sampling of the state space for any given network realization and to extrapolate from the small fraction of states sampled to the full state space. This method yielded the $\sqrt{N}$ dependence referred to above.

The weighted sampling is, however, not without problems; it might in principle undersample the state space. The number of cycles found in the average state space might not be representative for the overall number of cycles, as there might be small fractions of state space with very high number of attractors dominating the total number of attractors.

This is indeed the case. One can prove rigorously that the number of attractors grows faster than any power for the $K = 2$ Kauffman net. One might still argue, however, that for biological applications the result for the "average state space" is relevant, as biological systems are not too big anyway. The hormone regulation network of mammals contains of the order of 100 elements, the gene regulation network of the order of 20 000 elements.

3.4.4 The K = N Kauffman Network

Mean-field theory holds for the fully connected network $K = N$ and we can evaluate the average number and length of cycles using probability arguments.

The Random Walk Through Configuration Space We consider an orbit starting from an arbitrary configuration Σ_0 at time $t = 0$. The time evolution generates a series of states

$$\Sigma_0,\ \Sigma_1,\ \Sigma_2,\ \ldots$$

through the configuration space of size $\Omega = 2^N$. We consider all Σ_t to be uncorrelated, viz we consider a random walk. This assumption holds due to the large connectivity $K = N$.

Closing the Random Walk The walk through configuration space continues until we hit a previously visited point, see Fig. 3.10. We define by

- q_t: the probability that the trajectory remains unclosed after t steps;
- p_t: the probability of terminating the excursion exactly at time t.
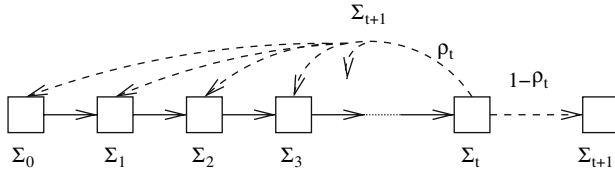
Fig. 3.10 A random walk in configuration space. The relative probability of closing the loop at time t, $\rho_t = (t+1)/\Omega$, is the probability that $\Sigma_{t+1} \equiv \Sigma_{t'}$, with a certain $t' \in [0,t]$

If the trajectory is still open at time t, we have already visited $t+1$ different sites (including the sites Σ_0 and Σ_t). Therefore, there are $t+1$ ways of terminating the walk at the next time step. The relative probability of termination is then $\rho_t = (t+1)/\Omega$ and the overall probability p_{t+1} to terminate the random walk at time $t+1$ is

$$p_{t+1} = \rho_t\, q_t = \frac{t+1}{\Omega}\, q_t\ .$$

The probability of still having an open trajectory after $t+1$ steps is

$$q_{t+1} = q_t(1-\rho_t) = q_t\left(1-\frac{t+1}{\Omega}\right) = q_0\prod_{i=1}^{t}\left(1-\frac{i}{\Omega}\right), \qquad q_0 = 1\ .$$

The phase space $\Omega = 2^N$ diverges in the thermodynamic limit $N \to \infty$ and the approximation

$$q_t = \prod_{i=1}^{t}\left(1-\frac{i}{\Omega}\right) \approx \prod_{i=1}^{t} e^{-i/\Omega} = e^{-\Sigma_i i/\Omega} = e^{-t(t+1)/(2\Omega)} \tag{3.22}$$

becomes exact in this limit. For large times t we have $t(t+1)/(2\Omega) \approx t^2/(2\Omega)$ in Eq. (3.22). The probability

$$\sum_{t=1}^{\infty} p_t = \int_0^{\infty} dt\, \frac{t}{\Omega}\, e^{-t^2/(2\Omega)} = 1$$

for the random walk to close at all is unity.

Cycle Length Distribution The probability $\langle N_c(L)\rangle$ that the system contains a cycle of length L is

$$\langle N_c(L)\rangle = \frac{q_{t=L}}{\Omega}\frac{\Omega}{L} = \frac{\exp[-L^2/(2\Omega)]}{L}\ , \tag{3.23}$$

where we used Eq. (3.22). $\langle\cdots\rangle$ denotes an ensemble average over realizations. In deriving Eq. (3.23) we used the following considerations:

(i) The probability that Σ_{t+1} is identical to Σ_0 is $1/\Omega$.

(ii)   There are Ω possible starting points (factor Ω).
(iii) Factor $1/L$ corrects for the overcounting of cycles when considering the L possible starting sites of the L-cycle.

Average Number of Cycles We are interested in the mean number $\bar{N}_c$ of cycles,

$$\bar{N}_c = \sum_{L=1}^{\infty} \langle N_c(L) \rangle \simeq \int_{L=1}^{\infty} dL \, \langle N_c(L) \rangle . \tag{3.24}$$

When going from the sum $\sum_L$ to the integral $\int dL$ in Eq. (3.24) we neglected terms of order unity. We find

$$\bar{N}_c = \int_1^{\infty} dL \, \frac{\exp[-L^2/(2\Omega)]}{L} = \underbrace{\int_{1/\sqrt{2\Omega}}^{1} du \, \frac{e^{-u^2}}{u}}_{\equiv I_1} + \underbrace{\int_1^{\infty} du \, \frac{e^{-u^2}}{u}}_{\equiv I_2} ,$$

where we rescaled the variable by $u = L/\sqrt{2\Omega}$. For the separation $\int_{1/\sqrt{2\Omega}}^{\infty} = \int_{1/\sqrt{2\Omega}}^{c} + \int_c^{\infty}$ of the integral above we used $c = 1$ for simplicity; any other finite value for c would do also the job.

The second integral, I_2, does not diverge as $\Omega \to \infty$. For I_1 we have

$$I_1 = \int_{1/\sqrt{2\Omega}}^{1} du \, \frac{e^{-u^2}}{u} = \int_{1/\sqrt{2\Omega}}^{1} du \, \frac{1}{u} \left(1 - u^2 + \frac{1}{2} u^4 + \dots \right)$$

$$\approx \ln(\sqrt{2\Omega}) , \tag{3.25}$$

since all further terms $\propto \int_{1/\sqrt{2\Omega}}^{1} du \, u^{n-1} < \infty$ for $n = 2, 4, \dots$ and $\Omega \to \infty$. The average number of cycles is then

$$\bar{N}_c = \ln(\sqrt{2^N}) + O(1) = \frac{N \ln 2}{2} + O(1) \tag{3.26}$$

for the $N = K$ Kauffman net in thermodynamic limit $N \to \infty$.

Mean Cycle Length The average length $\bar{L}$ of a random cycle is

$$\bar{L} = \frac{1}{\bar{N}_c} \sum_{L=1}^{\infty} L \langle N_c(L) \rangle \approx \frac{1}{\bar{N}_c} \int_1^{\infty} dL L \, \frac{\exp[-L^2/(2\Omega)]}{L}$$

$$= \frac{1}{\bar{N}_c} \int_1^{\infty} dL \, e^{-L^2/(2\Omega)} = \frac{\sqrt{2\Omega}}{\bar{N}_c} \int_{1/\sqrt{2\Omega}}^{\infty} du \, e^{-u^2} \tag{3.27}$$

after rescaling with $u = L/\sqrt{2\Omega}$ and using Eq. (3.23). The last integral on the right-hand-side of Eq. (3.27) converges for $\Omega \to \infty$ and the mean cycle length $\bar{L}$ consequently scales as

$$\bar{L} \sim \Omega^{1/2}/N = 2^{N/2}/N \tag{3.28}$$

for the $K = N$ Kauffman net, when using Eq. (3.24), $\bar{N}_c \sim N$.

3.5 Applications

3.5.1 Living at the Edge of Chaos

Gene Expression Networks and Cell Differentiation Kauffman introduced the N–K model in the late 1960s for the purpose of modeling the dynamics and time evolution of networks of interacting genes, i.e. the gene expression network. In this model an active gene might influence the expression of any other gene, e.g. when the protein transcribed from the first gene influences the expression of the second gene.

The gene expression network of real-world cells is not random. The web of linkages and connectivities among the genes in a living organism is, however, very intricate, and to model the gene–gene interactions as randomly linked is a good zero-th order approximation. One might then expect to gain a generic insight into the properties of gene expression networks; insights that are independent of the particular set of linkages and connectivities realized in any particular living cell.

Dynamical Cell Differentiation Whether random or not, the gene expression network needs to result in a stable dynamics in order for the cell to keep functioning. Humans have only a few hundreds of different cell types in their bodies. Considering the fact that every single cell contains the identical complete genetic material, in 1969 Kauffman proposed an, at that time revolutionary, suggestion that every cell type corresponds to a distinct dynamical state of the gene expression network. It is natural to assume that these states correspond to attractors, viz in general to cycles. The average length $\bar{L}$ of a cycle in a N–K Kauffman net is

$$\bar{L} \sim 2^{\alpha N}$$

in the chaotic phase, e.g. for $N = K$ where $\alpha = 1/2$, see Eq. (3.28), The mean cycle length $\bar{L}$ is exponentially large; consider that $N \approx 20\,000$ for the human genome. A single cell would take the universe's lifetime to complete a single cycle, which is an unlikely setting. It then follows that gene expression networks of living organisms cannot be operational in the chaotic phase.

Living at the Edge of Chaos If the gene expression network cannot operate in the chaotic phase there are but two possibilities left: the frozen phase or the critical point. The average cycle length is short in the frozen phase, see Sect. 3.4.2, and the dynamics stable. The system is consequently very resistant to damage of the linkages.

But what about Darwinian evolution? Is too much stability good for the adaptability of cells in a changing environment? Kauffman suggested that gene expression networks operate *at the edge of chaos*, an expression that has become legendary. By this he meant that networks close to criticality may benefit from the stability properties of the close-by frozen phase and at the same time exhibit enough sensitivity to changes in the network structure so that Darwinian adaption remains possible.

But how can a system reach criticality by itself? For the N–K network there is no extended critical phase, only a single critical point $K = 2$. In Chap. 4 we will

discuss mechanisms that allow certain adaptive systems to evolve their own internal parameters autonomously in such a way that they approach the critical point. This phenomenon is called "self-organized criticality".

One could then assume that Darwinian evolution trims the gene expression networks towards criticality: Cells in the chaotic phase are unstable and die; cells deep in the frozen phase cannot adapt to environmental changes and are selected out in the course of time.

3.5.2 The Yeast Cell Cycle

The Cell Division Process Cells have two tasks: to survive and to multiply. When a living cell grows too big, a cell division process starts. The cell cycle has been studied intensively for the budding yeast. In the course of the division process the cell goes through a distinct set of states

$$G_1 \rightarrow S \rightarrow G_2 \rightarrow M \rightarrow G_1 \,,$$

with G_1 being the "ground state" in physics slang, viz the normal cell state and the chromosome division takes place during the M phase. These states are characterized by distinct gene activities, i.e. by the kinds of proteins active in the cell. All eukaryote cells have similar cell division cycles.

The Yeast Gene Expression Network From the ≈ 800 genes involved only $11 - 13$ core genes are actually regulating the part of the gene expression network responsible for the division process; all other genes are more or less just descendants of the core genes. The cell dynamics contains certain checkpoints, where the cell division process can be stopped if something were to go wrong. When eliminating the checkpoints a core network with only 11 elements remains. This network is shown in Fig. 3.11.

Boolean Dynamics The full dynamical dependencies are not yet known for the yeast gene expression network. The simplest model is to assume

$$\sigma_i(t) = \begin{cases} 1 & \text{if } a_i(t) > 0 \\ 0 & \text{if } a_i(t) \leq 0 \end{cases} \,, \qquad a_i(t) = \sum_j w_{ij}\sigma_j(t) \,, \qquad (3.29)$$

i.e. a boolean dynamics for the binary variables $\sigma_i(t) = 0, 1$ representing the activation/deactivation of protein i, with couplings $w_{ij} = \pm 1$ for an excitatory/inhibitory functional relation.

Fixpoints The 11-site network has 7 attractors, all cycles of length 1, viz fixpoints. The dominating fixpoint has an attractor basin of 1764 states, representing about 72% of the state space $\Omega = 2^{11} = 2048$. Remarkably, the protein activation pattern of the dominant fixpoint corresponds exactly to that of the experimentally determined G_1 ground state of the living yeast cell.
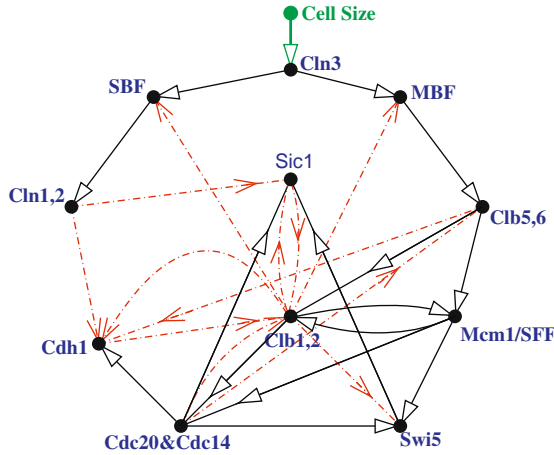
Fig. 3.11 The $N = 11$ core network responsible for the yeast cell cycle. Acronyms denote protein names, solid arrows excitatory connections and dashed arrows inhibitory connections. Cln3 is inactive in the resting state G_1 and becomes active when the cell reaches a certain size (top), initiating the cell division process (compare Li et al., 2004)

The Cell Division Cycle In the G_1 ground state the protein Cln3 is inactive. When the cell reaches a certain size it becomes expressed, i.e. it becomes active. For the network model one then just starts the dynamics by setting

$$\sigma_{Cln3} \rightarrow 1, \qquad \text{at} \quad t = 0$$

in the G_1 state. The ensuing simple boolean dynamics, induced by Eq. (3.29), is depicted in Fig. 3.12.

The remarkable result is that the system follows an attractor pathway that runs through all experimentally known intermediate cell states, reaching the ground state G_1 in 12 steps.

Comparison with Random Networks The properties of the boolean network depicted in Fig. 3.11 can be compared with those of a random boolean network. A random network of the same size and average connectivity would have more attractors with correspondingly smaller basins of attraction. Living cells clearly need a robust protein network to survive in harsh environments.

Nevertheless, the yeast protein network shows more or less the same susceptibility to damage as a random network. The core yeast protein network has an average connectivity of $\langle K \rangle = 27/11 \simeq 2.46$. The core network has only $N = 11$ sites, a number far too small to allow comparison with the properties of N–K networks in the thermodynamic limit $N \rightarrow \infty$. Nevertheless, an average connectivity of 2.46 is remarkably close to $K = 2$, i.e. the critical connectivity for N–K networks.

Life as an Adaptive Network Living beings are complex and adaptive dynamical systems; a subject that we will further dwell on in Chap. 5. The here discussed
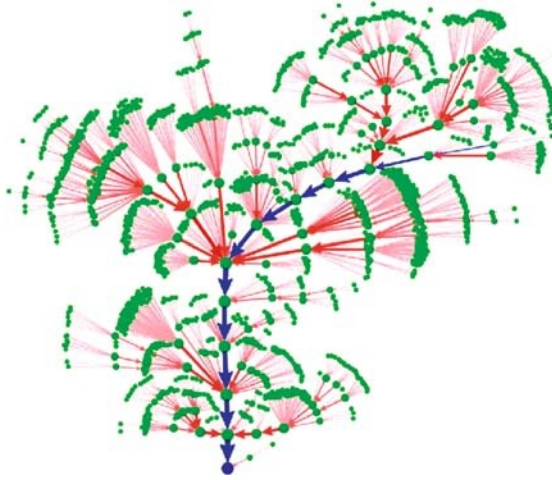
Fig. 3.12 The yeast cell cycle as an attractor trajectory of the gene expression network. Shown are the 1764 states (*green dots*, out of the $2^{11} = 2048$ states in phase space Ω) making up the basin of attraction of the biologically stable G_1 state (at the bottom). After starting with the excited G_1 normal state (the first state in the biological pathway represented by *blue arrows*), compare Fig. 3.11, the boolean dynamics runs through the known intermediate states (blue arrows) until the G_1 states attractor is again reached, representing the two daughter cells (from Li et al., 2004)

preliminary results on the yeast gene expression network indicate that this statement is not just an abstract notion. Adaptive regulative networks constitute the core of all living.

3.5.3 Application to Neural Networks

Time Encoding by Random Neural Networks There is some debate in neuroscience whether, and to which extent, time encoding is used in neural processing.

– Ensemble Encoding: Ensemble encoding is present when the activity of a sensory input is transmitted via the firing of certain ensembles of neurons. Every sensory input, e.g. every different smell sensed by the nose, has its respective neural ensemble.
– Time Encoding: Time encoding is present if the same neurons transmit more than one piece of sensory information by changing their respective firing patterns.

Cyclic attractors in a dynamical ensemble are an obvious tool to generate time encoded information. For random boolean networks as well as for random neural networks appropriate initial conditions, corresponding to certain activity patterns of the primary sensory organs, will settle into a cycle, as discussed in Sect. 3.4. The random network may then be used to encode initial firing patterns by the time sequence
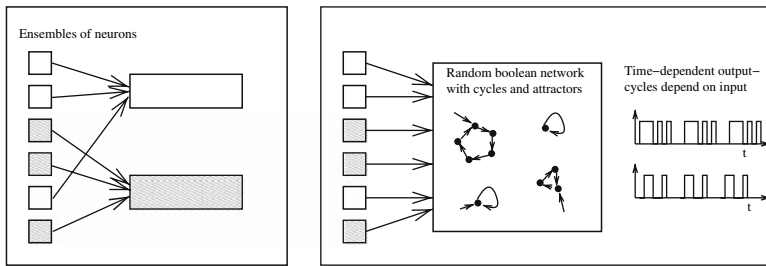
Fig. 3.13 Illustration of ensemble (**a**) and time (**b**) encoding. *Left*: All receptor neurons corresponding to the same class of input signals are combined, as as occurs in the nose for different odors. *Right*: The primary input signals are mixed together by a random neural network close to criticality and the relative weights are time encoded by the output signal
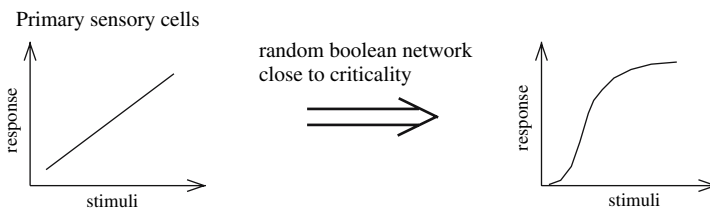
Fig. 3.14 The primary response of sensory receptors can be enhanced by many orders of magnitude using the non-linear amplification properties of a random neural network close to criticality

of neural activities resulting from the firing patterns of the corresponding limiting cycle, see Fig. 3.13.

Critical Sensory Processing The processing of incoming information is qualitatively different in the various phases of the *N–K* model, as discussed in Sect. 3.3.1.

The chaotic phase is unsuitable for information processing, any input results in an unbounded response and saturation. The response in the frozen phase is strictly proportional to the input and is therefore well behaved, but also relatively uninteresting. The critical state, on the other hand, has the possibility of nonlinear signal amplification.

Sensory organs in animals can routinely process physical stimuli, such as light, sound, pressure or odorant concentrations, which vary by many orders of magnitude in intensity. The primary sensory cells, e.g. the light receptors in the retina, have, however a linear sensibility to the intensity of the incident light, with a relatively small dynamical range. It is therefore conceivable that the huge dynamical range of sensory information processing of animals is a collective effect, as it occurs in a random neural network close to criticality. This mechanism, which is plausible from the view of possible genetic encoding mechanisms, is illustrated in Fig. 3.14.

Exercises

$K = 1$ KAUFFMAN NET

Analyze some $K = 1$ Kauffman nets with $N = 3$ and a cyclic linkage tree: $\sigma_1 = f_1(\sigma_2)$, $\sigma_2 = f_2(\sigma_3)$, $\sigma_3 = f_3(\sigma_1)$. Consider:
(i) $f_1 = f_2 = f_3 =$ identity,
(ii) $f_1 = f_2 = f_3 =$ negation and
(iii) $f_1 = f_2 =$ negation, $f3 =$ identity.
Construct all cycles and their attraction basin.

$N = 4$ KAUFFMAN NET

Consider the $N = 4$ graph illustrated in Fig. 3.1. Assume all coupling functions to be generalized XOR-functions (1/0 if the number of input-1's is odd/even). Find all cycles.

SYNCHRONOUS VS. ASYNCHRONOUS UPDATING

Consider the dynamics of the three-site network illustrated in Fig. 3.3 under sequential asynchronous updating. At every time step first update σ_1 then σ_2 and then σ_3. Determine the full network dynamics, find all cycles and fixpoints and compare with the results for synchronous updating shown in Fig. 3.3.

THE HUEPE AND ALDANA NETWORK

Solve the boolean neural network with uniform coupling functions and noise,

$$
\sigma_i(t+1) \;=\; \begin{cases} \text{sign}\left(\sum_{j=1}^{K} \sigma_{i_j}(t)\right) & \text{with probability } 1 - \eta, \\[2ex] -\text{sign}\left(\sum_{j=1}^{K} \sigma_{i_j}(t)\right) & \text{with probability } \quad \eta, \end{cases}
$$

via mean-field theory, where $\sigma_i = \pm 1$, by considering the order parameter

$$
\Psi \;=\; \lim_{T \to \infty} \frac{1}{T} \int_0^T |s(t)| \, dt, \qquad s(t) \;=\; \lim_{N \to \infty} \frac{1}{N} \sum_{i=1}^{N} \sigma_i(t) \, .
$$

See Huepe and Aldana-González (2002) and additional hints in the solutions section.

BOND PERCOLATION

Consider a finite $L \times L$ two-dimensional square lattice. Write a code that generates a graph by adding with probability $p \in [0,1]$ nearest-neighbor edges. Try to develop an algorithm searching for a non-interrupted path of bonds from one edge to the opposite edge; you might consult web resources. Try to determine the critical p_c, for $p > p_c$, a percolating path should be present with probability 1 for very large systems L.

Further Reading

The interested reader may want to take a look at Kauffman's (1969) seminal work on random boolean networks, or to study his book (Kauffman, 1993). For a review on boolean networks please consult Aldana, Coppersmith and Kadanoff (2003).

Examples of additional applications of boolean network theory regarding the modeling of neural networks (Wang, Pichler and Ross, 1990) and of evolution (Bornholdt and Sneppen, 1998) are also recommended. Some further interesting original literature concerns the connection of Kauffman nets with percolation theory (Lam, 1988), as well as the exact solution of the Kauffman net with connectivity one (Flyvbjerg and Kjaer, 1988), numerical studies of the Kauffman net (Flyvbjerg, 1989; Kauffman, 1969, 1990; Bastolla and Parisi, 1998), as well as the modeling of the yeast reproduction cycle by boolean networks (Li et al., 2004).

Some of the new developments concern the stability of the Kauffman net (Bilke and Sjunnesson, 2001) and the number of attractors (Samuelsson and Troein, 2003) and applications to time encoding by the cyclic attractors (Huerta and Rabinovich, 2004) and nonlinear signal amplification close to criticality (Kinouchi and Copelli, 2006).

ALDANA-GONZALEZ, M., SUSAN COPPERSMITH, S., KADANOFF, L.P. 2003 *Boolean Dynamics with Random Couplings* In Kaplan, E., Marsden, J.E., Sreenivasan, K.R. (eds.) Perspectives and Problems in Nonlinear Science. A Celebratory Volume in Honor of Lawrence Sirovich, pp. 23–89. Springer Applied Mathematical Sciences Series, Berlin.

ALDANA-GONZALEZ, M., CLUZEL, P. 2003 A natural class of robust networks. *Proceedings of the National Academy of Sciences* **100**, 8710–8714.

BASTOLLA, U., PARISI, G. 1998 Relevant elements, magnetization and dynamical properties in Kauffman networks: A numerical study. *Physica D* **115**, 203–218.

BILKE, S., SJUNNESSON, F. 2001 Stability of the Kauffman model. *Physical Review E* **65**, 016129.

BORNHOLDT, S., SNEPPEN, K. 1998 Neutral mutations and punctuated equilibrium in evolving genetic networks. *Physical Review Letters* **81**, 236–239.

FLYVBJERG, H. 1989 Recent results for random networks of automata. *Acta Physica Polonica B* **20**, 321–349.

FLYVBJERG, H., KJAER, N.J. 1988 Exact solution of Kauffman model with connectivity one. *Journal of Physics A: Mathematical and General* **21**, 1695–1718.

HUEPE, C., ALDANA-GONZÁLEZ, M. 2002 Dynamical phase transition in a neural network model with noise: An exact solution. *Journal of Statistical Physics* **108**, 527–540.

HUERTA, R., RABINOVICH, M. 2004 Reproducible sequence generation in random neural ensembles. *Physical Review Letters* **93**, 238104.

KAUFFMAN, S. A. 1969 Metabolic stability and epigenesis in randomly constructed nets. *Journal of Theoretical Biology* **22**, 437–467.

KAUFFMAN, S.A. 1990 Requirements for evolvability in complex systems – orderly dynamics and frozen components. *Physica D* **42**, 135–152.

KAUFFMAN, S.A. 1993 *The Origins of Order: Self-organization and Selection in Evolution.* Oxford University Press.

KINOUCHI, O., COPELLI, M.   2006   Optimal dynamical range of excitable networks at critical-
    ity *Nature Physics* **2**, 348–352.

LAM, P.M.   1988   A percolation approach to the Kauffman model. *Journal of Statistical Physics*
    50, 1263–1269.

LI, F., LONG, T., LU, Y., OUYANG, Q., TANG, C.   2004   The yeast cell-cycle network is ro-
    bustly designed. *Proceedings of the National Academy Science* **101**, 4781–4786.

LUQUE, B., SOLE, R.V.   2000   Lyapunov exponents in random boolean networks. *Physica A*
    284, 33–45.

SAMUELSSON, B., TROEIN, C.   2003   Superpolynomial growth in the number of attractors in
    Kauffman networks. *Physical Review Letters* **90**, 098701.

SOMOGYI, R., SNIEGOSKI, C.A.   1996   Modeling the complexity of genetic networks: Under-
    standing multigenetic and pleiotropic regulation *Complexity* **1**, 45–63.

WANG, L., PICHLER, E.E., ROSS, J.   1990   Oscillations and chaos in neural networks – An ex-
    actly solvable model. *Proceedings of the National Academy of Sciences of the United States
    of America* **87**, 9467–9471.

Chapter 4
Cellular Automata and Self-Organized Criticality

The notion of "phase transition" is a key concept in the theory of complex systems. We encountered an important class of phase transitions in Chap. 3, viz transitions in the overall dynamical state induced by changing the average connectivity in networks of randomly interacting boolean variables.

The concept of phase transition originates from physics. At its basis lies the "Landau theory of phase transition", which we will discuss in this chapter. Right at the point of transition between one phase and another, systems behave in a very special fashion; they are said to be "critical". Criticality is reached normally when tuning an external parameter, such as the temperature for many physical phase transitions or the average connectivity for the case of random boolean networks.

The central question discussed in this chapter is whether "self-organized criticality" is possible in complex adaptive systems, i.e. whether a system can adapt its own parameters in a way to move towards criticality on its own, as a consequence of a suitable adaptive dynamics. The possibility of self-organized criticality is a very intriguing outlook. In this context, we discussed in Chap. 3, the notion of "life at the edge of chaos", viz the hypothesis that the dynamical state of living beings may be close to self-organized criticality.

We will introduce and discuss "cellular automata" in this chapter, an important and popular class of standardized dynamical systems. Cellular automata allow a very intuitive construction of models, such as the famous "sandpile model", showing the phenomenon of self-organized criticality. The chapter then concludes with a discussion of whether self-organized criticality occurs in the most adaptive dynamical system of all, namely in the context of long-term evolution.

4.1 The Landau Theory of Phase Transitions

Second-Order Phase Transitions Phase transitions occur in many physical systems when the number of components diverges, viz "macroscopic" systems. Every phase has characteristic properties. The key property, which distinguishes one phase
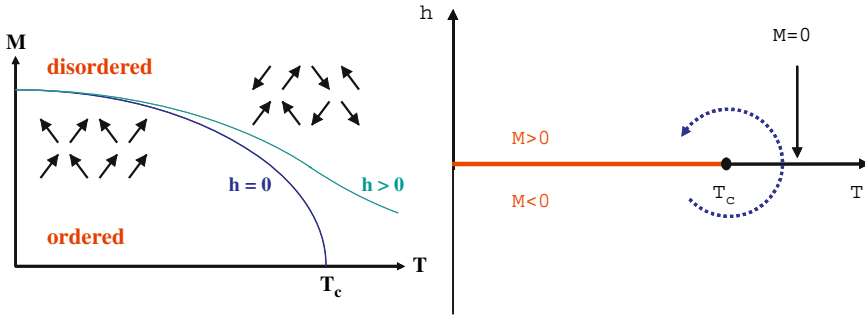
Fig. 4.1 Phase diagram of a magnet in an external magnetic field h. *Left*: The order parameter M (magnetization) as a function of temperature across the phase transition. The arrows illustrate typical arrangements of the local moments. In the ordered phase there is a net magnetic moment (magnetization). For $h = 0/h > 0$ the transition disorder–order is a sharp transition/crossover. *Right*: The $T - h$ phase diagram. A sharp transition occurs only for vanishing external field h

from another, is denoted the "order parameter". Mathematically one can classify the type of ordering according to the symmetry of the ordering breaks.

> *The Order Parameter. In a continuous or "second-order" phase transition the high-temperature phase has a higher symmetry than the low-temperature phase and the degree of symmetry breaking can be characterized by an order parameter ϕ.*

Note that all matter is disordered at high enough temperatures and ordered phases occur at low to moderate temperatures in physical systems.

Ferromagnetism in Iron The classical example for a phase transition is that of a magnet like iron. Above the Curie temperature of $T_c = 1043°$K the elementary magnets are disordered, see Fig. 4.1 for an illustration. They fluctuate strongly and point in random directions. The net magnetic moment vanishes. Below the Curie temperature the moments point on the average to a certain direction creating such a macroscopic magnetic field. Since magnetic fields are generated by circulating currents and since an electric current depends on time, one speaks of a breaking of "time-reversal symmetry" in the magnetic state of a ferromagnet like iron. Some further examples of order parameters characterizing phase transitions in physical systems are listed in Table 4.1.

Free Energy A statistical mechanical system takes the configuration with the lowest energy at zero temperature. A physical system at finite temperatures $T > 0$ does not minimize its energy but a quantity called the *free energy F*, which differs from the energy by a term proportional to the entropy and to the temperature[1].

Close to the transition temperature T_c the order parameter ϕ is small and one assumes within the Landau–Ginsburg model that the free energy density $f = F/V$,

---

[1] Details can be found in any book on thermodynamics and phase transitions, e.g. Callen (1985), they are, however, not necessary for an understanding of the following discussions.
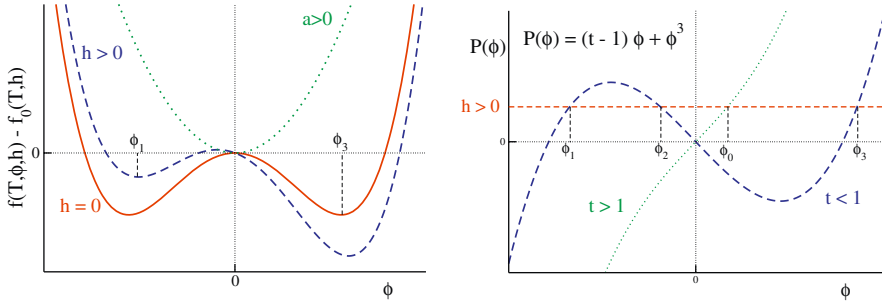
Fig. 4.2 *Left*: The functional dependence of the Landau–Ginzburg free energy $f(T,\phi,h) - f_0(T,h) = -h\phi + a\phi^2 + b\phi^4$, with $a = (t-1)/2$. Plotted is the free energy for $a < 0$ and $h > 0$ (*dashed line*) and $h = 0$ (*full line*) and for $a > 0$ (*dotted line*). *Right*: Graphical solution of Eq. (4.9) for a non-vanishing field $h \neq 0$; ϕ_0 is the order parameter in the disordered phase ($t > 1$, *dotted line*), ϕ_1, ϕ_3 the stable solutions in the order phase ($t < 1$, *dashed line*) and ϕ_2 the unstable solution, compare the *left-hand* side illustration

$$f = f(T, \phi, h),$$

can be expanded for a small order parameter ϕ and a small external field h:

$$f(T,\phi,h) = f_0(T,h) - h\phi + a\phi^2 + b\phi^4 + \dots \tag{4.1}$$

where the parameters $a = a(T)$ and $b = b(T)$ are functions of the temperature T and of an external field h, e.g. a magnetic field for the case of magnetic systems. Note the linear coupling of the external field h to the order parameter in lowest order and that $b > 0$ (stability for large ϕ), compare Fig. 4.2.

Spontaneous Symmetry Breaking All odd terms $\sim \phi^{2n+1}$ vanish in the expansion (4.1). The reason is simple. The expression (4.1) is valid for all temperatures close to T_c and the disordered high-temperature state is invariant under the symmetry operation

$$f(T,\phi,h) = f(T,-\phi,-h), \qquad \phi \leftrightarrow -\phi, \qquad h \leftrightarrow -h.$$

Table 4.1 Examples of important types of phase transitions in physical systems. When the transition is continuous/discontinuous one speaks of a second-/first-order phase transition. Note that most order parameters are non-intuitive. The superconducting state, notable for its ability to carry electrical current without dispersion, breaks what one calls the $U(1)$-gauge invariance of the normal (non-superconducting) metallic state

Transition	Type	Order parameter ϕ
Superconductivity	Second-order	U(1)-gauge
Magnetism	Mostly second-order	Magnetization
Ferroelectricum	Mostly second-order	Polarization
Bose–Einstein	Second-order	Amplitude of $k = 0$ state
Liquid–gas	First-order	Density

This relation must therefore hold also for the exact Landau–Ginsburg functional. When the temperature is lowered the order parameter ϕ will acquire a finite expectation value. One speaks of a "spontaneous" breaking of the symmetry inherent to the system.

The Variational Approach The Landau–Ginsburg functional (4.1) expresses the value that the free-energy would have for all possible values of ϕ. The true physical state, which one calls the "thermodynamical stable state", is obtained by finding the minimal $f(T, \phi, h)$ for all possible values of ϕ:

$$\delta f = \left(-h + 2a\phi + 4b\phi^3\right)\delta\phi = 0,$$
$$0 = -h + 2a\phi + 4b\phi^3, \tag{4.2}$$

where δf and $\delta\phi$ denote small variations of the free energy and of the order parameter, respectively. This solution corresponds to a minimum in the free energy if

$$\delta^2 f > 0, \qquad \delta^2 f = \left(2a + 12b\phi^2\right)(\delta\phi)^2. \tag{4.3}$$

One also says that the solution is "locally stable", since any change in ϕ from its optimal value would raise the free energy.

Solutions for $h = 0$ We consider first the case with no external field, $h = 0$. The solution of Eq. (4.2) is then

$$\phi = \begin{cases} 0 & \text{for } a > 0 \\ \pm\sqrt{-a/(2b)} & \text{for } a < 0 \end{cases}. \tag{4.4}$$

The trivial solution $\phi = 0$ is stable,

$$\left(\delta^2 f\right)_{\phi=0} = 2a(\delta\phi)^2, \tag{4.5}$$

if $a > 0$. The nontrivial solutions $\phi = \pm\sqrt{-a/(2b)}$ of Eq. (4.4) are stable,

$$\left(\delta^2 f\right)_{\phi\neq0} = -4a(\delta\phi)^2, \tag{4.6}$$

for $a < 0$. Graphically this is immediately evident, see Fig. 4.2. For $a > 0$ there is a single global minimum at $\phi = 0$, for $a < 0$ we have two symmetric minima.

Continuous Phase Transition We therefore find that the Ginsburg–Landau functional (4.1) describes continuous phase transitions when $a = a(T)$ changes sign at the critical temperature T_c. Expanding $a(T)$ for small $T - T_c$ we have

$$a(T) \sim T - T_c, \qquad a = a_0(t - 1), \qquad t = T/T_c, \qquad a_0 > 0,$$

where we have used $a(T_c) = 0$. For $T < T_c$ (ordered phase) the solution Eq. (4.4) then takes the form
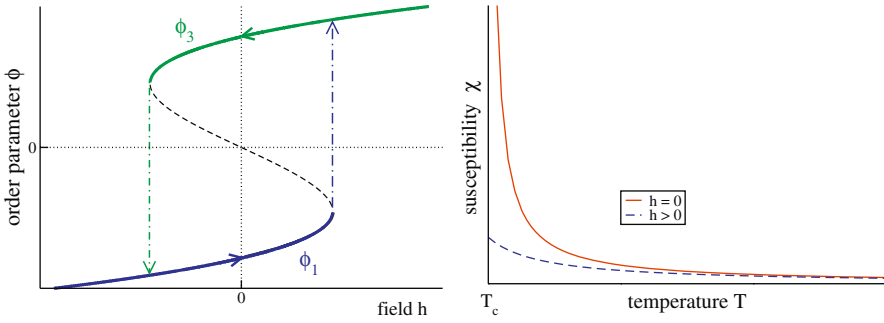
Fig. 4.3 *Left*: Discontinuous phase transition and hysteresis in the Landau model. Plotted is the solution $\phi = \phi(h)$ of $h = (t-1)\phi + \phi^3$ in the ordered phase ($t < 1$) when changing the field h. *Right*: The susceptibility $\chi = \partial\phi/\partial h$ for $h = 0$ (*solid line*) and $h > 0$ (*dotted line*). The susceptibility divergence in the absence of an external field ($h = 0$), compare Eq. (4.11)

$$\phi = \pm\sqrt{\frac{a_0}{2b}(1-t)}, \qquad t < 1, \qquad T < T_c . \qquad (4.7)$$

Simplification by Rescaling We can always rescale the order parameter ϕ, the external field h and the free energy density f such that $a_0 = 1/2$ and $b = 1/4$. We then have

$$a = \frac{t-1}{2}, \qquad f(T,\phi,h) - f_0(T,h) = -h\phi + \frac{t-1}{2}\phi^2 + \frac{1}{4}\phi^4$$

and

$$\phi = \pm\sqrt{1-t}, \qquad t = T/T_c \qquad (4.8)$$

for the non-trivial solution Eq. (4.7).

Solutions for h $\neq$ 0 The solutions of Eq. (4.2) are determined in rescaled form by

$$h = (t-1)\phi + \phi^3 \equiv P(\phi), \qquad (4.9)$$

see Fig. 4.2. In general one finds three solutions $\phi_1 < \phi_2 < \phi_3$. One can show (see the Exercises) that the intermediate solution is always locally instable and that ϕ_3 (ϕ_1) is globally stable for $h > 0$ ($h < 0$).

First-Order Phase Transition We note, see Fig. 4.2, that the solution ϕ_3 for $h > 0$ remains locally stable when we we vary the external field slowly (adiabatically)

$$(h > 0) \quad \rightarrow \quad (h = 0) \quad \rightarrow \quad (h < 0)$$

in the ordered state $T < T_c$. At a certain critical field, see Fig. 4.3, the order parameter changes sign abruptly, jumping from the branch corresponding to $\phi_3 > 0$ to the branch $\phi_1 < 0$. One speaks of hysteresis, a phenomenon typical for first-order phase transitions.

Susceptibility When the system is disordered and approaches the phase transition from above, it has an increased sensitivity towards ordering under the influence of an external field h.

> *Susceptibility. The susceptibility χ of a system denotes its response to an external field:*
>
> $$\chi = \left(\frac{\partial \phi}{\partial h}\right)_T , \tag{4.10}$$
>
> *where the subscript T indicates that the temperature is kept constant. The susceptibility measures the relative amount of the induced order $\phi = \phi(h)$.*

Diverging Response Taking the derivative with respect to the external field h in Eq. (4.9), $h = (t - 1)\phi + \phi^3$, we find for the disordered phase $T > T_c$,

$$1 = \left[(t-1) + 3\phi^2\right]\frac{\partial \phi}{\partial h}, \qquad \chi(T)\Big|_{h \to 0} = \frac{1}{t-1} = \frac{T_c}{T - T_c}, \tag{4.11}$$

since $\phi(h = 0) = 0$ for $T > T_c$. The susceptibility diverges at the phase transition for $h = 0$, see Fig. 4.3. This divergence is a typical precursor of ordering for a second-order phase transition. Exactly at T_c, viz at criticality, the response of the system is, strictly speaking, infinite.

A non-vanishing external field $h \neq 0$ induces a finite amount of ordering $\phi \neq 0$ at all temperatures and the phase transition is masked, compare Fig. 4.1. In this case, the susceptibility is a smooth function of the temperature, see Eq. (4.11) and Fig. 4.3.

4.2 Criticality in Dynamical Systems

Length Scales Any physical or complex system normally has well defined time and space scales. As an example we take a look at the Schrödinger equation for the hydrogen atom,

$$i\hbar \frac{\partial \Psi(t, \mathbf{r})}{\partial t} = H\Psi(t, \mathbf{r}), \qquad H = -\frac{\hbar^2 \Delta}{2m} - \frac{Ze^2}{|\mathbf{r}|},$$

where

$$\Delta = \frac{\partial^2}{\partial x^2} + \frac{\partial^2}{\partial y^2} + \frac{\partial^2}{\partial z^2}$$

is the Laplace operator. We do not need to know the physical significance of the parameters to realize that we can rewrite the differential operator H, called the "Hamilton" operator, as

$$H = -E_R\left(a_0^2\Delta + \frac{2a_0}{|\mathbf{r}|}\right), \qquad E_R = \frac{mZ^2e^4}{2\hbar^2}, \qquad a_0 = \frac{\hbar^2}{mZe^2} .$$

The length scale $a_0 = 0.53 \text{Å}/Z$ is called the "Bohr radius" and the energy scale $E_R = 13.6 \text{eV}$ the "Rydberg energy", which corresponds to a frequency scale of $E_R/\hbar = 3.39 \cdot 10^{15}$ Hz. The energy scale E_R determines the ground state energy and the characteristic excitation energies. The length scale a_0 determines the mean radius of the ground state wavefunction and all other radius-dependent properties.

Similar length scales can be defined for essentially all dynamical systems defined by a set of differential equations. The damped harmonic oscillator and the diffusion equations, e.g. are given by

$$\ddot{x}(t) - \gamma \dot{x}(t) + \omega^2 x(t) = 0, \qquad \frac{\partial \rho(t, \boldsymbol{r})}{\partial t} = D\Delta\rho(t, \boldsymbol{r}) . \qquad (4.12)$$

The parameters $1/\gamma$ and $1/\omega$, respectively, determine the time scales for relaxation and oscillation, and D is the diffusion constant.

Correlation Function A suitable quantity to measure and discuss the properties of the solutions of dynamical systems like the ones defined by Eq. (4.12) is the equal-time correlation function $S(r)$, which is the expectation value

$$S(r) = \langle \rho(t_0, \boldsymbol{x}) \rho(t_0, \boldsymbol{y}) \rangle, \qquad r = |\boldsymbol{x} - \boldsymbol{y}| . \qquad (4.13)$$

Here $\rho(t_0, \boldsymbol{x})$ denotes the particle density, for the case of the diffusion equation or when considering a statistical mechanical system of interacting particles. The exact expression for $\rho(t_0, \boldsymbol{x})$ in general depends on the type of dynamical system considered; for the Schrödinger equation $\rho(t, \boldsymbol{x}) = \Psi^*(t, \boldsymbol{x})\Psi(t, \boldsymbol{x})$, i.e. the probability to find the particle at time t at the point $\boldsymbol{x}$.

The equal-time correlation function then measures the probability to find a particle at position $\boldsymbol{x}$ when there is one at $\boldsymbol{y}$. $S(r)$ is directly measurable in scattering experiments and therefore a key quantity for the characterization of a physical system.

Correlation Length Of interest is the behavior of the equal-time correlation function $S(r)$ for large distances $r \to \infty$. In general we have two possibilities:

$$S(r)\Big|_{r\to\infty} \sim \begin{cases} e^{-r/\xi} & \text{non-critical} \\ 1/r^{d-2+\eta} & \text{critical} \end{cases} . \qquad (4.14)$$

In any "normal" (non-critical) system, correlations over arbitrary large distances cannot be built up, and the correlation function decays exponentially with the "correlation length" ξ. The notation $d - 2 + \eta > 0$ for the decay exponent of the critical system is a convention from statistical physics, where $d = 1, 2, 3, \ldots$ is the dimensionality of the system.

Scale-Invariance and Self-Similarity If a control parameter, often the temperature, of a physical system is tuned such that it sits exactly at the point of a phase transition, the system is said to be critical. At this point there are no characteristic length scales.
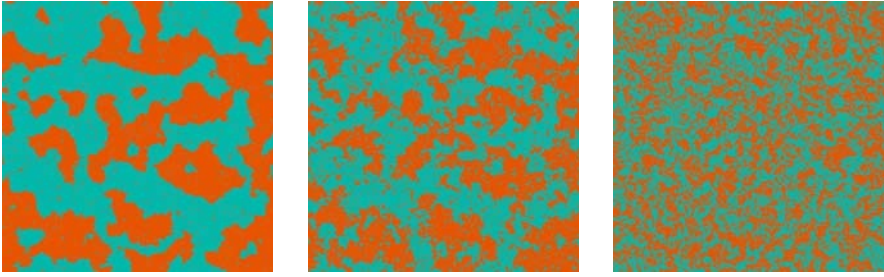
Fig. 4.4 Simulation of the 2D-Ising model $H = \sum_{<i,j>} \sigma_i \sigma_j$, $<i,j>$ nearest neighbors on a square lattice. Two magnetization orientations $\sigma_i = \pm 1$ correspond to the dark/light dots. For $T < T_c$ (*left*, ordered), $T \approx T_c$ (middle, critical) and $T > T_c$ (*right*, disordered). Note the occurrence of fluctuations at all length scales at criticality (self-similarity)

Scale Invariance. If a measurable quantity, like the correlation function, decays like a power of the distance $\sim (1/r)^\delta$, with a critical exponent δ, the system is said to be critical or scale-invariant.

Power laws have no scale; they are self-similar,

$$S(r) \;=\; c_0 \left(\frac{r_0}{r}\right)^\delta \;\equiv\; c_1 \left(\frac{r_1}{r}\right)^\delta \,, \qquad\qquad c_0\, r_0^\delta = c_1\, r_1^\delta \,,$$

for arbitrary distances r_0 and r_1.

Universality at the Critical Point The equal-time correlation function $S(r)$ is scale-invariant at criticality, compare Eq. (4.14). This is a surprising statement, since we have seen before that the differential equations determining the dynamical system have well defined time and length scales. How then does the solution of a dynamical system become effectively independent of the parameters entering its governing equations?

Scale invariance implies that fluctuations occur over all length scales, albeit with varying probabilities. This can be seen by observing snapshots of statistical mechanical simulations of simple models, compare Fig. 4.4. The scale invariance of the correlation function at criticality is a central result of the theory of phase transitions and statistical physics. The properties of systems close to a phase transition are not determined by the exact values of their parameters, but by the structure of the governing equations and their symmetries. This circumstance is denoted "universality" and constitutes one of the reasons for classifying phase transitions according to the symmetry of their order parameters, see Table 4.1.

Autocorrelation Function The equal-time correlation function $S(r)$ measures real-space correlations. The corresponding quantity in the time domain is the autocorrelation function

$$\Gamma(t) \;=\; \frac{\langle A(t+t_0)A(t_0)\rangle - \langle A\rangle^2}{\langle A^2\rangle - \langle A\rangle^2} \,, \qquad\qquad (4.15)$$

which can be defined for any time-dependent measurable quantity A, e.g. $A(t) = \rho(t,r)$. Note that the autocorrelations are defined relative to $\langle A \rangle^2$, viz the mean (time-independent) fluctuations. The denominator in Eq. (4.15) is a normalization convention, namely $\Gamma(0) \equiv 1$.

In the non-critical regime, viz the diffusive regime, no long-term memory is present in the system and all information about the initial state is lost exponentially,

$$\Gamma(t) \sim e^{-t/\tau}, \qquad t \to \infty. \tag{4.16}$$

τ is called the relaxation time. The relaxation or autocorrelation time τ is the time scale of diffusion processes.

Dynamical Critical Exponent The relaxation time entering Eq. (4.16) diverges at criticality, as does the real-space correlation length ξ entering Eq. (4.14). One can then define an appropriate exponent z, dubbed the "dynamical critical exponent" z, in order to relate the two power laws for τ and ξ via

$$\tau \sim \xi^z, \qquad \text{for} \qquad \xi = |T - T_c|^{-\nu} \to \infty.$$

The autocorrelation time is divergent in the critical state $T \to T_c$.

Self-Organized Criticality We have seen that phase transitions can be characterized by a set of exponents describing the respective power laws of various quantities like the correlation function or the autocorrelation function. The phase transition occurs generally at a single point, viz $T = T_c$ for a thermodynamical system. At the phase transition the system becomes effectively independent of the details of its governing equations, being determined by symmetries.

It then comes as a surprise that there should exist complex dynamical systems that attain a critical state for a finite range of parameters. This possibility, denoted "self-organized criticality" and the central subject of this chapter, is to some extent counter intuitive. We can regard the parameters entering the evolution equation as given externally. Self-organized criticality then signifies that the system effectively adapts to changes in the external parameters, e.g. to changes in the given time and length scales, in such a way that the stationary state becomes independent of those changes.

4.2.1 1/f Noise

So far we have discussed the occurrence of critical states in classical thermodynamics and statistical physics. We now ask ourselves for experimental evidence that criticality might play a central role in certain time-dependent phenomena.

***1/f* Noise** Per Bak and coworkers have pointed out that the ubiquitous $1/f$ noise, well known from electrical engineering, should result from a self-organized

phenomenon. One can postulate the noise to be generated by a continuum of weakly coupled damped oscillators representing the environment.

Power Spectrum of a Single Damped Oscillator A system with a single relaxation time τ, see Eq. (4.12), has a Lorentzian power spectrum

$$S(\omega, \tau) = Re \int_0^\infty dt\, e^{i\omega t} e^{-t/\tau} = Re\frac{-1}{i\omega - 1/\tau} = \frac{\tau}{1 + (\tau\omega)^2} \,.$$

For large frequencies $\omega \gg 1/\tau$ the power spectrum falls off like $1/\omega^2$.

Distribution of Oscillators The combined power or frequency spectrum of a continuum of oscillators is determined by the distribution $D(\tau)$ of relaxation times τ. For a critical system relaxation occurs over all time scales, as discussed in Sect. 4.2 and we may assume a scale-invariant distribution

$$D(\tau) \approx \frac{1}{\tau^\alpha} \tag{4.17}$$

for the relaxation times τ. This distribution of relaxation times yields a frequency spectrum

$$S(\omega) = \int d\tau\, D(\tau) \frac{\tau}{1 + (\tau\omega)^2} \sim \int d\tau \frac{\tau^{1-\alpha}}{1 + (\tau\omega)^2}$$
$$= \frac{1}{\omega\, \omega^{1-\alpha}} \int d(\omega\tau)\, \frac{(\omega\tau)^{1-\alpha}}{1 + (\tau\omega)^2} \sim \omega^{\alpha-2} \,. \tag{4.18}$$

For $\alpha = 1$ we obtain $1/\omega$, the typical behavior of $1/f$ noise.

The question is then how assumption (4.17) can be justified. The wide-spread appearance of $1/f$ noise can only happen when scale-invariant distribution of relaxation times are ubiquitous, viz if they were self-organized. The $1/f$ noise therefore constitutes an interesting motivation for the search of possible mechanisms leading to self-organized criticality.

4.3 Cellular Automata

Cellular automata are finite state lattice systems with discrete local update rules.

$$z_i \rightarrow f_i(z_i, z_{i+\delta}, \ldots), \qquad z_i \in [0, 1, \ldots, n] \,, \tag{4.19}$$

where $i + \delta$ denote neighboring sites of site i. Each site or "cell" of the lattice follows a prescribed rule evolving in discrete time steps. At each step the new value for a cell depends only on the current state of itself and on the state of its neighbors.

Cellular automata differ from the dynamical networks we studied in Chap. 3, in two aspects:

(i) The update functions are all identical: $f_i() \equiv f()$, viz they are translational invariant.

(ii) The number n of states per cell is usually larger than 2 (boolean case).

Cellular automata can give rise to extremely complex behavior despite their deceptively simple dynamical structure. We note that cellular automata are always updated synchronously and never sequentially or randomly. The state of all cells is updated simultaneously.

Number of Update Rules The number of possible update rules is huge. Take, e.g. a two-dimensional model (square lattice), where each cell can take only one of two possible states,

$$z_i = 0, \quad \text{(dead)}, \qquad z_i = 1, \quad \text{(alive)} .$$

We consider, for simplicity, rules for which the evolution of a given cell to the next time step depends on the current state of the cell and on the values of each of its eight nearest neighbors. In this case there are

$$2^9 = 512 \text{ configurations}, \qquad 2^{512} = 1.3 \times 10^{154} \text{ possible rules} ,$$

since any one of the 512 configurations can be mapped independently to "live" or "dead". For comparison note that the universe is only of the order of 3×10^{17} seconds old.

Totalistic Update Rules It clearly does not make sense to explore systematically the consequences of arbitrary updating rules. One simplification is to consider a mean-field approximation that results in a subset of rules called "totalistic". For mean-field rules the new state of a cell depends only on the total number of living neighbors and on its own state. The eight-cell neighborhood has

$$9 \text{ possible total occupancy states of neighboring sites},$$
$$2 \cdot 9 = 18 \text{ configurations}, \qquad 2^{18} = 262,144 \text{ totalistic rules} .$$

This is a large number, but it is exponentially smaller than the number of all possible update rules for the same neighborhood.

4.3.1 Conway's Game of Life

The "game of life" takes its name because it attempts to simulate the reproductive cycle of a species. It is formulated on a square lattice and the update rule involves the eight-cell neighborhood. A new offspring needs exactly three parents in its neighborhood. A living cell dies of loneliness if it has less than two live neighbors, and of overcrowding if it has more than three live neighbors. A living cell feels comfortable with two or three live neighbors; in this case it survives. The complete set of updating rules is listed in Table 4.2.

Living Isolated Sets   The time evolution of an initial set of a cluster of living cells can show extremely varied types of behavior. Fixpoints of the updating rules, such as a square

$$\left\{(0,0),(1,0),(0,1),(1,1)\right\}$$

of four neighboring live cells, survive unaltered. There are many configurations of living cells which oscillate, such as three live cells in a row or column,

$$\left\{(-1,0),(0,0),(1,0)\right\}, \qquad \left\{(0,-1),(0,0),(0,1)\right\}.$$

It constitutes a fixpoint of $f(f(.))$, alternating between a vertical and a horizontal bar. The configuration

$$\left\{(0,0),(0,1),(0,2),(1,2),(2,1)\right\}$$

is dubbed "glider", since it returns to its initial shape after four time steps but is displaced by $(-1,1)$, see Fig. 4.5. It constitutes a fixpoint of $f(f(f(f(.))))$ times the translation by $(-1,1)$. The glider continues to propagate until it encounters a cluster of other living cells.

The Game of Life as a Universal Computer   It is interesting to investigate, from an engineering point of view, all possible interactions between initially distinct sets of living cells in the game of life. In this context one finds that it is possible to employ gliders for the propagation of information over arbitrary distances. One can prove that arbitrary calculations can be performed by the game of life, when identifying the gliders with bits. Suitable and complicated initial configurations are necessary for this purpose, in addition to dedicated living subconfigurations performing logical computations, in analogy to electronic gates, when hit by one or more gliders.

4.3.2 The Forest Fire Model

The forest fires automaton is a very simplified model of real-world forest fires. It is formulated on a square lattice with three possible states per cell,

Table 4.2 Updating rules for the game of life; $z_i = 0, 1$ corresponds to empty and living cells. An "x" as an entry denotes what is going to happen for the respective number of living neighbors

$z_i(t)$	$z_i(t+1)$	Number of living neighbors				
		0	1	2	3	4..8
0	1				x	
	0	x	x	x		x
1	1			x	x	
	0	x	x			x

(a) block
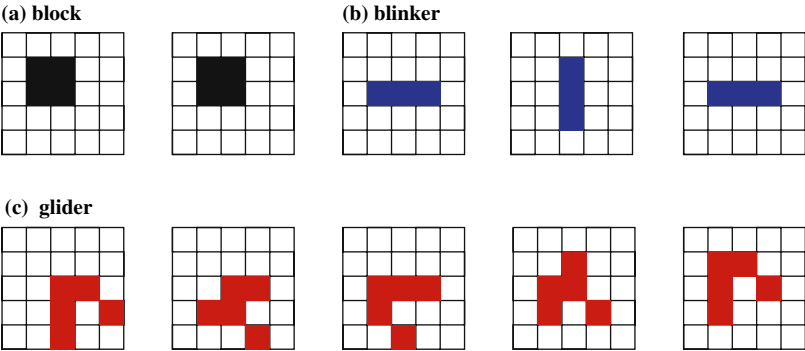
(b) blinker

(c) glider

Fig. 4.5 Time evolution of some living configurations for the game of life, see Table 4.2. (**a**) The "block"; it quietly survives. (**b**) The "blinker"; it oscillates with period 2. (c) The "glider"; it shifts by $(-1, 1)$ after four time steps

$$z_i = 0, \quad \text{(empty)}, \qquad z_i = 1, \quad \text{(tree)}, \qquad z_i = 2, \quad \text{(fire)} .$$

A tree sapling can grow on every empty cell with probability $p < 1$. There is no need for nearby parent trees, as sperms are carried by wind over wide distances. Trees do not die in this model, but they catch fire from any burning nearest neighbor tree. The rules are:

$z_i(t)$	$z_i(t+1)$	Condition
Empty	Tree	With probability $p < 1$
Tree	Tree	No fire close by
Tree	Fire	At least one fire close by
Fire	Empty	Always

The forest fire automaton differs from typical rules, such as Conway's game of life, because it has a stochastic component. In order to have an interesting dynamics one needs to adjust the growth rate p as a function of system size, so as to keep the fire burning continuously. The fires burn down the whole forest when trees grow too fast. When the growth rate is too low, on the other hand, the fires, being surrounded by ashes, may die out completely.

When adjusting the growth rate properly one reaches a steady state, the system having fire fronts continually sweeping through the forest, as is observed for real-world forest fires; this is illustrated in Fig. 4.6. In large systems stable spiral structures form and set up a steady rotation.

Criticality and Lightning The forest fire model, as defined above, is not critical, since the characteristic time scale $1/p$ for the regrowth of trees governs the dynamics. This time scale translates into a characteristic length scale $1/p$, which can be observed in Fig. 4.6, via the propagation rule for the fire.
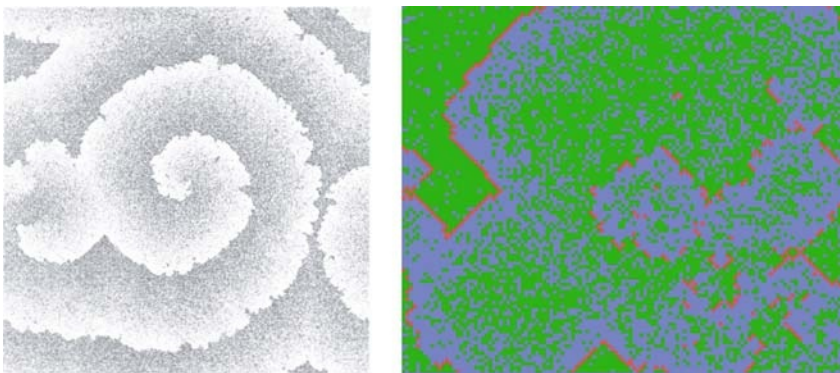
Fig. 4.6 Simulations of the forest fire model. *Left*: Fires burn in characteristic spirals for a growth probability $p = 0.005$ and no lightning, $f = 0$ (from Clar, Drossel and Schwabl, 1996). *Right*: A snapshot of the forest fire model with a growth probability $p = 0.06$ and a lightning probability $f = 0.0001$. Note the characteristic fire fronts with trees in front and ashes behind

Self-organized criticality can, however, be induced in the forest fire model when introducing an additional rule, namely that a tree might ignite spontaneously with a small probability f, when struck by lightning, causing also small patches of forest to burn. We will not discuss this mechanism in detail here, treating instead in the next section the occurrence of self-organized criticality in the sandpile model on a firm mathematical basis.

4.4 The Sandpile Model and Self-Organized Criticality

Self-Organized Criticality We have learned in Chap. 3 about the concept "life at the edge of chaos". Namely, that certain dynamical and organizational aspects of living organisms may be critical. Normal physical and dynamical systems, however, show criticality only for selected parameters, e.g. $T = T_c$, see Sect. 4.1. For criticality to be biologically relevant, the system must evolve into a critical state starting from a wide range of initial states – one speaks of "self-organized criticality".

The Sandpile Model Per Bak and coworkers introduced a simple cellular automaton that mimics the properties of sandpiles, i.e. the BTW model. Every cell is characterized by a force

$$z_i = z(x, y) = 0, 1, 2, \ldots, \qquad x, y = 1, \ldots, L$$

on a finite $L \times L$ lattice. There is no one-to-one correspondence of the sandpile model to real-world sandpiles. Loosely speaking one may identify the force z_i with the slope of real-world sandpiles. But this analogy is not rigorous, as the slope of a real-world sandpile is a continuous variable. The slopes belonging to two neighboring

cells should therefore be similar, whereas the values of z_i and z_j on two neighboring cells can differ by an arbitrary amount within the sandpile model.

The sand begins to topple when the slope gets too big:

$$z_j \;\rightarrow\; z_j - \Delta_{ij}, \qquad \text{if} \qquad z_j > K \;,$$

where K is the threshold slope and with the toppling matrix

$$\Delta_{i,j} \;=\; \begin{cases} 4 & i = j \\ -1 & i,j \quad \text{nearest neighbors} \\ 0 & \text{otherwise} \end{cases} \;. \tag{4.20}$$

This update rule is valid for the four-cell neighborhood $\{(0,\pm 1),(\pm 1,0)\}$. The threshold K is arbitrary, a shift in K simply shifts z_i. It is customary to consider $K = 3$. Any initial random configuration will then relax into a steady-state final configuration (called the stable state) with

$$z_i \;=\; 0,\ 1,\ 2,\ 3, \qquad \text{(stable state)} \;.$$

Open Boundary Conditions The update rule Eq. (4.20) is conserving:

Conserving Quantities. If there is a quantity that is not changed by the update rule it is said to be conserving.

The sandpile model is locally conserving. The total height $\sum_j z_j$ is constant due to $\sum_j \Delta_{i,j} = 0$. Globally, however, it is not conserving, as one uses open boundary conditions for which excess sand is lost at the boundary. When a site at the boundary topples, some sand is lost there and the total $\sum_j z_j$ is reduced by one.

However, here we have only a vague relation of the BTW model to real-world sandpiles. The conserving nature of the sandpile model mimics the fact that sand grains cannot be lost in real-world sandpiles. This interpretation , however, contrasts with the previously assumed correspondence of z_i with the slope of real-world sandpiles.

Avalanches When starting from a random initial state with $z_i \ll K$ the system settles in a stable configuration when adding "grains of sand" for a while. When a grain of sand is added to a site with $z_i = K$

$$z_i \;\rightarrow\; z_i + 1, \qquad z_i = K \;,$$

a toppling event is induced, which may in turn lead to a whole series of topplings. The resulting avalanche is characterized by its duration t and the size s of affected sites. It continues until a new stable configuration is reached. In Fig. 4.7 a small avalanche is shown.

Distribution of Avalanches We define with $D(s)$ and $D(t)$ the distributions of the size and of the duration of avalanches. One finds that they are scale-free,

Step 1				
3	0	3	2	3
1	2	3	1	0
2	3	3+1	1	3
3	1	0	2	0
0	2	1	3	1

Step 2				
3	0	3	2	3
1	2	4	1	0
2	4	0	2	3
3	1	1	2	0
0	2	1	3	1

Step 3				
3	0	4	2	3
1	4	0	2	0
3	0	2	2	3
3	2	1	2	0
0	2	1	3	1

Step 4				
3	2	0	3	3
2	0	2	2	0
3	1	2	2	3
3	2	1	2	0
0	2	1	3	1
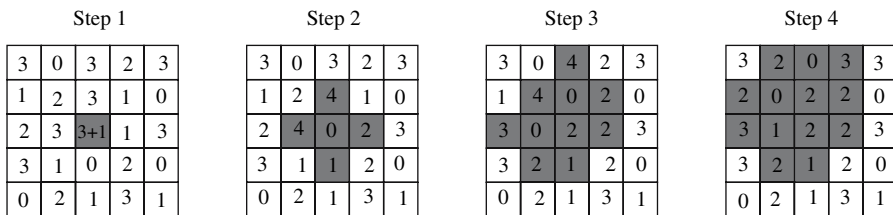
Fig. 4.7 The progress of an avalanche, with duration $t = 3$ and size $s = 13$, for a sandpile configuration on a 5×5 lattice with $K = 3$. The height of the sand in each cell is indicated by the numbers. The shaded region is where the avalanche has progressed. The avalanche stops after step 3

$$D(s) \sim s^{-\alpha_s}, \qquad D(t) \sim t^{-\alpha_t}, \tag{4.21}$$

as we will discuss in the next section. Equation (4.21) expresses the essence of self-organized criticality. We expect these scale-free relations to be valid for a wide range of cellular automata with conserving dynamics, independent of the special values of the parameters entering the respective update functions. Numerical simulations and analytic approximations for $d = 2$ dimensions yield

$$\alpha_s \approx \frac{5}{4}, \qquad \alpha_t \approx \frac{3}{4}.$$

Conserving Dynamics and Self-Organized Criticality We note that the toppling events of an avalanche are (locally) conserving. Avalanches of arbitrary large sizes must therefore occur, as sand can be lost only at the boundary of the system. One can indeed prove that Eqs. (4.21) are valid only for locally conserving models. Self-organized criticality breaks down as soon as there is a small but non-vanishing probability to lose sand somewhere inside the system.

Features of the Critical State The empty board, when all cells are initially empty, $z_i \equiv 0$, is not critical. The system remains in the frozen phase when adding sand; compare Chap. 3, as long as most $z_i < K$. Adding one sand corn after the other the critical state is slowly approached. There is no way to avoid the critical state.

Once the critical state is achieved the system remains critical. This critical state is paradoxically also the point at which the system is dynamically most unstable. It has an unlimited susceptibility to an external driving (adding a grain of sand), using the terminology of Sect. 4.1, as a single added grain of sand can trip avalanches of arbitrary size.

It needs to be noted that the dynamics of the sandpile model is deterministic, once the grain of sand has been added, and that the disparate fluctuations in terms of induced avalanches are features of the critical state per se and not due to any hidden stochasticity, as discussed in Chap. 2, or due to any hidden deterministic chaos.

4.5 Random Branching Theory

Branching theory deals with the growth of networks via branching. Networks generated by branching processes are loopless; they typically arise in theories of evolutionary processes. Avalanches have an intrinsic relation to branching processes: At every time step the avalanche can either continue or stop.

Branching in Sandpiles A typical update during an avalanche is of the form

$$
\begin{array}{lll}
\text{time 0:} & z_i \rightarrow z_i - 4 & z_j \rightarrow z_j + 1 \;, \\
\text{time 1:} & z_i \rightarrow z_i + 1 & z_j \rightarrow z_j - 4 \;,
\end{array}
$$

when two neighboring cells i and j initially have $z_i = K + 1$ and $z_j = K$. This implies that an avalanche typically intersects with itself. Consider, however, a general d-dimensional lattice with $K = 2d - 1$. The self-interaction of the avalanche becomes unimportant in the limit $1/d \rightarrow 0$ and the avalanche can be mapped rigorously to a random branching process. Note that we encountered an analogous situation in the context of high-dimensional or random graphs, discussed in Chap. 1, which are also loopless in the thermodynamic limit.

Binary Random Branching In $d \rightarrow \infty$ the notion of neighbors loses meaning, avalanches then have no spatial structure. Every toppling event affects $2d$ neighbors, on a d-dimensional hypercubic lattice. However, only the cumulative probability of toppling of the affected cells is relevant, due to the absence of geometric constraints in the limit $d \rightarrow \infty$. All that is important then is the question whether an avalanche continues, increasing its size continuosly, or whether it stops.

We can therefore consider the case of binary branching, viz that a toppling event creates two new active sites.

> *Binary Branching.*
>   *An active site of an avalanche topples with the probability p and creates two new active sites.*

For $p < 1/2$ the number of new active sites decreases on the average and the avalanche dies out. $p_c = 1/2$ is the critical state with (on the average) conserving dynamics. See Fig. 4.8 for some examples of branching processes.

Distribution of Avalanche Sizes The properties of avalanches are determined by the probability distribution,

$$
P_n(s, p), \qquad \sum_{s=1}^{\infty} P_n(s, p) = 1 \;,
$$

describing the probability to find an avalanche of size s in a branching process of order n. Here s is the (odd) number of sites inside the avalanche, see Figs. 4.8 and 4.9 for some examples.
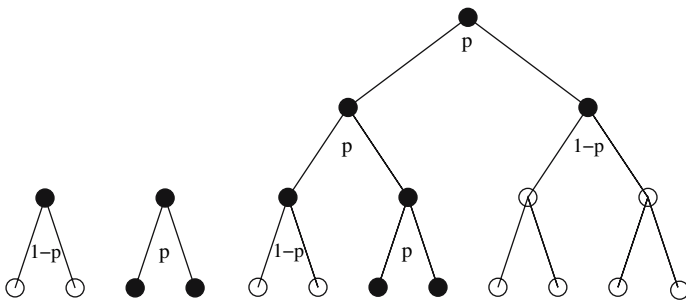
Fig. 4.8 Branching processes. *Left*: The two possible processes of order $n = 1$. *Right*: A generic process of order $n = 3$ with an avalanche of size $s = 7$

Generating Function Formalism In Chap. 3, we introduced the generating functions for probability distribution. This formalism is very useful when one has to deal with independent stochastic processes, as the joint probability of two independent stochastic processes is equivalent to the simple multiplication of the corresponding generating functions.

We define via

$$f_n(x,p) = \sum_s P_n(s,p)x^s, \qquad f_n(1,p) = \sum_s P_n(s,p) = 1 \qquad (4.22)$$

the generating functional $f_n(x,p)$ for the probability distribution $P_n(s,p)$. We note that

$$P_n(s,p) = \frac{1}{s!} \left. \frac{\partial^s f_n(x,p)}{\partial x^s} \right|_{x=0}, \qquad n, p \text{ fixed .} \qquad (4.23)$$

Small Avalanches For small s and large n one can evaluate the probability for small avalanches to occur by hand and one finds for the corresponding generating functionals:

$$P_n(1,p) = 1 - p, \qquad P_n(3,p) = p(1-p)^2, \qquad P_n(5,p) = 2p^2(1-p)^3 ,$$

compare Figs. 4.8 and 4.9. Note that $P_n(1,p)$ is the probability to find an avalanche of just one site.

The Recursion Relation For generic n the recursion relation

$$f_{n+1}(x,p) = x(1-p) + xp f_n^2(x,p) \qquad (4.24)$$

is valid. To see why, one considers building the branching network backwards, adding a site at the top:

- With the probability $(1 - p)$
  one adds a single-site avalanche described by the generating functional x.
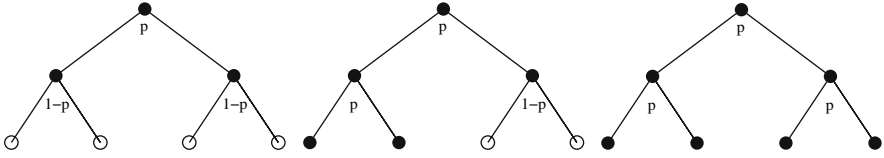
Fig. 4.9 Branching processes of order $n = 2$ with avalanches of sizes $s = 3, 5, 7$ (*left, middle, right*) and boundaries $\sigma = 0, 2, 4$

– With the probability p
  one adds a site, described by the generating functional x, which generated two
  active sites, described each by the generating functional $f_n(x, p)$.

The Self-Consistency Condition   For large n and finite x the generating functionals $f_n(x, p)$ and $f_{n+1}(x, p)$ become identical, leading to the self-consistency condition

$$f_n(x, p) \ = \ f_{n+1}(x, p) \ = \ x(1 - p) + xp\, f_n^2(x, p) \, , \tag{4.25}$$

with the solution

$$f(x, p) \ \equiv \ f_n(x, p) \ = \ \frac{1 - \sqrt{1 - 4x^2 p(1 - p)}}{2xp} \tag{4.26}$$

for the generating functional $f(x, p)$. The normalization condition

$$f(1, p) \ = \ \frac{1 - \sqrt{1 - 4^2 p(1 - p)}}{2p} \ = \ \frac{1 - \sqrt{(1 - 2p)^2}}{2p} \ = \ 1$$

is fulfilled for $p \in [0, 1/2]$. For $p > 1/2$ the last step in above equation would not be correct.

The Subcritical Solution   Expanding Eq. (4.26) in powers of x^2 we find terms like

$$\frac{1}{p} \left[4p(1 - p) \right]^k \frac{(x^2)^k}{x} \ = \ \frac{1}{p} \left[4p(1 - p) \right]^k x^{2k-1} \, .$$

Comparing this with the definition of the generating functional Eq. (4.22) we note that $s = 2k - 1$, $k = (s + 1)/2$ and that

$$P(s, p) \ \sim \ \frac{1}{p} \sqrt{4p(1 - p)} \left[4p(1 - p) \right]^{s/2} \ \sim \ e^{-s/s_c(p)} \, , \tag{4.27}$$

where we have used the relation

$$a^{s/2} = e^{\ln(a^{s/2})} = e^{-s(\ln a)/(-2)}, \qquad a = 4p(1-p),$$

and where we have defined the avalanche correlation size

$$s_c(p) = \frac{-2}{\ln[4p(1-p)]}, \qquad \lim_{p \to 1/2} s_c(p) \to \infty.$$

For $p < 1/2$ the size correlation length $s_c(p)$ is finite and the avalanche is consequently not scale-free, see Sect. 4.2. The characteristic size of an avalanche $s_c(p)$ diverges for $p \to p_c = 1/2$. Note that $s_c(p) > 0$ for $p \in]0,1[$.

The Critical Solution We now consider the critical case with

$$p = 1/2, \qquad 4p(1-p) = 1, \qquad f(x,p) = \frac{1 - \sqrt{1-x^2}}{x}.$$

The expansion of $\sqrt{1-x^2}$ with respect to x is

$$\sqrt{1-x^2} = \sum_{k=0}^{\infty} \frac{\frac{1}{2}\left(\frac{1}{2}-1\right)\left(\frac{1}{2}-2\right)\cdots\left(\frac{1}{2}-k+1\right)}{k!} \left(-x^2\right)^k$$

in Eq. (4.26) and therefore

$$P_c(k) \equiv P(s = 2k-1, p = 1/2) \sim \frac{\frac{1}{2}\left(\frac{1}{2}-1\right)\left(\frac{1}{2}-2\right)\cdots\left(\frac{1}{2}-k+1\right)}{k!}(-1)^k.$$

This expression is still unhandy. We are, however, only interested in the asymptotic behavior for large avalanche sizes s. For this purpose we consider the recursive relation

$$P_c(k+1) = \frac{1/2-k}{k+1}(-1)P_c(k) = \frac{1 - 1/(2k)}{1+1/k}P_c(k)$$

in the limit of large $k = (s+1)/2$, where $1/(1+1/k) \approx 1 - 1/k$,

$$P_c(k+1) \approx \left[1 - 1/(2k)\right]\left[1 - 1/k\right]P_c(k) \approx \left[1 - 3/(2k)\right]P_c(k).$$

This asymptotic relation leads to

$$\frac{P_c(k+1) - P_c(k)}{1} = \frac{-3}{2k}P_c(k), \qquad \frac{\partial P_c(k)}{\partial k} = \frac{-3}{2k}P_c(k),$$

with the solution

$$P_c(k) \sim k^{-3/2}, \qquad D(s) = P_c(s) \sim s^{-3/2}, \qquad \alpha_s = \frac{3}{2}, \qquad (4.28)$$

for large k, s, since $s = 2k - 1$.

Distribution of Relaxation Times The distribution of the duration n of avalanches can be evaluated in a similar fashion. For this purpose one considers the probability distribution function

$$Q_n(\sigma, p)$$

for an avalanche of duration n to have σ cells at the boundary, see Fig. 4.9.

One can then derive a recursion relation analogous to Eq. (4.24) for the corresponding generating functional and solve it self-consistently. We leave this as an exercise for the reader.

The distribution of avalanche durations is then given by considering $Q_n = Q_n$ ($\sigma = 0, p = 1/2$), i.e. the probability that the avalanche stops after n steps. One finds

$$Q_n \sim n^{-2}, \qquad D(t) \sim t^{-2}, \qquad \alpha_t = 2 . \qquad (4.29)$$

Tuned or Self-Organized Criticality? The random branching model discussed in this section had only one free parameter, the probability p. This model is critical only for $p \to p_c = 1/2$, giving rise to the impression that one has to fine tune the parameters in order to obtain criticality, just like in ordinary phase transitions.

This, however, is not the case. As an example we could generalize the sandpile model to continuous forces $z_i \in [0, \infty]$ and to the update rules

$$z_i \to z_i - \Delta_{ij}, \qquad \text{if} \qquad z_i > K ,$$

and

$$\Delta_{i,j} = \begin{cases} K & i = j \\ -cK/4 & i, j \quad \text{nearest neighbors} \\ -(1-c)K/8 & i, j \quad \text{next-nearest neighbors} \\ 0 & \text{otherwise} \end{cases} \qquad (4.30)$$

for a square-lattice with four nearest neighbors and eight next-nearest neighbors (Manhattan distance). The update rules are conserving,

$$\sum_j \Delta_{ij} = 0, \qquad \forall c \in [0, 1] .$$

For $c = 1$ this corresponds to the continuous field generalization of the BTW model. The model defined by Eqs. (4.30), which has not yet been studied in the literature, might be expected to map in the limit $d \to \infty$ to an appropriate random branching model with $p = p_c = 1/2$ and to be critical for all values of the parameters K and c, due to its conserving dynamics.

4.6 Application to Long-Term Evolution

An application of the techniques developed in this chapter can be used to study a model for the evolution of species proposed by Bak and Sneppen.
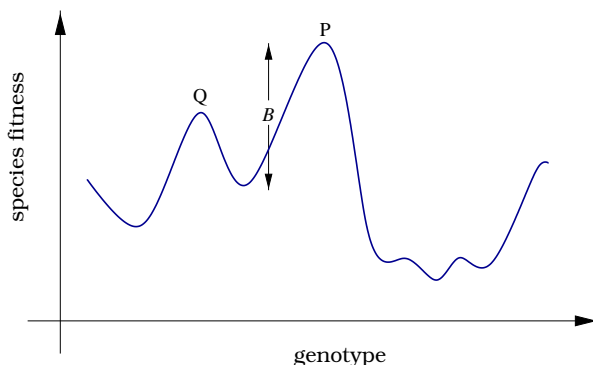
Fig. 4.10 A one-dimensional fitness landscape. A species evolving from an adaptive peak *P* to a new adaptive peak *Q* needs to overcome the fitness barrier *B*

Fitness Landscapes Evolution deals with the adaption of species and their fitness relative to the ecosystem they live in.

> *Fitness Landscapes.   The function that determines the chances of survival of a species, its fitness, is called the fitness landscape.*

In Fig. 4.10 a simple fitness landscape, in which there is only one dimension in the genotype (or phenotype)[2] space, is illustrated.

The population will spend most of its time in a local fitness maximum, whenever the mutation rate is low with respect to the selection rate, since there are fitness barriers, see Fig. 4.10, between adjacent local fitness maxima. Mutations are random processes and the evolution from one local fitness maximum to the next can then happen only through a stochastic escape, a process we discussed in Chap. 2.

Coevolution It is important to keep in mind for the following discussion that an ecosystem, and with it the respective fitness landscapes, is not static on long time scales. The ecosystem is the result of the combined action of geophysical factors, such as the average rainfall and temperature, and biological influences, viz the properties and actions of the other constituting species. The evolutionary progress of one species will therefore, in general, trigger adaption processes in other species appertaining to the same ecosystem, a process denoted "coevolution".

Evolutionary Time Scales In the model of Bak and Sneppen there are no explicit fitness landscapes like the one illustrated in Fig. 4.10. Instead the model attempts to mimic the effects of fitness landscapes, viz the influence of all the other species making up the ecosystem, by a single number, the "fitness barrier". The time needed for a stochastic escape from one local fitness optimum increases exponentially with

---

[2] The term "genotype" denotes the ensemble of genes. The actual form of an organism, the "phenotype", is determined by the genotype plus environmental factors, like food supply during growth.

the barrier height. We may therefore assume that the average time t it takes to mutate across a fitness barrier of height B scales as

$$t = t_0 e^{B/T} , \tag{4.31}$$

where t_0 and T are constants. The value of t_0 merely sets the time scale and is not important. The parameter T depends on the mutation rate, and the assumption that mutation is low implies that T is small compared with the typical barrier heights B in the landscape. In this case the time scales t for crossing slightly different barriers are distributed over many orders of magnitude and only the lowest barrier is relevant.

The Bak and Sneppen Model The Bak and Sneppen model is a phenomenological model for the evolution of barrier heights. The number N of species is fixed and each species has a respective barrier

$$B_i = B_i(t) \in [0,1], \qquad t = 0, 1, 2, \dots$$

for its further evolution. The initial $B_i(0)$ are drawn randomly from $[0,1]$. The model then consists of the repetition of two steps:

(1) The times for a stochastic escape are exponentially distributed, see Eq. (4.31). It is therefore reasonable to assume that the species with the lowest barrier B_i mutates and escapes first. After escaping, it will adapt quickly to a new local fitness maximum. At this point it will then have a new barrier for mutation, which is assumed to be uniformly distributed in $[0,1]$.
(2) The fitness function for a species i is given by the ecological environment it lives in, which is made up of all the other species. When any given species mutates it therefore influences the fitness landscape for a certain number of other species. Within the Bak and Sneppen model this translates into assigning new random barriers B_j for $K-1$ neighbors of the mutating species i.

The Bak and Sneppen model therefore tries to capture two essential ingredients of long-term evolution: The exponential distribution of successful mutations and the interaction of species via the change of the overall ecosystem, when one constituting species evolves.

The Random Neighbor Model The topology of the interaction between species in the Bak–Sneppen model is unclear. It might be chosen as two-dimensional, if the species are thought to live geographically separated, or one-dimensional in a toy model. In reality the topology is complex and can be assumed to be, in first approximation, random, resulting in the soluble random neighbor model.

Evolution of Barrier Distribution Let us discuss qualitatively the redistribution of barrier heights under the dynamics, the sequential repetition of step (1) and (2) above, see Fig. 4.11. The initial barrier heights are uniformly distributed over the interval $[0,1]$ and the lowest barrier, removed in step (1), is small. The new heights
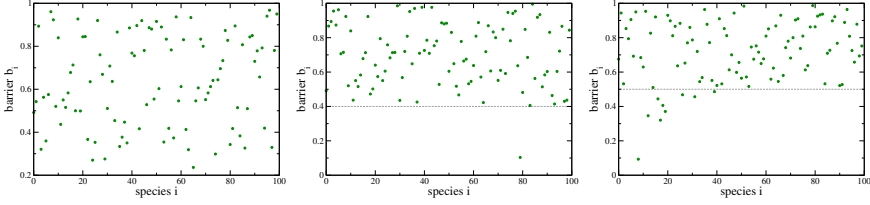
Fig. 4.11 The barrier values (dots) for a 100 species one-dimensional Bak–Sneppen model after 50, 200 and 1600 steps of a simulation. The horizontal line in each frame represents the approximate position of the upper edge of the "gap". A few species have barriers below this level, indicating that they were involved in an avalanche at the moment when the snapshot of the system was taken

reassigned in step (1) and (2) will therefore lead, on the average, to an increase of the average barrier height with passing time.

With increasing average barrier height the characteristic lowest barrier is also raised and eventually a steady state will be reached, just as in the sandpile model discussed previously. It turns out that the characteristic value for the lowest barrier is about $1/K$ at equilibrium in the mean-field approximation and that the steady state is critical.

Molecular Field Theory In order to solve the Bak–Sneppen model, we define the barrier distribution function,

$$p(x,t) ,$$

viz the probability to find a barrier of hight $x \in [0,1]$ at time step $t = 1, 2, \dots$. In addition, we define with $Q(x)$ the probability to find a barrier above x:

$$Q(x) = \int_x^1 dx'\, p(x'), \qquad Q(0) = 1, \qquad Q(1) = 0 . \qquad (4.32)$$

The dynamics is governed by the size of the smallest barrier. The distribution function $p_1(x)$ for the lowest barrier is

$$p_1(x) = N p(x) Q^{N-1}(x) , \qquad (4.33)$$

given by the probability $p(x)$ for one barrier (out of the N barriers) to have the barrier height x, while all the other $N-1$ barriers are larger. $p_1(x)$ is normalized,

$$\int_0^1 dx\, p_1(x) = (-N) \int_0^1 dx\, Q^{N-1}(x) \frac{\partial Q(x)}{\partial x} = -Q^N(x) \Big|_{x=0}^{x=1} = 1 ,$$

where we used $p(x) = -Q'(x)$, $Q(0) = 1$ and $Q(1) = 0$, see Eq. (4.32).

Time Evolution of Barrier Distribution The time evolution for the barrier distribution consists in taking away one (out of N) barrier, the lowest, via

$$p(x,t) - \frac{1}{N} p_1(x,t) \,,$$

and by removing randomly $K - 1$ barriers from the remaining $N - 1$ barriers, and adding K random barriers:

$$p(x,t+1) = p(x,t) - \frac{1}{N} p_1(x,t) \tag{4.34}$$
$$- \frac{K-1}{N-1} \left(p(x,t) - \frac{1}{N} p_1(x,t) \right) + \frac{K}{N} \,.$$

We note that $p(x,t+1)$ is normalized whenever $p(x,t)$ and $p_1(x,t)$ were normalized correctly:

$$\int_0^1 dx \, p(x,t+1) = 1 - \frac{1}{N} - \frac{K-1}{N-1} \left(1 - \frac{1}{N} \right) + \frac{K}{N}$$
$$= \left(1 - \frac{K-1}{N-1} \right) \frac{N-1}{N} + \frac{K}{N} = \frac{N-K}{N} + \frac{K}{N} \equiv 1 \,.$$

Stationary Distribution After many iterations of Eq. (4.34) the barrier distribution will approach a stationary solution $p(x,t+1) = p(x,t) \equiv p(x)$, as can be observed from the numerical simulation shown in Fig. 4.11. The stationary distribution corresponds to the fixpoint condition

$$0 = p_1(x) \frac{1}{N} \left(\frac{K-1}{N-1} - 1 \right) - p(x) \frac{K-1}{N-1} + \frac{K}{N}$$

of Eq. (4.34). Using the expression $p_1 = Np\,Q^{N-1}$, see Eq. (4.33), for $p_1(x)$ we then have

$$0 = Np(x) Q^{N-1}(x)(K-N) - p(x)(K-1)N + K(N-1) \,.$$

Using $p(x) = -\frac{\partial Q(x)}{\partial x}$ we obtain

$$0 = N(N-K) \frac{\partial Q(x)}{\partial x} Q^{N-1} + (K-1)N \frac{\partial Q(x)}{\partial x} + K(N-1)$$

$$0 = N(N-K) Q^{N-1} dQ + (K-1)N\,dQ + K(N-1)\,dx \,.$$

We can integrate this last expression with respect to x,

$$0 = (N-K) Q^N(x) + (K-1)N Q(x) + K(N-1)(x-1) \,, \tag{4.35}$$

where we took care of the boundary condition $Q(1) = 0$, $Q(0) = 1$.

Solution in the Thermodynamic Limit The polynomial Eq. (4.35) simplifies in the thermodynamic limit, with $N \to \infty$ and $K/N \to 0$, to
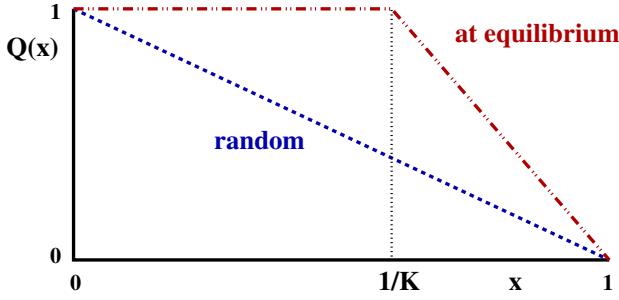
Fig. 4.12 The distribution $Q(x)$ to find a fitness barrier larger than $x \in [0, 1]$ for the Bak and Sneppen model, for the case of random barrier distribution (*dashed line*) and the stationary distribution (*dashed-dotted line*), compare Eq. (4.38)

$$0 \;=\; Q^N(x) + (K-1)\,Q(x) - K\,(1-x) \,. \tag{4.36}$$

We note that $Q(x) \in [0, 1]$ and that $Q(0) = 1$, $Q(1) = 0$. There must therefore be some $x \in]0, 1[$ for which $0 < Q(x) < 1$. Then

$$Q^N(x) \to 0, \qquad Q(x) \approx \frac{K}{K-1}\,(1-x) \,. \tag{4.37}$$

Equation (4.37) remains valid as long as $Q < 1$, or $x > x_c$:

$$1 \;=\; \frac{K}{K-1}(1-x_c), \qquad x_c \;=\; \frac{1}{K} \,.$$

We then have in the limit $N \to \infty$

$$\lim_{N \to \infty} Q(x) \;=\; \begin{cases} 1 & \text{for } x < 1/K \\ (1-x)K/(K-1) & \text{for } x > 1/K \end{cases}, \tag{4.38}$$

compare Fig. 4.12, and, using $p(x) = -\partial Q(x)/\partial x$,

$$\lim_{N \to \infty} p(x) \;=\; \begin{cases} 0 & \text{for } x < 1/K \\ K/(K-1) & \text{for } x > 1/K \end{cases}. \tag{4.39}$$

This result compares qualitatively well with the numerical results presented in Fig. 4.11. Note, however, that the mean-field solution Eq. (4.39) does not predict the exact critical barrier height, which is somewhat larger for $K = 2$ and a one-dimensional arrangement of neighbors, as in Fig. 4.11.

1/N Corrections Equation 4.39 cannot be rigorously true for $N < \infty$, since there is a finite probability for barriers with $B_i < 1/K$ to reappear at every step. One can expand the solution of the self-consistency Eq. (4.35) in powers of $1/N$. One finds
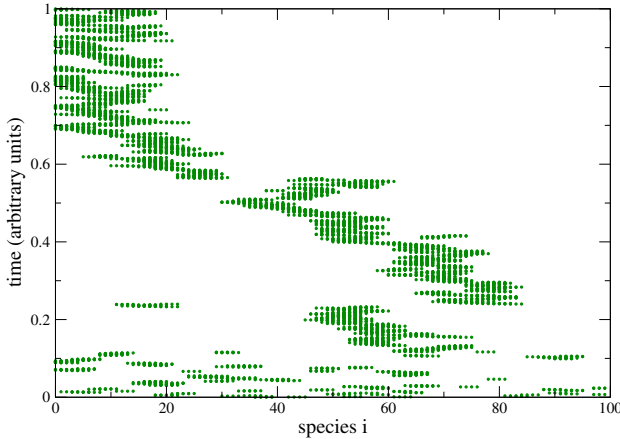
Fig. 4.13 A time series of evolutionary activity in a simulation of the one-dimensional Bak–Sneppen model with $K = 2$ showing coevolutionary avalanches interrupting the punctuated equilibrium. Each dot represents the action of choosing a new barrier value for one species

$$p(x) \simeq \begin{cases} K/N \text{ for } x < 1/K \\ K/(K-1) \text{ for } x > 1/K \end{cases} . \tag{4.40}$$

We leave the derivation as an exercise for the reader.

Distribution of the Lowest Barrier If the barrier distribution is zero below the self-organized threshold $x_c = 1/K$ and constant above, then the lowest barrier must be below x_c with equal probability:

$$p_1(x) \quad \rightarrow \quad \begin{cases} K \text{ for } x < 1/K \\ 0 \text{ for } x > 1/K \end{cases}, \qquad \int_0^1 dx \, p_1(x) = 1 . \tag{4.41}$$

Equations 4.41 and 4.33 are consistent with Eq. (4.40) for $x < 1/K$.

Coevolution and Avalanches When the species with the lowest barrier mutates we assign new random barrier heights to it and to its K-1 neighbors. This causes an avalanche of evolutionary adaptations whenever one of the new barriers becomes the new lowest fitness barrier. One calls this phenomenon "coevolution" since the evolution of one species drives the adaption of other species belonging to the same ecosystem. We will discuss this and other aspects of evolution in more detail in Chap. 5. In Fig. 4.13 this process is illustrated for the one-dimensional model. The avalanches in the system are clearly visible and well separated in time. In between the individual avalanches the barrier distribution does not change appreciably; one speaks of a "punctuated equilibrium".

Critical Coevolutionary Avalanches In Sect. 4.5 we discussed the connection between avalanches and random branching. The branching process is critical when it goes on with a probability of 1/2. To see whether the coevolutionary avalanches within the Bak and Sneppen model are critical we calculate the probability p_{bran} that

at least one of the K new, randomly selected, fitness barriers will be the new lowest barrier.

With probability x one of the new random barriers is in $[0, x]$ and below the actual lowest barrier, which is distributed with $p_1(x)$, see Eq. (4.41). We then have

$$p_{\text{bran}} = K \int_0^1 p_1(x) x \, dx = K \int_0^{1/K} K x \, dx = \frac{K^2}{2} x^2 \Big|_0^{1/K} \equiv \frac{1}{2},$$

viz the avalanches are critical. The distribution of the size s of the coevolutionary avalanches is then

$$D(s) \sim \left(\frac{1}{s}\right)^{3/2},$$

as evaluated within the random branching approximation, see Eq. (4.28), and independent of K. The size of a coevolutionary avalanche can be arbitrarily large and involve, in extremis, a finite fraction of the ecosystem, compare Fig. 4.13.

Features of the Critical State The sandpile model evolves into a critical state under the influence of an external driving, when adding one grain of sand after another. The critical state is characterized by a distribution of slopes (or heights) z_i, one of its characteristics being a discontinuity; there is a finite fraction of slopes with $z_i = Z - 1$, but no slope with $z_i = Z$, apart from some of the sites participating in an avalanche.

In the Bak and Sneppen model the same process occurs, but without external drivings. At criticality the barrier distribution $p(x) = \partial Q(x)/\partial x$ has a discontinuity at $x_c = 1/K$, see Fig. 4.12. One could say, cum grano salis, that the system has developed an "internal phase transition", namely a transition in the barrier distribution $p(x)$, an internal variable. This emergent state for $p(x)$ is a many-body or collective effect, since it results from the mutual reciprocal interactions of the species participating in the formation of the ecosystem.

Exercises

SOLUTIONS OF THE LANDAU–GINZBURG FUNCTIONAL
    Determine the order parameter for $h \neq 0$ via Eq. (4.9) and Fig. 4.2. Discuss the local stability condition Eq. (4.3) for the three possible solutions and their global stability. Note that $F = fV$, where F is the free energy, f the free energy density and V the volume.

ENTROPY AND SPECIFIC HEAT WITHIN THE LANDAU MODEL
    Determine the entropy $S(T) = \frac{\partial F}{\partial T}$ and the specific heat $c_V = T \frac{\partial S}{\partial T}$ within the Landau–Ginzburg theory Eq. (4.1) for phase transitions.

THE GAME OF LIFE
    Consider the evolution of the following states, see Fig. 4.5, under the rules for Conway's game of life:

{(0,0),(1,0),(0,1),(1,1)}
{(0,-1),(0,0),(0,1)}
{(0,0),(0,1),(1,0),(−1,0),(0,−1)}
{(0,0),(0,1),(0,2),(1,2),(2,1)}

The prediction may be checked with the Java-applet at
`http://www.ibiblio.org/\-lifepatterns`.

THE GAME OF LIFE ON A SMALL-WORLD NETWORK

Write a program to simulate the game of life on a 2D lattice. Consider this lattice as a network with every site having edges to its eight neighbors. Rewire the network such that (a) the local connectivities $z_i \equiv 8$ are retained for every site and (b) a small-world network is obtained. This can be achieved by cutting two arbitrary links with probability p and rewiring the four resulting stubs randomly. Define an appropriate dynamical order parameter and characterize the changes as a function of the rewiring probability. Compare the chapters "Graph Theory and Small-World Networks" and "Chaos, Bifurcations and Diffusion".

THE FOREST FIRE MODEL

Develop a mean-field theory for the forest fire model by introducing appropriate probabilities to find cells with trees, fires and ashes. Find the critical number of nearest neighbors Z for fires to continue burning.

THE REALISTIC SANDPILE MODEL

Propose a cellular automata model that simulates the physics of real-world sandpiles somewhat more realistically than the BTW model. The cell values $z(x,y)$ should correspond to the local height of the sand. Write a program to simulate the model.

THE RANDOM BRANCHING MODEL

Derive the distribution of avalanche durations Eq. (4.29) in analogy to the steps explained in Sect. 4.5.

THE BAK AND SNEPPEN MODEL

Write a program to simulate the Bak and Sneppen model in Sect. 4.6 and compare it with the molecular field solution Eq. (4.35).

Further Reading

Introductory texts to cellular automata and to the game of life are Wolfram (1986), Creutz (1997) and Berlekamp, Conway and Guy (1982). For a review of the forest fire and several related models, see Clar, Drossel and Schwabl (1996); for a review of sandpiles, see Creutz (2004), and for a general review of self-organized criticality, see Paczuski and Bak (1999). Exemplary textbooks on statistical physics and phase transitions have been written by Callen (1985) and Goldenfeld (1992).

Some general features of $1/f$ noise are discussed by Press (1978); its possible relation to self-organized criticality has been postulated by Bak, Tang and Wiesenfeld (1987). The formulation of the Bak and Sneppen (1993) model for long-term

coevolutionary processes and its mean-field solution are discussed by Flyvbjerg, Sneppen and Bak (1993).

The interested reader may also glance at some original research literature, such as a numerical study of the sandpile model (Priezzhev, Ktitarev and Ivashkevich, 1996) and the application of random branching theory to the sandpile model (Zapperi, Lauritsen and Stanley, 1995). The connection of self-organized criticality to local conservation rules is worked out by Tsuchiya and Katori (2000), and the forest fire model with lightning is introduced by Drossel and Schwabl (1992).

BAK, P. AND SNEPPEN, K.   1993   Punctuated equilibrium and criticality in a simple model of evolution. *Physical Review Letters* **71**, 4083–4086.

BAK, P., TANG, C. AND WIESENFELD, K.   1987   Self-organized criticality: An explanation of $1/f$ noise. *Physical Review Letters* **59**, 381–384.

BERLEKAMP, E., CONWAY, J. AND GUY, R.   1982   *Winning Ways for your Mathematical Plays, Vol. 2.* Academic Press, New York.

CALLEN, H.B.   1985   *Thermodynamics and Introduction to Thermostatistics.* Wiley, New York.

CLAR, S., DROSSEL, B. AND SCHWABL, F.   1996   Forest fires and other examples of self-organized criticality. *Journal of Physics: Condensed Matter* **8**, 6803–6824.

CREUTZ, M.   1997   *Cellular automata and self-organized criticality.* In Some new directions in science on computers, G. Bhanot, S. Chen and P. Seiden, eds. pp. 147–169 (World Scientific, Singapore).

CREUTZ, M.   2004   Playing with sandpiles. *Physica A* **340**, 521–526.

DROSSEL, B. AND SCHWABL, F.   1992   Self-organized critical forest-fire model *Physical Review Letters* **69**, 1629–1632.

FLYVBJERG, H., SNEPPEN, K. AND BAK, P.   1993   Mean field theory for a simple model of evolution. *Physical Review Letters* **71**, 4087–4090.

GOLDENFELD, N.   1992   *Lectures on Phase Transitions and the Renormalization Group.* Perseus Publishing.

NEWMAN, M.E.J., PALMER, R.G.   2002   *Models of Extinction.* Oxford University Press.

PACZUSKI, M., BAK. P.   1999   *Self organization of complex systems.* In: Proceedings of 12th Chris Engelbrecht Summer School; also available as `http://www.arxiv.org/abs/cond-mat/9906077`.

PRESS, W.H.   1978   Flicker noises in astronomy and elsewhere. *Comments on Modern Physics, Part C* **7**, 103–119.

PRIEZZHEV, V.B., KTITAREV, D.V., IVASHKEVICH, E.V.   1996   Formation of avalanches and critical exponents in an abelian sandpile model. *Physical Review Letters* **76**, 2093–2096.

TSUCHIYA, T., KATORI, M.   2000   Proof of breaking of self-organized criticality in a nonconservative abelian sandpile model. *Physical Review Letters* **61**, 1183–1186.

WOLFRAM, S., EDITOR   1986   *Theory and Applications of Cellular Automata.* World Scientific (Singapore).

ZAPPERI, S., LAURITSEN, K.B., STANLEY, H.E.   1995   Self-organized branching processes: Mean-field theory for avalanches. *Physical Review Letters* **75**, 4071–4074.

Chapter 5
Statistical Modeling of Darwinian Evolution

Adaptation and evolution are quasi synonymous in popular language and Darwinian evolution is a prime application of complex adaptive system theory. We will see that adaptation does not happen automatically and discuss the concept of "error catastrophe" as a possible root for the downfall of a species. Venturing briefly into the mysteries surrounding the origin of life, we will investigate the possible advent of a "quasispecies" in terms of mutually supporting hypercycles. The basic theory of evolution is furthermore closely related to game theory, the mathematical theory of interacting agents, viz of rationally acting economic persons.

We will learn in this chapter, on the one hand, that every complex dynamical system has its distinct characteristics to be considered. In the case of Darwinian evolution these are concepts like fitness, selection and mutation. General notions from complex system theory are, on the other hand, important for a thorough understanding. An example is the phenomenon of stochastic escape discussed in Chap. 2, which is operative in the realm of Darwinian evolution.

5.1 Introduction

Microevolution The ecosystem of the earth is a complex and adaptive system. It formed via Darwinian evolution through species differentiation and adaptation to a changing environment. A set of inheritable traits, the genome, is passed from parent to offspring and the reproduction success is determined by the outcome of random mutations and natural selection – a process denoted "microevolution"[1]

Asexual Reproduction. *One speaks of asexual reproduction when an individual has a single parent.*

---

[1] Note that the term "macroevolution", coined to describe the evolution at the level of organisms, is nowadays somewhat obsolete.

Here we consider mostly models for asexual reproduction, though most concepts can be easily generalized to the case of sexual reproduction.

Basic Terminology Let us introduce some basic variables needed to formulate the approach.

– Population M: The number of individuals.
  We assume here that M does not change with time, modeling the competition for a limited supply of resources.
– Genome N: Size of the genome.
  We encode the inheritable traits by a set of N binary variables,

$$\mathbf{s} = (s_1, s_2, \ldots, s_N), \qquad s_i = \pm 1 .$$

  N is considered fixed.
– Generations
  We consider time sequences of non-overlapping generations, like in a wheat field. The population present at time t is replaced by their offspring at generation $t + 1$.

In Table 5.1 some typical values for the size N of the genome are listed. Note the three orders of magnitude between simple eucaryotic life forms and the human genome.

State of the Population The state of the population at time t can be described by specifying the genomes of all the individuals,

$$\{\mathbf{s}^{\alpha}(t)\}, \qquad \alpha = 1 \ldots M, \qquad \mathbf{s} = (s_1, \ldots, s_N) .$$

We define by

$$X_{\mathbf{s}}(t), \qquad \sum_{\mathbf{s}} X_{\mathbf{s}}(t) = M , \qquad (5.1)$$

the number of individuals with genome $\mathbf{s}$ for each of the 2^N points $\mathbf{s}$ in the genome space. Typically, most of these occupation numbers vanish; biological populations are extremely sparse in genome space.

Table 5.1 Genome size N and the spontaneous mutation rates μ, compare Eq. (5.3), per base for two RNA-based bacteria and DNA-based eucaryotes. From Jain and Krug (2006) and Drake, Charlesworth and Charlesworth (1998)

Organism	Genome size	Rate per base	Rate per genome
Bacteriophage $Q\beta$	4.5×10^3	1.4×10^{-3}	6.5
Bacteriophage λ	4.9×10^4	7.7×10^{-8}	0.0038
E. Coli	4.6×10^6	5.4×10^{-10}	0.0025
C. Elegans	8.0×10^7	2.3×10^{-10}	0.018
Mouse	2.7×10^9	1.8×10^{-10}	0.49
Human	3.2×10^9	5.0×10^{-11}	0.16

Combinatorial Genetics of Alleles Classical genetics focuses on the presence (or absence) of a few characteristic traits. These traits are determined by specific sites, denoted "loci", in the genome. The genetic realizations of these specific loci are called "alleles". Popular examples are alleles for blue, brown and green eyes.

Combinatorial genetics deals with the frequency change of the appearance of a given allele resulting from environmental changes during the evolutionary process. Most visible evolutionary changes are due to a remixing of alleles, as mutation induced changes in the genome are relatively rare; compare the mutation rates listed in Table 5.1.

Beanbag Genetics Without Epistatic Interactions One calls "epistasis" the fact that the effect of the presence of a given allele in a given locus may depend on which alleles are present in some other loci. Classical genetics neglects epistatic interactions. The resulting picture is often called "beanbag genetics", as if the genome were nothing but a bag carrying the different alleles within itself.

Genotype and Phenotype We note that the physical appearance of an organism is not determined exclusively by gene expression. One distinguishes between the genotype and the phenotype.

– The Genotype: The genotype of an organism is the class to which that organism belongs as determined by the DNA that was passed to the organism by its parents at the organism's conception.
– The Phenotype: The phenotype of an organism is the class to which that organism belongs as determined by the physical and behavioral characteristics of the organism, for example its size and shape, its metabolic activities and its pattern of movement.

Selection acts, strictly speaking, only upon phenotypes, but only the genotype is bequeathed. The variations in phenotypes then act as a source of noise for the selection process.

Speciation One denotes by "speciation" the process leading to the differentiation of an initial species into two distinct species. Speciation occurs due to adaptation to different ecological niches, often in distinct geographical environments. We will not treat the various theories proposed for speciation here.

5.2 Mutations and Fitness in a Static Environment

Constant Environment We consider here the environment to be static; an assumption that is justified for the case of short-term evolution. This assumption clearly breaks down for long time scales, as already discussed in Chap. 4 since the evolutionary change of one species might lead to repercussions all over the ecosystem to which it appertains.

Independent Individuals An important issue in the theory of evolution is the emergence of specific kinds of social behavior. Social behavior can only arise if the individuals of the same population interact. We discuss some of these issues in Sect. 5.6 in the context of game theory. Until then we assume non-interacting individuals, which implies that the fitness of a given genetic trait is independent of the frequency of this and of other alleles, apart from the overall competition for resources.

Constant Mutation Rates We furthermore assume that the mutation rates are

– constant over time,
– independent of the locus in the genome, and
– not subject to genetic control.

Any other assumption would require a detailed microbiological modeling; a subject beyond our scope.

Stochastic Evolution The evolutionary process can then be modeled as a three-stage stochastic process:

1. Reproduction: The individual α at generation t is the offspring of an individual α' living at generation $t - 1$. Reproduction is thus represented as a stochastic map

$$\alpha \quad \longrightarrow \quad \alpha' = G_t(\alpha) \,, \tag{5.2}$$

   where $G_t(\alpha)$ is the parent of the individual α, and is chosen at random among the M individuals living at generation $t - 1$.
2. Mutation: The genomes of the offspring differ from the respective genomes of their parents through random changes.
3. Selection: The number of surviving offspring of each individual depends on its genome; it is proportional to its "fitness", which is a functional of the genome.

Point Mutations and Mutation Rate Here we consider mostly independent point mutations, namely that every element of the genome is modified independently of the other elements,

$$s_i^\alpha(t) \;=\; -s_i^{G_t(\alpha)}(t - 1) \qquad \text{with probability } \mu \,, \tag{5.3}$$

where the parameter $\mu \in [0, 1/2]$ is the microscopic "mutation rate". In real organisms, more complex phenomena take place, like global rearrangements of the genome, copies of some part of the genome, displacements of blocks of elements from one location to another, and so on. The values for the real-world mutation rates μ for various species listed in Table 5.1 are therefore to be considered as effective mutation rates.

Fitness and Fitness Landscape The fitness $W(\mathbf{s})$, also called "Wrightian fitness", of a genotype trait $\mathbf{s}$ is proportional to the average number of offspring an individual possessing the trait $\mathbf{s}$ has. It is strictly positive and can therefore be written as

$$W(\mathbf{s}) \;=\; e^{kF(\mathbf{s})} \;\; \propto \;\; \text{average number of offspring of } \mathbf{s}. \tag{5.4}$$
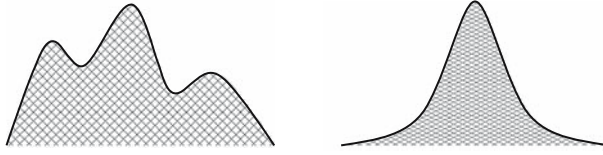
Fig. 5.1 (Smooth) one-dimensional model fitness landscapes $F(\mathbf{s})$. Real-world fitness landscapes, however, contain discontinuities. *Left*: A fitness landscape with peaks and valleys, metaphorically also called a "rugged landscape". *Right*: A fitness landscape containing a single smooth peak, as described by Eq. (5.23)

Selection acts in first place upon phenotypes, but we neglect here the difference, considering the variations in phenotypes as a source of noise, as discussed above. The parameters in Eq. (5.4) are denoted:

– $W(\mathbf{s})$: Wrightian fitness,
– $F(\mathbf{s})$: fitness landscape,
– k: inverse selection temperature, and
– $w(\mathbf{s})$: Malthusian fitness, when rewriting Eq. (5.4) as $W(\mathbf{s}) = e^{w(\mathbf{s})\Delta t}$, where Δt is the generation time.

We will work here with discrete time, viz with non-overlapping generations, and therefore make use only of the Wrightian fitness $W(\mathbf{s})$.

Fitness of Individuals Versus Fitness of Species We remark that this notion of fitness is a concept defined at the level of individuals in a homogeneous population. The resulting fitness of a species or of a group of species needs to be explicitly evaluated and is model-dependent.

Fitness Ratios The assumption of a constant population size makes the reproductive success a *relative* notion. Only the ratios

$$\frac{W(\mathbf{s}_1)}{W(\mathbf{s}_2)} = \frac{e^{kF(\mathbf{s}_1)}}{e^{kF(\mathbf{s}_2)}} = e^{k[F(\mathbf{s}_1)-F((\mathbf{s}_2)]} \tag{5.5}$$

are important. It follows that the quantity $W(\mathbf{s})$ is defined up to a proportionality constant and, accordingly, the fitness landscape $F(\mathbf{s})$ only up to an additive constant, much like the energy in physics.

The Fitness Landscape The graphical representation of the fitness function $F(\mathbf{s})$ is not really possible for real-world fitness functions, due to the high dimensional 2^N of the genome space. It is nevertheless customary to draw a fitness landscape, like the one shown in Fig. 5.1. However, one must bear in mind that these illustrations are not to be taken at face value, apart from model considerations.

The Fundamental Theorem of Natural Selection The so-called fundamental theorem of natural selection, first stated by Fisher in 1930, deals with adaptation in the

absence of mutations and in the thermodynamic limit $M \to \infty$. An infinite population allows one to neglect fluctuations.

The theorem states that the average fitness of the population cannot decrease in time under these circumstances, and that the average fitness becomes stationary only when all individuals in the population have the maximal reproductive fitness.

The proof is straightforward. We define by

$$\langle W \rangle_t \equiv \frac{1}{M} \sum_\alpha W(\mathbf{s}^\alpha(t)) = \frac{1}{M} \sum_\mathbf{s} W(\mathbf{s}) X_\mathbf{s}(t) , \tag{5.6}$$

the average fitness of the population. Note that the $\sum_\mathbf{s}$ in Eq. (5.6) contains 2^N terms. The evolution equations are given in the absence of mutations by

$$X_\mathbf{s}(t+1) = \frac{W(\mathbf{s})}{\langle W \rangle_t} X_\mathbf{s}(t) , \tag{5.7}$$

where $W(\mathbf{s})/\langle W \rangle_t$ is the relative reproductive success. The overall population size remains constant,

$$\sum_\mathbf{s} X_\mathbf{s}(t+1) = \frac{1}{\langle W \rangle_t} \sum_\mathbf{s} X_\mathbf{s}(t) W(\mathbf{s}) = M , \tag{5.8}$$

where we have used Eq. (5.6) for $\langle W \rangle_t$. Then

$$\langle W \rangle_{t+1} = \frac{1}{M} \sum_\mathbf{s} W(\mathbf{s}) X_\mathbf{s}(t+1) = \frac{\frac{1}{M} \sum_\mathbf{s} W^2(\mathbf{s}) X_\mathbf{s}(t)}{\frac{1}{M} \sum_{\mathbf{s}'} W(\mathbf{s}') X_{\mathbf{s}'}(t)}$$

$$= \frac{\langle W^2 \rangle_t}{\langle W \rangle_t} \geq \langle W \rangle_t . \tag{5.9}$$

The steady state

$$\langle W \rangle_{t+1} = \langle W \rangle_t, \qquad \langle W^2 \rangle_t = \langle W \rangle_t^2 ,$$

is only possible when all individuals $1 \ldots M$ in the population have the same fitness, viz the same genotype.

5.3 Deterministic Evolution

Mutations are random events and the evolution process is therefore a stochastic process. But stochastic fluctuations become irrelevant in the limit of infinite population size $M \to \infty$; they average out. In this limit the equations governing evolution become deterministic and only the average transition rates are relevant. One can then study in detail the condition necessary for adaptation to occur for various mutation rates.

5.3.1 Evolution Equations

The Mutation Matrix The mutation matrix

$$Q_\mu(\mathbf{s}' \to \mathbf{s}), \qquad \sum_{\mathbf{s}} Q_\mu(\mathbf{s}' \to \mathbf{s}) = 1 \qquad (5.10)$$

denotes the probabilities of obtaining a genotype $\mathbf{s}$ when attempting to reproduce an individual with genotype $\mathbf{s}'$. The mutation rates $Q_\mu(\mathbf{s}' \to \mathbf{s})$ may depend on a parameter μ determining the overall mutation rate. The mutation matrix includes the absence of any mutation, viz the transition $Q_\mu(\mathbf{s}' \to \mathbf{s}')$. It is normalized.

Deterministic Evolution with Mutations We generalize Eq. (5.7), which is valid in the absence of mutations, by including the effect of mutations via the mutation matrix $Q_\mu(\mathbf{s}' \to \mathbf{s})$:

$$X_\mathbf{s}(t+1)/M \;=\; \left(\sum_{\mathbf{s}'} X_{\mathbf{s}'}(t) W(\mathbf{s}') Q_\mu(\mathbf{s}' \to \mathbf{s}) \right) \bigg/ \left(\sum_{\mathbf{s}'} W_{\mathbf{s}'} X_{\mathbf{s}'}(t) \right),$$

or

$$x_\mathbf{s}(t+1) \;=\; \frac{\sum_{\mathbf{s}'} x_{\mathbf{s}'}(t) W(\mathbf{s}') Q_\mu(\mathbf{s}' \to \mathbf{s})}{\langle W \rangle_t}, \qquad \langle W \rangle_t = \sum_{\mathbf{s}'} W_{\mathbf{s}'} x_{\mathbf{s}'}(t), \qquad (5.11)$$

where we have introduced the normalized population variables

$$x_\mathbf{s}(t) \;=\; \frac{X_\mathbf{s}(t)}{M}, \qquad \sum_{\mathbf{s}} x_\mathbf{s}(t) = 1 . \qquad (5.12)$$

The evolution dynamics Eq. (5.11) retains the overall size $\sum_\mathbf{s} X_\mathbf{s}(t)$ of the population, due to the normalization of the mutation matrix $Q_\mu(\mathbf{s}' \to \mathbf{s})$, Eq. (5.10).

The Hamming Distance The Hamming distance

$$d_\mathrm{H}(\mathbf{s}, \mathbf{s}') \;=\; \sum_{i=1}^{N} \frac{(s_i - s_i')^2}{4} \;=\; \frac{N}{2} - \frac{1}{2} \sum_{i=1}^{N} s_i s_i' \qquad (5.13)$$

measures the number of units that are different in two genome configurations $\mathbf{s}$ and $\mathbf{s}'$, e.g. before and after the effect of a mutation event.

The Mutation Matrix for Point Mutations We consider the simplest mutation pattern, viz the case of fixed genome length N and random transcription errors afflicting only individual loci. For this case, namely point mutations, the overall mutation probability

$$Q_\mu(\mathbf{s}' \to \mathbf{s}) = \mu^{d_\mathrm{H}}(1-\mu)^{N-d_\mathrm{H}} \;\propto\; \exp\Big([\log(\mu) - \log(1-\mu)] d_H \Big)$$

$$\propto\; \exp\left(\beta \sum_i s_i s_i' \right) \qquad (5.14)$$

is the product of the independent mutation probabilities for all loci $i = 1, \ldots, N$. The parameters in Eq. (5.14) denote:

– d_H: the Hamming distance $d_H(\mathbf{s}, \mathbf{s}')$ given by Eq. (5.13),
– μ: the mutation rate μ defined in Eq. (5.3), and
– β: an effective inverse temperature as defined by

$$\beta = \frac{1}{2} \log \left(\frac{1 - \mu}{\mu} \right).$$
(5.15)

The relation of the evolution equation (5.14) to the partition function of a thermo-dynamical system, hinted at by the terminology "inverse temperature" will become evident below. One has

$$\sum_{\mathbf{s}} Q_\mu(\mathbf{s}' \to \mathbf{s}) = \sum_{d_H} \binom{N}{d_H} (1 - \mu)^{N - d_N} \mu^{d_N} = (1 - \mu + \mu)^N \equiv 1$$

and the mutation matrix defined by Eq. (5.14) is consequently normalized.

Evolution Equations for Point Mutations Using the exponential representation $W(\mathbf{s}) = \exp[kF(\mathbf{s})]$, see Eq. (5.4), of the fitness $W(\mathbf{s})$ and Eq. (5.14) for the mutation matrix, we can write the evolution Eq. (5.12) via

$$x_{\mathbf{s}}(t + 1) = \frac{1}{\langle W \rangle_t} \sum_{\mathbf{s}'} x_{\mathbf{s}'}(t) \exp \left(\beta \sum_i s_i s_i' + kF(\mathbf{s}') \right)$$
(5.16)

in a form that is suggestive of a statistical mechanics analogy.

Evolution Equations in Linear Form The evolution Eq. (5.16) is non-linear in the dynamical variables $x_{\mathbf{s}}(t)$, due to the normalization factor $1/\langle W \rangle_t$. A suitable change of variables does, however, allow the evolution equation to be cast into a linear form.

For this purpose we introduce the unnormalized variables $y_{\mathbf{s}}(t)$ via

$$x_{\mathbf{s}}(t) = \frac{y_{\mathbf{s}}(t)}{\sum_{\mathbf{s}'} y_{\mathbf{s}'}(t)}, \qquad \langle W \rangle_t = \sum_{\mathbf{s}} W(\mathbf{s}) x_{\mathbf{s}}(t) = \frac{\sum_{\mathbf{s}} W(\mathbf{s}) y_{\mathbf{s}}(t)}{\sum_{\mathbf{s}'} y_{\mathbf{s}'}(t)}.$$
(5.17)

Note that $y_{\mathbf{s}}(t)$ are determined by Eq. (5.17) implicitly and that the normalization $\sum_{\mathbf{s}'} y_{\mathbf{s}'}(t)$ can be chosen freely for every generation $t = 1, 2, 3, \ldots$. The evolution Eq. (5.16) then becomes

$$y_{\mathbf{s}}(t + 1) = Z_t \sum_{\mathbf{s}'} y_{\mathbf{s}'}(t) \exp \left(\beta \sum_i s_i s_i' + kF(\mathbf{s}') \right),$$
(5.18)

where

$$Z_t = \frac{\sum_{\mathbf{s}'} y_{\mathbf{s}'}(t + 1)}{\sum_{\mathbf{s}} W(\mathbf{s}) y_{\mathbf{s}}(t)}.$$

Choosing a different normalization for $y_{\mathbf{s}}(t)$ and for $y_{\mathbf{s}}(t+1)$ we may achieve $Z_t \equiv 1$. Equation (5.18) is then linear in $y_{\mathbf{s}}(t)$.

Statistical Mechanics of the Ising Model In the following we will make use of analogies to notations commonly used in statistical mechanics. The reader unfamiliar with the mathematics of the one-dimensional Ising model may skip the mathematical details and concentrate on the interpretation of the results.

We write the linear evolution Eq. (5.18) as

$$y_{\mathbf{s}}(t+1) \;=\; \sum_{\mathbf{s}'} e^{\beta H[\mathbf{s},\mathbf{s}']} y_{\mathbf{s}'}(t), \qquad y_{\mathbf{s}(t+1)} \;=\; \sum_{\mathbf{s}(t)} e^{\beta H[\mathbf{s}(t+1),\mathbf{s}(t)]} y_{\mathbf{s}(t)}\,, \qquad (5.19)$$

where we denote by $H[\mathbf{s},\mathbf{s}']$ an effective Hamiltonian

$$\beta H[\mathbf{s},\mathbf{s}'] \;=\; \beta \sum_i s_i s_i' + kF(\mathbf{s}')\,, \qquad (5.20)$$

and where we renamed the variables $\mathbf{s}$ by $\mathbf{s}(t+1)$ and $\mathbf{s}'$ by $\mathbf{s}(t)$. Equation (5.19) can be solved iteratively,

$$\begin{aligned}
y_{\mathbf{s}(t+1)} &= \sum_{\mathbf{s}(t),\dots,\mathbf{s}(0)} e^{\beta H[\mathbf{s}(t+1),\mathbf{s}(t)]} \cdots e^{\beta H[\mathbf{s}(1),\mathbf{s}(0)]} y_{\mathbf{s}(0)} \\
&= \langle \mathbf{s}(t+1)|e^{\beta H}|y(0)\rangle\,, \qquad (5.21)
\end{aligned}$$

with the two-dimensional Ising-type Hamiltonian

$$\beta H \;=\; \beta \sum_{i,t} s_i(t+1)s_i(t) + k\sum_t F(\mathbf{s}(t))\,, \qquad (5.22)$$

and the states $y_{\mathbf{s}}(t) = \langle \mathbf{s}|y(t)\rangle$ in the bra-ket notation of quantum mechanics.[2] We are interested in the asymptotic state $t \to \infty$ of the system, which corresponds to the last time layer $\lim_{t\to\infty} |y(t+1)>$.

A Short Detour: The Bra-ket Notation For convenience we explain, without digging into mathematical niceties, the fundamentals of the very convenient bra-ket notation, which is widely used in physics. One denotes with the "bra" $\langle y|$ and with the "ket" $|y\rangle$ just the respective row and column vectors

$$\langle y| \;\hat{=}\; (y_1^*, y_2^*, \dots, y_{2^N}^*), \qquad |y\rangle \;\hat{=}\; \begin{pmatrix} y_1 \\ \vdots \\ y_{2^N} \end{pmatrix}, \qquad y_j \;\hat{=}\; y_{\mathbf{s}}$$

of a vector $\mathbf{y}$, where y_j^* is the conjugate complex of y_j^*. Our variables are, however, all real and $y_j^* \equiv y_j$. The scalar product $\mathbf{x} \cdot \mathbf{y}$ of two vectors is then

---

[2] The following derivation can be understood disregarding the bra-ket notation, which is, however, helpful for the reader interested in the cross-correlations to quantum mechanics.

$$\mathbf{x} \cdot \mathbf{y} \equiv \sum_j x_j^* y_j = \langle x | y \rangle .$$

The expectation value $\langle A \rangle_y$ is given in bra-ket notation as

$$\langle A \rangle_y = \sum_{i,j} y_i^* A_{ij} y_j = \langle y | A | y \rangle ,$$

where A_{ij} are the elements of the matrix A.

5.3.2 Beanbag Genetics – Evolutions Without Epistasis

The Fujiyama Landscape The fitness function

$$F(\mathbf{s}) = \sum_{i=1}^N h_i s_i, \qquad W(\mathbf{s}) = \prod_{i=1}^N e^{k h_i s_i} , \qquad (5.23)$$

is denoted the "Fujiyama landscape" since it corresponds to a single smooth peak as illustrated in Fig. 5.1. To see why, we consider the case $h_i > 0$ and rewrite Eq. (5.23) as

$$F(\mathbf{s}) = \mathbf{s}_0 \cdot \mathbf{s}, \qquad \mathbf{s}_0 = (h_1, h_2, \ldots, h_N) .$$

The fitness of a given genome $\mathbf{s}$ is directly proportional to the scalar product with the master sequence $\mathbf{s}_0$, with a well defined gradient pointing towards the master sequence.

The Fujiyama Hamiltonian No epistatic interactions are present in the smooth peak landscape Eq. (5.23). In terms of the corresponding Hamiltonian, see Eq. (5.22), this fact expresses itself as

$$\beta H = \beta \sum_{i=1}^N H_i, \qquad \beta H_i = \beta \sum_t s_i(t+1) s_i(t) + k h_i \sum_t s_i(t) . \qquad (5.24)$$

Every locus i corresponds exactly to the one-dimensional $t = 1, 2, \ldots$ Ising-model βH_i in an effective uniform magnetic field $k h_i$.

The Transfer Matrix The Hamiltonian Eq. (5.24) does not contain interactions between different loci of the genome; we can just consider a single Hamiltonian H_i and find for the iterative solution Eq. (5.21)

$$\langle y_i(t+1) | e^{\beta H_i} | y_i(0) \rangle = \langle y_i(t+1) | \left(\prod_{t'=0}^t T_{t'} \right) | y_i(0) \rangle , \qquad (5.25)$$

with the 2×2 transfer matrix $T_t = e^{\beta H_i[s_i(t+1), s_i(t)]}$ given by

$$(T_t)_{\sigma, \sigma'} = < \sigma | T_t | \sigma' >, \qquad T_t = \begin{pmatrix} e^{\beta + k h_i} & e^{-\beta} \\ e^{-\beta} & e^{\beta - k h_i} \end{pmatrix} , \qquad (5.26)$$

where we have used $\sigma, \sigma' = \pm 1$ and the symmetrized form

$$\beta H_i = \beta \sum_t s_i(t+1)s_i(t) + \frac{kh_i}{2} \sum_t \left[s_i(t+1) + s_i(t) \right] .$$

of the one-dimensional Ising model.

Eigenvalues of the Transfer Matrix We consider

$$h_i \equiv 1$$

and evaluate the eigenvalues ω of T_t:

$$\omega^2 - 2\omega e^\beta \cosh(k) + e^{2\beta} - e^{-2\beta} = 0 .$$

The solutions are

$$\omega_{1,2} = e^\beta \cosh(k) \pm \sqrt{e^{2\beta} \cosh^2(k) - e^{2\beta} + e^{-2\beta}} .$$

The larger eigenvalue ω_1 thus has the form

$$\omega_1 = e^\beta \cosh(k) + \sqrt{e^{2\beta} \sinh^2(k) + e^{-2\beta}} . \tag{5.27}$$

Eigenvectors of the Transfer Matrix For $\omega_1 > \omega_2$ the eigenvector $|\omega_1\rangle$ corresponding to the larger eigenvalue ω_1 dominates in the $t \to \infty$ limit and its components determine the genome distribution. It is determined by

$$\begin{pmatrix} \langle +|\omega_1\rangle \\ \langle -|\omega_1\rangle \end{pmatrix} = \begin{pmatrix} A_+ \\ A_- \end{pmatrix}, \qquad \left(e^{\beta+k} - \omega_1 \right) A_+ + e^{-\beta} A_- = 0 ,$$

where

$$\omega_1 - e^{\beta+k} = \sqrt{e^{2\beta} \sinh^2(k) + e^{-2\beta}} - e^\beta \sinh(k) .$$

This yields

$$\begin{pmatrix} A_+ \\ A_- \end{pmatrix} = \frac{1}{\sqrt{N_\omega}} \left(\frac{e^{-\beta}}{\sqrt{e^{2\beta} \sinh^2(k) + e^{-2\beta}} - e^\beta \sinh(k)} \right), \tag{5.28}$$

with the normalization

$$N_\omega = A_+^2 + A_-^2 = e^{-2\beta} + e^{2\beta} \sinh^2(k)$$
$$+ \left(e^{2\beta} \sinh^2(k) + e^{-2\beta} \right) + 2e^\beta \sinh(k) \sqrt{e^{2\beta} \sinh^2(k) + e^{-2\beta}}$$
$$= 2e^{-2\beta} + e^{2\beta} \sinh^2(k) - 2e^\beta \sinh(k) \sqrt{e^{2\beta} \sinh^2(k) + e^{-2\beta}} .$$

The Order Parameter The one-dimensional Ising model does not have phase transitions. Thus we reach the conclusion that evolution in the Fujiyama landscape takes

place in a single phase, where there is always some degree of adaptation. One can evaluate the amount of adaptation by introducing the order parameter[3]

$$m = \lim_{t \to \infty} \langle s(t) \rangle = A_+ - A_- \,, \tag{5.29}$$

which corresponds to the uniform magnetization in the Ising model analogy. One obtains

$$m = \frac{1}{N_\omega} \left[e^{-\beta} - \sqrt{e^{2\beta} \sinh^2(k) + e^{-2\beta}} + e^{\beta} \sinh(k) \right] . \tag{5.30}$$

In order to interpret this result for the amount m of adaptation in the smooth Fujiyama landscape we recall that (see Eqs. (5.15) and (5.4))

$$\beta = \frac{1}{2} \log\left(\frac{1-\mu}{\mu}\right), \qquad W(\mathbf{s}) = e^{kF(\mathbf{s})} \,,$$

where μ is the mutation rate for point mutations. Thus we see that, whenever the fitness landscape does not vanish ($k > 0$), there is some degree of adaptation for any non-zero value of β, i.e. for any mutation rate μ smaller than 1/2.

5.3.3 Epistatic Interactions and the Error Catastrophe

The result of the previous Sect. 5.3.2, i.e. the occurrence of adaptation in a smooth fitness landscape for any non-trivial model parameter, is due to the absence of epistatic interactions in the smooth fitness landscape. Epistatic interactions introduce a phase transition to a non-adapting regime once the mutation rate becomes too high.

The Sharp Peak Landscape One possibility to study this phenomenon is the limiting case of very strong epistatic interactions; in this case, a single element of the genotype does not give any information on the value of the fitness. This fitness is defined by the equation

$$W(\mathbf{s}) = \begin{cases} 1 & \text{if } \mathbf{s} = \mathbf{s}_0 \\ 1 - \sigma & \text{otherwise} \end{cases} . \tag{5.31}$$

It is also denoted a fitness landscape with a "tower". In this case, all genome sequences have the same fitness, which is lower than the one of the master sequence $\mathbf{s}_0$. The corresponding landscape $F(\mathbf{s})$, defined by $W(\mathbf{s}) = e^{kF(\mathbf{s})}$ is then equally discontinuous. This landscape has no gradient pointing towards the master sequence of maximal fitness.

Relative Notation We define by x_k the fraction of the population whose genotype has a Hamming distance k from the preferred genotype,

---

[3] The concept of order parameters in the theory of phase transition is discussed in Chap. 4.

$$x_k(t) = \frac{1}{M} \sum_{\mathbf{s}} \delta_{d_H(\mathbf{s},\mathbf{s}_0),k} X_\mathbf{s}(t) \ . \tag{5.32}$$

The evolution equations can be formulated entirely in terms of these x_k; they correspond to the fraction of the population being k point mutations away from the master sequence.

Infinite Genome Limit We take the $N \to \infty$ limit and scale the mutation rate, see Eq. (5.3),

$$\mu = u/N \ , \tag{5.33}$$

for point mutations such that the average number of mutations

$$u = N\mu$$

occurring at every step remains finite.

The Absence of Back Mutations We consider starting from the optimal genome $\mathbf{s}_0$ and consider the effect of mutations. Any successful mutation increases the distance k from the optimal genome $\mathbf{s}_0$. Assuming $u \ll 1$ in Eq. (5.33) implies that

– multiple mutations do not appear, and that
– one can neglect back mutations that reduce the value of k, since they have a relative probability proportional to

$$\frac{k}{N-k} \ll 1 \ .$$

The Linear Chain Model The model so defined consequently has the structure of a linear chain. $k = 0$ being the starting point of the chain.

We have two parameters: u, which measures the mutation rate and σ, which measures the strength of the selection. Remembering that the fitness $W(\mathbf{s})$ is proportional to the number of offspring, see Eq. (5.31), we then find

$$x_0(t+1) = \frac{1}{\langle W \rangle} \left[x_0(t)(1-u) \right] , \tag{5.34}$$

$$x_1(t+1) = \frac{1}{\langle W \rangle} \left[u x_0(t) + (1-u)(1-\sigma)x_1(t) \right] ; \tag{5.35}$$

$$x_k(t+1) = \frac{1}{\langle W \rangle} \left[u x_{k-1}(t) + (1-u)x_k(t) \right](1-\sigma) , \qquad k > 1, \tag{5.36}$$

where $\langle W \rangle$ is the average fitness. These equations describe a linear chain model as illustrated in Fig. 5.2. The population of individuals with the optimal genome x_0 constantly loses members due to mutations. But it also has a higher number of offspring than all other populations due to its larger fitness.

$$x_0 \longrightarrow x_1 \longrightarrow x_2 \longrightarrow x_3 \longrightarrow x_4 \longrightarrow$$
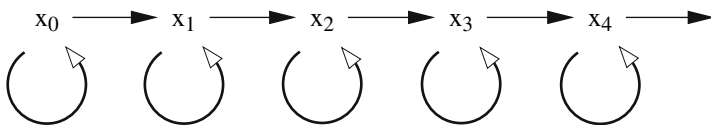
Fig. 5.2 The linear chain model for the tower landscape, Eq. (5.31), with k denoting the number of point mutations necessary to reach the optimal genome. The population fraction $x_{k+1}(t+1)$ is only influenced by the value of x_k and its own value at time t

Stationary Solution The average fitness of the population is given by

$$\langle W \rangle = x_0 + (1-\sigma)(1-x_0) = 1 - \sigma(1-x_0) . \tag{5.37}$$

We look for the stationary distribution $\{x_k^*\}$. The equation for x_0^* does not involve the x_k^* with $k > 0$:

$$x_0^* = \frac{x_0^*(1-u)}{1-\sigma(1-x_0^*)}, \qquad 1 - \sigma(1-x_0^*) = 1-u .$$

The solution is

$$x_0^* = \begin{cases} 1-u/\sigma & \text{if } u < \sigma \\ 0 & \text{if } u \geq \sigma \end{cases} , \tag{5.38}$$

due to the normalization condition $x_0^* \leq 1$. For $u > \sigma$ the model becomes ill defined. The stationary solutions for the x_k^* are for $k = 1$

$$x_1^* = \frac{u}{1 - \sigma(1-x_0^*) - (1-u)(1-\sigma)} x_0^* ,$$

which follows directly from Eqs. (5.35) and (5.37), and for $k > 1$

$$x_k^* = \frac{(1-\sigma)u}{1 - \sigma(1-x_0^*) - (1-u)(1-\sigma)} x_{k-1}^* , \tag{5.39}$$

which follows from Eqs. (5.36) and (5.37).

Phase Transition and the Order Parameter We can thus distinguish two regimes determined by the magnitude of the mutation rate $\mu = u/N$ relative to the fitness parameter σ, with

$$u = \sigma$$

being the transition point. In physics language the epistatic interaction corresponds to many-body interactions and the occurrence of a phase transition in the sharp peak model is due to the many-body interactions which were absent in the smooth fitness landscape model considered in Sect. 5.3.2.

The Adaptive Regime and Quasispecies In the regime of small mutation rates, $u < \sigma$, one has $x_0^* > 0$ and in fact the whole population lies a finite distance away from the preferred genotype. To see why, we note that
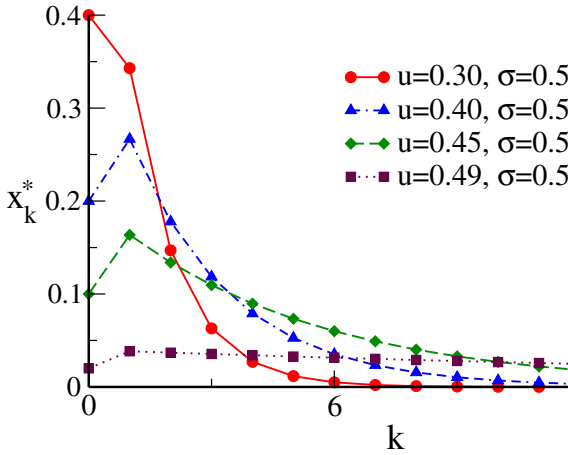
Fig. 5.3 Quasispecies formation within the sharp peak fitness landscape, Eq. (5.31). The stationary population densities x_k^*, see Eq. (5.39), are peaked around the genome with maximal fitness, $k = 0$. The population tends to spread out in genome space when the overall mutation rate u approaches the critical point $u \to \sigma$

$$\sigma(1 - x_0^*) = \sigma(1 - 1 + u/\sigma) = u$$

and take a look at Eq. (5.39):

$$\frac{(1-\sigma)u}{1 - u - (1-u)(1-\sigma)} = \left(\frac{1-\sigma}{1-u}\right)\left(\frac{u}{\sigma}\right) \leq 1, \qquad \text{for } u < \sigma.$$

The x_k^* therefore form a geometric series,

$$x_k^* \sim \left(\frac{1-\sigma}{1-u}\frac{u}{\sigma}\right)^k,$$

which is summable when $u < \sigma$. In this adaptive regime the population forms what Manfred Eigen denoted a "quasispecies", see Fig. 5.3.

> *Quasispecies.* *A quasispecies is a population of genetically close but not identical individuals.*

The Wandering Regime and The Error Threshold In the regime of a large mutation rate, $u > \sigma$, we have $x_k^* = 0, \forall k$. In this case, a closer look at the finite genome situation shows that the population is distributed in an essentially uniform way over the whole genotype space. The infinite genome limit therefore becomes inconsistent, since the whole population lies an infinite number of mutations away from the preferred genotype. In this *wandering regime* the effects of finite population size are prominent.

Error Catastrophe.   The transition from the adaptive (quasispecies) regime to the wandering regime is denoted the "error threshold" or "error catastrophe".

The notion of error catastrophe is a quite generic feature of quasispecies theory, independent of the exact nature of the fitness landscape containing epistatic interactions. A quasispecies can no longer adapt, once its mutation rate becomes too large. In the real world the error catastrophe implies extinction.

5.4 Finite Populations and Stochastic Escape

Punctuated Equilibrium Evolution is not a steady process, there are regimes of rapid increase of the fitness and phases of relative stasis. This kind of overall dynamical behavior is denoted the "punctuated equilibrium".

In this context, adaptation can result either from local optimization of the fitness of a single species or via coevolutionary avalanches, as discussed in Chap. 4.

The Neutral Regime.   The stage where evolution is essentially driven by random mutations is called the neutral (or wandering) regime.

The quasispecies model is inconsistent in the neutral regime. In fact, the population spreads out in genome space in the neutral regime and the infinite population limit is no longer reachable. In this situation, the fluctuations of the reproductive process in a finite population have to be taken into account.

Deterministic Versus Stochastic Evolution Evolution is driven by stochastic processes, since mutations are random events. Nevertheless, randomness averages out and the evolution process becomes deterministic in the thermodynamic limit, as discussed in Sect. 5.3, when the number M of individuals diverges, $M \to \infty$.

Evolutionary processes in populations with a finite number of individuals differ from deterministic evolution quantitatively and sometimes also qualitatively, the later being our focus of interest here.

Stochastic Escape.   Random mutations in a finite population might lead to a decrease in the fitness and to a loss of the local maximum in the fitness landscape with a resulting dispersion of the quasispecies.

We have given a general account of the theory of stochastic escape in Chap. 2. Here we will discuss in some detail under which circumstances this phenomenon is important in evolutionary processes of small populations.

5.4.1 Strong Selective Pressure and Adaptive Climbing

Adaptive Walks We consider a coarse-grained description of population dynamics for finite populations. We assume that

(a)   the population is finite,
(b)   the selective pressure is very strong, and
(c)   the mutation rate is small.

It follows from (b) that one can represent the population by a single point in genome space; the genomes of all individuals are taken to be equal. The evolutionary dynamics is then the following:

(A)   At each time step, only one genome element of some individual in the population mutates.
(B)   If, because of this mutation, one obtains a genotype with higher fitness, the new genotype spreads rapidly throughout the entire population, which then moves altogether to the new position in genome space.
(C)   If the fitness of the new genotype is lower, the mutation is rejected and the population remains at the old position.

   Physicists would call this type of dynamics a Monte Carlo process at zero temperature. As is well known, this algorithm does not lead to a global optimum, but to a "typical" local optimum. Step **(C)** holds only for the infinite population limit. We will relax this condition further below.

The Random Energy Model It is thus important to investigate the statistical properties of the local optima, which depend on the properties of the fitness landscape. A suitable approach is to assume a random distribution of the fitness.

   The Random Energy Model.   The fitness landscape $F(\mathbf{s})$ is uniformly distributed between 0 and 1.

The random energy model is illustrated in Fig. 5.4.

Local Optima in the Random Energy Model Let us denote by N the number of genome elements. The probability that a point with fitness $F(\mathbf{s})$ is a local optimum is simply given by

$$F^N = F^N(\mathbf{s}),$$

since we have to impose that the N nearest neighbors

$$(s_1,\ldots,-s_i,\ldots,s_N),\qquad (i=1,\ldots,N),\qquad \mathbf{s} = (s_1,\ldots,s_N),$$

of the point have fitness less than F. The probability that a point in genome space is a local optimum is given by

$$P\{\text{local optimum}\} = \int_0^1 F^N dF = \frac{1}{N+1},\tag{5.40}$$
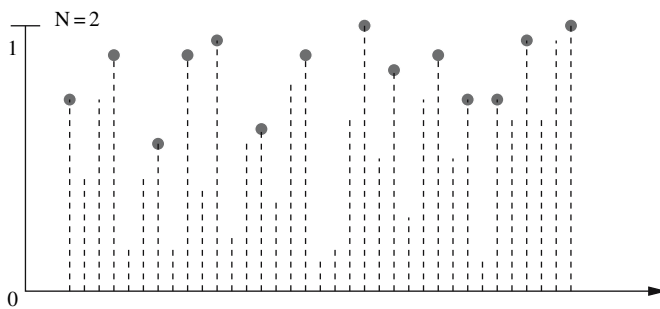
Fig. 5.4 Local fitness optima in a one-dimensional random fitness distribution; the number of neighbors is two. This simplified picture does not corresponds directly to the $N = 2$ random energy model, for which there are just $2^2 = 4$ states in genome space. It shows, however, that random distributions may exhibit an enormous number of local optima (*filled circles*), which are characterized by lower fitness values both on the left-hand side as well as on the right-hand side

since the fitness F is equally distributed in $[0, 1]$. There are therefore many local optima, namely $2^N/(N+1)$. A schematic picture of the large number of local optima in a random distribution is given in Fig. 5.4.

Average Fitness at a Local Optimum The typical fitness of a local optimum is

$$F_{typ} \;=\; \frac{1}{1/(N+1)} \int_0^1 F F^N \mathrm{d}F \;=\; \frac{N+1}{N+2} \;=\; \frac{1+1/N}{1+2/N} \;\approx\; 1 - 1/N\,, \qquad (5.41)$$

viz very close the global optimum of 1, when the genome length N is large. At every successful step the distance from the top is divided, on average, by a factor of 2.

Successful Mutations We now consider the adaptation process. Any mutation results in a randomly distributed fitness of the offspring. A mutation is successful whenever the fitness of the offspring is bigger than the fitness of its parent. The typical fitness attained after ℓ successful steps is then of the order of

$$1 - \frac{1}{2^{\ell+1}}\,,$$

when starting ($l = 0$) from an average initial fitness of 1/2. It follows that the typical number of successful mutations after which an optimum is attained is

$$F_{typ} \;=\; 1 - 1/N \;=\; 1 - \frac{1}{2^{\ell_{typ}+1}}, \qquad \ell_{typ} + 1 \;=\; \frac{\log N}{\log 2}\,, \qquad (5.42)$$

i.e. it is relatively small.

The Time Needed for One Successful Mutation Even though the number of successful mutations Eq. (5.42) needed to arrive at the local optimum is small, the time to climb to the local peak can be very long; see Fig. 5.5 for an illustration of the climbing process.
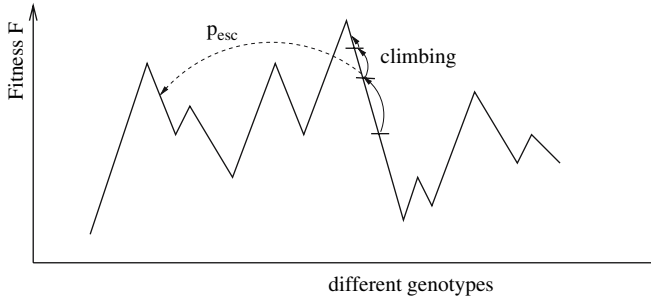
Fig. 5.5 Climbing process and stochastic escape. The higher the fitness, the more difficult it becomes to climb further. With an escape probability p_{esc} the population jumps somewhere else and escapes a local optimum

We define by

$$t_F = \sum_n n P_n, \qquad n : \text{ number of generations}$$

the average number of generations necessary for the population with fitness F to achieve one successful mutation, with P_n being the probability that it takes exactly n generations. We obtain:

$$t_F = 1(1-F) + 2(1-F)F + 3(1-F)F^2 + 4(1-F)F^3 + \cdots$$

$$= \frac{1-F}{F} \sum_{n=0}^{\infty} n F^n = \frac{1-F}{F}\left(F\frac{\partial}{\partial F}\sum_{n=0}^{\infty} F^n\right) = (1-F)\frac{\partial}{\partial F}\frac{1}{1-F}$$

$$= \frac{1}{1-F} . \tag{5.43}$$

The average number of generations necessary to further increase the fitness by a successful mutation diverges close to the global optimum $F \to 1$.

The Total Climbing Time Every successful mutation decreases the distance $1-F$ to the top by 1/2 and therefore increases the factor $1/(1-F)$ on the average by 2. The typical number ℓ_{typ}, see Eq. (5.42), of successful mutations needed to arrive at a local optimum determines, via Eq. (5.43), the expected total number of generations T_{opt} to arrive at the local optimum. It is therefore on the average

$$T_{opt} = 1 t_F + 2 t_F + 2^2 t_F + \ldots + 2^{\ell_{typ}} t_F$$

$$= t_F \frac{1 - 2^{\ell_{typ}+1}}{1 - 2} \approx t_F 2^{\ell_{typ}+1} = t_F e^{(\ell_{typ}+1)\log 2}$$

$$\approx t_F e^{\log N} = \frac{N}{1-F} \approx 2N , \tag{5.44}$$

where we have used Eq. (5.42) and $F \approx 1/2$ for a typical starting fitness. The time needed to climb to a local maximum in the random fitness landscape is therefore proportional to the length of the genome.

5.4.2 Adaptive Climbing Versus Stochastic Escape

In Sect. 5.4.1 the average properties of adaptive climbing have been evaluated. We now take the fluctuations in the reproductive process into account and compare the typical time scales for a stochastic escape with those for adaptive climbing.

Escape Probability When a favorable mutation appears it spreads instantaneously into the whole population, under the condition of strong selection limit, as assumed in our model.

We consider a population situated at a local optimum or very close to a local optimum. Every point mutation then leads to a lower fitness and the probability p_{esc} for stochastic escape is

$$p_{esc} \approx u^M \, ,$$

where M is the number of individuals in the population and $u \in [0, 1]$ the mutation rate per genome, per individual and per generation, compare Eq. (5.33). The escape can only happen when a mutation occurs in every member of the population within the same generation (see also Fig. 5.5). If a single individual does not mutate it retains its higher fitness of the present local optimum and all other mutations are discarded within the model, assuming a strong selective pressure.

Stochastic Escape and Stasis We now consider a population climbing towards a local optimum. The probability that the fitness of a given individual increases is $(1 - F)u$. It needs to mutate with a probability u and to achieve a higher fitness, when mutating, with probability $1 - F$. We denote by

$$a = 1 - (1 - F)u$$

the probability that the fitness of an individual does not increase with respect to the current fitness F of the population. The probability q_{bet} that at least one better genotype is found is then given by

$$q_{bet} = 1 - a^M \, .$$

Considering a population close to a local optimum, a situation typical for real-world ecosystems, we can then distinguish between two evolutionary regimes:

– Adaptive Walk: The escape probability p_{esc} is much smaller than the probability to increase the fitness, $q_{bet} \gg p_{esc}$. The population continuously increases its fitness via small mutations.
– The Wandering Regime: Close to a local optimum the adaptive dynamics slows down and the probability of stochastic escape p_{esc} becomes comparable to that

of an adaptive process, $p_{esc} \approx q_{bet}$. The population wanders around in genome space, starting a new adaptive walk after every successful escape.

Typical Escape Fitness During the adaptive walk regime the fitness F increases steadily, until it reaches a certain typical fitness F_{esc} for which the probability of stochastic escape becomes substantial, i.e. when $p_{esc} \approx q_{bet}$ and

$$p_{esc} = u^M = 1 - [1 - (1 - F_{esc})u]^M = q_{bet}$$

holds. As $(1 - F_{esc})$ is then small we can expand the above expression in $(1 - F_{esc})$,

$$u^M \approx 1 - [1 - M(1 - F_{esc})u] = M(1 - F_{esc})u \,,$$

obtaining

$$1 - F_{esc} = u^{M-1}/M \,. \tag{5.45}$$

The fitness F_{esc} necessary for the stochastic escape to become relevant is exponentially close to the global optimum $F = 1$ for large populations M.

The Relevance of Stochastic Escape The stochastic escape occurs when a local optimum is reached, or when we are close to a local optimum. We may estimate the importance of the escape process relative to that of the adaptive walk by comparing the typical fitness F_{typ} of a local optimum achieved by a typical climbing process with the typical fitness F_{esc} needed for the escape process to become important:

$$F_{typ} = 1 - \frac{1}{N} \equiv F_{esc} = 1 - \frac{u^{M-1}}{M}, \qquad \frac{1}{N} = \frac{u^{M-1}}{M} \,,$$

where we have used Eq. (5.41) for F_{typ}. The above condition can be fulfilled only when the number of individuals M is much smaller than the genome length N, as $u < 1$. The phenomena of stochastic escape occurs only for very small populations.

5.5 Prebiotic Evolution

Prebiotic evolution deals with the question of the origin of life. Is it possible to define chemical autocatalytic networks in the primordial soup having properties akin to those of the metabolistic reaction networks going on continuously in every living cell?

5.5.1 Quasispecies Theory

The quasispecies theory was introduced by Manfred Eigen to describe the evolution of a system of information carrying macromolecules through a set of equations for chemical kinetics,

$$\frac{d}{dt}x_i \;=\; \dot{x}_i \;=\; W_{ii}x_i + \sum_{j \neq i} W_{ij}x_j - x_i\phi(t) \,, \tag{5.46}$$

where the x_i denote the concentrations of $i = 1 \dots N$ molecules. W_{ii} is the (auto-catalytic) self-replication rate and the off-diagonal terms $W_{i,j}$ $(i \neq j)$ the respective mutation rates.

Mass Conservation We can choose the flux $-x\phi(t)$ in Eigen's equations (5.46) for prebiotic evolution such that the total concentration C, viz the total mass

$$C \;=\; \sum_i x_i$$

is conserved for long times. Summing Eq. (5.46) over i we obtain

$$\dot{C} \;=\; \sum_{ij} W_{ij}x_j - C\phi, \qquad \phi(t) \;=\; \sum_{ij} W_{ij}x_j(t) \,, \tag{5.47}$$

for a suitable choice for the field $\phi(t)$, leading to

$$\dot{C} \;=\; \phi\,(1-C), \qquad \frac{d}{dt}(C-1) \;=\; -\phi\,(C-1) \,. \tag{5.48}$$

The total concentration $C(t)$ will therefore approach 1 for $t \to \infty$ for $\phi > 0$, which we assume to be the case here, implying total mass conservation. In this case the autocatalytic rates W_{ii} dominate with respect to the transmolecular mutation rates W_{ij} $(i \neq j)$.

Quasispecies We can write the evolution equation (5.46) in matrix form

$$\frac{d}{dt}\,x(t) \;=\; (W - 1\phi)\,x(t), \qquad x = \begin{pmatrix} x_1 \\ x_1 \\ \dots \\ x_N \end{pmatrix}, \tag{5.49}$$

where W is the matrix $\{W_{ij}\}$. We assume here for simplicity a symmetric mutation matrix $W_{ij} = W_{ji}$. The solutions of the linear differential equation (5.49) are then given in terms of the eigenvectors e_λ of W:

$$W e_\lambda \;=\; \lambda\, e_\lambda, \qquad x \;=\; \sum_\lambda a_\lambda\, e_\lambda, \qquad \dot{a}_\lambda \;=\; [\lambda - \phi(t)] a_\lambda \,.$$

The eigenvector $e_{\lambda_{\max}}$ with the largest eigenvalue $\lambda_{\max}$ will dominate for $t \to \infty$, due to the overall mass conservation Eq. (5.48). The flux will adapt to the largest eigenvalue,

$$\lim_{t \to \infty} \left(\lambda_{\max} - \phi(t) \right) \;\to\; 0 \,,$$

leading to the stationary condition $\dot{x}_i = 0$ for the evolution Eq. (5.49) in the long time limit.

Fig. 5.6 The simplest hypercycle. A and B are self-replicating molecules. A acts as a catalyst for B, i.e. the replication rate of B increases with the concentration of A. Likewise the presence of B favors the replication of A
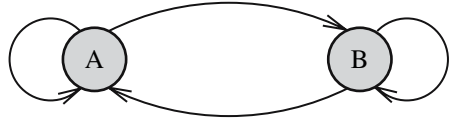
If W is diagonal (no mutations) a single macromolecule will remain in the primordial soup for $t \to \infty$. For small but finite mutation rates W_{ij} ($i \neq j$), a quasispecies will emerge, made up of different but closely related macromolecules.

The Error Catastrophe The mass conservation equation (5.48) cannot be retained when the mutation rates become too big, viz when the eigenvectors e_λ become extended. In this case the flux $\phi(t)$ diverges, see Eq. (5.47), and the quasispecies model consequently becomes inconsistent. This is the telltale sign of the error catastrophe.

The quasispecies model Eq. (5.46) is equivalent to the random energy model for microevolution studied in Sect. 5.4, with the autocatalytic rates W_{ii} corresponding to the fitness of the x_i, which corresponds to the states in genome space. The analysis carried through in Sect. 5.3.3 for the occurrence of an error threshold is therefore also valid for Eigen's prebiotic evolutionary equations.

5.5.2 Hypercycles and Autocatalytic Networks

The macromolecular evolution equations (5.46) do not contain terms describing the catalysis of molecule i by molecule j. This process is, however, important both for the prebiotic evolution, as stressed by Manfred Eigen, as well as for the protein reaction network in living cells.

> *Hypercycles. Two or more molecules may form a stable catalytic (hyper) cycle when the respective intermolecular catalytic rates are large enough to mutually support their respective synthesis.*

An illustration of some hypercycles is given in Figs. 5.6 and 5.7. The most likely chemical candidate for the constituent molecules is RNA, functioning both enzymatically and as a precursor of the genetic material. One speaks also of an "RNA world".

Reaction Networks We disregard mutations in the following and consider the catalytic reaction equations

$$\dot{x}_i = x_i \left(\lambda_i + \sum_j \omega_{ij} x_j - \phi \right) \tag{5.50}$$
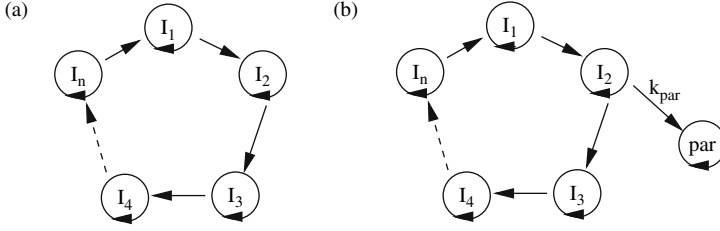
Fig. 5.7 Hypercycles of higher order. (**a**) A hypercycle of order n consists of n cyclically coupled self-replicating molecules I_i, and each molecule provides catalytic support for the subsequent molecule in the cycle. (**b**) A hypercycle with a single self-replicating parasitic molecule "par" coupled to it via k_{par}. The parasite gets catalytic support from I_2 but does not give back catalytic support to the molecules in the hypercycle

$$\phi = \sum_k x_k \left(\lambda_k + \sum_j \omega_{kj} x_j \right) , \qquad (5.51)$$

where x_i are the respective concentrations, λ_i the autocatalytic growth rates and ω_{ij} the transmolecular catalytic rates. The field ϕ has been chosen, Eq. (5.51), such that the total concentration $C = \sum_i x_i$ remains constant

$$\dot{C} = \sum_i \dot{x}_i = \sum_i x_i \left(\lambda_i + \sum_j \omega_{ij} x_j \right) - C\phi = (1 - C)\phi \rightarrow 0$$

for $C \rightarrow 1$.

The Homogeneous Network We consider the case of homogeneous "interactions" $\omega_{i \neq j}$ and uniformly distributed autocatalytic growth rates:

$$\omega_{i \neq j} = \omega, \qquad \omega_{ii} = 0, \qquad \lambda_i = \alpha i , \qquad (5.52)$$

compare Fig. 5.8, leading to

$$\dot{x}_i = x_i \left(\lambda_i + \omega \sum_{j \neq i} x_j - \phi \right) = x_i \left(\lambda_i + \omega - \omega x_i - \phi \right) , \qquad (5.53)$$

where we have used $\sum_i x_i = 1$. The fixed points x_i^* of Eq. (5.53) are

$$x_i^* = \begin{cases} (\lambda_i + \omega - \phi)/\omega \\ 0 \end{cases} \qquad \lambda_i = \alpha, 2\alpha, \dots, N\alpha , \qquad (5.54)$$

where the non-zero solution is valid for $\lambda_i - \omega - \phi > 0$. The flux ϕ in Eq. (5.54) needs to obey Eq. (5.51), as the self-consistency condition.

The Stationary Solution The case of homogeneous interactions, Eq. (5.52), can be solved analytically. Dynamically, the $x_i(t)$ with the largest growth rates λ_i will dominate and obtain a non-zero steady-state concentration x_i^*. We may therefore assume that there exists an $N^* \in [1, N]$ such that
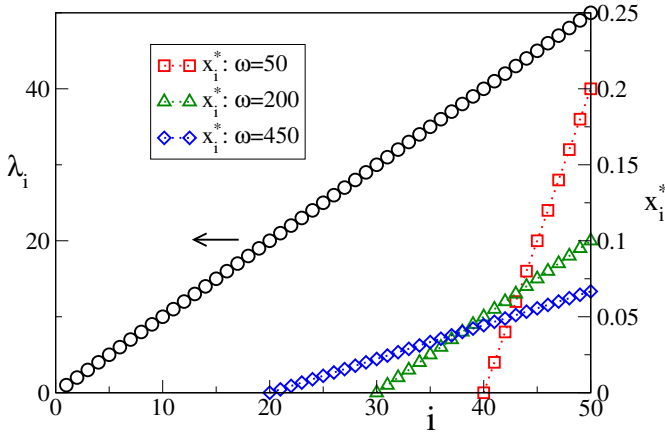
Fig. 5.8 The autocatalytic growth rates λ_i (*left axis*), as in Eq. (5.52) with $\alpha = 1$, and the stationary solution x_i^* (*right axis*) of the concentrations, Eq. (5.55), constituting a prebiotic quasispecies, for various mean intercatalytic rates ω. The *horizontal axis* $i = 1, 2, \ldots, 50$ denotes the respective molecules

$$x_i^* = \begin{cases} (\lambda_i + \omega - \phi)/\omega & N^* \leq i \leq N \\ 0 & 1 \leq i < N^* \end{cases}, \tag{5.55}$$

compare Fig. 5.8, where N^* and ϕ are determined by the normalization condition

$$1 = \sum_{i=N^*}^{N} x_i^* = \sum_{i=N^*}^{N} \frac{\lambda_i + \omega - \phi}{\omega} = \frac{\alpha}{\omega} \sum_{i=N^*}^{N} i + \left[\frac{\omega - \phi}{\omega}\right] \left(N + 1 - N^*\right)$$

$$= \frac{\alpha}{2\omega} \left[N(N+1) - N^*(N^* - 1)\right] + \left[\frac{\omega - \phi}{\omega}\right] \left(N + 1 - N^*\right) \tag{5.56}$$

and by the condition that $x_i^* = 0$ for $i = N^* - 1$:

$$0 = \frac{\lambda_{N^*-1} + \omega - \phi}{\omega} = \frac{\alpha(N^* - 1)}{\omega} + \frac{\omega - \phi}{\omega} . \tag{5.57}$$

We eliminate $(\omega - \phi)/\omega$ from Eqs. (5.56) and (5.57) for large N, N^*:

$$\frac{2\omega}{\alpha} \simeq N^2 - (N^*)^2 - 2N^* (N - N^*)$$

$$= N^2 - 2N^*N + (N^*)^2 = (N - N^*)^2 .$$

The number of surviving species $N - N^*$ is therefore

$$N - N^* \simeq \sqrt{\frac{2\omega}{\alpha}} , \tag{5.58}$$

which is non-zero for a finite and positive inter-molecular catalytic rate ω. A hypercycle of mutually supporting species (or molecules) has formed.

The Origin of Life The scientific discussions concerning the origin of life are highly controversial to date and it is speculative whether hypercycles have anything to do with it. Nevertheless it is interesting to point out that Eq. (5.58) implies a clear division between molecules $i = N^*, \ldots, N$ which can be considered to form a primordial "life form" separated by molecules $i = 1, \ldots, N^* - 1$ belonging to the "environment", since the concentrations of the latter are reduced to zero. This clear separation between participating and non-participating substances is a result of the non-linearity of the reaction equations (5.50). The linear evolution equations (5.46) would, on the other hand, result in a continuous density distribution, as illustrated in Fig. 5.3 for the case of the sharp peak fitness landscape. One could then conclude that life is possible only via cooperation, resulting from non-linear evolution equations.

5.6 Coevolution and Game Theory

Coevolution In the discussion so far we first considered the evolution of a single species and then in Sect. 5.5.2, the stabilization of an "ecosystem" made of a hypercycle of mutually supporting species.

> *Coevolution. When two or more species form an interdependent ecosystem the evolutionary progress of part of the ecosystem will generally induce co-evolutionary changes also in the other species.*

One can view the coevolutionary process also as a change in the respective fitness landscapes, see Fig. 5.9. A prominent example of phenomena arising from coevolution is the "red queen" phenomenon.

> *The Red Queen Phenomenon. When two or more species are interdependent then "It takes all the running, to stay in place" (from Lewis Carroll's children's book "Through the Looking Glass").*

A well-known example of the red queen phenomenon is the "arms race" between predator and prey commonly observed in natural ecosystems.

Avalanches and Punctuated Equilibrium In Chap. 4 we discussed the Bak and Sneppen model of coevolution. It may explain the occurrence of coevolutionary avalanches within a state of punctuated equilibrium.

> *Punctuated Equilibrium. Most of the time the ecosystem is in equilibrium, in the neutral phase. Due to rare stochastic processes periods of rapid coevolutionary processes are induced.*
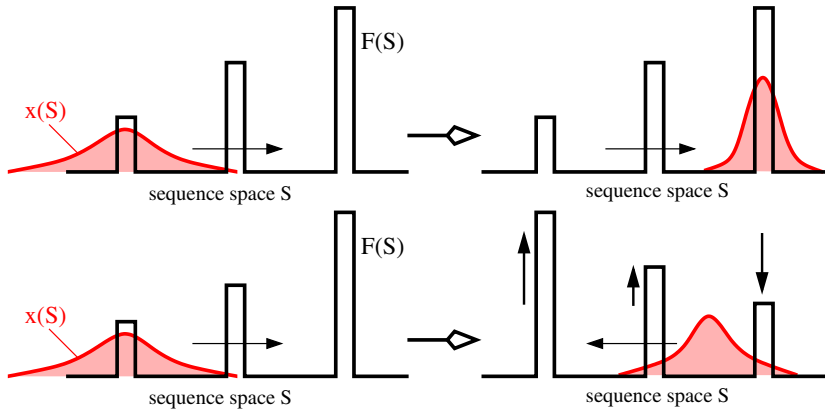
Fig. 5.9 *Top*: Evolutionary process of a single (quasi) species in a fixed fitness landscape (fixed ecosystem), here with tower-like structures, see Eq. (5.31). *Bottom*: A coevolutionary process might be regarded as changing the respective fitness landscapes

The term punctuated equilibrium was proposed by Gould and Eldredge in 1972 to describe a characteristic feature of the evolution of simple traits observed in fossil records. In contrast to the gradualistic view of evolutionary changes, these traits typically show long periods of stasis interrupted by very rapid changes.

The random events leading to an increase in genome optimization might be a rare mutation bringing one or more individuals to a different peak in the fitness landscape (microevolution) or a coevolutionary avalanche.

Strategies and Game Theory One is often interested, in contrast to the stochastic considerations discussed so far, in the evolutionary processes giving rise to very specific survival strategies. These questions can be addressed within game theory, which deals with strategically interacting agents in economics and beyond. When an animal meets another animal it has to decide, to give an example, whether confrontation, cooperation or defection is the best strategy. The basic elements of game theory are:

– Utility: Every participant, also called an agent, plays for himself, trying to maximize its own utility.
– Strategy: Every participant follows a set of rules of what to do when encountering an opponent; the strategy.
– Adaptive Games: In adaptive games the participants change their strategy in order to maximize future return. This change can be either deterministic or stochastic.
– Zero-Sum Games: When the sum of utilities is constant, you can only win what the others lose.
– Nash Equilibrium: Any strategy change by a participant leads to a reduction of his utility.

Hawks and Doves This simple evolutionary game tries to model competition in terms of expected utilities between aggressive behavior (by the "hawk") and peaceful (by the "dove") demeanor. The rules are:

Dove meets Dove	$A_{DD} = V/2$	They divide the territory.
Hawk meets Dove	$A_{HD} = V, A_{DH} = 0$	The Hawk gets all the territory, the Dove retreats and gets nothing.
Hawk meets Hawk	$A_{HH} = (V - C)/2$	They fight, get injured, and win half the territory.

The expected returns, the utilities, can be cast in matrix form,

$$A = \begin{pmatrix} A_{HH} & A_{HD} \\ A_{DH} & A_{DD} \end{pmatrix} = \begin{pmatrix} \frac{1}{2}(V - C) & V \\ 0 & \frac{V}{2} \end{pmatrix}.$$

A is denoted the "payoff" matrix. The question is then, under which conditions it pays to be peaceful or aggressive.

Adaptation by Evolution The introduction of reproductive capabilities for the participants turns the hawks-and-doves game into an evolutionary game. In this context one considers the behavioral strategies to result from the expression of distinct alleles.

The average number of offspring of a player is proportional to its fitness, which in turn is assumed to be given by its expected utility,

$$\begin{aligned} \dot{x}_H &= \left(A_{HH} x_H + A_{HD} x_D - \phi(t) \right) x_H \\ \dot{x}_D &= \left(A_{DH} x_H + A_{DD} x_D - \phi(t) \right) x_D \end{aligned}, \tag{5.59}$$

where x_D and x_H are the density of doves and hawks, respectively, and where the flux

$$\phi(t) = x_H A_{HH} x_H + x_H A_{HD} x_D + x_D A_{DH} x_H + x_D A_{DD} x_D$$

ensures an overall constant population, $x_H + x_D = 1$.

The Steady State Solution We are interested in the steady-state solution of Eq. (5.59), with $\dot{x}_D = 0 = \dot{x}_H$. Setting

$$x_H = x, \qquad x_D = 1 - x,$$

we find

$$\phi(t) = \frac{x^2}{2}(V - C) + Vx(1 - x) + \frac{V}{2}(1 - x)^2 = \frac{V}{2} - \frac{C}{2}x^2$$

and

$$\dot{x} = \left(\frac{V - C}{2}x + V(1 - x) - \phi(t) \right) x = \left(\frac{V}{2} - \frac{V}{2}x + \frac{C}{2}(x^2 - x) \right) x$$

$$= \frac{C}{2} x \left(x^2 - \frac{C+V}{C} x + \frac{V}{C} \right) = \frac{C}{2} x (x-1)(x-C/V)$$

$$= -\frac{d}{dx} V(x),$$

with

$$V(x) = -\frac{x^2}{4} V + \frac{x^3}{6}(V+C) - \frac{x^4}{8} C.$$

The steady state solution is given by

$$V'(x) = 0, \qquad x = V/C,$$

apart from the trivial solution $x = 0$ (no hawks) and $x = 1$ (only hawks). For $V > C$ there will be no doves left in the population, but for $V < C$ there will be an equilibrium with $x = V/C$ hawks and $1 - V/C$ doves. A population consisting exclusively of cooperating doves ($x = 0$) is unstable against the intrusion of hawks.

The Prisoner's Dilemma The payoff matrix of the prisoner's dilemma is given by

$$A = \begin{pmatrix} R & S \\ T & P \end{pmatrix} \qquad \begin{matrix} T > R > P > S \\ 2R > S + T \end{matrix} \qquad \begin{matrix} \text{cooperator} \triangleq \text{dove} \\ \text{defector} \triangleq \text{hawk} \end{matrix}. \qquad (5.60)$$

Here "cooperation" between the two prisoners is implied and not cooperation between a suspect and the police. The prisoners are best off if both keep silent. The standard values are

$$T = 5, \qquad R = 3, \qquad P = 1, \qquad S = 0.$$

The maximal global utility NR is obtained when everybody cooperates, but in a situation where agents interact randomly, the only stable Nash equilibrium is when everybody defects, with a global utility NP:

$$\text{reward for cooperators} = R_c = \left[RN_c + S(N - N_c) \right]/N,$$

$$\text{reward for defectors} = R_d = \left[TN_c + P(N - N_c) \right]/N,$$

where N_c is the number of cooperators and N the total number of agents. The difference is

$$R_c - R_d \sim (R - T)N_c + (S - P)(N - N_c) < 0,$$

as $R - T < 0$ and $S - P < 0$. The reward for cooperation is always smaller than that for defecting.

Evolutionary Games on a Lattice The adaptive dynamics of evolutionary games can change completely when the individual agents are placed on a regular lattice and when they adapt their strategies based on past observations. A possible simple rule is the following:
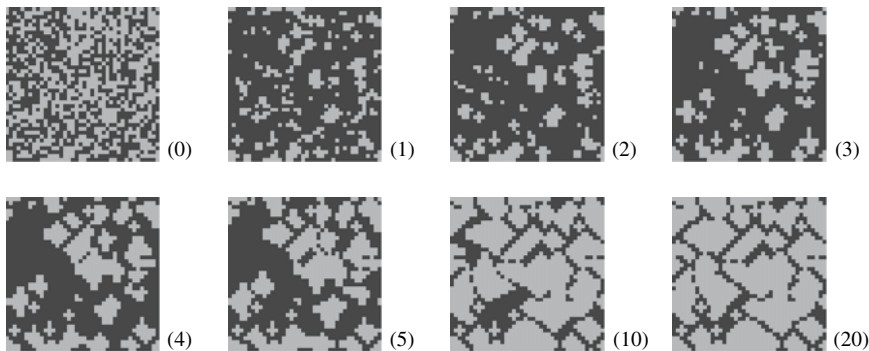
Fig. 5.10 Time series of the spatial distribution of cooperators (*gray*) and defectors (*black*) on a lattice of size $N = 40 \times 40$. The time is given by the numbers of generations in brackets. Initial condition: Equal number of defectors and cooperators, randomly distributed. Parameters for the payoff matrix, $\{T; R; P; S\} = \{3.5; 3.0; 0.5; 0.0\}$ (from Schweitzer, Behera and Mühlenbein, 2002)

– At each generation (time step) every agent evaluates its own payoff when inter-
  acting with its four neighbors, as well as the payoff of its neighbors.
– The individual agent then compares his own payoff one-by-one with the payoffs
  obtained by his four neighbors.
– The agent then switches his strategy (to cooperate or to defect) to the strategy of
  his neighbor if the neighbor received a higher payoff.

This simple rule can lead to complex real-space patterns of defectors intruding in a background of cooperators, see Fig. 5.10. The details depend on the value chosen for the payoff matrix.

Nash Equilibria and Coevolutionary Avalanches Coevolutionary games on a lattice eventually lead to an equilibrium state, which by definition has to be a Nash equilibrium. If such a state is perturbed from the outside, a self-critical coevolutionary avalanche may follow, in close relation to the sandpile model discussed in Chap. 4.

Exercises

THE ONE-DIMENSIONAL ISING MODEL
   Solve the one-dimensional Ising model

$$H = J\sum_i s_i s_{i+1} + B \sum_i s_i$$

by the transfer matrix method presented in Sect. 5.3.2 and calculate the free energy $F(T,B)$, the magnetization $M(T,B)$ and the susceptibility $\chi(T) = \lim_{B \to 0} \frac{\partial M(T,B)}{\partial B}$.

ERROR CATASTROPHE

For the prebiotic quasispecies model Eq. (5.49) consider tower-like autocatalytic reproduction rates W_{jj} and mutation rates W_{ij} ($i \neq j$) of the form

$$W_{ii} = \begin{cases} 1 & i = 1 \\ 1 - \sigma & i > 1 \end{cases}, \qquad W_{ij} = \begin{cases} u_+ & i = j+1 \\ u_- & i = j-1 \\ 0 & i \neq j \text{ otherwise} \end{cases},$$

with $\sigma, u_\pm \in [0,1]$. Determine the error catastrophe for the two cases $u_+ = u_- \equiv u$ and $u_+ = u$, $u_- = 0$. Compare it to the results for the tower landscape discussed in Sect. 5.3.3.

Hint: For the stationary eigenvalue equation (5.49), with $\dot{x}_i = 0$ ($i = 1, \ldots$), write x_{j+1} as a function of x_j and x_{j-1}. This two-step recursion relation leads to a 2×2 matrix. Consider the eigenvalues/vectors of this matrix, the initial condition for x_1, and the normalization condition $\sum_i x_i < \infty$ valid in the adapting regime.

MODELS OF LIFE

Go to the Internet, e.g. http://cmol.nbi.dk/javaapp.php, and try a few JAVA applets simulating models of life. Select a model of your choice and study the literature given.

HYPERCYCLES

Consider the reaction equations (5.50) and (5.51) for $N = 2$ molecules and a homogeneous network. Find the fixpoints and discuss their stability.

THE PRISONER'S DILEMMA ON A LATTICE

Consider the stability of intruders in the prisoner's dilemma Eq. (5.60) on a square lattice, as the one illustrated in Fig. 5.10. Namely, the case of just one and of two adjacent defectors/cooperators in a background of cooperators/defectors. Who survives?

NASH EQUILIBRIUM

Examine the Nash equilibrium and its optimality for the following two-player game:

Each player acts either cautiously or riskily. A player acting cautiously always receives a low pay-off. A player playing riskily gets a high pay-off if the other player also takes a risk. Otherwise, the risk-taker obtains no reward.

Further Reading

A comprehensive account of the earth's biosphere can be found in Smil (2002); a review article on the statistical approach to Darwinian evolution in Peliti (1997) and Drossel (2001). Further general textbooks on evolution, game-theory and hypercycles are Nowak (2006), Kimura (1983), Eigen (1971), Eigen and Schuster (1979) and Schuster (2001). For a review article on evolution and speciation see Drossel (2001).

The relation between life and self-organization is further discussed by Kauffman (1993), a review of the prebiotic RNA world can be found in Orgel (1998) and critical discussions of alternative scenarios for the origin of life in Orgel (1998) and Pereto (2005).

The original formulation of the fundamental theorem of natural selection was given by Fisher (1930), and the original introduction of the term "punctuated equilibrium" by Eldredge and Gould (1972). For the reader interested in coevolutionary games we refer to Ebel and Bornholdt (2002); for an interesting application of game theory to world politics as an evolving complex system see Cederman (1997).

CEDERMAN, L.-E. 1997 *Emergent Actors in World Politics.* Princeton University Press.

DRAKE, J.W., CHARLESWORTH, B., CHARLESWORTH, D. 1998 Rates of spontaneous mutation. *Genetics* **148**, 1667–1686.

DROSSEL, B. 2001 Biological evolution and statistical physics. *Advances in Physics* **2**, 209–295.

EBEL, H., BORNHOLDT, S. 2002 Coevolutionary games on networks. *Physical Review E* **66**, 056118.

EIGEN, M. 1971 Self organization of matter and the evolution of biological macromolecules. *Naturwissenschaften* **58**, 465.

EIGEN, M., SCHUSTER, P. 1979 *The Hypercycle - A Principle of Natural Self-Organization.* Springer, Berlin.

ELDREDGE, N., GOULD, S.J. 1972 *Punctuated Equilibria: An alternative to Phyletic Gradualism.* T.J.M. Schopf, J.M. Thomas (eds.), Models in Paleobiology. Freeman and Cooper, San Francisco.

FISHER, R.A. 1930 *The Genetical Theory of Natural Selection.* Dover, New York.

JAIN, K., KRUG, J. 2006 *Adaptation in simple and complex fitness landscapes.* In Bastolla, U., Porto, M, Roman, H.E., Vendruscolo, M. (eds.) Structural Approaches to Sequence Evolution: Molecules, Networks and Populations. AG Porto, Darmstadt.

KIMURA, M. 1983 *The Neutral Theory of Molecular Evolution.* Cambridge University Press.

KAUFFMAN, S.A. 1993 *The Origins of Order.* Oxford University Press.

NOWAK, M.A. 2006 *Evolutionary Dynamics: Exploring the Equations of Life.* Harvard University Press.

ORGEL, L.E 1998 The origin of life: A review of facts and speculations. *Trends in Biochemical Sciences* **23**, 491–495.

PELITI, L. 1997 *Introduction to the statistical theory of Darwinian evolution.* ArXiv preprint cond-mat/9712027.

PERETO, J. 2005 Controversies on the origin of life. *International Microbiology* **8**, 23–31.

SCHUSTER, H.G. 2001 *Complex Adaptive Systems – An Introduction.* Scator, Saarbrücken.

SMIL, V. 2002 *The Earth's Biosphere: Evolution, Dynamics, and Change.* MIT Press, Cambridge.

SCHWEITZER, F., BEHERA, L., MÜHLENBEIN, H. 2002 Evolution of Cooperation in a Spatial Prisoner's Dilemma. *Advances in Complex Systems* **5**, 269–299.

Chapter 6
Synchronization Phenomena

Here we consider the dynamics of complex systems constituted of interacting local computational units that have their own non-trivial dynamics. An example for a local dynamical system is the time evolution of an infectious disease in a certain city that is weakly influenced by an ongoing outbreak of the same disease in another city; or the case of a neuron in a state where it fires spontaneously under the influence of the afferent axon potentials.

A fundamental question is then whether the time evolutions of these local units will remain dynamically independent of each other or whether, at some point, they will start to change their states all in the same rhythm. This is the notion of "synchronization", which we will study throughout this chapter.

6.1 Frequency Locking

The Driven Harmonic Oscillator For introductory purposes we consider the driven harmonic oscillator

$$\ddot{x} + \gamma \dot{x} + \omega_0^2 x \ = \ F \left(e^{i\omega t} + c.c. \right), \qquad \gamma > 0 . \tag{6.1}$$

In the absence of external driving, $F \equiv 0$, the solution is

$$x(t) \ \sim \ e^{\lambda t}, \qquad \lambda_{\pm} = -\frac{\gamma}{2} \pm \sqrt{\frac{\gamma^2}{4} - \omega_0^2} , \tag{6.2}$$

which is damped/critical/overdamped for $\gamma < 2\omega_0$, $\gamma = 2\omega_0$ and $\gamma > 2\omega_0$.

Frequency Locking In the long time limit, $t \to \infty$, the dynamics of the system follows the external driving, for all $F \neq 0$, due the damping $\gamma > 0$. We therefore consider the ansatz

$$x(t) \ = \ a e^{i\omega t} + c.c., \tag{6.3}$$

where the amplitude a may contain an additional time-independent phase. Using this ansatz for Eq. (6.1) we obtain

$$
\begin{aligned}
F &= a\left(-\omega^2 + i\omega\gamma + \omega_0^2\right) \\
&= -a\left(\omega^2 - i\omega\gamma - \omega_0^2\right) = -a\left(\omega + i\lambda_+\right)\left(\omega + i\lambda_-\right),
\end{aligned}
$$

where the eigenfrequencies $\lambda_\pm$ are given by Eq. (6.2). The solution for the amplitude a can then be written in terms of $\lambda_\pm$ or alternatively as

$$
a = \frac{-F}{\left(\omega^2 - \omega_0^2\right) - i\omega\gamma} . \tag{6.4}
$$

The response becomes divergent, viz $a \to \infty$, at resonance $\omega = \omega_0$ and small damping $\gamma \to 0$.

The General Solution The driven, damped harmonic oscillator Eq. (6.1) is an inhomogeneous linear differential equation and its general solution is given by the superposition of the special solution Eq. (6.4) with the general solution of the homogeneous system Eq. (6.2). The latter dies out for $t \to \infty$ and the system synchronizes with the external driving frequency ω.

6.2 Synchronization of Coupled Oscillators

Limiting Cycles A free rotation

$$
x(t) = r\left(\cos(\omega t + \phi_0), \sin(\omega t + \phi_0)\right), \qquad \theta(t) = \omega t + \theta_0, \qquad \dot{\theta} = \omega
$$

often occurs (in suitable coordinates) as limiting cycles of dynamical systems, see Chap. 2.

Coupled Dynamical Systems We consider a collection of individual dynamical systems $i = 1, \dots, N$, which have limiting cycles with natural frequencies ω_i. The coupled system then obeys

$$
\dot{\theta}_i = \omega_i + \sum_{j=1}^{N} \Gamma_{ij}(\theta_i, \theta_j), \qquad i = 1, \dots, N, \tag{6.5}
$$

where the Γ_{ij} are suitable coupling constants.

The Kuramoto Model A particularly tractable choice for the coupling constants Γ_{ij} has been proposed by Kuramoto:

$$
\Gamma_{ij}(\theta_i, \theta_j) = \frac{K}{N} \sin(\theta_j - \theta_i), \tag{6.6}
$$
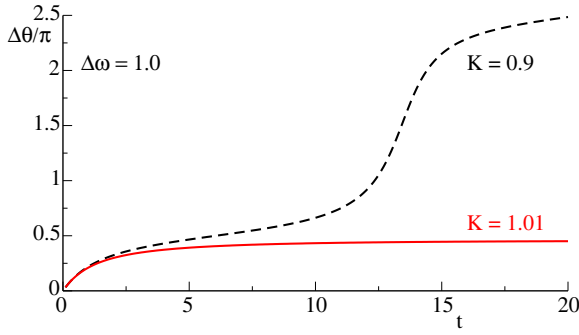
Fig. 6.1 The relative phase $\Delta\theta(t)$ of two coupled oscillators, obeying Eq. (6.7), with $\Delta\omega = 1$ and a critical coupling strength $K_c = 1$. For an undercritical coupling strength $K = 0.9$ the relative phase increases steadily, for an overcritical coupling $K = 1.01$ it locks

where $K \geq 0$ is the coupling strength and the factor $1/N$ ensures that the model is well behaved in the limit $N \to \infty$.

Two Coupled Oscillators We consider first the case $N = 2$:

$$\dot{\theta}_1 = \omega_1 + \frac{K}{2}\sin(\theta_2 - \theta_1), \qquad \dot{\theta}_2 = \omega_2 + \frac{K}{2}\sin(\theta_1 - \theta_2),$$

or

$$\Delta\dot{\theta} = \Delta\omega - K\sin(\Delta\theta), \qquad \Delta\theta = \theta_2 - \theta_1, \qquad \Delta\omega = \omega_2 - \omega_1. \tag{6.7}$$

The system has a fixpoint $\Delta\theta^*$ for which

$$\frac{d}{dt}\Delta\theta^* = 0, \qquad \sin(\Delta\theta^*) = \frac{\Delta\omega}{K} \tag{6.8}$$

and therefore

$$\Delta\theta^* \in [-\pi/2, \pi/2], \qquad K > |\Delta\omega|. \tag{6.9}$$

We analyze the stability of this fixpoint using $\Delta\theta = \Delta\theta^* + \delta$ and Eq. (6.7). We obtain

$$\frac{d}{dt}\delta = -(K\cos\Delta\theta^*)\,\delta, \qquad \delta(t) = \delta_0 e^{-K\cos\Delta\theta^* t}.$$

The fixpoint is stable since $K > 0$ and $\cos\Delta\theta^* > 0$, due to Eq. (6.9). We therefore have a bifurcation.

- For $K < |\Delta\omega|$ there is no phase coherence between the two oscillators, they are drifting with respect to each other.
- For $K > |\Delta\omega|$ there is phase locking and the two oscillators rotate together with a constant phase difference.

This situation is illustrated in Fig. 6.1.

Natural Frequency Distribution We now consider the case of many coupled oscillators, $N \to \infty$. The individual systems have different individual frequencies ω_i with a probability distribution

$$g(\omega) \,=\, g(-\omega), \qquad \int_{-\infty}^{\infty} g(\omega)\,\mathrm{d}\omega \,=\, 1 \,. \qquad (6.10)$$

We note that the choice of a zero average frequency

$$\int_{-\infty}^{\infty} \omega g(\omega)\,\mathrm{d}\omega \,=\, 0$$

implicit in Eq. (6.10) is actually generally possible, as the dynamical equations (6.5) and (6.6) are invariant under a global translation

$$\omega \;\to\; \omega + \Omega, \qquad \theta_i \;\to\; \theta_i + \Omega t \,,$$

with Ω being the initial non-zero mean frequency.

The Order Parameter The complex order parameter

$$r e^{i\psi} \,=\, \frac{1}{N} \sum_{j=1}^{N} e^{i\theta_j} \qquad (6.11)$$

is a macroscopic quantity that can be interpreted as the collective rhythm produced by the assembly of the interacting oscillating systems. The radius $r(t)$ measures the degree of phase coherence and $\psi(t)$ corresponds to the average phase.

Molecular Field Representation We rewrite the order parameter definition Eq. (6.11) as

$$r e^{i(\psi-\theta_i)} \,=\, \frac{1}{N} \sum_{j=1}^{N} e^{i(\theta_j-\theta_i)}, \qquad r\sin(\psi-\theta_i) \,=\, \frac{1}{N} \sum_{j=1}^{N} \sin(\theta_j - \theta_i) \,,$$

retaining the imaginary component of the first term. Inserting the second expression into the governing equation (6.5) we find

$$\dot{\theta}_i \,=\, \omega_i + \frac{K}{N} \sum_{j} \sin(\theta_j - \theta_i) \,=\, \omega_i + Kr\sin(\psi - \theta_i) \,. \qquad (6.12)$$

The motion of every individual oscillator $i = 1, \dots, N$ is coupled to the other oscillators only through the mean-field phase ψ; the coupling strength being proportional to the mean-field amplitude r.

The individual phases θ_i are drawn towards the self-consistently determined mean phase ψ, as can be seen in the numerical simulations presented in Fig. 6.2. Mean-field theory is exact for the Kuramoto model. It is nevertheless non-trivial to solve, as the self-consistency condition (6.11) needs to be fulfilled.
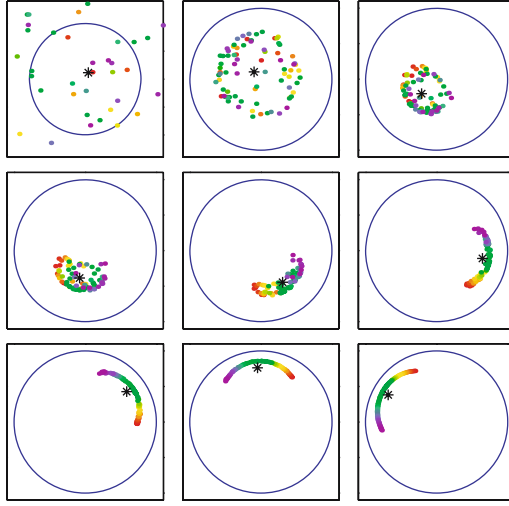
Fig. 6.2 Spontaneous synchronization in a network of limit cycle oscillators with distributed individual frequencies. Color coding: slowest (*red*)–fastest (*violet*) natural frequency. With respect to Eq. (6.5) an additional distribution of individual radii $r_i(t)$ has been assumed, the asterisk denotes the mean field $re^{i\psi} = \sum_i r_i e^{i\theta_i}/N$, compare Eq. (6.11), and the individual radii $r_i(t)$ are slowly relaxing (from Strogatz, 2001)

The Rotating Frame of Reference We consider the thermodynamic limit

$$N \to \infty, \qquad r(t) \to r, \qquad \psi(t) \to \Omega t$$

and transform via

$$\theta_i \to \theta_i + \psi = \theta_i + \Omega t, \qquad \dot{\theta}_i \to \theta_i + \Omega, \qquad \omega_i \to \omega + \Omega$$

to the rotating frame of reference. The governing equation (6.12) then becomes

$$\dot{\theta}_i = \omega_i - Kr\sin(\theta_i). \qquad (6.13)$$

This expression is identical to the one for the case of two coupled oscillators, Eq. (6.7), when substituting Kr by K. It then follows directly that $\omega_i = Kr$ constitutes a special point.

Drifting and Locked Components Equation (6.13) has a fixpoint θ_i^* for which $\dot{\theta}_i^* = 0$ and

$$Kr\sin(\theta_i^*) = \omega_i, \qquad |\omega_i| < Kr, \qquad \theta_i^* \in [-\frac{\pi}{2}, \frac{\pi}{2}]. \qquad (6.14)$$

$\dot{\theta}_i^* = 0$ in the rotating frame of reference means that the participating limit cycles oscillate with the average frequency ψ; they are "locked" to ψ, see Figs. 6.2 and 6.3.
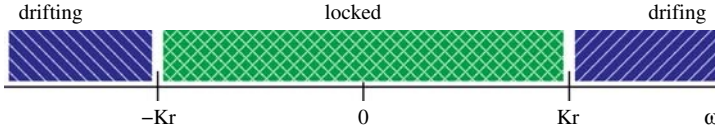
Fig. 6.3 The region of locked and drifting natural frequencies $\omega_i \to \omega$ within the Kuramoto model

For $|\omega_i| > Kr$ the participating limit cycle *drifts*, i.e. $\dot{\theta}_i$ never vanishes. They do, however, slow down when they approach the locked oscillators, see Eq. (6.13) and Fig. 6.1.

Stationary Frequency Distribution We denote by

$$\rho(\theta, \omega)\, d\theta$$

the fraction of drifting oscillators with natural frequency ω that lie between θ and $\theta + d\theta$. It obeys the continuity equation

$$\frac{\partial \rho}{\partial t} + \frac{\partial}{\partial \theta}\left(\rho\, \dot{\theta}\right) = 0 \,,$$

where $\rho\, \dot{\theta}$ is the respective current density. In the stationary case, $\dot{\rho} = 0$, the stationary frequency distribution $\rho(\theta, \omega)$ needs to be inversely proportional to the speed

$$\dot{\theta} = \omega - Kr\sin(\theta) \,.$$

The oscillators pile up at slow places and thin out at fast places on the circle. Hence

$$\rho(\theta, \omega) = \frac{C}{|\omega - Kr\sin(\theta)|}, \qquad \int_{-\pi}^{\pi} \rho(\theta, \omega)\, d\theta = 1 \,, \qquad (6.15)$$

for $\omega > 0$, where C is an appropriate normalization constant.

Formulation of the Self-Consistency Condition We write the self-consistency condition (6.11) as

$$\langle e^{i\theta} \rangle = \langle e^{i\theta} \rangle_{\text{locked}} + \langle e^{i\theta} \rangle_{\text{drifting}} = re^{i\psi} \equiv r \,, \qquad (6.16)$$

where the brackets $\langle \cdot \rangle$ denote population averages and where we have used the fact that we can set the average phase ψ to zero.

Locked Contribution The locked contribution is

$$\langle e^{i\theta} \rangle_{\text{locked}} = \int_{-Kr}^{Kr} e^{i\theta^*(\omega)} g(\omega)\, d\omega = \int_{-Kr}^{Kr} \cos\left(\left(\theta^*(\omega)\right)\right) g(\omega)\, d\omega \,,$$

where we have assumed $g(\omega) = g(-\omega)$ for the distribution $g(\omega)$ of the natural frequencies within the rotating frame of reference. Using Eq. (6.14),
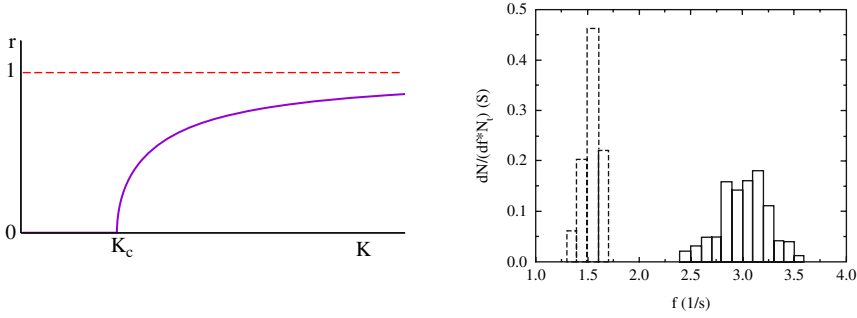
Fig. 6.4 *Left*: The solution $r = \sqrt{1 - K_c/K}$ for the order parameter r in the Kuramoto model. *Right*: Normalized distribution for the frequencies of clappings of one chosen individual from 100 samplings (Néda et al., 2000a,b)

$$\mathrm{d}\omega = Kr\cos\theta^* \, \mathrm{d}\theta^* \, ,$$

for $\theta^*(\omega)$ we obtain

$$\langle e^{i\theta} \rangle_{\text{locked}} = \int_{-\pi/2}^{\pi/2} \cos(\theta^*) \, g(Kr\sin\theta^*) \, Kr\cos(\theta^*) \, \mathrm{d}\theta^* \qquad (6.17)$$

$$= Kr \int_{-\pi/2}^{\pi/2} \cos^2(\theta^*) \, g(Kr\sin\theta^*) \, \mathrm{d}\theta^* \, .$$

The Drifting Contribution The drifting contribution

$$\langle e^{i\theta} \rangle_{\text{drifting}} = \int_{-\pi}^{\pi} \mathrm{d}\theta \int_{|\omega|>Kr} \mathrm{d}\omega \, e^{i\theta} \rho(\theta, \omega) g(\omega) = 0$$

to the order parameter actually vanishes. Physically this is clear: oscillators that are not locked to the mean field cannot contribute to the order parameter. Mathematically it follows from $g(\omega) = g(-\omega)$, $\rho(\theta + \pi, -\omega) = \rho(\theta, \omega)$ and $e^{i(\theta+\pi)} = -e^{i\theta}$.

Second-Order Phase Transition The population average $\langle e^{i\theta} \rangle$ of the order parameter Eq. (6.16) is then just the locked contribution Eq. (6.17)

$$r = \langle e^{i\theta} \rangle \equiv \langle e^{i\theta} \rangle_{\text{locked}} = Kr \int_{-\pi/2}^{\pi/2} \cos^2(\theta^*) \, g(Kr\sin\theta^*) \, \mathrm{d}\theta^* \, . \qquad (6.18)$$

For $K < K_c$ Eq. (6.18) has only the trivial solution $r = 0$; for $K > K_c$ a finite order parameter $r > 0$ is stabilized, see Fig. 6.4. We therefore have a second-order phase transition, as discussed in Chap. 4.

Critical Coupling The critical coupling strength K_c can be obtained considering the limes $r \to 0+$ in Eq. (6.18):

$$1 = K_c g(0) \int_{-\pi/2}^{\pi/2} \cos^2 \theta^* \, d\theta^* = K_c g(0) \frac{\pi}{2}, \qquad K_c = \frac{2}{\pi g(0)} \, . \qquad (6.19)$$

The self-consistency condition Eq. (6.18) can actually be solved exactly with the result

$$r = \sqrt{1 - \frac{K_c}{K}}, \qquad K_c = \frac{2}{\pi g(0)} \, , \qquad (6.20)$$

as illustrated in Fig. 6.4.

The Physics of Rhythmic Applause A nice application of the Kuramoto model is the synchronization of the clapping of an audience after a performance, which happens when everybody claps at a slow frequency and in tact. In this case the distribution of "natural clapping frequencies" is quite narrow and $K > K_c \propto 1/g(0)$.

When an individual wants to express especial satisfaction with the performance he/she increases the clapping frequency by about a factor of 2, as measured experimentally, in order to increase the noise level, which just depends on the clapping frequency. Measurements have shown, see Fig. 6.4, that the distribution of natural clapping frequencies is broader when the clapping is fast. This leads to a drop in $g(0)$ and then $K < K_c \propto 1/g(0)$. No synchronization is possible when the applause is intense.

6.3 Synchronization of Relaxation Oscillators

The synchronization of the limiting cycle oscillators discussed in Sect. 6.2 is very slow, see Fig. 6.2, as the information between the different oscillators is exchanged only indirectly via the molecular field, which is an averaged quantity. Relaxational oscillators, like the van der Pol oscillator discussed in Chap. 2, do, on the other hand, have a non-uniform cycle and the timing of the stimulation of one element by another is important. This is a characteristic property of real-world neurons in particular and of many models of artificial neurons, like so-called integrate-and-fire models.

Terman–Wang Oscillators There are many variants of relaxation oscillators relevant for describing integrate-and-fire neurons, starting from the classical Hodgkin–Huxley equations. Here we discuss the particularly transparent dynamical system introduced by Terman and Wang, namely

$$\begin{aligned} \dot{x} &= f(x) - y + I & f(x) &= 3x - x^3 + 2 \\ \dot{y} &= \epsilon \left(g(x) - y \right) & g(x) &= \alpha \left(1 + \tanh(x/\beta) \right) \end{aligned} \qquad (6.21)$$

Here x corresponds in neural terms to the membrane potential and I represents the external stimulation to the neural oscillator. The amount of dissipation is given by

$$\frac{\partial \dot{x}}{\partial x} + \frac{\partial \dot{y}}{\partial y} = 3 - 3x^2 - \epsilon = 3(1 - x^2) - \epsilon \, .$$
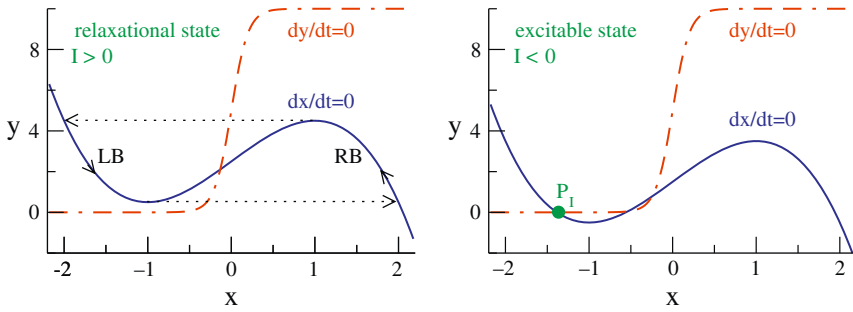
Fig. 6.5 The $\dot{y} = 0$ (*thick dashed-dotted lines*) and the $\dot{x} = 0$ (*thick full lines*) isocline of the Terman–Wang oscillator, Eq. (6.21), for $\alpha = 5$, $\beta = 0.2$, $\epsilon = 0.1$. *Left*: $I = 0.5$ with the limiting relaxational cycle for $\epsilon \ll 1$ (*thin dotted line with arrows*). *Right*: $I = -0.5$ with the stable fixpoint: P_I

For small $\epsilon \ll 1$ the system takes up energy for membrane potentials $|x| < 1$ and dissipates energy for $|x| > 1$.

Fixpoints The fixpoints are determined via

$$\begin{aligned} \dot{x} &= 0 & y &= f(x) + I \\ \dot{y} &= 0 & y &= g(x) \end{aligned}$$

by the intersection of the two functions $f(x) + I$ and $g(x)$, see Fig. 6.5. We find two parameter regimes:

– For $I \geq 0$ we have one unstable fixpoint (x^*, y^*) with $x^* \simeq 0$.
– For $I < 0$ and $|I|$ large enough we have two additional fixpoints given by the crossing of the sigmoid $\alpha(1 + \tanh(x/\beta))$ with the left branch (LB) of the cubic $f(x) = 3x - x^3 + 2$, with one fixpoint being stable.

The stable fixpoint P_I is indicated in Fig. 6.5.

The Relaxational Regime For the case $I > 0$ the Terman–Wang oscillator relaxes in the long time limit to a periodic solution, see Fig. 6.5, which is very similar to the limiting relaxation oscillation of the Van der Pol oscillator discussed in Chap. 2.

Silent and Active Phases In its relaxational regime, the periodic solution jumps very fast (for $\epsilon \ll 1$) between trajectories that approach closely the right branch (RB) and the left branch (LB) of the $\dot{x} = 0$ isocline. The time development on the RB and the LB are, however, not symmetric, see Figs. 6.5 and 6.6, and we can distinguish two regimes:

The Silent Phase. We call the relaxational dynamics close to the LB ($x < 0$) of the $\dot{x} = 0$ isocline the silent phase or the refractory period.
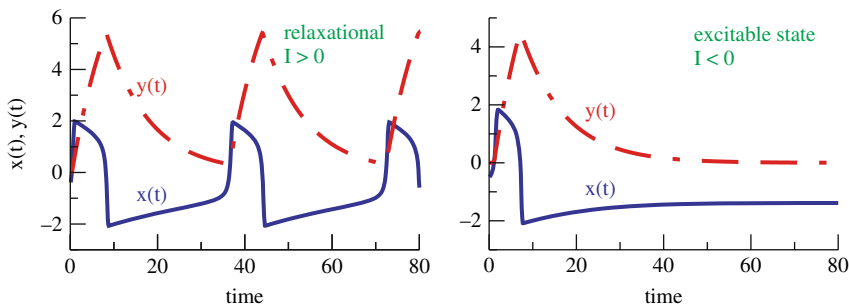
Fig. 6.6 Sample trajectories $y(t)$ (*thick dashed-dotted lines*) and $x(t)$ (*thick full lines*) of the Terman–Wang oscillator Eq. (6.21) for $\alpha = 5$, $\beta = 0.2$, $\epsilon = 0.1$. *Left*: $I = 0.5$ exhibiting spiking behavior. *Right*: $I = -0.5$, relaxing to the stable fixpoint

> *The Active Phase. We call the relaxational dynamics close to the RB ($x > 0$) of the $\dot{x} = 0$ isocline the active phase.*

The relative rate of the time development $\dot{y}$ in the silent and active phases are determined by the parameter α, compare Eq. (6.21).

The active phase on the RB is far from the $\dot{y} = 0$ isocline for $\alpha \gg 1$, see Fig. 6.5, and the time development $\dot{y}$ is then fast. The silent phase on the LB is, however, always close to the $\dot{y} = 0$ isocline and the system spends considerable time there.

The Spontaneously Spiking State and the Separation of Time Scales In its relaxational phase, the Terman–Wang oscillator can therefore be considered as a spontaneously spiking neuron, see Fig. 6.6, with the spike corresponding to the active phase, which might be quite short compared to the silent phase for $\alpha \gg 1$.

The Terman–Wang differential equations (6.21) are examples of a standard technique within dynamical system theory, the coupling of a slow variable, y, to a fast variable, x, which results in a separation of time scales. When the slow variable $y(t)$ relaxes below a certain threshold, see Fig. 6.6, the fast variable $x(t)$ responds rapidly and resets the slow variable. We will encounter further applications of this procedure in Chap. 7.

The Excitable State The neuron has an additional phase with a stable fixpoint P_I on the LB (within the silent region), for negative external stimulation (suppression) $I < 0$. The dormant state at the fixpoint P_I is "excitable": A positive external stimulation above a small threshold will force a transition into the active phase, with the neuron spiking continuously.

Synchronization via Fast Threshold Modulation Limit cycle oscillators can synchronize, albeit slowly, via the common molecular field, as discussed in Sect. 6.2. A much faster synchronization can be achieved via *fast threshold synchronization* for a network of interacting relaxation oscillators.
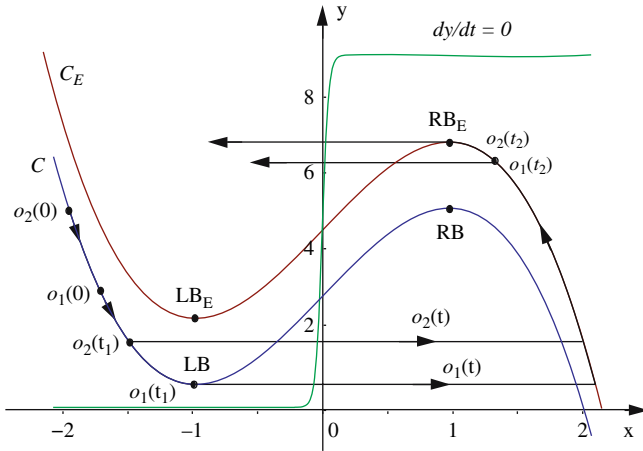
Fig. 6.7 Fast threshold modulation for two excitatory coupled Terman–Wang oscillators, Eq. (6.21) $o_1 = o_1(t)$ and $o_2 = o_2(t)$, which start at time 0. When o_1 jumps at $t = t_1$ the cubic $\dot{x} = 0$ isocline for o_2 is raised from C to C_E. This induces o_2 to jump as well. Note that the jumping from the right branches (RB and RB_E) back to the left branches occurs in the reverse order: o_2 jumps first (from Wang, 1999)

The idea is simple. Relaxational oscillators have distinct states during their cycle; we called them the "silent phase" and the "active phase" for the case of the Terman–Wang oscillator. We then assume that a neural oscillator in its (short) active phase changes the threshold I of the other neural oscillator in Eq. 6.21 as

$$I \rightarrow I + \Delta I, \qquad \Delta I > 0 \,,$$

such that the second neural oscillator changes from an excitable state to the oscillating state. This process is illustrated graphically in Fig. 6.7. In neural terms: when the first neuron fires, the second neuron follows suit.

Propagation of Activity We consider a simple model

$$\boxed{1} \quad \Rightarrow \quad \boxed{2} \quad \Rightarrow \quad \boxed{3} \quad \Rightarrow \quad \dots$$

of $i = 1, \dots, N$ coupled oscillators $x_i(t), y_i(t)$, all being initially in the excitable state with $I_i \equiv -0.5$. They are coupled via fast threshold modulation, specifically via

$$\Delta I_i(t) = \Theta(x_{i-1}(t)) \,, \tag{6.22}$$

where $\Theta(x)$ is the Heaviside step function. That is, we define an oscillator i to be in its active phase whenever $x_i > 0$. The resulting dynamics is shown in Fig. 6.8. The chain is driven by setting the first oscillator of the chain into the spiking state for a certain period of time. All other oscillators start to spike consecutively in rapid sequence.
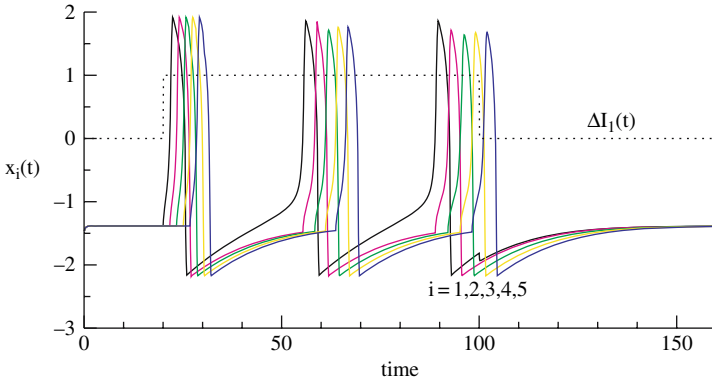
Fig. 6.8 Sample trajectories $x_i(t)$ (lines) for a line of coupled Terman–Wang oscillators, Eq. (6.21) for $\alpha = 10$, $\beta = 0.2$, $\epsilon = 0.1$ and $I = -0.5$ in excitable states. For $t \in [20, 100]$ a driving current $\Delta I_1 = 1$ is added to the first oscillator. x_1 then starts to spike, driving the other oscillators one by one via a fast threshold modulation

6.4 Synchronization and Object Recognition in Neural Networks

Temporal Correlation Theory The neurons in the brain have time-dependent activities and can be described by generalized relaxation oscillators. The *temporal correlation theory* assumes that not only the average activities of individual neurons (the spiking rate) are important, but also the relative phasing of the individual spikes. Indeed, experimental evidence points towards object definition in the visual cortex via synchronized firing.

The LEGION Network of Coupled Relaxation Oscillators As an example of how object definition via coupled relaxation oscillators can be achieved we consider the LEGION (local excitatory globally inhibitory oscillator network) network by Terman and Wang. Each oscillator i is defined as

$$\begin{aligned}
\dot{x}_i &= f(x_i) - y_i + I_i + S_i + \rho & f(x) &= 3x - x^3 + 2 \\
\dot{y}_i &= \epsilon\left(g(x_i) - y_i\right) & g(x) &= \alpha\left(1 + \tanh(x/\beta)\right)
\end{aligned} \qquad (6.23)$$

There are two terms in addition to the ones necessary for the description of a single oscillator, compare Eq. (6.21):

ρ : a random-noise term and

S_i : the interneural interaction.

Interneural Interaction The interneural interaction is given for the LEGION network by

$$S_i = \sum_{l \in N(i)} T_{il}\,\Theta(x_l - x_c) - W_z\Theta(z - z_c) , \qquad (6.24)$$
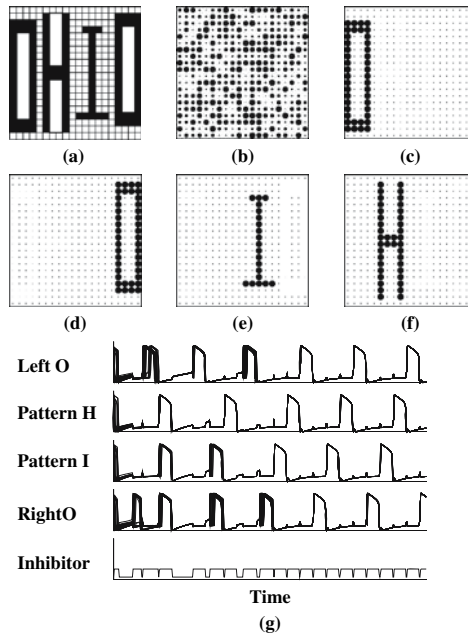
Fig. 6.9 (**a**) A pattern used to stimulate a 20×20 LEGION network. (**b**) Initial random activities of the relaxation oscillators. (**c**, **d**, **e**, **f**) Snapshots of the activities at different sequential times. (**g**) The corresponding time-dependent activities of selected oscillators and of the global inhibitor (from Wang, 1999)

where $\Theta(z)$ is the Heaviside step function. The parameters have the following meaning:

$T_{il} > 0$: Interneural excitatory couplings.

$N(i)$: Neighborhood of neuron i.

x_c : Threshold determining the active phase.

z : Variable for the global inhibitor.

$-W_z < 0$: Coupling to the global inhibitor z.

z_c : Threshold for the global inhibitor.

Global Inhibition Global inhibition is a quite generic strategy for neural networks with selective gating capabilities. A long-range or global inhibition term assures that only one or only a few of the local computational units are active coinstantaneously. In the context of the Terman–Wang LEGION network it is assumed to have the dynamics

$$\dot{z} = (\sigma_z - z)\phi, \qquad \phi > 0, \qquad (6.25)$$

where the binary variable σ_z is determined by the following rule:

$\sigma_z = 1$ if at least one oscillator is active.

$\sigma_z = 0$ if all oscillators are silent or in the excitable state.

This rule is very non-biological, the LEGION network is just a proof of the principle for object definition via fast synchronization. When at least one oscillator is in its active phase the global inhibitor is activated, $z \rightarrow 1$, and inhibition is turned off whenever the network is completely inactive.

Simulation of the LEGION Network A simulation of a 20×20 LEGION network is presented in Fig. 6.9. We observe the following:

– The network is able to discriminate between different input objects.
– Objects are characterized by the coherent activity of the corresponding neurons, while neurons not belonging to the active object are in the excitable state.
– Individual input objects pop up randomly one after the other.

Working Principles of the LEGION Network The working principles of the LEGION network are the following:

– When the stimulus begins there will be a single oscillator k, which will jump first into the active phase, activating the global inhibitor, Eq. (6.25), via $\sigma_z \rightarrow 1$. The noise term $\sim \rho$ in Eq. (6.23) determines the first active unit randomly from the set of all units receiving an input signal $\sim I_i$, whenever all input signals have the same strength.
– The global inhibitor then suppresses the activity of all other oscillators, apart from the stimulated neighbors of k, which also jump into the active phase, having set the parameters such that

$$I + T_{ik} - W_z > 0, \qquad I : \text{stimulus}$$

is valid. The additional condition

$$I - W_z < 0$$

assures, that units receiving an input, but not being topologically connected to the cluster of active units, are suppressed. No two distinct objects can then be activated coinstantaneously.
– This process continues until all oscillators representing the stimulated pattern are active. As this process is very fast, all active oscillators fire nearly simultaneously, compare also Fig. 6.8.
– When all oscillators in a pattern oscillate in phase, they also jump back to the silent state simultaneously. At that point the global inhibitor is turned off: $\sigma_z \rightarrow 0$ in Eq. (6.25) and the game starts again with a different pattern.

Discussion Even though the network nicely performs its task of object recognition via coherent oscillatory firing, there are a few aspects worth noting:

– The functioning of the network depends on the global inhibitor triggered by the specific oscillator that jumps first. This might be difficult to realize in biological networks, like the visual cortex, which do not have well defined boundaries.
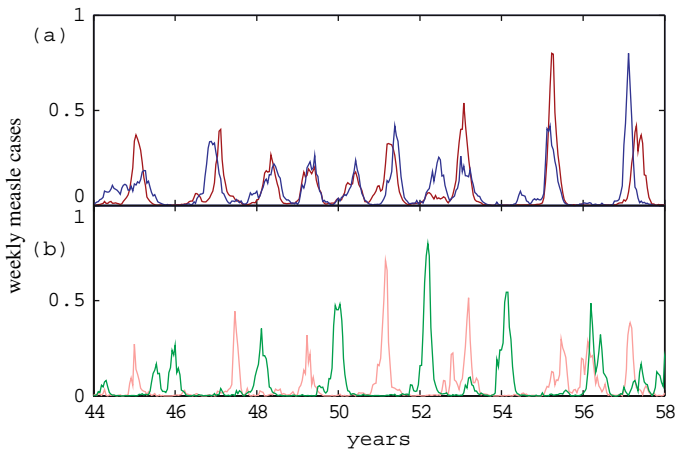
Fig. 6.10 Observation of the number of infected persons in a study on illnesses. (**a**) Weekly cases of measle cases in Birmingham (*red line*) and Newcastle (*blue line*). (**b**) Weekly cases of measle cases in Cambridge (*green line*) and in Norwich (*pink line*) (from He, 2003)

– The first active oscillator sequentially recruits all other oscillators belonging to its pattern. This happens very fast via the mechanism of rapid threshold modulation. The synchronization is therefore not a collective process in which the input data is processed in parallel; a property assumed to be important for biological networks.
– The recognized pattern remains active for exactly one cycle and no longer.

We notice, however, that the design of neural networks capable of fast synchronization via a collective process remains a challenge, since collective processes have an inherent tendency towards slowness, due to the need to exchange information, e.g. via molecular fields. Without reciprocal information exchange, a true collective state, as an emergent property of the constituent dynamical units, is not possible.

6.5 Synchronization Phenomena in Epidemics

There are illnesses, like measles, that come and go recurrently. Looking at the local statistics of measle outbreaks, see Fig. 6.10, one can observe that outbreaks occur in quite regular time intervals within a given city. Interestingly though, these outbreaks can be either in phase (synchronized) or out of phase between different cities.

The oscillations in the number of infected persons are definitely not harmonic, they share many characteristics with relaxation oscillations, which typically have silent and active phases, compare Sect. 6.3.

The SIRS Model A standard approach to model the dynamics of infectious diseases is the SIRS model. At any time an individual can belong to one of the three classes:

S	S	S	I	R	R	R	S	S	State
1	2	3	4	5	6	7	8	9	Time

Fig. 6.11 Example of the course of an individual infection within the SIRS model with an infection time $\tau_I = 1$ and a recovery time $\tau_R = 3$. The number of individuals recovering at time t is just the sum of infected individuals at times $t-1$, $t-2$ and $t-3$, compare Eq. (6.26)

    S : susceptible,

    I : infected,

    R : recovered.

The dynamics is governed by the following rules:

(a) Susceptibles pass to the infected state, with a certain probability, after coming into contact with one infected individual.
(b) Infected individuals pass to the recovered state after a fixed period of time τ_I.
(c) Recovered individuals return to the susceptible state after a recovery time τ_R, when immunity is lost, and the S→I→R→ S cycle is complete.

When $\tau_I \to \infty$ (lifelong immunity) the model reduces to the SIR-model.

The Discrete Time Model We consider a discrete time SIRS model with $t = 1, 2, 3, \ldots$ and $\tau_I = 1$: The infected phase is normally short and we can use it to set the unit of time. The recovery time τ_R is then a multiple of $\tau_I = 1$.
We define with

    x_t the fraction of infected individuals at time t,

    s_t the percentage of susceptible individuals at time t,

which obey

$$s_t = 1 - x_t - \sum_{k=1}^{\tau_R} x_{t-k} = 1 - \sum_{k=0}^{\tau_R} x_{t-k} , \tag{6.26}$$

as the fraction of susceptible individuals is just 1 minus the number of infected individuals minus the number of individuals in the recovery state, compare Fig. 6.11.

The Recursion Relation We denote with a the rate of transmitting an infection when there is a contact between an infected individual and a susceptible individual:

$$x_{t+1} = ax_t s_t = ax_t \left(1 - \sum_{k=0}^{\tau_R} x_{t-k} \right) . \tag{6.27}$$

Relation to the Logistic Map For $\tau_R = 0$ the discrete time SIRS model (6.27) reduces to the logistic map

$$x_{t+1} = ax_t (1 - x_t) ,$$

which we studied in Chap. 2. For $a < 1$ it has only the trivial fixpoint $x_t \equiv 0$, the illness dies out. The non-trivial steady state is
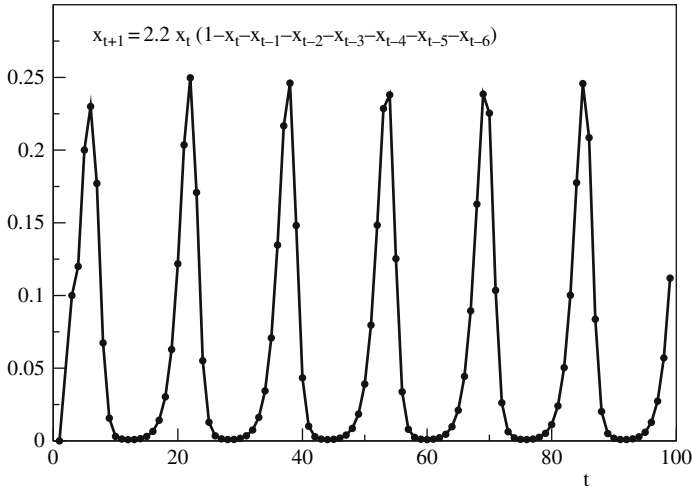
Fig. 6.12 Example of a solution to the SIRS model, Eq. (6.27), for $\tau_R = 5$. The number of infected individuals might drop to very low values during the silent phase in between two outbreaks as most of the population is first infected and then immunized during an outbreak

$$x^{(1)} = 1 - \frac{1}{a}, \qquad \text{for} \quad 1 < a < 3 .$$

For $a = 3$ there is a Hopf bifurcation and for $a > 3$ the system oscillates with a period of 2. Equation 6.27 has a similar behavior, but the resulting oscillations may depend on the initial condition and for $\tau_R \gg \tau_I \equiv 1$ show features characteristic of relaxation oscillators, see Fig. 6.12.

Two Coupled Epidemic Centers We consider now two epidemic centers with variables

$$s_t^{(1,2)}, \qquad x_t^{(1,2)} ,$$

denoting the fraction of susceptible/infected individuals in the respective cities. Different dynamical couplings are conceivable, via exchange or visits of susceptible or infected individuals. We consider with

$$x_{t+1}^{(1)} = a\left(x_t^{(1)} + e x_t^{(2)}\right) s_t^{(1)}, \qquad x_{t+1}^{(2)} = a\left(x_t^{(2)} + e x_t^{(1)}\right) s_t^{(2)} \qquad (6.28)$$

the visit of a small fraction e of infected individuals to the other center. Equation (6.28) determines the time evolution of the epidemics together with Eq. (6.26), generalized to both centers.

In Phase Versus Out of Phase Synchronization We have seen in Sect. 6.2 that a strong coupling of relaxation oscillators during their active phase leads in a quite natural way to a fast synchronization. Here the active phase corresponds to an outbreak of the illness and Eq. (6.28) indeed implements a coupling equivalent to the fast threshold modulation discussed in Sect. 6.3, since the coupling is proportional to the fraction of infected individuals.
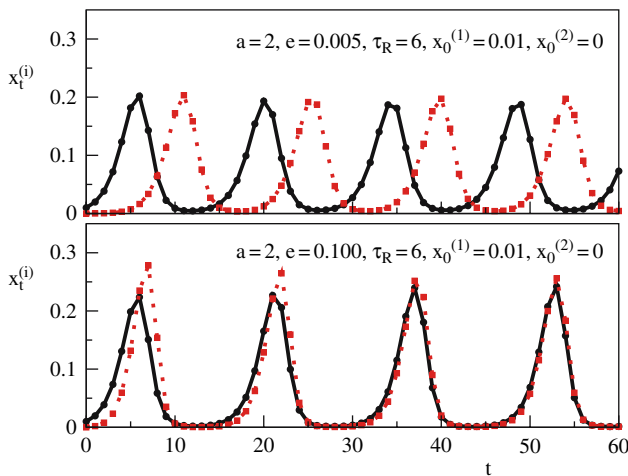
Fig. 6.13 Time evolution of the fraction of infected individuals $x^{(1)}(t)$ and $x^{(2)}(t)$ within the SIRS model, Eq. (6.28), for two epidemic centers $i = 1, 2$ with recovery times $\tau_R = 6$ and infection rates $a = 2$, see Eq. (6.27). For a very weak coupling $e = 0.005$ (*top*) the outbreaks occur out of phase, for a moderate coupling $e = 0.1$ (*bottom*) in phase

In Fig. 6.13 we present the results from a numerical simulation of the coupled model, illustrating the typical behavior. We see that the outbreaks of epidemics in the SIRS model indeed occur in phase for a moderate to large coupling constant e. For very small coupling e between the two centers of epidemics on the other hand, the synchronization becomes antiphase, as is sometimes observed in reality, see Fig. 6.10.

Time Scale Separation The reason for the occurrence of out of phase synchronization is the emergence of two separate time scales in the limit $t_R \gg 1$ and $e \ll 1$. A small seed $\sim eax^{(1)}s^{(2)}$ of infections in the second city needs substantial time to induce a full-scale outbreak, even via exponential growth, when e is too small. But in order to remain in phase with the current outbreak in the first city the outbreak occurring in the second city may not lag too far behind. When the dynamics is symmetric under exchange $1 \leftrightarrow 2$ the system then settles in antiphase cycles.

Exercises

THE DRIVEN HARMONIC OSCILLATOR
   Solve the driven harmonic oscillator, Eq. (6.1), for all times t and compare it
   with the long time solution $t \rightarrow \infty$, Eqs. (6.3) and (6.4).
THE TERMAN–WANG OSCILLATOR

Discuss the stability of the fixpoints of the Terman–Wang oscillator, Eq. (6.21). Linearize the differential equations around the fixpoint solution and consider the limit $\beta \to 0$.

THE SIRS MODEL – ANALYTICAL

Find the fixpoints $x_t \equiv x^*$ of the SIRS model, Eq. (6.27), for all τ_R, as a function of a and study their stability for $\tau_R = 0, 1$.

THE SIRS MODEL – NUMERICAL

Study the SIRS model, Eq. (6.27), numerically for various parameters a and $\tau_R = 0, 1, 2, 3$. Try to reproduce Figs. 6.12 and 6.13.

Further Reading

A nice review of the Kuramoto model, together with historical annotations has been published by Strogatz (2000). Some of the material discussed in this chapter requires a certain background in theoretical neuroscience, see e.g. Dayan and Abbott (2001).

We recommend that the interested reader takes a look at some of the original research literature, such as the exact solution of the Kuramoto (1984) model, the Terman and Wang (1995) relaxation oscillators, the concept of fast threshold synchronization (Somers and Kopell, 1993), the temporal correlation hypothesis for cortical networks (von der Malsburg and Schneider, 1886), and its experimental studies (Gray et al., 1989), the LEGION network (Terman and Wang, 1995), the physics of synchronized clapping (Néda et al., 2000a,b) and synchronization phenomena within the SIRS model of epidemics (He and Stone, 2003).

DAYAN, P., ABBOTT, L.F. 2001 *Theoretical Neuroscience: Computational and Mathematical Modeling of Neural Systems.* MIT Press, Cambridge.

GRAY, C.M., KÖNIG, P., ENGEL, A.K., SINGER, W. 1989 Oscillatory responses in cat visual cortex exhibit incolumnar synchronization which reflects global stimulus properties. *Nature* **338**, 334–337.

HE, D., STONE, L. 2003 Spatio-temporal synchronization of recurrent epidemics. *Proceedings of the Royal Society London B* **270**, 1519–1526.

KURAMOTO, Y. 1984 *Chemical Oscillations, Waves and Turbulence.* Springer, Berlin.

NÉDA, Z., RAVASZ, E., VICSEK, T., BRECHET, Y., BARABÁSI, A.L. 2000a Physics of the rhythmic applause. *Physical Review E* **61**, 6987–6992.

NÉDA, Z., RAVASZ, E., VICSEK, T., BRECHET, Y., BARABÁSI, A.L. 2000b The sound of many hands clapping. *Nature* **403**, 849–850.

SOMERS, D., KOPELL, N. 1993 Rapid synchronization through fast threshold modulation. *Biological Cybernetics* **68**, 398–407.

STROGATZ, S.H. 2000 From Kuramoto to Crawford: exploring the onset of synchronization in populations of coupled oscillators. *Physica D* **143**, 1–20.

STROGATZ, S.H. 2001 Exploring complex networks. *Nature* **410**, 268–276.

TERMAN, D., WANG, D.L. 1995 Global competition and local cooperation in a network of neural oscillators. *Physica D* **81**, 148–176.

VON DER MALSBURG, C., SCHNEIDER, W. 1886 A neural cocktail-party processor. *Biological Cybernetics* **54**, 29–40.

WANG, D.L. 1999 *Relaxation Oscillators and Networks.* In Webster, J.G. (ed.) Encyclopedia of electrical and electronic engineers, pp. 396–405, Wiley, New York.

Chapter 7
Elements of Cognitive Systems Theory

The brain is without doubt the most complex adaptive system known to humanity, arguably also a complex system about which we know very little.

Throughout this book we have considered and developed general guiding principles for the understanding of complex networks and their dynamical properties; principles and concepts transcending the details of specific layouts realized in real-world complex systems. We follow the same approach here, considering the brain as just one example of what is called a cognitive system, a specific instance of what one denotes, cum grano salis, a living dynamical system.

In the first part we will treat general layout considerations concerning dynamical organizational principles, an example being the role of diffuse controlling and homeostasis for stable long-term cognitive information processing. Special emphasis will be given to the motivational problem – how the cognitive system decides what to do – in terms of survival parameters of the living dynamical system and the so-called emotional diffusive control.

In the second part we will discuss two specific generalized neural networks implementing various aspects of these general principles: a dense and homogeneous associative network (dHAN) for environmental data representation and associative thought processes, and the simple recurrent network (SRN) for concept extraction from universal prediction tasks.

7.1 Introduction

We start with a few basic considerations concerning the general setting.

What is a Cognitive System? A cognitive system may be either biological, like the brain, or artificial. It is, in both instances, a dynamical system embedded into an environment, with which it mutually interacts.

> *Cognitive Systems. A cognitive system is a continuously active complex adaptive system autonomously exploring and reacting to the environment with the capability to "survive".*
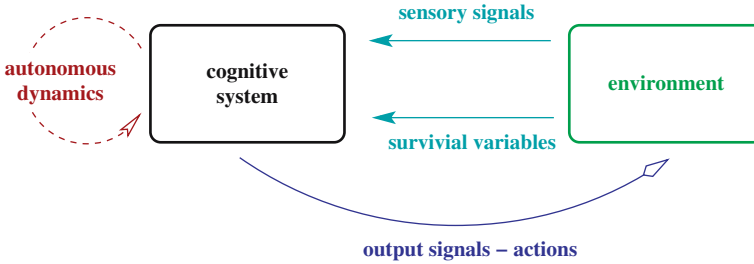
Fig. 7.1 A cognitive system is placed in an environment (compare Sect. 7.2.4) from which it receives two kinds of signals. The status of the survival parameters, which it needs to regulate (see Sect. 7.3.2), and the standard sensory input. The cognitive system generates output signals via its autonomous dynamics, which act back onto the outside world, viz the environment

For a cognitive system, the only information source about the outside is given, to be precise, by its sensory data input stream, viz the changes in a subset of variables triggered by biophysical processes in the sensory organs or sensory units. The cognitive system does therefore not react directly to environmental events but to the resulting changes in the sensory data input stream, compare Fig. 7.1.

Living Dynamical Systems A cognitive system is an instance of a living dynamical system, being dependent on a functioning physical support unit, the body. The cognitive system is terminated when its support unit ceases to work properly.

> *Living Dynamical Systems.   A dynamical system is said to "live" in an abstract sense if it needs to keep the ongoing dynamical activity in certain parameter regimes.*

As an example we consider a dynamical variable $y(t) \geq 0$, part of the cognitive system, corresponding to the current amount of pain or hunger. This variable could be directly set by the physical support unit, i.e. the body, of the cognitive system, telling the dynamical system about the status of its support unit.

The cognitive system can influence the value of $y(t)$ indirectly via its motor output signals, activating its actuators, e.g. the limbs. These actions will, in general, trigger changes in the environment, like the uptake of food, which in turn will influence the values of the respective survival variables. One could then define the termination of the cognitive system when $y(t)$ surpasses a certain threshold y_c. The system "dies" when $y(t) > y_c$. These issues will be treated in depth in Sects. 7.2.4 and 7.3.2.

Cognition Versus Intelligence A cognitive system is not necessarily intelligent, but it might be in principle. Cognitive system theory presumes that artificial intelligence can be achieved only once autonomous cognitive systems have been developed. This stance is somewhat in contrast with the usual paradigm of artificial intelligence (AI), which follows an all-in-one-step approach to intelligent systems.

Universality Simple biological cognitive systems are dominated by cognitive capabilities and algorithms hard-wired by gene expression. These features range

from simple stimulus–response reactions to sophisticated internal models for limb dynamics.

A priori information is clearly very useful for task solving in particular and for cognitive systems in general. A main research area in AI is therefore the development of efficient algorithms making maximal use of a priori information about the environment. A soccer-playing robot normally does not acquire the ball dynamics from individual experience. Newton's law is given to the robot by its programmer and hard-wired within its code lines.

Cognitive system theory examines, on the other hand, universal principles and algorithms necessary for the realization of an autonomous cognitive system. This chapter will be devoted to the discussion and possible implementations of such universal principles.

A cognitive system should therefore be able to operate in a wide range of environmental conditions, performing tasks of different kinds. A rudimentary cognitive system does not need to be efficient. Performance boosting specialized algorithms can always be added afterwards.

A Multitude of Possible Formulations Fully functional autonomous cognitive systems may possibly have very different conceptual foundations. The number of consistent approaches to cognitive system theory is not known, it may be substantial. This is a key difference to other areas of research treated in this book, like graph theory, and is somewhat akin to ecology, as there are a multitude of fully functional ecological systems.

It is, in any case, a central challenge to scientific research to formulate and to examine self-consistent building principles for rudimentary but autonomous cognitive systems. The venue treated in this chapter represents a specific approach towards the formulation and the understanding of the basic requirements needed for the construction of a cognitive system.

Biologically Inspired Cognitive Systems Cognitive system theory has two long-term targets: To understand the functioning of the human brain and to develop an autonomous cognitive system. The realization of both goals is still far away, but they may be combined to a certain degree. The overall theory is however at an early stage and it is presently unclear to which extent the first implemented artificial cognitive systems will resemble our own cognitive organ, the brain.

7.2 Foundations of Cognitive Systems Theory

7.2.1 Basic Requirements for the Dynamics

Homeostatic Principles Several considerations suggest that self-regulation via adaptive means, viz homeostatic principles, are widespread in the domain of life in general and for biological cognitive systems in particular.

– There are concrete instances for neural algorithms, like the formation of topological neural maps, based on general, self-regulating feedback. An example is the topological map connecting the retina to the primary optical cortex.
– The number of genes responsible for the development of the brain is relatively low, perhaps a few thousands. The growth of about 100 billion neurons and of around 10^{15} synapses can only result in a functioning cognitive system if very general self-regulating and self-guiding algorithms are used.
– The strength and the number of neural pathways interconnecting different regions of the brain or connecting sensory organs to the brain may vary substantially during development or during lifetime, e.g. as a consequence of injuries. This implies, quite generally, that the sensibility of neurons to the average strength of incoming stimuli must be adaptive.

It is tempting to speak in this context of "target-oriented self-organization", since mere "blind", viz basic self-organizational processes might be insufficient tools for the successful self-regulated development of the brain in a first step and of the neural circuits in a second step.

Self-Sustained Dynamics Simple biological neural networks, e.g. the ones in most worms, just perform stimulus–response tasks. Highly developed mammal brains, on the other side, are not directly driven by external stimuli. Sensory information influences the ongoing, self-sustained neuronal dynamics, but the outcome cannot be predicted from the outside viewpoint.

Indeed, the human brain is on the whole occupied with itself and continuously active even in the sustained absence of sensory stimuli. A central theme of cognitive systems theory is therefore to formulate, test and implement the principles that govern the autonomous dynamics of a cognitive system.

Transient State Versus Fluctuation Dynamics There is a plurality of approaches for the characterization of the time development of a dynamical system. A key questions in this context regards the repeated occurrence of well defined dynamical states, that is, of states allowing for a well defined characterization of the current dynamical state of the cognitive system, like the ones illustrated in Fig. 7.2.

Transient States. *A transient state of a dynamical system corresponds to a quasistationary plateau in the value of the variables.*

Transient state dynamics can be defined mathematically in a rigorous way. It is present in a dynamical system if the governing equations of the system contain parameters that regulate the length of the transient state, viz whenever it is possible, by tuning theses parameters, to prolong the length of the plateaus arbitrarily.

In the case of the human brain, several experiments indicate the occurrence of spontaneously activated transient neural activity patterns in the cortex.[1] It is therefore natural to assume that both fluctuating states and those corresponding to

---

[1] See, e.g., Abeles et al. (1995) and Kenet et al. (2003).
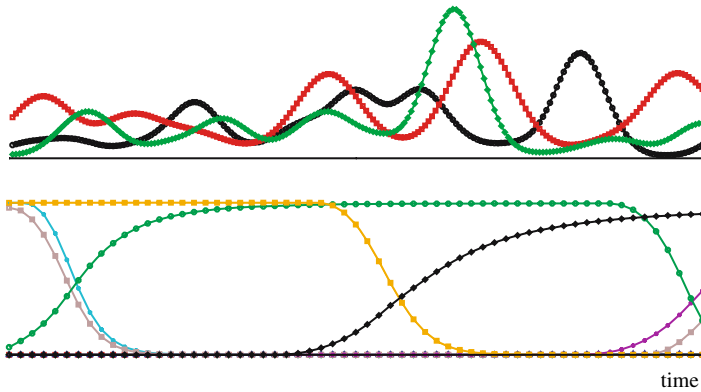
Fig. 7.2 Fluctuating *(top)* and transient state *(bottom)* dynamics

transient activity are characteristic for biological inspired cognitive systems. In this chapter we will especially emphasize the transient state dynamics and discuss the functional roles of the transient attractors generated by this kind of dynamics.

Competing Dynamics The brain is made up of many distinct regions that are highly interconnected. The resulting dynamics is thought to be partly competing.

> *Competing Dynamics. A dynamical system made up of a collection of interacting centers is said to show competing dynamics if active centers try to suppress the activity level of the vast majority of competing centers.*

In neural network terminology, competing dynamics is also called a *winners-take-all* setup. In the extreme case, when only a single neuron is active at any given time, one speaks of a *winner-take-all* situation.

> *The Winning Coalition. In a winners-take-all network the winners are normally formed by an ensemble of mutually supportive centers, which one also denotes the "winning coalition".*

A winning coalition needs to be stable for a certain minimal period of time, in order to be well characterized. Competing dynamics therefore frequently results in transient state dynamics.

Competing dynamics in terms of dynamically forming winning coalitions is a possible principle for achieving the target-oriented self-organization needed for a self-regulating autonomously dynamical systems. We will treat this subject in detail in Sect. 7.4.

States-of-the-Mind and the Global Workspace A highly developed cognitive system is capable of generating autonomously a very large number of different transient states, which represent the "states-of-the-mind". This feature plays an important role in present-day investigations of the neural correlates of consciousness,

which we shall now briefly mention for completeness. We will not discuss the relation of cognition and consciousness any further in this chapter.

Edelman and Tononi[2] argued that these states-of-the-mind can be characterized by "critical reentrant events", constituting transient conscious states in the human brain. Several authors have proposed the notion of a "global workspace". This workspace would be the collection of neural ensembles contributing to global brain dynamics. It could serve, among other things, as an exchange platform for conscious experience and working memory[3]. The constituting neural ensembles of the global workspace have also been dubbed "essential nodes", i.e. ensembles of neurons responsible for the explicit representation of particular aspects of visual scenes or other sensory information[4].

Spiking Versus Non-Spiking Dynamics Neurons emit an axon potential called a spike, which lasts about a millisecond. They then need to recover for about 10 ms, the refractory period. Is it then important for a biologically inspired cognitive system to use spiking dynamics? We note here in passing that spiking dynamics can be generated by interacting relaxation oscillators, as discussed in Chap. 6.

The alternative would be to use a network of local computational units having a continuously varying activity, somewhat akin to the average spiking intensity of neural ensembles. There are two important considerations in this context:

– At present, it does not seem plausible that spiking dynamics is a condition *sine qua non* for a cognitive system. It might be suitable for a biological system, but not a fundamental prerequisite.
– Typical spiking frequencies are in the range of 5–50 spikes per second. A typical cortical neuron receives input from about ten thousand other neurons, viz 50–500 spikes per millisecond. The input signal for typical neurons is therefore quasicontinuous.

The exact timing of neural spikes is clearly important in many areas of the brain, e.g. for the processing of acoustic data. Individual incoming spikes are also of relevance, when they push the postsynaptic neuron above the firing threshold. However, the above considerations indicate a reduced importance of precise spike timing for the average all-purpose neuron.

Continuous Versus Discrete Time Dynamics Neural networks can be modeled either by using a discrete time formulation $t = 1, 2, 3, \ldots$ or by employing continuous time $t \in [0, \infty]$.

Synchronous and Asynchronous Updating. A dynamical system with discrete time is updated synchronously (asynchronously) when all variables are evaluated simultaneously (one after another).

---

[2] See Edelman and Tononi (2000).

[3] See Dehaene and Naccache (2003), and Baars and Franklin (2003).

[4] See Crick and Koch (2003).

For a continuous time formulation there is no difference between synchronous and asynchronous updating however, it matters for a dynamical system with discrete time, as we discussed in Chap. 3.

The dynamics of a cognitive system needs to be stable. This condition requires that the overall dynamical feature cannot depend, e.g., on the number of components or on the local numerical updating procedure. Continuous time is therefore the only viable option for real-world cognitive systems.

Continuous Dynamics and Online Learning The above considerations indicate that a biologically inspired cognitive system should be continuously active.

> *Online Learning.* When a neural network type system learns during its normal mode of operation one speaks of "online learning". The case of "offline learning" is given when learning and performance are separated in time.

Learning is a key aspect of cognition and online learning is the only possible learning paradigm for an autonomous cognitive system. Consequently there can be no distinct training and performance modes. We will come back to this issue in Sect. 7.4.3.

7.2.2 Cognitive Information Processing Versus Diffusive Control

A cognitive system is an (exceedingly) complex adaptive system per excellence. As such it needs to be adaptive on several levels.

Biological considerations suggest to use a network of local computational units with primary variables $x_i = (x_i^0, x_i^1, \ldots)$. Typically x_i^0 would correspond to the average firing rate and the other x_i^α ($\alpha = 1, \ldots$) would characterize different dynamical properties of the ensemble of neurons represented by the local computational unit as well as the (incoming) synaptic weights.

The cognitive system, as a dynamical system, is governed by a set of differential equations, such as

$$\dot{x}_i = f_i(x_1, \ldots, x_N), \qquad i = 1, \ldots, N . \qquad (7.1)$$

Primary and Secondary Variables The functions f_i governing the time evolution equation (7.1) of the primary variables $\{x_i\}$ generally depend on a collection of parameters $\{\gamma_i\}$, such as learning rates, firing thresholds, etc.:

$$f_i(x_1, \ldots, x_N) = f_i(\gamma_1, \gamma_2, \ldots | x_1, x_2, \ldots) . \qquad (7.2)$$

The time evolution of the system is fully determined by Eq. (7.1) whenever the parameters γ_j are unmutable, that is, genetically predetermined. Normally , however, the cognitive system needs to adjust a fraction of these parameters with time, viz

$$\dot{\gamma}_i = g_i(\gamma_1, \gamma_2, \ldots | x_1, x_2, \ldots) , \qquad (7.3)$$

In principle one could merge $\{x_j\}$ and $\{\gamma_i\}$ into one large set of dynamical variables $\{y_l\} = \{\gamma_i | x_j\}$. It is, however, meaningful to keep them separated whenever their respective time evolution differs qualitatively and quantitatively.

> *Fast and Slow Variables. When the average rate changes of two variables $x = x(t)$ and $y = y(t)$ are typically very different in magnitude, $|\dot{x}| \gg |\dot{y}|$, then one calls $x(t)$ the fast variable and $y(t)$ the slow variable.*

The parameters $\{\gamma_j\}$ are, per definition, slow variables. One can then also call them "secondary variables" as they follow the long-term average of the primary variables $\{x_i\}$.

Adaptive Parameters A cognitive system needs to self-adapt over a wide range of structural organizations, as discussed in Sect. 7.2.1. Many parameters relevant for the sensibility to presynaptic activities, for short-term and long-term learning, to give a few examples, need therefore to be adaptive, viz time-dependent.

> *Metalearning. The time evolution of the slow variables, the parameters, is called "metalearning" in the context of cognitive systems theory.*

With (normal) learning we denote the changes in the synaptic strength, i.e. the connections between distinct local computational units. Learning (of memories) therefore involves part of the primary variables.

The other primary variables characterize the current state of a local computational unit, such as the current average firing rate. Their time evolution corresponds to the actual *cognitive information processing*, see Fig. 7.3.

Diffusive Control Neuromodulators, like dopamine, serotonin, noradrenaline and acetylcholine, serve in the brain as messengers for the transmission of general information about the internal status of the brain, and for overall system state control. A release of a neuromodulator by the appropriate specialized neurons does not influence individual target neurons, but extended cortical areas.

> *Diffusive Control. A signal by a given part of a dynamical system is called a "diffusive control signal" if it tunes the secondary variables in an extended region of the system.*

A diffusive control signal does not influence the status of individual computational units directly, i.e. their primary variables. Diffusive control has a wide range of tasks. It plays an important role in metalearning and reinforcement learning.

As an example of the utility of diffusive control signals we mention the "learning from mistakes" approach, see Sect. 7.2.4. Within this paradigm synaptic plasticities are degraded after an unfavorable action has been performed. For this purpose a diffusive control signal is generated by a mistake with the effect that all previously active synapses are weakened.

$$\boxed{\begin{array}{c} \text{primary} \quad \text{secondary} \\[4pt] \boxed{\quad x \quad w \quad} \quad \boxed{\quad \gamma \quad \gamma' \quad} \\[8pt] \boxed{\begin{array}{ll} \dot{x} : & \text{cognitive information processing} \\ \dot{w} : & \text{learning} \\ \dot{\gamma} : & \text{metalearning} \\ \dot{\gamma}' = 0 & \end{array}} \end{array}}$$
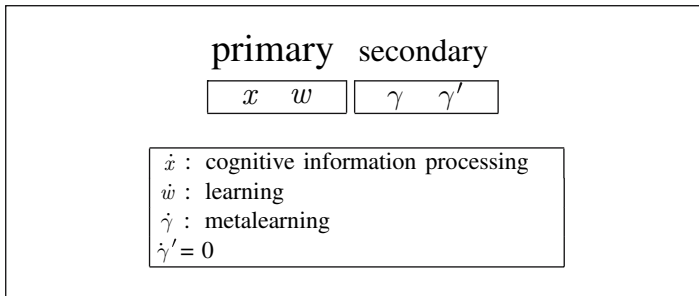
Fig. 7.3 General classification scheme for the variables and the parameters of a cognitive system. The variables can be categorized as primary variables and as secondary variables (parameters). The primary variables can be subdivided into the variables characterizing the current state of the local computational units x and into generalized synaptic weights w. The "parameters" γ are slow variables adjusted for homeostatic regulation. The true unmutable (genetically predetermined) parameters are γ'

7.2.3 Basic Layout Principles

There is, at present, no fully developed theory for real-world cognitive systems. Here we discuss some recent proposals for a possible self-consistent set of requirements for a biologically inspired cognitive system.

(A)   Absence of A Priori Knowledge About the Environment
      Preprogrammed information about the outside world is normally a necessary ingredient for the performance of robotic systems at least within the artificial intelligence paradigm. However, a rudimentary system needs to perform dominantly on the base of universal principles.

(B)   Locality of Information Processing
      Biologically inspired models need to be scalable and adaptive to structural modifications. This rules out steps in information processing needing non-local information, as is the case for the standard back-propagation algorithm, viz the minimization of a global error function.

(C)   Modular Architecture
      Biological observations motivate a modular approach, with every individual module being structurally homogeneous. An autonomous cognitive system needs modules for various cognitive tasks and diffusive control. Well defined interface specifications are then needed for controlled intermodular information exchange. Homeostatic principles are necessary for the determination of the intermodule connections, in order to allow for scalability and adaptability to structural modifications.

(D)   Metalearning via Diffusive Control
      Metalearning, i.e. the tuning of control parameters for learning and sensitivity to internal and external signals, occurs exclusively via diffusive control.

The control signal is generated by diffusive control units, which analyze the overall status of the network and become active when certain conditions are achieved.

(E)   Working Point Optimization

The length of the stability interval of the transient states relative to the length of the transition time from one state-of-mind to the next (the working point of the system) needs to be self-regulated by homeostatic principles.

Learning influences the dynamical behavior of the cognitive system in general and the time scales characterizing the transient state dynamics in particular. Learning rules therefore need to be formulated in a way that autonomous working point optimization is guaranteed.

The Central Challenge The discovery and understanding of universal principles, especially for cognitive information processing, postulated in (A)–(F) is the key to ultimately understanding the brain or to building an artificial cognitive system. In Sect. 7.5 we will discuss an example for a universal principle, namely environmental model building via universal prediction tasks.

The Minimal Set of Genetic Knowledge No cognitive system can be universal in a strict sense. Animals, to give an example, do not need to learn that hunger and pain are negative reward signals. This information is genetically preprogrammed. Other experiences are not genetically fixed, e.g. some humans like the taste of coffee, others do not.

No cognitive system could be functioning with strictly zero a priori knowledge, it would have no "purpose". A minimal set of goals is necessary, as we will discuss further in depth in Sect. 7.3. A minimal goal of fundamental significance is to "survive" in the sense that certain internal variables need to be kept within certain parameter ranges. A biological cognitive system needs to keep the pain and hunger signals that it receives from its own body at low average levels, otherwise its body would die. An artificial system could be given corresponding tasks.

Consistency of Local Information Processing with Diffusive Control We note that the locality principle (B) for cognitive information processing is consistent with non-local diffusive control (D). Diffusive control regulates the overall status of the system, like attention focusing and sensibilities, but it does not influence the actual information processing directly.

Logical Reasoning Versus Cognitive Information Processing Very intensive research on logical reasoning theories is carried out in the context of AI. From (A) it follows that logical manipulation of concepts is, however, not suitable as a basic framework for universal cognitive systems. Abstract concepts cannot be formed without substantial knowledge about the environment, but this knowledge is acquired by an autonomous cognitive system only step-by-step during its "lifetime".

7.2.4 Learning and Memory Representations

With "learning" one denotes quite generally all modifications that influence the dynamical state and the behavior. One distinguishes the learning of memories and actions.

> *Memories.   By memory one denotes the storage of a pattern found within the incoming stream of sensory data, which presumably encodes information about the environment.*

The storage of information about its own actions, i.e. about the output signals of a cognitive system is also covered by this definition. Animals do not remember the output signal of the motor cortex directly, but rather the optical or acoustical response of the environment as well as the feedback of its body via appropriate sensory nerves embedded in the muscles.

The Outside World – The Cognitive System as an Abstract Identity A rather philosophical question is whether there is, from the perspective of a cognitive system, a true outside world. The alternative would be to postulate that only the internal representations of the outside world, i.e. the environment, are known to the cognitive system. For all practical purposes it is useful to postulate an environment existing independently of the cognitive system.

It is, however, important to realize that the cognitive system per se is an abstract identity, i.e. the dynamical activity patterns. The physical support, i.e. computer chips and brain tissue, are not part of the cybernetic or of the human cognitive system, respectively. We, as cognitive systems, are abstract identities and the physical brain tissue therefore also belongs to our environment!

One may differentiate this statement to a certain extent, as direct manipulations of our neurons may change the brain dynamics directly. This may possibly occur without our external and internal sensory organs noticing the manipulatory process. In this respect the brain tissue is distinct from the rest of the environment, since changes in the rest of the environment influence the brain dynamics exclusively via internal, such as a pain signal, or external, e.g. an auditory signal, sensory inputs.

For practical purposes, when designing an artificial environment for a cognitive system, the distinction between a directly observable part of the outside world and the non-observable part becomes important. Only the observable part generates, per definition, sensorial stimuli, but one needs to keep in mind that the actions of the cognitive system may also influence the non-observable environment.

Classification of Learning Procedures It is customary to broadly classify possible learning procedures. We discuss briefly the most important cases of learning algorithms; for details we refer to the literature.

– Unsupervised Learning: The system learns completely by itself, without any external teacher.

– Supervised Learning: Synaptic changes are made "by hand", by the external teacher and not determined autonomously. Systems with supervised learning in most cases have distinguished periods for training and performance (recall).
– Reinforcement Learning: Any cognitive system faces the fundamental dilemma of action selection, namely that the final success or failure of a series of actions may often be evaluated only at the end. When playing a board game one knows only at the end whether one has won or lost.

  Reinforcement learning denotes strategies that allow one to employ the positive or negative reward signal obtained at the end of a series of actions to either rate the actions taken or to reinforce the problem solution strategy.
– Learning from Mistakes: Random action selection will normally result in mistakes and not in success. In normal life learning from mistakes is therefore by far more important than learning from positive feedback.
– Hebbian Learning: Hebbian learning denotes a specific instance of a linear synaptic modification procedure in neural networks.

  – Spiking Neurons: For spiking neurons Hebbian learning results in a long-term potentiation (LTP) of the synaptic strength when the presynaptic neuron spikes shortly before the postsynaptic neuron (causality principle). The reversed spiking timing results in long-term depression (LTD).
  – Neurons with Continuous Activity: The synaptic strength is increased when both postsynaptic and presynaptic neurons are active. Normally one assumes the synaptic plasticity to be directly proportional to the product of postsynaptic and presynaptic activity levels.

Learning Within an Autonomous Cognitive System Learning within an autonomous cognitive system with self-induced dynamics is, strictly speaking, unsupervised. Direct synaptic modifications by an external teacher are clearly not admissible. But also reinforcement learning is, at its basis, unsupervised, as the system has to select autonomously what it accepts as a reward signal.

The different forms of learning are, however, significant when taking the internal subdivision of the cognitive system into various modules into account. In this case a diffusive control unit can provide the reward signal for a cognitive information processing module. Also internally supervised learning is conceivable.

Runaway Synaptic Growth Learning rules in a continuously active dynamical system need careful considerations. A learning rule might foresee fixed boundaries, viz limitations, for the variables involved in learning processes and for the parameters modified during metalearning. In this case when the parameter involved reaches the limit, learning might potentially lead to saturation, which is suboptimal for information storage and processing. With no limits encoded the continuous learning process might lead to unlimited synaptic weight growth.

Runaway Learning. When a specific learning rule acts over time continuously with the same sign it might lead to an unlimited growth of the affected variables.

Any instance of runaway growth needs to be avoided, as it will inevitably lead the system out of suitable parameter ranges. This is an example of the general problem of working point optimization, see Sect. 7.2.3.

A possible solution, for the case of Hebbian learning, is to adapt the sum of active incoming synaptic strengths towards a constant value. This procedure leads to both LTP and LTD; an explicit rule for LTD is then not necessary.

Biological Memories Higher mammalian brains are capable of storing information in several distinct ways. Both experimental psychology and neuroscience are investigating the different storage capabilities and suitable nomenclatures have been developed. Four types of biophysical different storing mechanisms have been identified so far:

(i)   Long-Term Memory: The brain is made up by a network of neurons that are interconnected via synapses. All long-term information is therefore encoded, directly or indirectly, in the respective synaptic strengths.
(ii) Short-Term Memory: The short-term memory corresponds to transient modifications of the synaptic strength. These modifications decay after a characteristic time, which may be of the order of minutes.
(iii) Working Memory: The working memory corresponds to firing states of individual neurons or neuron ensembles that are kept active for a certain period, up to several minutes, even after the initial stimulus has subsided.
(iv) Episodic Memory: The episodic memory is mediated by the hippocampus, a separate neural structure. The core of the hippocampus, called CA3, contains only about $3 \cdot 10^5$ neurons (for humans). All daily episodic experiences, from the visit to the movie theater to the daily quarrel with the spouse, are kept active by the hippocampus. A popular theory of sleep assumes that fixation of the episodic memory in the cortex occurs during dream phases when sleeping.

In Sect. 7.4 we will treat a generalized neural network layout implementing both short-term as well as long-term synaptic plasticities, discussing the role of their interplay for long-term memory formation.

Learning and Memory Representations The representation of the environment, via suitable filtering of prominent patterns from the sensory input data stream, is a basic need for any cognitive system. We discuss a few important considerations.

– Storage Capacity: Large quantities of new information needs to be stored without erasing essential memories.

   Sparse/Distributed Coding. A network of local computational units in which only a few units are active at any given time is said to use "sparse coding". If on the average half of the neurons are active, one speaks of "distributed coding".

Neural networks with sparse coding have a substantially higher storage capacity than neural networks with an average activity of 1/2. The latter have a storage capacity scaling only linearly with the number of nodes. A typical value for the storage capacity is in this case 14%, with respect to the system size.[5]

In the brain only a few percent of all neurons are active at any given time. Whether this occurs in order to minimize energy consumption or to maximize the storage capacity is not known.

– Forgetting: No system can acquire and store new information forever. There are very different approaches to how to treat old information and memories.

> *Catastrophic Forgetting and Fading Memory. One speaks of "catastrophic forgetting" if all previously stored memories are erased whenever the system surpasses its storages capacity. The counterpoint is called "fading memory".*

Recurrent neural networks[6] with distributed coding forget catastrophically. Cognitive systems can only work with a fading memory, when old information is overwritten slowly.[7]

– The Embedding Problem: There is no isolated information. Any new information is only helpful if the system can embed it into the web of existing memories. This embedding, at its basic level, needs to be an automatic process, since any search algorithm would blast away any available computing power.

In Sect. 7.4 we will present a cognitive module for environmental data representation, which allows for a crude but automatic embedding.

– Generalization Capability: The encoding used for memories must allow the system to work with noisy and incomplete sensory data. This is a key requirement that one can regard as a special case of a broader generalization capability necessary for universal cognitive systems.

An efficient data storage format would allow the system to automatically find, without extensive computations, common characteristics of distinct input patterns. If all patterns corresponding to "car" contain elements corresponding to "tires" and "windows" the data representation should allow for an automatic prototyping of the kind "car = tires + windows".

Generalization capabilities and noise tolerance are intrinsically related. Many different neural network setups have this property, due to distributed and overlapping memory storage.

---

[5] This is a standard result for so called Hopfield neural networks, see e.g. Ballard (2000).

[6] A neural network is denoted "recurrent" when loops dominate the network topology.

[7] For a mathematically precise definition, a memory is termed fading when forgetting is scale-invariant, viz having a power law functional time dependence.

7.3 Motivation, Benchmarks and Target-Oriented Self-Organization

Key issues to be considered for the general layout of a working cognitive system are:

– Cognitive Information Processing: Cognitive information processing involves the dynamics of the primary variables, compare Sect. 7.2.3. We will discuss a possible modular layout in Sect. 7.3.1.
– Diffusive Control: Diffusive control is at the heart of homeostatic self-regulation for any cognitive system. The layout of the diffusive control depends to a certain extent on the specific implementation of the cognitive modules. We will therefore restrict ourselves here to general working principles.
– Decision Processes: Decision making in a cognitive system depends strongly on the specifics of its layout. A few general guidelines may be formulated for biologically inspired cognitive systems; we will discuss these in Sect. 7.3.2

7.3.1 Cognitive Tasks

Basic Cognitive Tasks A rudimentary cognitive system needs at least three types of cognitive modules. The individual modules comprise cognitive units for

(a) environmental data representation via unsupervised learning (compare Sect. 7.2.4),
(b) modules for model building of the environment via internal supervised learning, and
(c) action selection modules via learning by reinforcement or learning by error.

We mention here in passing that the assignment of these functionalities to specific brain areas is an open issue, one possibility being a delegation to the cortex, the cerebellum and to the basal ganglia, respectively.

Data Representation and Model Building In Sect. 7.4 we will treat in depth the problem of environmental data representation and automatic embedding. Let us note here that the problem of model building is not an all-in-one-step operation. Environmental data representation and basic generalization capabilities normally go hand in hand, but this feature falls far short of higher abstract concept generation.

An example of a basic generalization process is, to be a little more concrete, the generation of the notion of a "tree" derived by suitable averaging procedures out of many instances of individual trees occurring in the visual input data stream.

Time Series Analysis and Model Building The analysis of the time sequence of the incoming sensory data has a high biological survival value and is, in addition, at the basis of many cognitive capabilities. It allows for quite sophisticated model

building and for the generation of abstract concepts. In Sect.7.5 we will treat a neu-
ral network setup allowing for universal abstract concept generation, resulting from
the task to predict the next incoming sensory data; a task that is independent of the
nature of the sensory data and in this sense universal. When applied to a linguistic
incoming data stream, the network generates, with zero prior grammatical knowl-
edge, concepts like "verb", "noun" and so on.

7.3.2 Internal Benchmarks

Action selection occurs in an autonomous cognitive system via internal reinforce-
ment signals. The reward signal can be either genetically predetermined or internally
generated. To give a high-level example: We might find it positive to win a chess
game if playing against an opponent but we may also enjoy losing when playing
with our son or daughter. Our internal state is involved when selecting the reward
signal.

   We will discuss the problem of action selection by a cognitive system first on a
phenomenological level and then relate these concepts to the general layout in terms
of variables and diffusive control units.

Action Selection Two prerequisites are fundamental to any action taken by a cog-
nitive system:

(α) Objective: No decision can be taken without an objective of what to do. A
     goal can be very general or quite specific. "I am bored, I want to do something
     interesting" would result in a general explorative strategy, whereas "I am thirsty
     and I have a cup of water in my hand" will result in a very concrete action,
     namely drinking.
(β) Situation Evaluation: In order to decide between many possible actions the sys-
     tem needs to evaluate them. We define by "situation" the combined attributes
     characterizing the current internal status and the environmental conditions.

> Situation = (internal status) + (environmental conditions)
> Situation → value

   The situation "(thirsty) + (cup with water in my hands)" will normally be eval-
uated positively, the situation "(sleepy) + (cup with water in my hand)" on the
other hand not.

Evaluation and Diffusive Control The evaluation of a situation goes hand in hand
with feelings and emotions. Not only for most human does the evaluation belong to
the domain of diffusive control. The reason being that the diffusive control units, see
Sect. 7.2.2, are responsible for keeping an eye on the overall status of the cognitive
system; they need to evaluate the internal status constantly in relation to what is
happening in the outside world, viz in the sensory input.

Primary Benchmarks Any evaluation needs a benchmark: What is good and what is bad for oneself? For a rudimentary cognitive system the benchmarks and motivations are given by the fundamental need to survive: If certain parameter values, like hunger and pain signals arriving from the body, or more specific signals about protein support levels or body temperature, are in the "green zone", a situation, or a series of events leading to the present situation, is deemed good. Appropriate corresponding "survival variables" need to be defined for an artificial cognitive system.

> *Survival Parameters. We denote the parameters regulating the condition of survival for a living dynamical system as survival parameters.*

The survival parameters are part of the sensory input, compare Fig. 7.1, as they convene information about the status of the body, viz the physical support complex for the cognitive system. The survival parameters affect the status of selected diffusive control units; generally they do not interact directly with the cognitive information processing.

Rudimentary Cognitive Systems A cognitive system will only survive if its benchmarking favors actions that keep the survival parameters in the green zone.

> *Fundamental Genetic Preferences. The necessity for biological or artificial cognitive systems to keep the survival parameters in a given range corresponds to primary goals, which are denoted "fundamental genetic preferences".*

The fundamental genetic preferences are not "instincts" in the classical sense, as they do not lead deterministically and directly to observable behavior. The cognitive system needs to learn which of its actions satisfy the genetic preferences, as it acquires information about the world it is born into only by direct personal experiences.

> *Rudimentary Cognitive Systems. A rudimentary cognitive system is determined fully by its fundamental genetic preferences.*

A rudimentary cognitive system is very limited with respect to the complexity level that its actions can achieve, since they are all directly related to primary survival. The next step in benchmarking involves the diffusive control units.

Secondary Benchmarks and Emotional Control Diffusive control units are responsible for keeping an eye on the overall status of the dynamical system. We can divide the diffusive control units into two classes:

– Neutral Units: These diffusive control units have no preferred activity level.
– Emotional Units: These diffusive control units have a (genetically determined) preferred activity level.

Secondary benchmarks involve the emotional diffusive control units. The system tries to keep the activity level of those units in a certain green zone.

Emotions.   By emotions we denote for a cognitive system the goals resulting from the desire to keep emotional diffusive control units at a preprogrammed level.

We note that the term *emotion* is to a certain extent controversial here. The relation of real emotions experienced by biological cognitive systems, e.g. us humans, to the above definition from cognitive system theory is unclear at present.

Emotional control is very powerful. An emotional diffusive control signal like "playing is good when you are not hungry or thirsty", to give an example, can lead a cognitive system to slowly develop very complex behavioral patterns. Higher-order explorative strategies, like playing, can be activated when the fundamental genetic preferences are momentarily satisfied.

Tertiary Benchmarks and Acquired Tastes   The vast majority of our daily actions is not directly dictated by our fundamental genetic preferences. A wish to visit a movie theater instead of a baseball match cannot be tracked back in any meaningful way to the need to survive, to eat and to sleep.

Many of our daily actions are also difficult to directly relate to emotional control. The decision to eat an egg instead of a toast for breakfast involves partly what one calls acquired tastes or preferences.

Acquired Preferences.   A learned connection, or association, between environmental sensory input signals and the status of emotional control units is denoted as an acquired taste or preference.

The term "acquired taste" is used here in a very general context, it could contain both positive or negative connotations, involve the taste of food or the artistic impression of a painting.

Humans are able to go even one step further. We can establish positive/negative feedback relations between essentially every internal dynamical state of the cognitive system and emotional diffuse control, viz we can set ourselves virtually any goal and task. This capability is called "freedom of will" in everyday language. This kind of freedom of will is an emergent feature of certain complex but deterministic dynamical systems and we sidestep here the philosophically rather heavy question of whether the thus defined freedom of will corresponds to the true freedom of will.[8]

The Inverse Pyramid   An evolved cognitive system will develop complex behavioral patterns and survival strategies. The delicate balance of internal benchmarks needed to stabilize complex actions goes beyond the capabilities of the primary genetic preferences. The necessary fine tuning of emotional control and acquired preferences is the domain of the diffusive control system.

---

[8] From the point of view of dynamical systems theory effective freedom of action is conceivable in connection to a true dynamical phase transition, like the ones discussed in the Chap. 3 possibly occurring in a high-level cognitive system. Whether dynamical phase transitions are of relevance for the brain of mammals, e.g. in relation to the phenomenon of consciousness, is a central and yet completely unresolved issue.

culturally and intellectually acquired motivations

secondary objectives and benchmarks

fundamental genetic
preferences
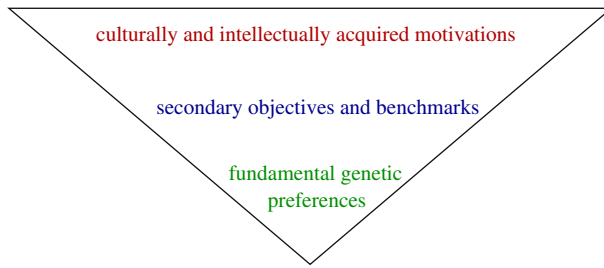
Fig. 7.4 The inverse pyramid for the internal benchmarking of complex and universal cognitive systems. The secondary benchmarks correspond to the emotional diffusive control and the culturally acquired motivations to the tertiary benchmarks, the acquired preferences. A rudimentary cognitive system contains only the basic genetic preferences, viz the preferred values for the survival variables, for action selection

Climbing up the ladder of complexity, the cognitive system effectively acquires a de facto freedom of action. The price for this freedom is the necessity to benchmark internally any possible action against hundreds and thousands of secondary and tertiary desires and objectives, which is a delicate balancing problem.

The layers of internal benchmarking can be viewed as an inverse benchmarking pyramid, see Fig. 7.4 for an illustration. The multitude of experiences and tertiary preferences plays an essential role in the development of the inverse pyramid; an evolved cognitive system is more than the sum of its genetic or computer codes.

7.4 Competitive Dynamics and Winning Coalitions

Most of the discussions presented in this chapter so far were concerned with general principles and concepts. We will now discuss a functional basic cognitive module implementing the concepts treated in the preceding sections. This network is useful for environmental data representation and storage and shows a continuous and self-regulated transient state dynamics in terms of associative thought processes. For some of the more technical details we refer to the literature.

7.4.1 General Considerations

The Human Associative Database The internal representation of the outside world is a primary task of any cognitive system with universal cognitive capabilities, i.e. capabilities that are suitable for a certain range of environments that are not explicitly encoded in genes or in software. Associations between distinct representations of the environment play an important role in human thought processes and may rank evolutionary among the first cognitive capabilities not directly determined

by gene expression. Humans dispose of a huge commonsense knowledge base, organized dominantly via associations. These considerations imply that associative information processing plays a basic role in human thinking.

Associative Thought Processes.   An associative thought process is the spontaneous generation of a time series of transient memory states with a high associative overlap.

Associative thought processes are natural candidates for transient state dynamics (see Sect. 7.2.1). The above considerations indicate that associative thought processes are, at least in part, generated directly in the cognitive modules responsible for the environmental data representation. Below we will define the notion of "associative" overlaps, see Eqs. (7.4) and (7.5).

The Winners-Take-All Network Networks in which the attractors are given by finite clusters of active sites, the "winners", are suitable candidates for data storage-because (i) they have a very high storage capacity and (ii) the competitive dynamics is directly controllable when clique encoding is used.

Cliques.   A fully connected subgraph of a network is called a clique, compare Chap. 1.

Cliques are natural candidates for winning coalitions of mutually supporting local computing units.

Data Embedding Data is meaningless when not embedded into the context of other, existing data. When properly embedded, data transmutes to information, see the discussion in Sect. 7.2.4.

Sparse networks with clique encoding allow for a crude but automatic embedding, viz embedding with zero computational effort. Any memory state added to an existing network in the form of a clique, compare Fig. 7.5, will normally share nodes with other existing cliques, viz with other stored memories. It thus automatically acquires an "associative context". The notion of associative context or associative overlap will be defined precisely below, see Eqs. (7.4) and (7.5).

Inhibitory Background Winners-take-all networks function on the basis of a strong inhibitory background. In Fig. 7.5 a few examples of networks with clique encoding are presented. Fully connected clusters, the cliques, mutually excite themselves. The winning coalition suppresses the activities of all other sites, since there is at least one inhibitory link between one of the sites belonging to the winning coalition and any other site. All cliques therefore form stable attractors.

The storage capacity is very large, due to the sparse coding. The 48-site network illustrated in Fig. 7.5 has 236 stable memory states (cliques). We note for comparison that maximally $6 \approx 1.4 * N$ memories could be stored for a $N = 48$ network with distributed coding.

Discontinuous Synaptic Strengths The clique encoding works when the excitatory links are weak compared to the inhibitory background. This implies that any given link cannot be weakly inhibitory; the synaptic strength is discontinuous,
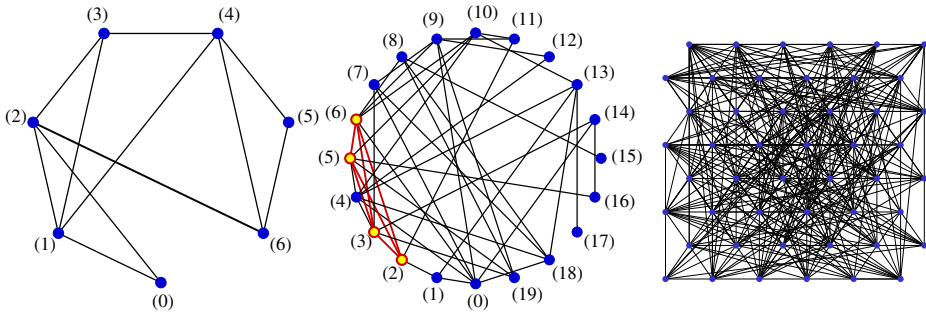
Fig. 7.5 Illustration of winners-take-all networks with clique encoding. Shown are the excitatory links. Sites not connected by a line are inhibitorily connected. *Left*: This 7-site network contains the cliques (0,1,2), (1,2,3), (1,3,4), (4,5,6) and (2,6). *Middle*: This 20-site network contains 19, 10 and 1 cliques with 2, 3 and 4 sites. The only 4-site clique (2,3,5,6) is highlighted. *Right*: This 48-site network contains 2, 166, 66 and 2 cliques (a total of 236 memories) with 2, 3, 4 and 5 sites, respectively. Note the very high density of links

see Fig. 7.6. This is admissible, as cognitive systems theory is based on generalized local computational units and not on real neurons.

Discontinuous synaptic strengths also arise generically when generating effective neural networks out of biological neural nets. Biological neurons come in two types, excitatory neurons and inhibitory interneurons. A biological neuron has either exclusively excitatory or inhibitory outgoing synapses, never both types. Most effective neurons used for technical neural networks have, on the other hand, synaptic strengths of both signs. Thus, when mapping a biological network to a network of effective neurons one has to eliminate one degree of freedom, e.g. the inhibitory interneurons.

> *Integrating out Degrees of Freedom. A transformation of a model (A) to a model (B) by eliminating certain degrees of freedom occurring in (A), but not in (B) is called "integrating out a given degree of freedom", a notion of widespread use in theoretical physics.*

This transformation depends strongly on the properties of the initial model. Consider the small biological network depicted in Fig. 7.6, for the case of strong inhibitory synaptic strength. When the interneuron is active/inactive the effective (total) influence of neuron (1) on neuron (2) will be strongly negative/weakly positive.[9]

---

[9] We note that general n-point interactions could also be generated when eliminating the interneurons. "n-point interactions" are terms entering the time evolution of dynamical systems depending on $(n-1)$ variables. Normal synaptic interactions are 2-point interactions, as they involve two neurons, the presynaptic and the postsynaptic neuron. When integrating out a degree of freedom, like the activity of the interneurons, general n-point interactions are generated. The postsynaptic neuron is then influenced only when $(n-1)$ presynaptic neurons are active simultaneously. n-point interactions are normally not considered in neural networks theory. They complicate the analysis of the network dynamics considerably.
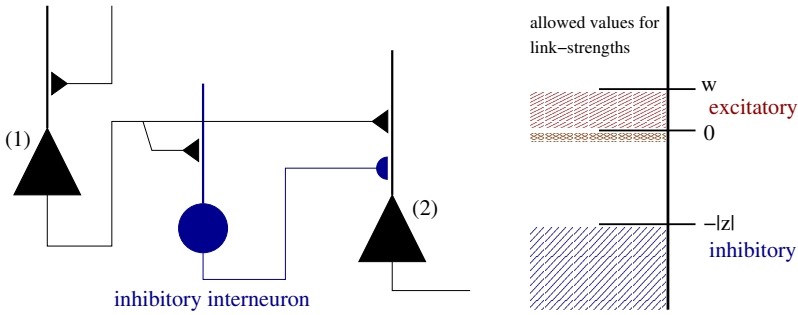
Fig. 7.6 Synaptic strengths might be discontinuous when using effective neurons. *Left*: A case network of biological neurons consisting of two neurons with exhibitory couplings (1) and (2) and an inhibitory interneuron. The effective synaptic strength (1)→(2) might be weakly positive or strongly negative depending on the activity status of the interneuron. The *vertical lines* symbolize the dendritic tree, the *thin lines* the axons ending with respective synapses. *Right*: The resulting effective synaptic strength. Weak inhibitory synaptic strengths do not occur. For the significance of the small negative allowed range for w_{ij} compare the learning rule Eq. (7.13) (from Gros, 2007b)

Transient Attractors The network described so far has many stable attractors, i.e. the cliques. These patterns are memories representing environmental data found as typical patterns in the incoming sensory data stream.

It clearly does not make sense for a cognitive system to remain stuck for eternity in stable attractors. Every attractor of a cognitive system needs to be a transient attractor,[10] i.e. to be part of the transient state dynamics.

There are many ways in dynamical systems theory by which attractors can become unstable. The purpose of any cognitive system is cognitive information processing and associative thought processes constitute the most fundamental form of cognitive information processing. We therefore discuss here how memories can take part, in the form of transient attractors, in associative thought processes.

Associative Overlaps Let us denote by $x_i \in [0,1]$ the activities of the network ($i = 1,\ldots,N$) and by

$$x_i^{(\alpha)}, \qquad \alpha = 1,\ldots,N^{(m)}$$

the activation patterns of the $N^{(m)}$ stable attractors, the memories. In winners-take-all networks $x_i^{(\alpha)} \to 0,1$.

For the seven-site network illustrated in Fig. 7.5 the number of cliques is $N^{(m)} = 5$ and for the clique $\alpha = (0,1,2)$ the activities approach $x_i^{(0,1,2)} \to 1$ (i=0,1,2) for members of the winning coalition and $x_j^{(0,1,2)} \to 0$ ($j = 3,4,5,6$) for the out-of-clique units.

---

[10] Here we use the term "transient attractor" as synonymous with "attractor ruin", an alternative terminology from dynamical system theory.

Associative Overlap of Order Zero. We define the associative overlap of zero order

$$A_0[\alpha, \beta] = \sum_{i=0}^{N} x_i^{(\alpha)} x_i^{(\beta)} \tag{7.4}$$

for two memory states α and β and for a network using clique encoding.

The associative overlap of order zero just counts the number of common constituting elements.

For the seven-site network shown in Fig. 7.5 we have $A_0[(0,1,2),(2,6)] = 1$ and $A_0[(0,1,2),(1,2,3)] = 2$.

Associative Overlap of Order 1. We define by

$$A_1[\alpha, \beta] = \sum_{\gamma \neq \alpha, \beta} \left(\sum_i x_i^{(\alpha)} (1 - x_i^{(\beta)}) x_i^{(\gamma)} \right) \left(\sum_j x_j^{(\gamma)} (1 - x_j^{(\alpha)}) x_j^{(\beta)} \right) \tag{7.5}$$

the associative overlap of first order for two memory states α and β and a network using clique encoding.

The associative overlap of order 1 is the sum of multiplicative associative overlap of zero order that the disjunct parts of two memory states α and β have with all third memory states γ. It counts the number of associative links connecting two memories.

For the seven-site network shown in Fig. 7.5 we have $A_1[(0,1,2),(4,5,6)] = 2$ and $A_1[(0,1,2),(1,3,4)] = 1$.

Associative Thought Processes Associative thought processes convenes maximal cognitive information processing when they correspond to a time series of memories characterized by high associative overlaps of order zero or one.

In Fig. 7.8 the orbits resulting from a transient state dynamics, which we will introduce in Sect. 7.4.2 are illustrated. Therein two consecutive winning coalitions have either an associative overlap of order zero, such as the transition $(0,1) \rightarrow (1,2,4,5)$ or of order 1, as the transition $(1,2,4,5) \rightarrow (3,6)$.

7.4.2 Associative Thought Processes

We now present a functioning implementation, in terms of a set of appropriate coupled differential equations, of the notion of associative thought processes as a time series of transient attractors representing memories in the environmental data representation module.

Reservoir Variables A standard procedure, in dynamical system theory, to control the long-term dynamics of a given variable of interest is to couple it to a second

Fig. 7.7 The reservoir functions $f_w(\varphi)$ (*solid line*) and $f_z(\varphi)$ (*dashed line*), see Eq. 7.7, of sigmoidal form with respective turning points $\varphi_c^{(f/z)}$ and width $\Gamma_\varphi = 0.05$
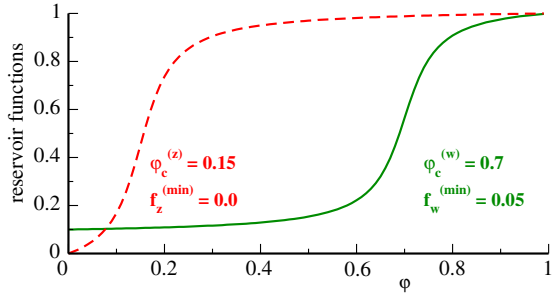
variable with much longer time scales. To be concrete we denote, as hitherto, by $x_i \in [0,1]$ the activities of the local computational units constituting the network and by

$$\varphi_i \in [0,1]$$

a second variable, which we denote *reservoir*. The differential equations

$$\dot{x}_i = (1-x_i)\,\Theta(r_i)\,r_i + x_i\,\Theta(-r_i)\,r_i \;, \tag{7.6}$$

$$r_i = \sum_{j=1}^{N} \left[f_w(\varphi_i)\Theta(w_{ij})w_{i,j} + z_{i,j}f_z(\varphi_j) \right] x_j \;, \tag{7.7}$$

$$\dot{\varphi}_i = \Gamma_\varphi^+ (1-\varphi_i)(1-x_i/x_c)\Theta(x_c - x_i) - \Gamma_\varphi^- \varphi_i \Theta(x_i - x_c) \;, \tag{7.8}$$

$$z_{ij} = -|z|\Theta(-w_{ij}) \tag{7.9}$$

generate associative thought processes. We now discuss some properties of Eqs. (7.6)–(7.9). The general form of these differential equations is termed the "Lotka–Volterra" type.

– Normalization: Equations (7.6)–(7.8) respect the normalization $x_i, \varphi_i \in [0,1]$, due to the prefactors $x_i, (1-x_i)$, φ_i and $(1-\varphi_i)$ in Eqs. (7.6) and (7.8), for the respective growth and depletion processes, and $\Theta(r)$ is the Heaviside step function.
– Synaptic Strength: The synaptic strength is split into excitatory and inhibitory contributions, $\propto w_{i,j}$ and $\propto z_{i,j}$, respectively, with $w_{i,j}$ being the primary variable: The inhibition $z_{i,j}$ is present only when the link is not excitatory, Eq. (7.9). With $z \equiv -1$ one sets the inverse unit of time.
– The Winners-Take-All Network: Equations (7.6) and (7.7) describe, in the absence of a coupling to the reservoir via $f_{z/w}(\varphi)$, a competitive winners-take-all neural network with clique encoding. The system relaxes towards the next attractor made up of a clique of Z sites $(p_1, \ldots, p_Z)$ connected excitatory via $w_{p_i,p_j} > 0$ $(i,j = 1, \ldots, Z)$.
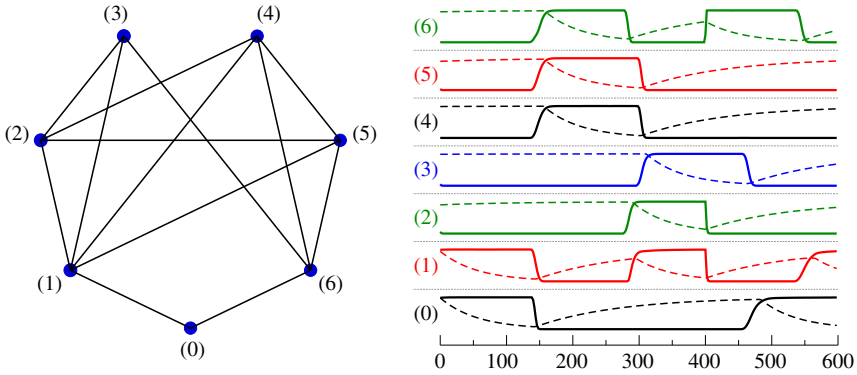
Fig. 7.8 *Left*: A seven-site network; shown are links with $w_{i,j} > 0$, containing six cliques, $(0,1)$, $(0,6)$, $(3,6)$, $(1,2,3)$, $(4,5,6)$ and $(1,2,4,5)$. *Right*: The activities $x_i(t)$ (*solid lines*) and the respective reservoirs $\varphi_i(t)$ (*dashed lines*) for the transient state dynamics $(0,1) \to (1,2,4,5) \to (3,6) \to (1,2,4,5)$

- Reservoir Functions: The reservoir functions $f_{z/w}(\varphi) \in [0,1]$ govern the interaction between the activity levels x_i and the reservoir levels φ_i. They may be chosen as washed out step functions of sigmoidal form[11] with a suitable width Γ_φ and inflection points $\varphi_c^{(w/z)}$, see Fig. 7.7.
- Reservoir Dynamics: The reservoir levels of the winning clique deplete slowly, see Eq. (7.8), and recovers only once the activity level x_i of a given site has dropped below x_c. The factor $(1 - x_i/x_c)$ occurring in the reservoir growth process, see the right-hand side of Eq. (7.8), serves as a stabilization of the transition between subsequent memory states.
- Separation of Time Scales: A separation of time scales is obtained when $\Gamma_\varphi^\pm$ are much smaller than the average strength of an excitatory link, $\bar{w}$, leading to transient state dynamics. Once the reservoir of a winning clique is depleted, it loses, via $f_z(\varphi)$, its ability to suppress other sites. The mutual intraclique excitation is suppressed via $f_w(\varphi)$.

Fast and Slow Thought Processes Figure 7.8 illustrates the transient state dynamics resulting from Eqs. (7.6)–(7.9), in the absence of any sensory signal. When the growth/depletion rates $\Gamma_\varphi^\pm \to 0$ are very small, the individual cliques turn into stable attractors.

The possibility to regulate the "speed" of the associative thought process arbitrarily by setting $\Gamma_\varphi^\pm$ is important for applications. For a working cognitive system it is

---

[11] A possible mathematical implementation for the reservoir functions, with $\alpha = w, z$, is $f_\alpha(\varphi) = f_\alpha^{(min)} + \left(1 - f_\alpha^{(min)}\right) \frac{\text{atan}[(\varphi - \varphi_c^{(\alpha)})/\Gamma_\varphi] - \text{atan}[(0 - \varphi_c^{(\alpha)})/\Gamma_\varphi]}{\text{atan}[(1 - \varphi_c^{(\alpha)})/\Gamma_\varphi] - \text{atan}[(0 - \varphi_c^{(\alpha)})/\Gamma_\varphi]}$. Suitable values are $\varphi_c^{(z)} = 0.15$, $\varphi_c^{(w)} = 0.7$ $\Gamma_\varphi = 0.05$, $f_w^{(min)} = 0.1$ and $f_z^{(min)} = 0$.
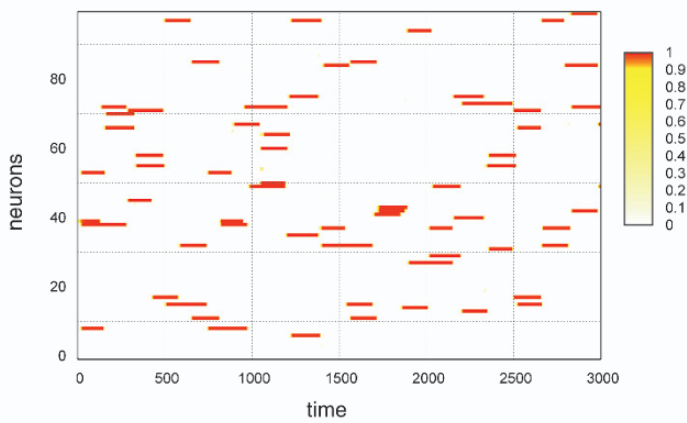
Fig. 7.9 Example of an associative thought process in a network containing 100 artificial neurons and 713 stored memories. The times runs horizontally, the site index vertically ($i = 1, \ldots, 100$). The neural activities $x_i(t)$ are color coded

enough if the transient states are just stable for a certain minimal period, anything longer just would be a "waste of time".

Cycles The system in Fig. 7.8 is very small and the associative thought process soon settles into a cycle, since there are no incoming sensory signals in the simulation of Fig. 7.8.

For networks containing a somewhat larger number of sites, see Fig. 7.9, the number of attractors can be very large. The network will then generate associative thought processes that will go on for very long time spans before entering a cycle. Cyclic "thinking" will normally not occur for real-world cognitive systems interacting continuously with the environment. Incoming sensory signals will routinely interfere with the ongoing associative dynamics, preempting cyclic activation of memories.

Dual Functionalities for Memories The network discussed here is a dense and homogeneous associative network (dHAN). It is homogeneous since memories have dual functionalities:

– Memories are the transient states of the associative thought process.
– Memories define the associative overlaps, see Eq. (7.5), between two subsequent transient states.

The alternative would be to use networks with two kinds of constituent elements, as in semantic networks. The semantic relation

| car | —— is —— | blue |
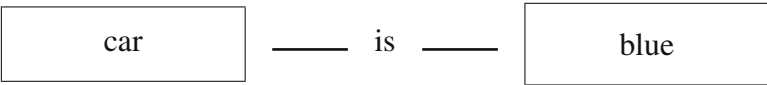
can be thought to be part of a (semantic) network containing the nodes "car" and "blue" linked by the relation "is". Such a network would contain two kinds of different constituting elements, the nodes and the links. The memories of the dHAN, on the other hand, are made up of cliques of nodes and it is therefore homogeneous.

A rudimentary cognitive system knows of no predefined concepts and cannot, when starting from scratch, initially classify data into "links" and "nodes". A homogeneous network is consequently the network of choice for rudimentary cognitive systems.

Dissipative Dynamics Interestingly, the phase space contracts at all times in the absence of external inputs. With respect to the reservoir variables, we have

$$\sum_i \frac{\partial \dot{\varphi}_i}{\partial \varphi_i} = -\sum_i \left[\Gamma_\varphi^+ (1 - x_i/x_c)\Theta(x_c - x_i) + \Gamma_\varphi^- \Theta(x_i - x_c) \right] \leq 0,$$

$\forall x_i \in [0,1]$, where we have used Eq. (7.8). We note that the diagonal contributions to the link matrices vanish, $z_{ii} = 0 = w_{ii}$, and therefore $\partial r_i/\partial x_i = 0$. The phase space consequently contracts also with respect to the activities,

$$\sum_i \frac{\partial \dot{x}_i}{\partial x_i} = \sum_i \left[\Theta(-r_i) - \Theta(r_i) \right] r_i \leq 0,$$

where we have used Eq. (7.6). The system is therefore strictly dissipative, compare Chap. 2 in the absence of external stimuli.

Recognition Any sensory stimulus arriving in the dHAN needs to compete with the ongoing intrinsic dynamics to make an impact. If the sensory signal is not strong enough, it cannot deviate the autonomous thought process. This feature results in an intrinsic recognition property of the dHAN: A background of noise will not influence the transient state dynamics.

7.4.3 Autonomous Online Learning

Sensory Stimuli Learning or training of the network occurs on the fly, during its normal mode of operation. There are no distinct modes for training and performance for a cognitive system. The sensory stimuli or training patterns $\{b_i^{(\text{ext})}(t)\}$ add to the respective growth rates r_i in Eq. (7.7),

$$r_i \rightarrow r_i + f_b(\varphi_i)\, b_i^{(\text{ext})}(t), \tag{7.10}$$

where $f_b(\varphi_i)$ is an appropriate coupling function, dependent on the local reservoir level φ_i. For simplicity one may take it to be identical with the reservoir

function $f_w(\varphi_i)$. A site active for a prolonged period depletes its own reservoir and consequently via $f_b(\varphi_i)$ it will lose its susceptibility to stimuli. Novel stimuli are then more likely to make an impact.

For neural networks with supervised learning there are explicit training phases were Hebbian-type synaptic changes $\sim b_i b_j$ are enforced by hand. An autonomous cognitive system has to decide by itself when to modify its own synaptic link strengths and how strong these changes ought to be.

Short-Term and Long-Term Synaptic Plasticities There are two fundamental considerations for the choice of the synaptic dynamics adequate for the dHAN.

– Learning is a very slow process without a short-term memory. Training patterns need to be presented to the network over and over again until substantial changes are induced into the link matrices. A short-term memory can speed up the learning process substantially as it stabilizes external patterns, thus giving the system time to consolidate long-term synaptic plasticity.
– Systems using sparse coding are based on a strong inhibitory background, the average inhibitory link strength $|z|$ is substantially larger than the average excitatory link strength $\bar{w}$,

$$|z| \gg \bar{w} .$$

It is then clear that gradual learning dominantly affects the excitatory links, as they are much smaller; small changes of large parameters do not lead to new transient attractors, nor do they influence the cognitive dynamics substantially.

We consequently consider both short-term and long-term modifications for the link matrices

$$w_{ij} = w_{ij}(t) = w_{ij}^S(t) + w_{ij}^L(t) , \tag{7.11}$$

where $w_{ij}^{S/L}$ correspond to the short/long-term synaptic plasticities. Note that short-term plasticities are also transient, they go away after a certain characteristic period, and that the long-term changes are essentially permanent.

The Negative Baseline Equation (7.9), $z_{ij} = -|z| \Theta(-w_{ij})$, states that the inhibitory link strength is either zero or $-|z|$, but is not changed directly during learning, in accordance to Eq. (7.11).

When a $w_{i,j}$ is slightly negative, as default (compare Fig. 7.6), the corresponding total link strength is inhibitory. When $w_{i,j}$ acquires, during learning, a positive value, the corresponding total link strength becomes excitatory. In this sense we have active excitatory synapses with $w_{i,j} > 0$ and inactive excitatory synapses with $w_{i,j} \lesssim 0$.

Short-Term Memory Dynamics It is reasonable to have a maximal possible value $W_S^{(\max)}$ for the transient short-term synaptic plasticities. An appropriate Hebbian-type autonomous learning rule is then

$$\dot{w}_{ij}^S(t) = \Gamma_S^+ \left(W_S^{(\max)} - w_{ij}^S \right) f_z(\varphi_i) f_z(\varphi_j) \Theta(x_i - x_c) \Theta(x_j - x_c) \tag{7.12}$$
$$- \Gamma_S^- w_{ij}^S .$$
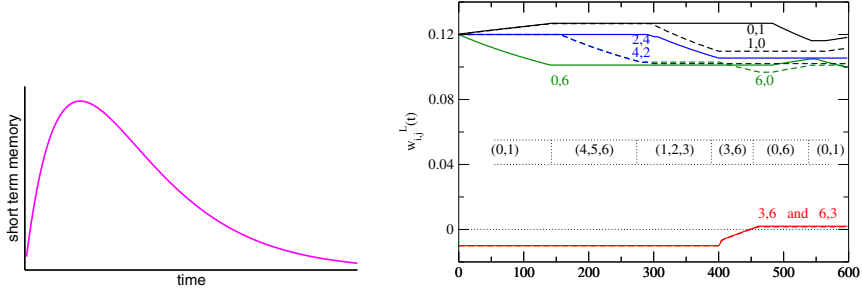
Fig. 7.10 *Left*: Typical activation pattern of the transient short-term plasticities of an excitatory link (short-term memory). *Right*: The time evolution of the long-term memory, for some selected links $w_{i,j}^L$ and the network illustrated in Fig. 7.8, without the link $(3,6)$. The transient states are $(0,1) \to (4,5,6) \to (1,2,3) \to (3,6) \to (0,6) \to (0,1)$. An external stimulus at sites (3) and (6) acts for $t \in [400, 410]$ with strength $b^{(\text{ext})} = 3.6$. The stimulus pattern $(3,6)$ has been learned by the system, as the $w_{3,6}$ and $w_{6,3}$ turned positive during the learning interval $\approx [400, 460]$. The learning interval is substantially longer than the bare stimulus length due to the activation of the short-term memory. Note the asymmetric decay of inactive links, compare Eq. (7.14) (from Gros, 2007b)

It increases rapidly when both the presynaptic and the postsynaptic centers are active, it decays to zero otherwise, see Fig. 7.10.

The coupling functions $f_z(\varphi)$ preempt prolonged self-activation of the short-term memory. When the presynaptic and the postsynaptic centers are active long enough to deplete their respective reservoir levels, the short-term memory is shut off via $f_z(\varphi)$, compare Fig. 7.7.

Working Point Optimization Dynamical systems normally retain their functionalities only when they keep their dynamical properties in certain regimes. They need to regulate their own working point, as discussed in Sect. 7.2.3. This is a long-term affair, it involves time-averaged quantities and is therefore a job for the long-term synaptic plasticities, w_{ij}^L.

Effective Incoming Synaptic Strength The average magnitude of the growth rates r_i, see Eq. (7.7), determine the time scales of the autonomous dynamics and thus the working point. $r_i(t)$ are, however, quite strongly time dependent. The effective incoming synaptic signal

$$\tilde{r}_i = \sum_j \left[w_{i,j} x_j + z_{i,j} x_j f_z(\varphi_j) \right] ,$$

which is independent of the postsynaptic reservoir, φ_i, is a more convenient control parameter, since $\tilde{r}_i$ tends to the sum of active incoming links,

$$\tilde{r}_i \to \sum_{j \in \alpha} w_{i,j} ,$$

for a transiently stable clique $\alpha = (p_1, \ldots, p_Z)$. The working point of the cognitive system is optimal when the effective incoming signal is, on the average, of comparable magnitude $r^{(opt)}$ for all sites,

$$\tilde{r}_i \;\rightarrow\; r^{(opt)} \;.$$

$r^{(opt)}$ is an unmutable parameter, compare Fig. 7.3.

Long-Term Memory Dynamics The long-term memory has two tasks: To encode stimulus patterns permanently and to keep the working point of the dynamical system in its desired range. Both tasks can be achieved by a single local learning rule,

$$\dot{w}_{ij}^L(t) = \Gamma_L^{(opt)} \Delta \tilde{r}_i \left[\left(w_{ij}^L - W_L^{(min)} \right) \Theta(-\Delta \tilde{r}_i) + \Theta(\Delta \tilde{r}_i) \right] \tag{7.13}$$
$$\cdot \Theta(x_i - x_c)\, \Theta(x_j - x_c),$$
$$- \Gamma_L^- \, d(w_{ij}^L)\, \Theta(x_i - x_c)\, \Theta(x_c - x_j) \;, \tag{7.14}$$

with

$$\Delta \tilde{r}_i \;=\; r^{(opt)} - \tilde{r}_i \;.$$

Some comments:

- Hebbian learning: The learning rule Eq. (7.13) is local and of Hebbian type. Learning occurs only when the presynaptic and the postsynaptic neurons are active. Weak forgetting, i.e. the decay of rarely used links , Eq. (7.14) is local too.
- Synaptic Competition: When the incoming signal is weak/strong, relative to the optimal value $r^{(opt)}$, the active links are reinforced/weakened, with $W_L^{(min)}$ being the minimal value for the w_{ij}. The baseline $W_L^{(min)}$ is slightly negative, compare Figs. 7.6 and 7.10.
  The Hebbian-type learning then takes place in the form of a competition between incoming synapses – frequently active incoming links will gain strength, on the average, on the expense of rarely used links.
- Asymmetric Decay of Inactive Links: The decay term $\propto \Gamma_L^- > 0$ in Eq. (7.14) is taken to be asymmetric, viz when the presynaptic neuron is inactive with the postsynaptic neuron being active. The strength of the decay is a suitable nonlinear function $d(w_{ij}^L)$ of the synaptic strength w_{ij}^L. Note that the opposite asymmetric decay, for which w_{ij}^L is weakened whenever the presynaptic/postsynaptic neurons are active/inactive, may potentially lead to the dynamical isolation of the currently active clique by suppressing excitatory out-of-clique synapses.
- Fast Learning of New Patterns: In Fig. 7.10 the time evolution of some selected w_{ij} from a simulation is presented. A simple input pattern is learned by the network. In this simulation the learning parameter $\Gamma_L^{(opt)}$ was set to a quite large value such that the learning occurred in one step (fast learning).
- Suppression of Runaway Synaptic Growth: The link dynamics, Eq. (7.13) suppresses synaptic runaway growth, a general problem common to adaptive and

continuously active neural networks. It has been shown that similar rules for discrete neural networks optimize the overall storage capacity.

– Long-Term Dynamical Stability: In Fig. 7.9 an example for an associative thought process is shown for a 100-site network containing 713 memories. When running the simulation for very long times one finds that the values of excitatory links w_{ij}^L tend to a steady-state distribution, as the result of the continuous online learning. The system is self-adapting.

Conclusions In this section we presented and discussed the concrete implementation of a module for the storage of environmental data, as given by patterns present in the input stimuli.

The key point is that this implementation fulfills all requirements necessary for an autonomous cognitive system, such as locality of information processing, unsupervised online learning, huge storage capacity, intrinsic generalization capacity and self-sustained transient state dynamics in terms of self-generated associative thought processes.

7.5 Environmental Model Building

The representation of environmental data, as discussed in Sect. 7.4, allows for simple associational reasoning. For anything more sophisticated, the cognitive system needs to learn about the structure of the environment itself, i.e. it has to build models of the environment.

The key question is then: Are there universal principles that allow for environmental model building without any a priori information about the environment? Principles that work independently of whether the cognitive system lives near a lakeside in a tropical rain forest or in an artificial cybernetical world.

Here we will discuss how *universal prediction tasks* allow for such universal environmental model building and for the spontaneous generation of abstract concepts.

7.5.1 The Elman Simple Recurrent Network

Innate Grammar Is the human brain completely empty at birth and can babies learn with the same ease any language, natural or artificial, with arbitrary grammatical organization? Or do we have certain gene determined predispositions toward certain innate grammatical structures? This issue has been discussed by linguists for decades.

In this context in 1990 Elman performed a seminal case study, examining the representation of time-dependent tasks by a simple recurrent network. This network is universal in the sense that no information about the content or structure of the input data stream is used in its layout.
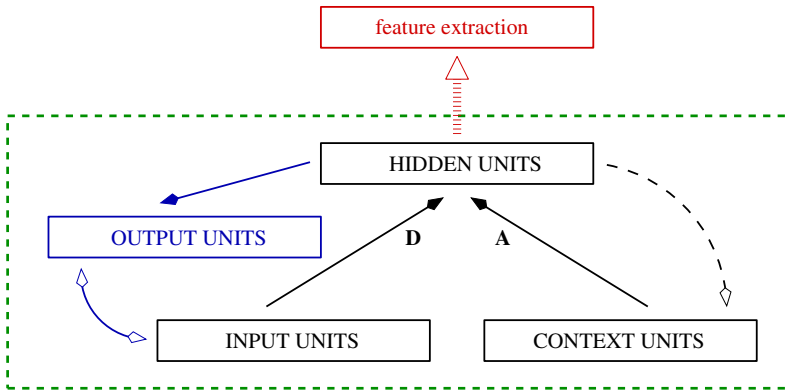
Fig. 7.11 The Elman simple recurrent network (inside the *dashed box*). The connections (**D**: input→hidden), (**A**: context→hidden) and (hidden→output) are trained via the backpropagation algorithm. At every time step the content of the hidden units is copied into the context units on a one-to-one basis. The difference between the output signal and the new input signal constitutes the error for the training. The hidden units generate abstract concepts that can be used for further processing by the cognitive system via standard feature extraction

Elman discovered that lexical classes are spontaneously generated when the network is given the task to predict the next word in an incoming data stream made up of natural sentences constructed from a reduced vocabulary.

The Simple Recurrent Network   When the task of a neural network extends into the time domain it needs a memory, otherwise comparison of current and past states is impossible. For the simple recurrent network, see Fig. 7.11, this memory is constituted by a separate layer of neurons denoted *context units.*

The simple recurrent network used by Elman employs discrete time updating. At every time step the following computations are performed:

1. The activities of the hidden units are determined by the activities of the input units and by the activities of the context units and the respective link matrices.
2. The activities of the output units are determined by the activities of the hidden units and the respective link matrix.
3. The activities of the hidden units are copied one-by-one to the context unit.
4. The next input signal is copied to the input units.
5. The activities of the output units are compared to the current input and the difference yields the error signal. The weight of the link matrices (input→hidden), (context→hidden) and (hidden→output) are adapted such to reduce the error signal. This procedure is called the back-propagation algorithm.

The Elman net does not conform in this form to the requirements needed for modules of a full-fledged cognitive system, see Sect. 7.2.1. It employs discrete time synchronous updating and non-local learning rules based on a global optimization condition, the so-called back-propagation algorithm. This drawback is, however,

not essential at this point, since we are interested here in the overall and generic properties of the simple recurrent network.

The Lexical Prediction Task The simple recurrent network works on a time series $x(t)$ of inputs

$$x(1), \ x(2), \ x(3), \ \ldots$$

which are presented to the network one after the other.

The network has the task to predict the next input. For the case studied by Elman the inputs $x(t)$ represented randomly encoded words out of a reduced vocabulary of 29 lexical items. The series of inputs corresponded to natural language sentences obeying English grammar rules. The network then had the task to predict the next word in a sentence.

The Impossible Lexical Prediction Task The task to predict the next word of a natural language sentence is impossible to fulfill. Language is non-deterministic, communication would otherwise convene no information.

The grammatical structure of human languages places constraints on the possible sequence of words, a verb is more likely to follow a noun than another verb, to give an example. The expected frequency of possible successors, implicit in the set of training sentences, is, however, deterministic and is reproduced well by the simple recurrent network.

Spontaneous Generation of Lexical Types Let us recapitulate the situation:

i.   The lexical prediction task given to the network is impossible to fulfill.
ii. The data input stream has a hidden grammatical structure.
iii. The frequency of successors is not random.

As a consequence, the network generates in its hidden layer representations of the 29 used lexical items, see Fig. 7.12. These representations, and this is the central result of Elman's 1990 study, have a characteristic hierarchical structure. Representations of different nouns, e.g. "mouse" and "cat", are more alike than the representations of a noun and a verb, e.g. "mouse" and "sleep". The network has generated spontaneously abstract lexical types like verb, nouns of animated objects and nouns of inanimate objects.

Tokens and Types The network actually generated representations of the lexical items dependent on the context, the tokens. There is not a unique representation of the item *boy*, but several, viz $boy_1, boy_2, \ldots$, which are very similar to each other, but with fine variations in their respective activation patterns. These depend on the context, as in the following training sentences:

<center>man_smell_BOY,   man_chase_BOY,   ...</center>

The simple recurrent network is thus able to generate both abstract lexical types and concrete lexical tokens.
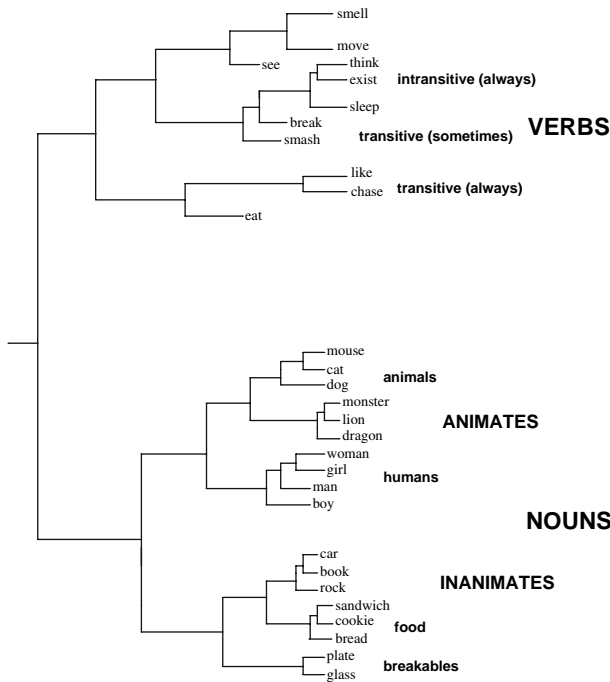
Fig. 7.12 Hierarchical cluster diagram of the hidden units activation pattern. Shown are the relations and similarities of the hidden unit activity patterns according to a hierarchical cluster analysis (from Elman, 2004)

Temporal XOR The XOR problem, see Fig. 7.13, is a standard prediction task in neural network theory. In its temporal version the two binary inputs are presented one after the other to the same input neuron as $x(t-1)$ and $x(t)$, with the task to predict the correct $x(t+1)$.

The XOR problem is not linearly decomposable, i.e. there are no constants a, b, c such that

$$x(t+1) \; = \; ax(t) + bx(t-1) + c \; ,$$

and this is why the XOR problem serves as a benchmark for neural prediction tasks. Input sequences like

$$\ldots \underbrace{0\,0\,0}\,\underbrace{1\,0\,1}\,\underbrace{1\,1\,0}\ldots$$

are presented to the network with the caveat that the network does not know when an XOR-triple starts. A typical result is shown in Fig. 7.13. Two out of three prediction results are random, as expected but every third prediction is quite good.

The Time Horizon Temporal prediction tasks may vary in complexity depending on the time scale τ characterizing the duration of the temporal dependencies in the input data $x(t)$. A well known example is the Markov process.

x(t-1)	x(t)	x(t+1)
0	0	0
0	1	1
1	0	1
1	1	0
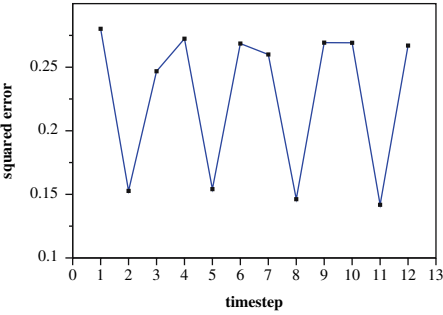
Fig. 7.13 The temporal XOR. *Left*: The prediction task. *Right*: The performance $(y(t+1) - x(t+1))^2$ ($y(t) \in [0,1]$) is the activity of the single output neuron of a simple recurrent network, see Fig. 7.11, with two neurons in the hidden layer after 600 sweeps through a 3000-bit training sequence

> *The Markov Assumption.*   *The distribution of possible $x(t)$ depends only on the value of the input at the previous time step, $x(t-1)$.*

For Markovian-type inputs the time correlation length of the input data is 1; $\tau = 1$. For the temporal XOR problem $\tau = 2$. In principle, the simple recurrent network is able to handle time correlations of arbitrary length. It has been tested with respect to the temporal XOR and to a letter-in-a-word prediction task. The performance of the network in terms of the accuracy of the prediction results, however, is expected to deteriorate with increasing τ.

7.5.2 Universal Prediction Tasks

Time Series Analysis The Elman simple recurrent network is an example of a neural network layout that is suitable for time series analysis. Given a series of vectors

$$x(t), \qquad t = 0, 1, 2, \ldots$$

one might be interested in forecasting $x(t+1)$ when $x(t)$, $x(t-1), \ldots$ are known. Time series analysis is very important for a wide range of applications and a plethora of specialized algorithms have been developed.

State Space Models Time series generated from physical processes can be described by "state space models". The daily temperature in Frankfurt is a complex function of the weather dynamics, which contains a huge state space of (mostly) unobservable variables. The task to predict the local temperature from only the knowledge of the history of previous temperature readings constitutes a time series analysis task.

Quite generally, there are certain deterministic or stochastic processes generating a series

$$s(t), \qquad t = 0, 1, 2, \ldots$$

of vectors in a state space, which is mostly unobservable. The readings $x(t)$ are then some linear or non-linear functions

$$x(t) \;=\; F[s(t)] + \eta(t) \tag{7.15}$$

of the underlying state space, possibly in addition to some noise $\eta(t)$. Equation (7.15) is denoted a state space model.

The Hidden Markov Process There are many possible assumptions for the state space dynamics underlying a given history of observables $x(t)$. For a hidden Markov process, to give an example, one assumes that

(a) $s(t+1)$ depends only on $s(t)$ (and not on any previous state space vector, the *Markov assumption*) and that
(b) the mapping $s(t) \rightarrow s(t+1)$ is stochastic.

The process is dubbed "hidden", because the state space dynamics is not directly observable.

The Elman State Space Model The Elman simple recurrent network is described by

$$s(t) \;=\; \sigma\Big[\mathbf{A}s(t-1) + \mathbf{D}x(t)\Big], \qquad \sigma[y] = \frac{1}{1 + e^{-y}} \;, \tag{7.16}$$

were $x(t)$ and $s(t)$ correspond to the activation patterns of input and hidden units, respectively. The $\mathbf{A}$ and $\mathbf{D}$ are the link matrices (context→hidden) and (input→hidden), compare Fig. 7.11, and $\sigma(y)$ is called the *sigmoid function*. The link matrix (hidden →output) corresponds to the prediction task $s(t) \rightarrow x(t+1)$ given to the Elman network.

The Elman simple recurrent network is, however, not a classical state space model. For a normal state space model the readings $x(t)$ depend only on the current state $s(t)$ of the underlying dynamical system, compare Eq. (7.15). Extracting $x(t)$ from Eq. (7.16), one obtains

$$x(t) \;=\; F[s(t), s(t-1)] \;, \tag{7.17}$$

which is a straightforward generalization of Eq. (7.15). The simple recurrent net has a memory since $x(t)$ in Eq. (7.17) depends both on $s(t)$ and on $s(t-1)$.

Neural Networks for Time Series Analysis The simple recurrent network can be generalized in several ways, e.g. additional hidden layers result in a non-linear state space dynamics. More complex layouts lead to more powerful prediction capabilities, but there is a trade-off. Complex neural networks with lots of hidden layers

and recurrent connections need very big training data. There is also the danger of overfitting the data, when the model has more free parameters than the input.

Time Series Analysis for Cognitive Systems For most technical applications one is interested exclusively in the time prediction capability of the algorithm employed. Pure time series prediction is, however, of limited use for a cognitive system. An algorithm that allows one to predict future events and that at the same time generates models of the environment is, however, extremely useful for a cognitive system.

This is the case for state space models, as they generate explicit proposals for the underlying environmental states describing the input data. For the simple recurrent network these proposals are generated in the hidden units. The activation state of the hidden units can be used by the network for further cognitive information processing via a simple feature extraction procedure, see Fig. 7.11, e.g. by a Kohonen layer.[12]

Possible and Impossible Prediction Tasks A cognitive system is generally confronted with two distinct types of prediction tasks.

– Possible Prediction Tasks: Examples are the prediction of the limb dynamics as a function of muscle activation or the prediction of physical processes like the motion of a ball in a soccer game.
– Impossible Prediction Tasks: When a series of events is unpredictable it is, however, important to be able to predict the class of the next events. When we drive with a car behind another vehicle we automatically generate in our mind a set of likely maneuvers that we we expect the vehicle in front of us to perform next. When we listen to a person speaking we generate expectancies of what the person is likely to utter next.

Universal Prediction Tasks and Abstract Concepts Impossible prediction tasks, like the lexical prediction task discussed in Sect. 7.5.1, lead to the generation of abstract concepts in the hidden layer, like the notion of "noun" and "verb". This is not a coincidence, but a necessary consequence of the task given to the network. Only classes of future events can be predicted in an impossible prediction task and not concrete instances. We may then formulate the key result of this section in the form of a lemma.

Universal Prediction Task Lemma. The task to predict future events leads to universal environmental model building for neural networks with state space layouts. When the prediction task is impossible to carry out, the network will automatically generate abstract concepts that can be used for further processing by the cognitive system.

---

[12] A Kohonen network is an example of a neural classifier via one-winner-takes-all architecture, see e.g. Ballard (2000).

Exercises

TRANSIENT STATE DYNAMICS

Consider a system containing two variables, $x, \varphi \in [0,1]$. Invent a system of coupled differential equations for which $x(t)$ has two transient states, $x \approx 1$ and $x \approx 0$. One possibility is to consider φ as a reservoir and to let $x(t)$ autoexcite/autodeplete itself when the reservoir is high/low.

The transient state dynamics should be rigorous. Write a code implementing the differential equations.

THE DIFFUSIVE CONTROL UNIT

Given are two signals $y_1(t) \in [0, \infty]$ and $y_2(t) \in [0, \infty]$. Invent a system of differential equations for variables $x_1(t) \in [0,1]$ and $x_2(t) \in [0,1]$ driven by the $y_{1,2}(t)$ such that $x_1 \to 1$ and $x_2 \to 0$ when $y_1 > y_2$ and vice versa. Note that $y_{1,2}$ are not necessarily normalized.

ASSOCIATIVE OVERLAPS AND THOUGHT PROCESSES

Consider the seven-site network of Fig. 7.5. Evaluate all pairwise associative overlaps of order zero and of order one between the five cliques, using Eqs. (7.4) and (7.5). Generate an associative thought process of cliques $\alpha_1, \alpha_2, \ldots$, where a new clique α_{t+1} is selected using the following simplified dynamics:

(1) α_{t+1} has an associative overlap of order zero with α_t and is distinct from α_{t-1}.
(2) If more than one clique satisfies criterium (1), then the clique with the highest associative overlap of order zero with α_t is selected.
(3) If more than one clique satisfies criteria (1)–(2), then one of them is drawn randomly.

Discuss the relation to the dHAN model treated in Sect.7.4.2.

Further Reading

For a general introduction to the field of artificial intelligence (AI), see Russell and Norvig (1995). For a handbook on experimental and theoretical neuroscience, see Arbib (2002). For exemplary textbooks on neuroscience, see Dayan and Abbott (2001) and for an introduction to neural networks, see Ballard (2000).

Somewhat more specialized books for further reading regarding the modeling of cognitive processes by small neural networks is that by McLeod, Plunkett and Rolls (1998) and on computational neuroscience that by O'Reilly and Munakata (2000).

For some relevant review articles on dynamical modeling in neuroscience the following are recommended: Rabinovich, Varona, Selverston and Abarbanel (2006); on reinforcement learning Kaelbling, Littman and Moore (1996), and on learning and memory storage in neural nets Carpenter (2001).

We also recommend to the interested reader to go back to some selected original literature dealing with 'simple recurrent networks in the context of grammar acquisition (Elman, 1990; 2004), with neural networks for time series prediction tasks (Dorffner, 1996), with "learning by error" (Chialvo and Bak, 1999), with the assignment of the cognitive tasks discussed in Sect.7.3.1 to specific mammal brain areas (Doya, 1999), with the effect on memory storage capacity of various Hebbian-type learning rules (Chechik, Meilijson and Ruppin, 2001) and with the concept of "associative thought processes" (Gros, 2005; 2007a,b).

It is very illuminating to take a look at the freely available databases storing human associative knowledge (Nelson, McEvoy and Schreiber, 1998) and (Liu and Singh, 2004).

ABELES M. ET AL. 1995 Cortical activity flips among quasi-stationary states. *Proceedings of the National Academy of Science, USA* **92**, 8616–8620.

ARBIB, M.A. 2002 *The Handbook of Brain Theory and Neural Networks.* MIT Press, Cambridge, MA.

BAARS, B.J., FRANKLIN, S. 2003 How conscious experience and working memory interact. *Trends in Cognitive Science* **7**, 166–172.

BALLARD, D.H. 2000 *An Introduction to Natural Computation.* MIT Press, Cambridge, MA.

CARPENTER, G.A. 2001 Neural-network models of learning and memory: Leading questions and an emerging framework. *Trends in Cognitive Science* **5**, 114–118.

CHECHIK, G., MEILIJSON, I., RUPPIN, E. 2001 Effective neuronal learning with ineffective Hebbian learning rules. *Neural Computation* **13**, 817.

CHIALVO, D.R., BAK, P. 1999 Learning from mistakes. *Neuroscience* **90**, 1137–1148.

CRICK, F.C., KOCH, C. 2003 A framework for consciousness. *Nature Neuroscience* **6**, 119–126.

DAYAN, P., ABBOTT, L.F. 2001 *Theoretical Neuroscience: Computational and Mathematical Modeling of Neural Systems.* MIT Press, Cambridge, MA.

DEHAENE, S., NACCACHE, L. 2003 Towards a cognitive neuroscience of consciousness: Basic evidence and a workspace framework. *Cognition* **79**, 1–37.

DORFFNER, G. 1996 Neural networks for time series processing. *Neural Network World* **6**, 447–468.

DOYA, K. 1999 What are the computations of the cerebellum, the basal ganglia and the cerebral cortex? *Neural Networks* **12**, 961–974.

EDELMAN, G.M., TONONI, G.A. 2000 *A Universe of Consciousness.* Basic Books, New York.

ELMAN, J.L. 1990 Finding structure in time. *Cognitive Science* **14**, 179-211.

ELMAN, J.L. 2004 An alternative view of the mental lexicon. *Trends in Cognitive Sciences* **8**, 301–306.

GROS, C. 2005 *Self-Sustained Thought Processes in a Dense Associative Network.* Springer Lecture Notes in Artificial Intelligence (KI2005) 3698, 375-388 (2005); also available as `http://arxiv.org/abs/q-bio.NC/0508032`.

GROS, C. 2007a *Autonomous dynamics in neural networks: The dHAN concept and associative thought processes.* Cooperative Behaviour in Neural Systems (Ninth Granada Lectures), P.L. Garrido, J. Marro, J.J. Torres (Eds.), AIP Conference Proceedings **887**, 129-138; also available as `http://arxiv.org/abs/q-bio.NC/0703002`.

GROS, C. 2007b Neural networks with transient state dynamics *New Journal of Physics* **9**, 109.

KAELBLING, L.P., LITTMAN, M.L., MOORE, A. 1996 Reinforcement learning: A survey. *Journal of Artificial Intelligence Research* **4**, 237–285.

KENET, T., BIBITCHKOV, D., TSODYKS, M., GRINVALD, A., ARIELI, A. 2003 Spontaneously emerging cortical representations of visual attributes. *Nature* **425**, 954–956.

LIU, H., SINGH, P. 2004 ConcepNet a practical commonsense reasoning tool-kit. *BT Technology Journal* **22**, 211–226.

NELSON, D.L., MCEVOY, C.L., SCHREIBER, T.A. 1998 *The University of South Florida word association, rhyme, and word fragment norms.* Homepage: `http://www.usf.edu/FreeAssociation`.

MCLEOD, P., PLUNKETT, K., ROLLS, E.T. 1998 *Introduction to Connectionist Modelling.* Oxford University Press.

O'REILLY, R.C., MUNAKATA, Y. 2000 *Computational Explorations in Cognitive Neuroscience: Understanding the Mind by Simulating the Brain.* MIT Press.

RABINOVICH, M.I., VARONA, P., SELVERSTON, A.I. AND ABARBANEL, H.D.I. 2006 Dynamical principles in neuroscience. *Review of Modern Physics* **78**, 1213–1256.

RUSSELL, S.J., P NORVIG, P. 1995 *Artificial intelligence: a modern approach.* Prentice-Hall, Englewood Cliffs, NJ.

Chapter 8
Solutions

Solutions to the Exercises of Chapter 1

DEGREE DISTRIBUTION

We list below a few freely available network databases. The main task of this exercise is to format a database of your choice in such a way that your program can read it.

Title	Address
Human Protein Reference Database	`http://www.hprd.org/download`
Database of Interacting Proteins	`http://dip.doe-mbi.ucla.edu`
EMBL Nucleotide Sequence Database	`http://www.ebi.ac.uk/embl`
NCBI GenBank	`http://www.ncbi.nlm.nih.gov/ Genbank`
DNA Data Bank of Japan	`http://www.ddbj.nig.ac.jp`
Saccharomyces Genome Database	`http://www.yeastgenome.org`
Database of Drosophila Genes & Genomes	`http://flybase.bio.indiana.edu`
Ensembl	`http://www.ensembl.org/info/ data`
UniProtKB/Swiss-Prot	`http://www.ebi.ac.uk/swissprot`
UniProtKB/TrEMBL	`http://www.ebi.ac.uk/trembl`
Protein Information Resource	`http://pir.georgetown.edu`
nrdb90: A Nonredundant Sequence Database	`http://www.ebi.ac.uk/~holm/ nrdb90`
Munich Information Center for Protein Sequences	`http://mips.gsf.de`
Center for Complex Network Research	`http://www.nd.edu/~networks`
Biomolecular Object Network Databank	`http://bond. unleashedinformatics.com`

ENSEMBLE FLUCTUATIONS

The probability that a given vertex has degree k is provided by p_k (see Eq. 1.4). Therefore, the probability that R vertices have degree k, viz $X_k = R$, is given by

$$P(X_k = R) = \binom{N}{R} p_k^R (1 - p_k)^{N-R} . \tag{8.1}$$

Considering the large-N limit and $N \gg R$ we find

$$P(X_k = R) = e^{-\lambda_k} \frac{(\lambda_k)^R}{R!}, \qquad \lambda_k = N p_k = \langle X_k \rangle , \tag{8.2}$$

as the binomial distribution, Eq. (8.1) reduces for $p_k \ll 1$ to the Poisson distribution, Eq. (8.2) in the thermodynamic limit $N \to \infty$.

SELF-RETRACING PATH APPROXIMATION

This exercise needs a background in Green's functions. One needs to find the one-particle Green's function $G(\omega)$ of single particle hopping with amplitude $t = 1$ (the entries of the adjacency matrix) on a random lattice. We denote by

$$G_0(\omega) = \frac{1}{\omega}, \qquad G(\omega) = \frac{1}{\omega - \Sigma(\omega)},$$

the single-site Green's function $G_0(\omega)$, viz the Green's function on an isolated vertex and with $\Sigma(\omega)$ the respective one-particle self-energy.

We may now expand the self-energy in terms of hopping processes, with the lowest-order process being to hop to the next site and back. Once the next site has been reached the process can be iterated. We then have

$$\Sigma(\omega) = zG(\omega), \qquad G(\omega) = \frac{1}{\omega - zG(\omega)},$$

which is just the starting point for the semi-circle law Eq. (1.12).

THE CLUSTERING COEFFICIENT

One Dimension: We prove Eq. (1.56) for the clustering coefficient

$$C = \frac{3(z-2)}{4(z-1)} \tag{8.3}$$

for a one-dimensional lattice with coordination number z.

The clustering coefficient C is defined by the average fraction of pairs of neighbors of a vertex, which are also neighbors of each other. Therefore, we first calculate the total number of pairs of neighbors of a given vertex,

$$\sum_{k=1}^{z-1} k = \frac{1}{2}z(z-1) . \tag{8.4}$$

Next we evaluate the connected pairs of neighbors for a given node. Starting on the left side where we find

$$\sum_{k=1}^{z/2-1} k = \frac{z}{4}\left(\frac{z}{2}-1\right) \tag{8.5}$$

for the number of connected neighbors with no interconnecting links crossing the given vertex. Now the links crossing the given vertex remain to be counted. Starting with the node that lies $z/2$ steps left from the first node to the right of the vertex, we find this one connected to vertex 1 on the opposite site, the next with vertex 2 and so on. Thus the number of crossing connections is

$$\frac{z}{4}\left(\frac{z}{2}-1\right) , \tag{8.6}$$

leading to the result for C:

$$C\frac{1}{2}z(z-1) = 3\frac{z}{4}\left(\frac{z}{2}-1\right), \qquad C = \frac{3(z-2)}{4(z-1)} .$$

General Dimensions: The arguments above can be generalized for lattices in arbitrary dimension d by some relatively simple arguments. Consider that we are now dealing with d coordinate or lattice lines traversing a certain node. Thus, in order to calculate the cluster coefficient for this case, we confine ourselves to a one-dimensional subspace and simply have to substitute z by z/d, the connectivity on the line, yielding

$$C_d = \frac{3(z/d-2)}{4(z/d-1)} = \frac{3(z-2d)}{4(z-d)} . \tag{8.7}$$

SCALE FREE GRAPHS

As an example of a possible solution a JAVA program is given below.

```java
import java.util.Arrays;
import java.util.Random;

public class scaleFreeGraphsExcercise {

    public scaleFreeGraphsExcercise() {
        super();
    }

    public static void main(String[ ] args) {
        int totalNodes = 500;
        int graph_matrix[ ][ ] = new int[totalNodes][totalNodes];
        Random rnd = new Random();
        for (int i = 1; i < totalNodes; i++) {
            int nodeB = calcNode(i - 1, rnd.nextDouble(), graph_matrix);
```

```java
                graph_matrix[nodeB][i] = graph_matrix[i][nodeB] = 1;
            }
            double dd[ ] = degreeDistribution(graph_matrix, totalNodes);
            Arrays.sort(dd);
            for (int i = totalNodes-1; i !=0; i--) {
                if (dd[i] > 0)
                    System.out.println(totalNodes-i+"\t-\t"+dd[i]);
            }
        }

    private static double[ ] degreeDistribution(int[ ][ ] graph, int max) {
            double degreeDistribution[ ] = new double[max];
            for (int i = 0; i < max; i++) {
                degreeDistribution[degree(i, graph, max)]++;
            }
            return degreeDistribution;
        }

    public static int degree(int node, int graph[ ][ ], int totalNodes) {
            int degree = 0;
            for (int i = 0; i < totalNodes; i++) {
                degree += graph[node][i];
            }
            return degree;
        }
    public static int calcNode(int max, double random, int graph[ ][ ]) {
            double degrees[ ] = new double[max];
            double cumulativePk = 0;
            int i = 0;
            int sumdegree = 0;
            for (i = 0; i < max; i++) {
                degrees[i] = (double) degree(i, graph, max);
                sumdegree += degrees[i];
            }
            for (i = 0; i < max; i++) {
                degrees[i] = (double) degrees[i] / sumdegree;
            }
            for (i = 0; i < max; i++) {
                cumulativePk += degrees[i];
                if (random <= cumulativePk)
                    return i;
            }
            return i;
        }
    }
```

THE SIR MODEL

This task has the form of a literature study. The probability generating functions formalism, treated in Sect. (1.2.2), can be applied to an interesting problem: the spreading of an infectious disease within a social network. Presentation of the results in the form of a short seminar is a recommendable option.

Solutions to the Exercises of Chapter 2

THE LORENZ MODEL

By linearizing the differential equations (2.19) around the fixpoint (x^*, y^*, z^*) we find

$$\dot{\tilde{x}} = -\sigma\tilde{x} + \sigma\tilde{y}\,,$$
$$\dot{\tilde{y}} = (-z^* + r)\tilde{x} - \tilde{y} - x^*\tilde{z}\,,$$
$$\dot{\tilde{z}} = y^*\tilde{x} + x^*\tilde{y} - b\tilde{z}\,,$$

where $\tilde{x} = x - x^*$, $\tilde{y} = y - y^*$, $\tilde{z} = z - z^*$ are small perturbations around the fixpoint and $\sigma = 10$ and $\beta = 8/3$. By the ansatz $\tilde{x} \sim \tilde{y} \sim \tilde{z} \sim e^{\lambda t}$ we can determine the eigenvalues λ_i in the above equation.

For the fixpoint $(x^*, y^*, z^*) = (0, 0, 0)$ we find the eigenvalues

$$(\lambda_1, \lambda_2, \lambda_3) = \left(-\frac{8}{3}, \frac{-11 - \sqrt{81 + 40r}}{2}, \frac{-11 + \sqrt{81 + 40r}}{2} \right)\,.$$

For $r < 1$ all three eigenvalues are negative and the fixpoint is stable. For $r = 1$ the last eigenvalue $\lambda_3 = (-11 + 11)/2 = 0$ is marginal. For $r > 1$ the fixpoint becomes unstable.

The stability of the non-trivial fixpoints, Eq. (2.20), for $1 < r < r_c$ can be proven in a similar way, leading to a cubic equation. You can either find the explicit analytical solutions via Cardano's method or solve them numerically, e.g. via Mathematica, Maple or Mathlab, and determine the critical r_c, for which at least one eigenvalue turns positive.

THE POINCARÉ MAP

In order to solve this problem you have first to inform yourself as to how to solve a differential equation in a numerically stable fashion. There is good literature available, also on the Internet.

THE HAUSDORFF DIMENSION

Dimension of a Line: To cover a line of length l we need *one* circle of diameter l. If we reduce the diameter of the circle to $l/2$ we require *two* circles to cover the line. Generally we require a factor of two more circles if we reduce the diameter to a half. From the definition of the Hausdorff dimension we obtain

$$D_H = -\frac{\log[N(l)/N(l')]}{\log[l/l']} = -\frac{\log[1/2]}{\log[2]} = 1 \, , \tag{8.8}$$

where we used $N(l) = 1$ and $N(l' = l/2) = 2$. Therefore, the line is one-dimensional.

The Dimension of the Cantor Set: If we reduce the diameter of the circles form l to $l/3$, we require a factor of *two* more circles to cover the Cantor set. Therefore we obtain the Hausdorff dimension

$$D_H = -\frac{\log[N(l)/N(l')]}{\log[l/l']} = -\frac{\log[1/2]}{\log[3]} \approx 0.6309 \, , \tag{8.9}$$

where we used $N(l) = 1$ and $N(l' = l/3) = 2$.

DRIVEN HARMONIC OSCILLATORS

In the long time limit the system oscillates with the frequency of the driving force. Hence, we can use the ansatz

$$x(t) = x_0 \cos(\omega t + \phi) \, , \tag{8.10}$$

where we have to determine the amplitude x_0 and the phase shift ϕ. Using this ansatz for the damped harmonic oscillator we find

$$(\omega_0^2 - \omega^2) x_0 \cos(\omega t + \phi) - \gamma x_0 \omega \sin(\omega t + \phi) = \epsilon \cos(\omega t) \, . \tag{8.11}$$

The amplitude x_0 and the phase shift ϕ can now be found by splitting above equation into $\sin(\omega t)$-terms and $\cos(\omega t)$-terms and comparing the prefactors. For the case $w = w_0$ we obtain $\phi = -\pi/2$ and $x_0 = \epsilon/(\gamma\omega)$. Note that $x_0 \to \infty$ for $\gamma \to 0$.

INFORMATION FLOW IN NETWORKS

Several aspects can be studied here: For example, for the information flow as a function of a vertex' degree, you will find a proportional correlation. Furthermore you can consider the standard deviation

$$\sqrt{\frac{1}{N}\sum_{i=1}^{N} (\rho_i - \langle\rho\rangle)^2} \tag{8.12}$$

of the mean information density when varying the mean coordination number of the random lattice, see Fig. 8.1.

STOCHASTIC RESONANCE

The exercise is kind of a numerical étude. Integrating the differential equation via Euler's method should work well. Try to change the parameters by hand in order to study the effects this has on the trajectories.
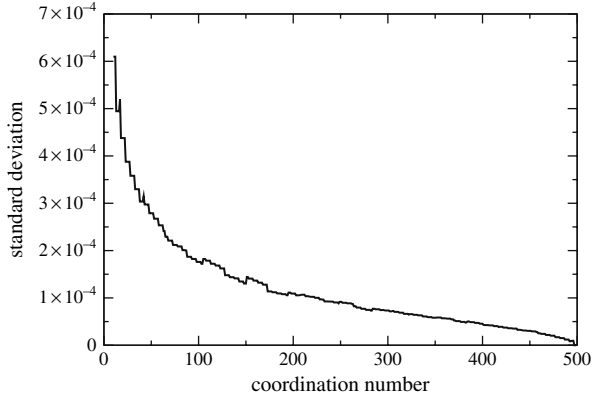
Fig. 8.1 Information flow in networks: The standard deviation, Eq. (8.12), of the mean information density decreases exponentially with the mean coordination number of the graph

Solutions to the Exercises of Chapter 3

THE $K = 1$ KAUFFMAN NET
The solutions are illustrated in Fig. 8.2.

THE $N = 4$ KAUFFMAN NET
The solution is illustrated in Fig. 8.3.

SYNCHRONOUS VS. ASYNCHRONOUS UPDATING
The solution is illustrated in Fig. 8.4.

THE HUEPE AND ALDANA NETWORK
As the exact solution can be found in the paper, we confine ourselves to some hints. You should start with the fraction of elements $\phi_N(t)$ with $+1$ at time t, which reduces to the probability $\phi(t)$ for $\sigma_i = +1$ in the $N \to \infty$ limit. You will then find that

$$s(t) = 2\phi(t) - 1 . \tag{8.13}$$

Afterwards one has to consider the probability I(t) for the output function to be positive, which gives us the recursion equation

$$\phi(t+1) = I(t)(1-\eta) + (1-I(t))\eta . \tag{8.14}$$

The relation between $I(t)$ and $\phi(t)$ is still unknown but can be calculated via

$$I(t) = \int_0^\infty P_{\xi(t)}(x)\mathrm{d}x \tag{8.15}$$

(i)

(ii)

(iii)
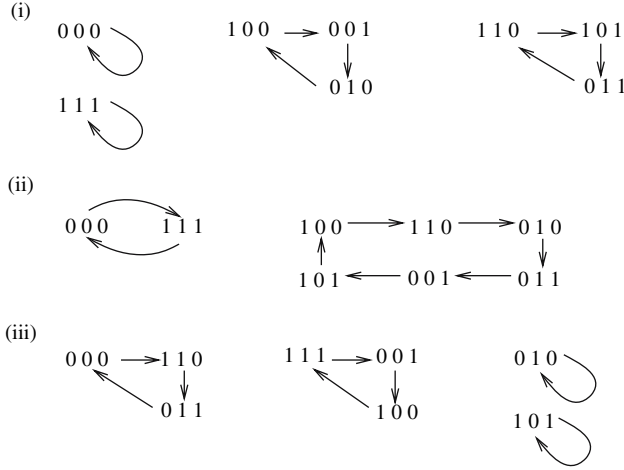
Fig. 8.2 Solution of $K = 1$, $N = 3$ Kauffman nets with a cyclic linkage tree $\sigma_1 = f_1(\sigma_2)$, $\sigma_2 = f_2(\sigma_3)$, $\sigma_3 = f_3(\sigma_1)$ for: (i) $f_1 = f_2 = f_3 =$ identity, (ii) $f_1 = f_2 = f_3 =$ negation and (iii) $f_1 = f_2 =$ negation, $f3 =$ identity
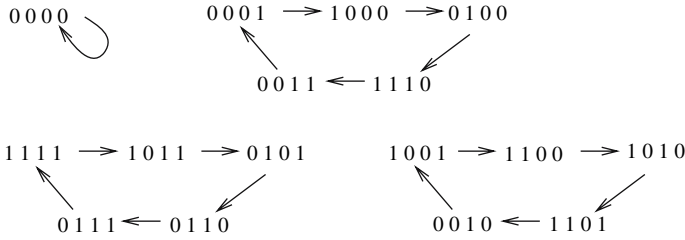
Fig. 8.3 Solution for the $N = 4$ Kauffman nets shown in Fig. 3.1, $\sigma_1 = f(\sigma_2, \sigma_3, \sigma_4)$, $\sigma_2 = f(\sigma_1, \sigma_2)$, $\sigma_3 = f(\sigma_2)$, $\sigma_4 = f(\sigma_3)$, with all coupling functions $f(\ldots)$ being the generalized XOR functions, which count the parity of the controlling elements

with $P_{\xi(t)}$ being the probability density function of the sum $\xi(t) = \sum_{j=1}^{K} \sigma_{i_j}(t)$, which can be represented as the K-fold of $P_{\sigma(t)}$ or in Fourier space:

$$\hat{P}_{\xi(t)} = \left[\hat{P}_{\sigma(t)} \right]^K . \tag{8.16}$$

For the probability density of $\sigma(t)$ the proper ansatz is:

$$P_{\sigma(t)} = \phi(t)\delta(x-1) + [1 - \phi(t)]\,\delta(x+1) . \tag{8.17}$$

After some calculus you should finally obtain the recursion relation for $s(t)$ and find both its fixed points and the critical value η_c.
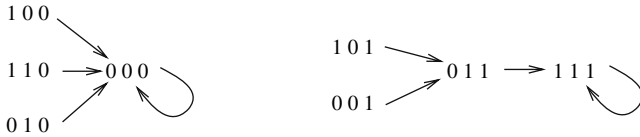
Fig. 8.4 Solution of the $N = 3$, $Z = 2$ network defined in Fig. 3.3, when using sequential asynchronous updating. The cycles completely change in comparison to the case of synchronous updating shown in Fig. 3.3

BOND PERCOLATION

The critical value p_c emerges to be $1/2$.[1] For an efficient algorithm implementing the percolation problem in C you may have a look at `http://www.santafe.edu/~mark/percolation`. This algorithm measures the number of vertices in the largest connected component. Visual simulations can be found on the Internet as well, e.g. `http://www.univ-bechar.dz/Boutiche/VRH/percolation.htm`.

Solutions to the Exercises of Chapter 4

SOLUTIONS OF THE LANDAU–GINZBURG FUNCTIONAL

The values $t = h = 0.1$ lead for Eq. (4.9) to the cubic equation

$$P(\phi) - h = \phi^3 - 0.9\phi - 0.1 = 0 , \tag{8.18}$$

which has one root $\phi_3 = 1$. The remaining quadratic equation can be solved analytically. One finds $\phi_1 \approx -0.89$ and $\phi_2 \approx -0.11$. Inserting these solutions into the derivative $P'(\phi)$ one obtains $P'(\phi_2) < 0$, which implies that ϕ_2 is an unstable fixpoint. ϕ_1 and ϕ_3 are, on the other hand, locally stable.

ENTROPY AND SPECIFIC HEAT WITHIN THE LANDAU MODEL

The free energy density is given by

$$f(T,\phi,h) - f_0(T,h) = \frac{t-1}{2}\phi^2 + \frac{1}{4}\phi^4 = -\frac{(t-1)^2}{4} ,$$

where we used $\phi^2 = 1 - t$. It follows that

$$\frac{\partial F}{\partial t} = -V\frac{t-1}{2} \qquad \Rightarrow \qquad S = \frac{\partial F}{\partial T} = \frac{V}{T_c}\frac{1-t}{2}$$

for the entropy S and where $t = T/T_c$. The specific heat C_V is then

---

[1] The reader interested in a rigorous mathematical proof may consult
KESTEN, H.1980 The critical probability of bond percolation on the square lattice equals 1/2. *Communications in Mathematical Physics* **74** 41–59.

"cross"

| Step 1 | Step 2 | Step 3 | Step 4 |

| Step 5 | Step 6 | Step 7 |
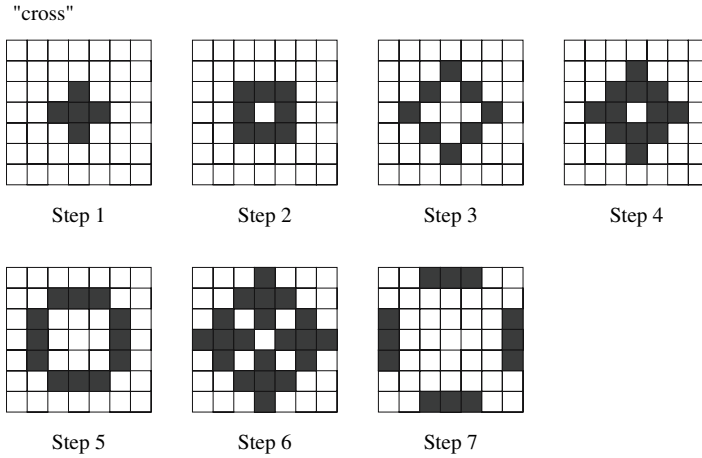
Fig. 8.5 Evolution of the pattern "cross" in the game of life: After seven steps it gets stuck in a fixed state with four blinkers

$$C_V \;=\; T_c \frac{\partial S}{\partial T} \;=\; -\frac{V}{2T_c}, \qquad T < T_c \,.$$

For $T > T_c$ the specific heat C_V vanishes, there is a jump at $T = T_c$.

THE GAME OF LIFE

The solutions have already been given in Fig. 4.5, apart from the cross $\{(0,0), (0,1),(1,0),(-1,0),(0,-1)\}$. For an illustration of its development see Fig. 8.5.

THE GAME OF LIFE ON A SMALL-WORLD NETWORK

The construction of a small-world net with conserving local connectivities $k_i \equiv 8$ is shown and explained in Fig. 8.6. An appropriate dynamical order parameter would be the density of life $\rho(t)$ at time t representing the fraction of living cells.[2]

THE FOREST FIRE MODEL

We define by x_t, x_f and x_e the densities of cells with trees, fires and ashes (empty), with $x_t + x_f + x_e = 1$. A site burns if there is at least one fire on one of the Z nearest-neighbor cells. The probability that none of Z cells is burning is $(1-x_f)^Z$, the probability that at least one out of Z is burning is $1 - (1-x_f)^Z$. We have than the updating rules

$$x_f(t+1) \;=\; \left[1 - (1 - x_f(t))^Z\right] x_t(t), \qquad x_e(t+1) \;=\; x_f(t) - p x_e(t),$$

[2] This problem has been surveyed in detail by

HUANG, S.-Y., ZOU, X.-W., TAN, Z.-J., JIN, Z.-Z. 2003 Network-induced non-equilibrium phase transition in the "Game of Life". *Physical Review E* **67** 026107.
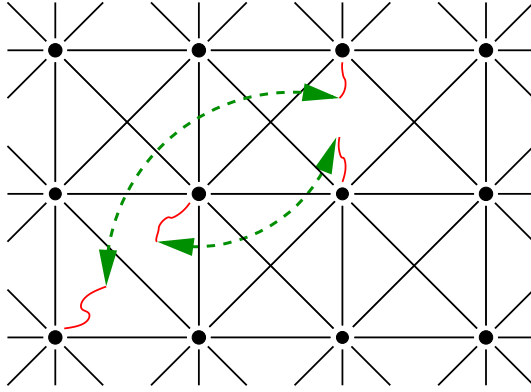
Fig. 8.6 Construction of a small-world network out of the game of life on a 2D-lattice: One starts with a regular arrangement of vertices where each one is connected to its eight nearest neighbors. Two arbitrarily chosen links (wiggled lines) are cut with probability p and the remaining stubs are rewired randomly as indicated by the dashed arrows. The result is a structure showing clustering as well as a fair amount of shortcuts between far away sites, as in the Watts and Strogatz model, Fig. 1.9, but with conserved connectivities $k_i \equiv 8$

The stationary solutions $x_e(t+1) = x_e(t) \equiv x_e^*$, etc., are

$$(1+p)x_e^* = x_f^*, \qquad 1 = x_f^* + x_t^* + x_f^*/(1+p), \qquad x_t^* = 1 - \frac{2+p}{1+p}x_f^*.$$

We then find a self-consistency condition for the stationary density x_f^* of fires,

$$x_f^* = \left[1 - (1 - x_f^*)^Z\right] \left(1 - \frac{2+p}{1+p}x_f^*\right), \qquad (8.19)$$

which in general needs to be solved numerically. For small densities of fires we expand

$$1 - (1 - x_f^*)^Z \approx 1 - (1 - Zx_f^* + Z(Z-1)/2(x_f^*)^2) = Zx_f^* - Z(Z-1)/2(x_f^*)^2$$

and find for Eq. (8.19)

$$\frac{1}{Z} = \left(1 - \frac{(Z-1)}{2}x_f^*\right) \left(1 - \frac{2+p}{1+p}x_f^*\right) \approx 1 - \left(\frac{(Z-1)}{2} + \frac{2+p}{1+p}\right)x_f^*.$$

The minimal number of neighbors for fires to burn continuously is $Z > 1$ in mean-field theory.

THE REALISTIC SANDPILE MODEL

The variable z_i should denote the true local height of a sandpile; the toppling starts when the slope becomes too big after adding grains of sand randomly,
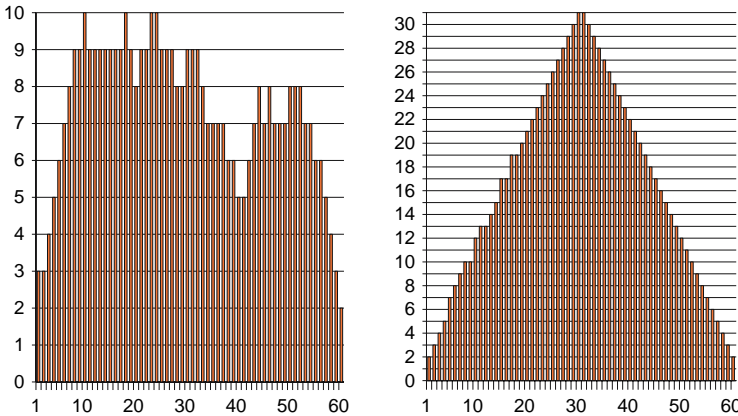
Fig. 8.7 Example of a simulation of a one-dimensional realistic sandpile model, see Eq. (8.20), with 60 cells, after 500 (left) and 2000 (right) time step

i.e. when the difference $z_i - z_j$ between two neighboring cells exceeds a certain threshold K. Site i then topples in the following fashion:

(i)   Look at the neighbor j of site i for which $z_i - z_j$ is biggest and transfer one grain of sand from i to j,

$$z_i \to z_i - 1, \qquad z_j \to z_j + 1 . \tag{8.20}$$

(ii)   If more than one neighbor satisfies the criteria in (i), select one of them randomly.
(iii)   Repeat step (i) until all neighbors j of i satisfy the condition $z_i \geq z_j + 1$.

The toppling process mimics a local instability. The avalanche can then proceed in two directions: forwards and backwards. Note that the toppling rule is conserving, sand is lost only at the boundaries.

This model leads to true sandpiles in the sense that it is highest in the center and lowest at the boundaries, compare Fig. 8.7. Note that there is no upper limit to z_i, only to the slope $|z_i - z_j|$.

THE RANDOM BRANCHING MODEL

For the probability Q_n for the avalanche to last $1 \ldots n$ time steps one can make the recursion ansatz:

$$Q_{n+1} = (1 - p) + p Q_n^2 , \tag{8.21}$$

in analogy to the recursion relation Eq. (4.24) for the functionals generating the distribution of avalanche sizes. The case here, however, is simpler, as one can work directly with probabilities: The probability Q_{n+1} to find an avalanche of duration $1 \ldots (n+1)$ is the probability $(1 - p)$ to find an an avalanche of length 1 plus the probability $p Q_n^2$ to branch one time step, generating two avalanches of length $1 \ldots n$.

In the thermodynamic limit we can replace the difference $Q_{n+1} - Q_n$ by the derivative $\frac{dQ_n}{dn}$ leading to the differential equation

$$\frac{dQ_n}{dn} = \frac{1}{2} + \frac{1}{2}Q_n^2 - Q_n, \quad \text{for} \quad p = p_c = \frac{1}{2}, \quad (8.22)$$

which can easily be solved by separation of variables. The derivative of the solution Q_n with respect to n is the probability of an avalanche to have a duration of exactly n steps.

$$Q_n = \frac{n}{n+2}, \quad (8.23)$$

$$D(t=n) = \frac{dQ_n}{dn} = \frac{2}{(n+2)^2} \sim n^{-2}.$$

Check that , Eq. (8.23) really solves , Eq. (8.22).

THE BAK AND SNEPPEN MODEL

In the $N \to \infty$ limit you will find the simulation results perfectly assorting with the molecular field solution; you should be aware that by increasing the number of species N you will also have to increase the number of iterations until the equilibrium is reached.

Solutions to the Exercises of Chapter 5

THE ONE-DIMENSIONAL ISING MODEL

For the one-dimensional Ising system the energy is

$$E = -J \sum_i S_i S_{i+1} - B \sum_i S_i ,$$

with $S_i = \pm 1$. The partition function

$$\mathscr{Z}_N = \mathscr{Z}_N(T,B) = \sum_n e^{-\beta E_n} = \sum_{S_1} \cdots \sum_{S_N} T_{S1,S2} T_{S2,S3} \ldots T_{SN,S1}$$

can be evaluated with the help of the 2×2 transfer matrix $T = \begin{pmatrix} e^{\beta(J+B)} & e^{-\beta J} \\ e^{\beta J} & e^{\beta(J-B)} \end{pmatrix}$.

It has the eigenvalues

$$\lambda_{1,2} = e^{\beta J} \cosh \beta B \pm \sqrt{e^{2\beta J} \cosh^2 \beta B - 2 \sinh 2\beta J} ,$$

leading to

$$\mathscr{Z}_N(T,B) = \sum_{S1,S2} \left(T^N \right)_{S1,S2} = (\lambda_1)^N + (\lambda_2)^N \simeq (\lambda_1)^N ,$$

for large N and $\lambda_1 \gg \lambda_2$. The free energy per particle is given by

$$\frac{F(T,B)}{N} = \frac{-kT}{N} \ln \mathscr{Z}_N(T,B) \,,$$

and the magnetization per particle by

$$\frac{M(T,B)}{N} = -\frac{\partial F(T,B)}{\partial B} = \left(1 + \frac{e^{-4\beta J}}{\sinh^2 \beta B} \right)^{-1/2} \,.$$

ERROR CATASTROPHE

First Case $u_- = 0$, $u_+ = u$: The fixpoint conditions read

$$0 = (1 - \sigma)x_i + ux_{i-1} - \phi x_i, \qquad i > 1 \,,$$
$$0 = x_1 - \phi x_1 \,,$$

where the x_i are the respective concentrations. Hence we can immediately write down the $N \times N$ reproduction rate matrix W:

$$W = \begin{pmatrix} 1 & 0 & 0 & 0 \cdots \\ u & (1-\sigma) & 0 & 0 \cdots \\ 0 & u & (1-\sigma) & 0 \cdots \\ \vdots & \vdots & \vdots & \vdots \ddots \end{pmatrix} \,, \tag{8.24}$$

whose diagonal elements obviously represent the eigenvalues. The largest eigenvalue is $1 = W_{11}$, and the corresponding eigenvector

$$e_1 = \frac{1}{\sqrt{N}} \left(1, \frac{u}{\sigma}, \left(\frac{u}{\sigma}\right)^2, \cdots, \left(\frac{u}{\sigma}\right)^{N-1} \right) \,. \tag{8.25}$$

This eigenvector is normalizable only for $u < \sigma$, viz $u = \sigma$ is the error threshold.

Second Case $u_- = u_+ = u$: The fixpoint conditions are

$$0 = (1 - \sigma)x_i + ux_{i-1} + ux_{i+1} - \phi x_i, \qquad i > 1 \,,$$
$$0 = x_1 + ux_2 - \phi x_1 \,.$$

The first equation is equivalent to

$$x_{i+1} = \frac{\phi + \sigma - 1}{u} x_i - x_{i-1}, \qquad i > 1 \,, \tag{8.26}$$

which can be cast into the 2×2 recursion form

$$\begin{pmatrix} x_i \\ x_{i+1} \end{pmatrix} = \begin{pmatrix} 0 & 1 \\ -1 & \frac{\phi + \sigma - 1}{u} \end{pmatrix} \begin{pmatrix} x_{i-1} \\ x_i \end{pmatrix} \,. \tag{8.27}$$

The largest eigenvalues of the above recursion matrix determine the scaling of x_i for large i. For the determination of the error threshold you may solve for the x_i numerically, using Eq. (8.26) and the mass-normalization condition $\sum_i x_i = 1$ for the self-consistent determination of the flux ϕ.

MODELS OF LIFE

This is very suitable for a small work study with a subsequent seminar.

HYPERCYCLES

The fixpoints (x_1^*, x_2^*) are given by

$$0 = x_1^* (\alpha + \omega x_2^* - \phi),$$
$$0 = x_2^* (2\alpha + \omega x_1^* - \phi),$$
$$\phi = \alpha x_1^* + 2\alpha x_2^* + 2\omega x_1^* x_2^*,$$

with the condition $x_1 + x_2 = 1$ for the total concentration and $x_1^*, x_2^* \geq 0$. Solving these equations we find $x_1^* = \frac{\omega - \alpha}{2\omega}$ and $x_2^* = \frac{\omega + \alpha}{2\omega}$ for $\omega > \alpha$. Otherwise, only the trivial solutions $(x_1^*, x_2^*) = (0, 1)$ and $(x_1^*, x_2^*) = (1, 0)$ are fixpoints. Linearizing the equations around the fixpoints leads us to the matrix

$$M = \begin{pmatrix} (\omega - \alpha)x_2^* - 4\omega x_1^* x_2^* & (\omega - \alpha)x_1^* - 2\omega(x_1^*)^2 \\ \omega x_2^* - 2\omega(x_2^*)^2 & \alpha + \omega x_1^* - 2\alpha x_2^* - 4\omega x_1^* x_2^* \end{pmatrix}. \tag{8.28}$$

For $(x_1^*, x_2^*) = (1, 0)$ the biggest eigenvalue of M is $\omega + \alpha$, which is positive for positive growth rates, so the fixpoint is unstable. For $(0, 1)$ one finds the condition $\omega < \alpha$ that guarantees all eigenvalues being negative. The analysis for $(\frac{\omega - \alpha}{2\omega}, \frac{\omega + \alpha}{2\omega})$ can hardly be accomplished by hand; it should be left to a computer algebra system like Maple, Mathematica or Mathlab.

THE PRISONER'S DILEMMA ON A LATTICE

We use first a general payoff matrix and then, specifically, $\{T; R; P; S\} = \{3.5; 3.0; 0.5; 0.0\}$ as in Fig. 5.10. We consider the four cases separately:

– *One Defector in the Background of Cooperators*
  The payoffs are
  intruding defector: $4 \times T \qquad = 4 \times 3.5 \quad = 14$
  cooperating neighbors: $3 \times R + 1 \times S = 3 \times 3 + 0 = 9$
  Therefore, the neighboring cooperators will become defectors in the next step.
– *Two Adjacent Defectors in the Background of Cooperators*
  The payoffs are:
  intruding defectors: $3 \times T + 1 \times P = 3 \times 3.5 + 0.5 = 11$
  cooperating neighbors: $3 \times R + 1 \times S = 3 \times 3 + 0 \qquad = 9$
  Therefore, the neighboring cooperators will become defectors in the next step.

– *One Cooperator in the Background of Defectors*
  The payoffs are:
  intruding cooperator: $4 \times S$ $= 4 \times 0$ $= 0$
  defecting neighbors: $3 \times P + 1 \times T = 3 \times 0.5 + 3.5 = 5$
  The cooperating intruder will die and in the next step only defectors will be present.

– *Two Adjacent Cooperators in the Background of Defectors*
  The payoffs are:
  intruding cooperators: $3 \times S + 1 \times R = 4 \times 0 + 3$ $= 3$
  defecting neighbors: $3 \times P + 1 \times T = 3 \times 0.5 + 3.5 = 5$
  The cooperating intruders will die and in the next step only defectors will be present.

One can go one step further and consider the case of three adjacent intruders. Not all intruders will then survive for the case of defecting intruders and not all intruders will die for the case of cooperating intruders.

NASH EQUILIBRIUM

The payoff matrix of this game is given by

$$A = \begin{pmatrix} L\ L \\ 0\ H \end{pmatrix}, \qquad L < H,$$

for the cautious/risky player, where L signifies the low payoff and H the high payoff. Denoting the number of cautious players by N_c we can compute the reward for participants playing cautiously or riskily, respectively and from this the global reward G:

$$R_c = [LN_c + L(N - N_c)]/N = L, \tag{8.29}$$
$$R_r = [0 \cdot N_c + H(N - N_c)]/N = H(N - N_c)/N, \tag{8.30}$$
$$G(N_c) = \frac{(N - N_c)^2}{N}H + N_c L. \tag{8.31}$$

The function $G(N_c)$ has two local maxima at $N_c = 0$ and $N_c = N$ representing the Nash equilibria with the first case being the optimal one for each player and the maximal global utility being NH.

Solutions to the Exercises of Chapter 6

DRIVEN HARMONIC OSCILLATORS

The all time solution can be obtained by combining the homogeneous solution (no external force) and one special solution (e.g. the long-time ansatz from Eqs. 6.3 and 6.4). Since the homogeneous solution is given by

$$x(t) \sim e^{\lambda t}, \qquad \lambda_{\pm} = -\frac{\gamma}{2} \pm \sqrt{\frac{\gamma^2}{4} - \omega_0^2}, \qquad (8.32)$$

with damping γ, this contribution vanishes in the limit $t \to 0$ and only the special solution survives.

THE TERMAN–WANG OSCILLATOR

We linearize Eq. (6.21) around the fixpoint (x^*, y^*) and consider the limit $\beta \to 0$,

$$\lim_{\beta \to \infty} \tanh(x/\beta) = \Theta(x) = \begin{cases} 0 & (x < 0) \\ 1 & (x > 0) \end{cases}.$$

We find, since $x^* < 0$ (compare Fig. 6.5),

$$\dot{\tilde{x}} = 3(1 - x^{*2})\tilde{x} - \tilde{y}$$
$$\dot{\tilde{y}} = -\epsilon \tilde{y}$$

where $\tilde{x} = x - x^*$ and $\tilde{y} = y - y^*$ are small perturbations around the fixpoint. By the ansatz $\tilde{x} \sim \tilde{y} \sim e^{\lambda t}$ we can determine the eigenvalues λ in the above equation. We obtain $\lambda_1 = 3(1 - x^{*2})$ and $\lambda_2 = -\epsilon$. The fixpoint $x^* \simeq 0$ is unstable, since $\lambda_1 \simeq 3 > 0$ for this case. The fixpoint at $|x^*| > 1$ is stable, since $\lambda_1 < 0$, $\lambda_2 < 0$ and $\tilde{x} \sim \tilde{y} \sim e^{\lambda t}$ decays in the long time limit.

THE SIRS MODEL – ANALYTICAL

The fixpoint equation reads

$$x^* = ax^* \left[1 - (\tau_R + 1)x^* \right]$$

with the solutions

$$x^* = 0 \qquad \text{or} \qquad x^* = \frac{a - 1}{a(\tau_R + 1)}$$

for general $\tau_R = 0, 1, 2, \ldots$. We examine the stability of x^* against a small perturbation $\tilde{x}_n$ by linearization using $x_n = x^* + \tilde{x}_n$:

$$\tilde{x}_{n+1} = -ax^* \sum_{k=0}^{\tau_R} \tilde{x}_{n-k} + a\tilde{x}_n \left[1 - (\tau_R + 1)x^* \right].$$

For the trivial fixed point $x^* = 0$ this reduces to

$$\tilde{x}_{n+1} = a\tilde{x}_n, \qquad \text{leading to the stability condition} \quad a < 1.$$

The analysis for the second fixed point with $\tau_R = 0$ runs analogously to the computation concerning the logistic map in Chap. 2. For $\tau_R = 1$ the situation becomes more complicated:

$$\tilde{x}_{n+1} = \frac{1}{2}(3-a)\tilde{x}_n + \frac{1}{2}(1-a)\tilde{x}_{n-1} .$$

With the common ansatz $\tilde{x}_n = \lambda^n$ for linear recurrence relations one finds the conditions

$$\left| -\frac{1}{4}a + \frac{3}{4} + \frac{1}{4}\sqrt{a^2 - 14a + 17} \right| < 1, \qquad \text{and} \qquad a^2 - 14a + 17 > 0 \quad (8.33)$$

for small perturbations to remain small and not to grow exponentially, i.e. $|\lambda| <$ 1. So a has to fulfill

$$1 < a < 7 - 4\sqrt{2} \approx 1.34 .$$

THE SIRS MODEL – NUMERICAL

If you have some programming experience the implementation will not pose any problem. It is recommended that you change the parameters over an adequate range and study the effects.

Solutions to the Exercises of Chapter 7

TRANSIENT STATE DYNAMICS

Driven Transient State Dynamics: The most simple solution to this problem would be to provide a signal $\phi(t)$, e.g. an oscillator and let $x(t)$ react on its behavior like

$$\dot{x} = (1-x)\theta(\phi - x_c)(\phi - x_c) + x\theta(x_c - \phi)(\phi - x_c) ,$$
$$\phi = \big(\cos(\omega t) + 1\big)/2 ,$$

with a critical $x_c \in [0,1]$, which determines the threshold for ϕ from which on the signal x is to autoexcite. As usual the prefactors $(1-x)$ and x guarantee the normalization of x and $(\phi - x_c)$ represents the growth rate being assumed as a linear function of ϕ.

Emerging Transient State Dynamics: In order to describe a situation with both variables mutually influencing each other, one may introduce several thresholds that make the reservoir ϕ deplete only if x is close to 1 and activity x to deplete when ϕ is almost 0 and vice versa,

$$\dot{x} = (1-x)\theta(\phi - 0.99)r + x\theta(0.01 - \phi)r ,$$
$$r = 2(\phi - 0.5) ,$$
$$\dot{\phi} = \Gamma^+(1-\phi)\theta(0.02 - x) + \Gamma^-\phi\theta(x - 0.98) .$$

Note that the parameters of the solution are very sensitive; most combinations result in a fixpoint attractor and in the absence of continuous dynamics. We

found $\Gamma^+ = \Gamma^- = 0.04$ to work in this case and yield a permanent excitation–depletion cycle.

THE DIFFUSIVE CONTROL UNIT

In analogy to the previous task the most simple ansatz for this problem would be the differential equations

$$\dot{x}_1 = (1-x_1)\theta(y_1-y_2)(y_1-y_2)+x_1\theta(y_2-y_1)(y_1-y_2)\,, \qquad (8.34)$$
$$\dot{x}_2 = (1-x_2)\theta(y_2-y_1)(y_2-y_1)+x_2\theta(y_1-y_2)(y_2-y_1)\,, \qquad (8.35)$$

where the Heaviside function decides when the value of the first unit x_1 is to grow, namely if $y_1 > y_2$, and when to deplete ($y_2 > y_1$) and the other way round for x_2.

ASSOCIATIVE OVERLAPS

We start by calculating all associative overlaps of degree zero, compare Fig. 7.5, for the six cliques (0,1,2), (1,2,3), (1,3,4), (4,5,6) and (2,6):

```
            |0  1  1  4
            |1  2  3  5  2
            |2  3  4  6  6
    ────────┼────────────
    0  1  2 |   2  1  0  1
    1  2  3 |2     2  0  1
    1  3  4 |1  2     1  0
    4  5  6 |0  0  1     1
    2  6    |1  1  0  1
```

Next we present two possible solutions, beginning with clique (012). The table contains seven columns, the first being the time step t followed by the nodes 0 to 6. Every row in the table indicates a time step. An active node at a time step is set to 1, inactive nodes are left empty.

t	0	1	2	3	4	5	6
0	1	1	1				
1		1	1	1			
2		1		1	1		
3	1	1	1				

t	0	1	2	3	4	5	6
0	1	1	1				
1		1	1	1			
2		1		1	1		
3					1	1	1
4			1				1
5	1	1	1				

The time evolutions coincide qualitatively with those illustrated in Fig. 7.8.

Index